University of Naples Federico II
Polytechnic and Basic Sciences School

Department of Chemical Sciences

Ph.D. in Chemical Sciences

Development of site-selective procedures towards biomedically relevant semi-synthetic polysaccharides

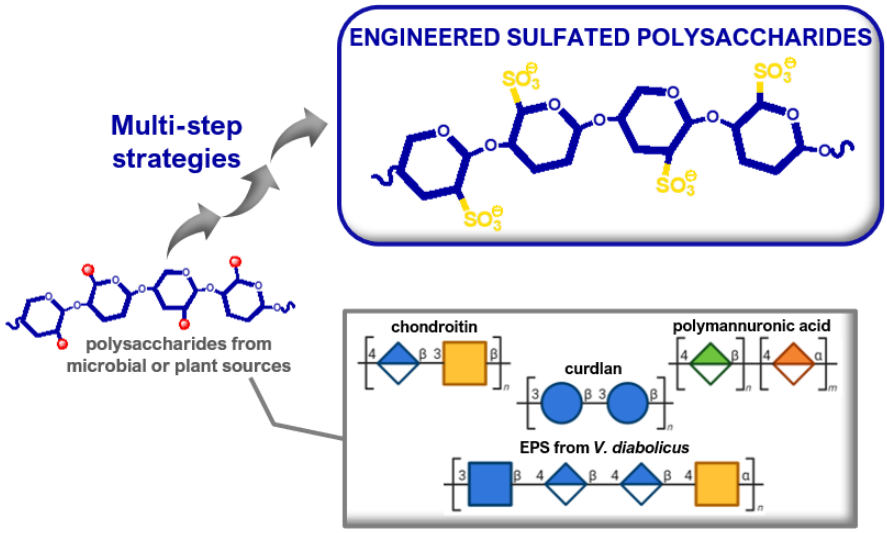

Giulia Vessella

Advisor:
prof. Emiliano Bedini

Examiner:
prof. Paola Manini

XXXIII Cycle 2018 – 2021
Coordinator: prof. Angela Lombardi

List of Symbols and Abbreviations

Ac	Acetyl
Ac_2O	Acetic anhydride
AcCl	Acetyl chloride
AcOEt	Ethyl acetate
AcOH	Acetic acid
Alloc	Allyloxycarbonyl
AT	Antithrombin
ATR	Attenuated Total Reflection
AW–300	Acid-Washed
Bn	Benzyl
BnBr	Benzyl bromide
BTSA	*N*,*O*-bis(trimethylsilyl)-acetamide
Bu_3N	Tributylammonium
Bz	Benzoyl
Bz_2O	Benzoic anhydride
BzCl	Benzoyl chloride
BzCN	Benzoyl cyanide
Cbz	Benzyloxycarbonyl
CD	Circular Dichroism
CdS	Curdlan sulfate
COSY	COrrelation SpectroscopY
Cp	Cyclopentadienyl
CS	Chondroitin sulfate
CSA	(+)-Camphor-10-sulfonic acid
DEA	Diethylamine
DEPT	Distorsionless Enhancement by Polarization Transfer
DeS	Dermatan sulfate
DF	Fucosylation Degree
DIPEA	*N*,*N*-Diisopropylethylamine
DMAc	*N*,*N*-Dimethylacetamide
DMAP	4-(Dimethylamino)pyridine
DMF	*N*,*N*-Dimethylformamide
DMI	1,3-Dimethyl-2-imidazolidinone
DMSO	Dimethylsulfoxide
DMTr	4,4′-Dimethoxytrityl
DMTrCl	4,4′-Dimethoxytrityl chloride
DQF	Double Quantum Filter

DS	Sulfation Degree
DTT	1,4-Dithiothreitol
ECM	Extracellular Matrix
EDC	1-(3-(Dimethylamino)propyl)-ethylcarbodiimide
EDTA	Ethylenediaminetetraacetic acid
EtI	Ethyl Iodide
Et_3N	Triethylamine
Et_3SiH	Triethyl silane
fCS	Fucosylated chondroitin sulfate
Fuc, F	Fucose
GAG	Glycosaminoglycan
GalNAc, N	2-Acetamido-2-deoxy-galactose (*N*-acetyl-galactosamine)
Glc	Glucose
GlcA, U	Glucuronic Acid
GlcNAc	2-Acetamido-2-deoxy-glucose (*N*-acetyl-glucosamine)
GPC	Gel Permeation Chromatography
GulA, G	Guluronic acid
HA	Hyaluronic acid
HCII	Heparin Cofactor II
HeP	Heparin
HEPES	*N*-(2-Hydroxyethyl)piperazine-*N'*-(2-ethanesulfonic acid)
HMBC	Heteronuclear Multiple Bond Correlation
HPLC	High Performance Liquid Chromatography
HP-SEC	High Performance Size Exclusion Chromatography
HS	Heparan sulfate
HSQC	Heteronuclear Single Quantum Coherence
ImH	Imidazole
i-Pr_2O	Diisopropyl ether
KS	Keratan sufate
LALS	Low-Angle Light Scattering
LMW	Low Molecular Weight
MALS	Multiangle Light Scattering
ManA, M	Mannuronic acid
MMTr	Monomethoxytrityl
$MPCH(OMe)_2$	*p*-methoxybenzaldehyde dimethyl acetal
MS	Molecular Sieves
MSTFA	*N*-methyl-*N*-(trimethylsilyl)-trifluoroacetamide
M_w	Molecular weight
n.d.	Not determined
NaOAc	Sodium acetate

NHS	*N*-hydroxysuccinimide
NH_4OAc	Ammonium acetate
NIS	*N*-iodosuccinimide
NMe_3	Trimethylamine
NOESY	Nuclear Overhauser Enhancement SpectroscopY
o.n.	overnight
PEO	Polyethylene oxide
PES	Polyethersulfone
PG	Proteoglycan
PivCl	Pivaloyl chloride
PMP	*p*-Methoxyphenyl
py	Pyridine
r.t.	Room temperature
RALS	Right-Angle Light Scattering
RI	Refractive Index
RU	Repeating Unit
SAR	Structure-activity Relationship
SAX	Strong Anion Exchange
SEC	Size Exclusion Chromatography
$SO_3 \cdot Me_3N$	Sulfur trioxide–trimethylamine
$SO_3 \cdot py$	Sulfur trioxide pyridine complex
SPR	Surface Plasmon Resonance
TBA	Tetrabutylammonium
TBAF	Tetrabutylammonium fluoride
TBAOAc	Tetrabutylammonium acetate
TBAOH	Tetrabutylammonium hydroxide
TBDMS	*t*-Butyldimethylsilyl
TBDPS	*t*-Butyldiphenylsilyl
TDMS	Thexyldimethylsilyl
Tf	Trifluoromethanesulfonate
TFA	Trifluoroacetic acid
TfOH	Trifluoromethanesulfonic acid
THF	Tetrahydrofuran
TIPS	Triisopropylsilyl
TMS	Trimethylsilyl
TMSOTf	Trimethylsilyl trifluoromethanesulfonate
TOCSY	TOtal Correlation SpectroscopY
TPPI	Time Proportional Phase Incrementation
Troc	2,2,2-Trichloroethoxycarbonyl
VIS	Viscosimeter

Table of Contents

List of Publications

Vessella, G., Esposito, F., Traboni, S., Di Meo, C., Iadonisi, A., Schiraldi, C., Bedini, E., **2021**. Exploiting Diol Reactivity for the Access to Unprecedented Low Molecular Weight Curdlan Sulfate Polysaccharides. *Carbohydr. Polym. 269*, 118324–11833, doi: 10.1016/j.carbpol.2021.118324.

Iadonisi, A., Traboni, S., Capasso, D., Bedini, E., Cuomo, S., Di Gaetano, S., Vessella, G., **2021**. Switchable Synthesis of Glycosyl Selenides or Diselenides with Direct Use of Selenium as the Selenating Agent. *Org. Chem. Front. 8*, 1823–1829. doi: 10.1039/D1QO00045D.

Traboni, S., Bedini, E., Landolfi, A., Vessella, G., Iadonisi, A., **2021**. Catalytic, Regioselective Sulfonylation of Carbohydrates with Dibutyltin Oxide under Solvent-Free Conditions. *Catalysts 11*, 202–210. doi: 10.1039/D1QO00045D.

Vessella, G., Vázquez, J.A., Valcárcel, J., Lagartera, L., Monterrey, D. T., Bastida, A., García-Junceda, E., Bedini, E., Fernández-Mayoralas, A., Revuelta, J., **2021**. Deciphering Structural Determinants in Chondroitin Sulfate Binding to FGF-2: Paving the Way to Enhanced Predictability of Their Biological Functions. *Polymers 13,* 313–328. doi: 10.3390/polym13020313.

Traboni, S., Bedini, E., Vessella, G., Iadonisi, A., **2020**. Solvent-Free Approaches in Carbohydrate Synthetic Chemistry: Role of Catalysis in Reactivity and Selectivity. *Catalyst 10*, 1142–1165. doi: 10.3390/catal10101142.

Traboni, S., Vessella, G., Bedini, E., Iadonisi, A., **2020**. Solvent-Free, under Air Selective Synthesis of α-Glycosides Adopting Glycosyl Chlorides as Donors. *Org. Biomol. Chem. 18*, 5157–5163. doi: 10.1039/d0ob01024c.

Vessella, G., Traboni, S., Laezza, A., Iadonisi, A., Bedini, E., **2020**. (Semi)-Synthetic Fucosylated Chondroitin Sulfate Oligo-and Polysaccharides. *Mar. Drugs 18*, 293–312. doi: 10.3390/md18060293.

Vessella, G., Traboni, S., Pirozzi, A.V.A., Laezza, A., Iadonisi, A., Schiraldi, C., Bedini, E., **2019**. A Study for the Access to a Semi-Synthetic Regioisomer of Natural Fucosylated Chondroitin Sulfate with Fucosyl Branches on *N*-Acetyl-Galactosamine Units. *Mar. Drugs 17*, 655-670. doi: 10.3390/md17120655.

Vessella, G., Traboni, S., Cimini, D., Iadonisi, A., Schiraldi, C., Bedini, E., **2019**. Development of Semisynthetic, Regioselective Pathways for Accessing the Missing Sulfation Patterns of Chondroitin Sulfate. *Biomacromolecules 20*, 3021–3030. doi: 10.1021/acs.biomac.9b00590.

Vessella, G., Casillo, A., Fabozzi, A., Traboni, S., Iadonisi, A., Corsaro, M.M., Bedini, E., **2019**. Synthesis of the Tetrasaccharide Repeating Unit of the Cryoprotectant Capsular Polysaccharide from: *Colwellia psychrerythraea* 34H. *Org. Biomol. Chem. 17*, 3129–3140. doi: 10.1039/c9ob00104b.

Abstract

Polysaccharides are highly abundant biopolymers, possessing enormous structural diversity and functional versatility. They naturally possess outstanding applications and uses, but their chemical manipulation can improve the given features and open the way to the development of new products and materials.

An important group of natural polysaccharides comprises the sulfated ones, which perform key biological functions. Among them, sulfated GAGs are the most abundant in animal species, where they play crucial roles in many physio-pathological processes. Thanks to their bioproperties, GAGs are currently used as therapeutics and biomaterials, however for many applications native GAGs may exhibit limitations linked to production cost, batch standardization, immunogenicity, degradability, or other aspects.

The biological functions of sulfated polysaccharides often depend on their selective binding to proteins, and it has been suggested —for GAGs primarily— that the sulfation pattern sequence might be able to encode functional information to this aim.

The obtainment of engineered sulfated polysaccharides (ESPs), by chemical or enzymatic modification of natural ones or by chemical synthesis of oligo- or polysaccharides, can lead to well-defined structures with a precise sulfation pattern, thus helping the elucidation of the effects of their structural parameters on the exhibited functions. Besides, ESPs can exhibit new and enhanced biological properties compared to their unmodified counterparts and can also be produced in large quantities at low costs from renewable raw materials or from microbial production, being an easier alternative to isolation of GAGs from animal tissues.

In this work, I investigated the possibility to achieve regioselective modifications of naturally occurring polysaccharides, exploiting suitably tailored multi-step

sequences, often embedding cyclic protecting groups for vicinal diols, to obtain GAG analogues or mimics.

I first focused the attention on the development of semi-synthetic pathways to structurally well-defined CS and fCS —two GAG family members— polysaccharides.

Starting from a microbial sourced unsulfated chondroitin and employing a modular approach, comprising regioselective steps together with sulfation and final deprotection, a library of twelve (semi)-homogeneous CSs, possessing almost all the possible sulfation patterns on the polymeric chain, was afforded.

A library of ten fCS structures, with a strict regiocontrol of both fucose branch position and sulfation pattern, was obtained by chemical glycosylation of suitably protected chondroitin polysaccharides, having selectively free hydroxyl position(s), with properly prepared L-fucose donors, followed by four additional steps (acetylation, selective cleavage of orthogonal protecting groups, sulfation, global deprotection).

A study for regioselective sulfation of other naturally occurring polysaccharides was also carried out. Three polymers were considered: (1) curdlan, a β-1→3-glucan produced, for commercial purposes, from mutant *Agrobacterium* strains; (2) an alginate polysaccharide, a copolymer of 1→4-linked β-D-ManA (M) and α-L-GulA, commercially available as an M-rich alginic acid; (3) a marine-sourced bacterial exopolysaccharide, resembling GAG structure due to the presence, in its backbone, of aminosugars and uronic acids. Differently sulfated species, some of them showing well-defined and unprecedented sulfation patterns, were obtained both by direct regioselective sulfation/desulfation reactions and by multi-step procedures, also including the use of cycling protecting groups.

CHAPTER 1
INTRODUCTION

1
INTRODUCTION

1.1. Carbohydrates: an Overview

Carbohydrates (also called saccharides or glycans) are one of the four major class of biomolecules and they have been established to be the most abundant organic molecules in Nature.

The basic structural units of glycans are named monosaccharides, aldehyde or ketone derivatives of straight chain polyhydroxyalcohols containing at least three carbon atoms. There are numerous, different, types of monosaccharides, which vary in their number of carbon atoms and in the arrangement of the hydrogen and oxygen atoms attached to the carbons. Monosaccharides can be classified according to the stereochemical configuration of the asymmetric carbon atom farthest from the carbonyl group. Two different groups can be distinguished depending on whether the hydroxyl group (or other non-H group) on the last asymmetric carbon is on the right (D series) or on the left (L series) in the Fischer projection. Most naturally occurring sugars belong to the D series, with some exceptions such as fucose and iduronic acid that have been found in the L form. Free monosaccharides can exist in open-chain or cyclic forms, the latter characterized by a hemiacetal (or hemiketal) group formed by the reaction between one of the hydroxyl groups of the chain and the carbonyl function. For reasons of chemical stability, five- and six-membered rings are most commonly formed, and the corresponding compounds are labelled as furanose and pyranose, respectively. Furthermore, the formation of the cyclic structure creates an additional asymmetric carbon (commonly called anomeric carbon); therefore, two diastereoisomeric forms can exist for each cyclic sugar and these are

designated as α- and β-anomers whether the absolute configurations at the anomeric carbon and the furthest stereogenic centre are the same (α anomer) or different (β anomer) (Seeberger, **2015**). The furanose and pyranose rings puckers to form different conformations. (Rao et al., **1998**) As concerning the most common pyranose form, it has been largely demonstrated that the $^4C_1$ chair conformation ($^1C_4$ for L-sugars) is the most energetically preferred pyranose ring structure (Brown and Levy, **1965**). Some exceptions occur rarely, as in the case of L-iduronic acid in heparan and dermatan sulfate that assumes a skew-boat form to accommodate mechanical stress and conformational flexibility (Casu et al., **1988**; Marszalek et al., **1998**).

Except for their roles as sources of energy for living organisms, sugars seldom occur in nature as monosaccharides. Diverse structures can be created by simply linking different monosaccharides through acetal bonds, called glycosidic bonds, between the hydroxyl oxygen of one sugar moiety and the anomeric carbon of another one; the resulting glycans are called oligosaccharides (usually less than a dozen monosaccharides) or polysaccharides (usually more than a dozen monosaccharides). The huge diversity of these oligomeric and polymeric structures arises not only from the choice of sugars, but also from the way they are linked. Several linkage positions are possible since each sugar usually possesses more than one unmodified hydroxyl group to which the anomeric carbon of another moiety can bind: this allows the construction both of linear and branched products. In addition, each anomeric carbon is a stereogenic centre and therefore each glycosidic linkage can be constructed having either the α- or β-configuration.

Not surprisingly for such a diverse group of molecules, the biological roles of glycans are remarkably varied. First, carbohydrates possess structural and modulatory functions: polymerized glycans serve a major role in nutrient storage and sequestration (*e.g.* starch and cellulose in plants and glycogen in animals);

also, carbohydrates coat the surface of eukaryotic and prokaryotic cells, acting as a physical barrier; furthermore, some glycans are important for maintenance of tissue structure, porosity, and integrity; finally, saccharide chains, externally located on most glycoproteins, are involved in folding of the polypeptide core and can also provide a general shield from proteases (Moremen et al., **2012**; Varki, **2011**).

Carbohydrates are also involved in specific recognition mechanisms through the interaction with other molecules, most commonly intrinsic and extrinsic glycan-binding proteins (GBPs). Intrinsic GBPs recognize glycans from the same organism, thus mediating cell–cell and cell–matrix interactions; conversely, the extrinsic GBPs are responsible for the recognition of glycans from pathogenic or symbiotic organisms (Schnaar, **2016**; Varki and Gagneux, **2015**). Actually, microbial pathogens, that invade multicellular animals, sometimes decorate themselves with glycan structures that are identical or nearly identical to those on host cell surfaces and this state of "molecular mimicry" allow them to successfully evade host immune response (Van Breedam et al., **2014**).

Thanks to this wide spectrum of activities, carbohydrates find numerous applications in various fields. They have become increasingly important in modern biotechnology and pharmaceutical industry, being essential components of small-molecule drugs, vaccines and nutrients (Brown et al., **2007**; Hudak and Bertozzi, **2014**; Mettu et al., **2020**). Finally many natural and synthetic glycans are key components for nanotechnology, bioenergy, and material science (O'Neill et al., **2015**; Penadés et al., **2015**).

1.2. Polysaccharides

As touched upon in the previous paragraph, polysaccharides are polymeric carbohydrates, consisting of several monosaccharides joined by acetal, or much

more rarely ketal, glycosidic bonds. A polysaccharide structure is usually built on a core of repeating subunits, either mono- or oligosaccharide moieties. They are often classified as homopolysaccharides, if the repeating unit is composed of a single type of sugar monomers, and heteropolysaccharides if it is composed of different types of monomers.

There is a wide range of naturally occurring polysaccharides derived from plants, microorganisms, fungi, marine organisms, and animals possessing magnificent structural diversity and functional versatility. In Table 1.1, some of the most important polysaccharides are summarized according to chemical structures; these include glucans (**1–7**), fructans (**10**), aminodeoxy-glucans (**11**,**12**), and polysaccharides with uronic acid units (**13**,**14**).

Table 1.1. Structure of polysaccharides of different origin.

Polysaccharide Type		Source	Main mono- or oligosaccharide components
Cellulose	**1**	Plants	β-(1→4)-D-glucose
Curdlan	**2**	Bacteria	β-(1→3)-D-glucose
Dextran	**3**	Bacteria	α-(1→6)-D-glucose main chain
Pullulan	**4**	Fungi	α-(1→6) linked maltotriosyl units
Starch	**5**	Plants	
Amylose	**6**		α-(1→4)-D-glucose
Amylopectin	**7**		α-(1→4)- and α-(1→6)-D-glucose
Xylan	**8**	Plants	β-(1→4)-D-xylose main chain
Guar	**9**	Plants	β-(1→4)-D-mannose main chain, D-galactose branches
Inulin	**10**	Plants	β-(1→2)-fructofuranose
Chitin	**11**	Animals	β-(1→4)-D-(*N*-acetyl)glucosamine
Chitosan	**12**		β-(1→4)-D-glucosamine
Alginate	**13**	Algae	α-(1→4)-L-guluronic acid β-(1→4)-D-mannuronic acid
Pectin	**14**	Plants	α-(1→4)-D-galacturonic acid

Polysaccharides have been recognized and exploited by man for centuries. A large number of polysaccharides obtained from plants, animals and microorganisms have been developed into commercially important products

(Loth, **2012**). From the chemist's point of view, their unique structures combined with many promising properties like hydrophilicity, biocompatibility, biodegradability (at least in the original state), stereoregularity, multichirality, and polyfunctionality (*i.e.* reactive functional groups that can be modified by various chemical reactions), provide an additional and important argument for their study as a valuable and renewable resource (Heinze et al., **2006a**).

1.2.1. Sulfated Polysaccharides

An important and complex group of natural polysaccharides comprises the sulfated ones, which perform diverse role in biological systems acting as structural components of tissue to signalling agents in physiological processes (Gama et al., **2015**).

In Nature, sulfated polysaccharides are highly diverse, possessing variations in the carbohydrate backbone, location of the sulfate group(s), and degree of sulfation. They are extensively distributed in marine algae and in animals, both mammals and invertebrates.

Marine sulfated polysaccharides show a high structural diversity and the main groups are classified, according to the saccharide backbone composition, in galactans, ulvans and fucans (Jiao et al., **2011**). Galactans (agarans and carrageenans) are mainly found in red seaweed, they show a linear polysaccharide backbone composed almost exclusively of L- and/or D-galactose and 3,6-anhydro-D- or L-galactose units sulfated to various extents (Campo et al., **2009**; Knutsen et al., **1994**). Ulvans, commonly isolated from green algae, are usually constituted of 3-*O*-sulfated-L-rhamnose residues linked to an uronic acid, such as D-glucuronic or L-iduronic acid or, in minor extent, to xylose, either sulfated or not at its *O*-2 position (Lahaye and Robic, **2007**). Finally, fucans, found in brown seaweed, are characterized by highly heterogeneous structures, composed of variously sulfated L-fucose units (Pomin and Mourão,

2008). Some of these polysaccharides have been found in animals too: for example, sulfated fucans and galactans, with a more regular structure than their analogues from seaweeds, have been isolated from some marine invertebrates (Pomin, **2009**). Despite that, the most common sulfated polysaccharides in animal kingdom are GAGs, highly negatively charged heteropolysaccharides, which represent essential components of the ECM, playing crucial biological roles (see paragraph 1.2.2).

Sulfated polysaccharides display a huge number of different biological functions, participating in several physiological and patho-physiological processes, such as the coagulation cascade, viral transmission and antioxidation (Clausen et al., **2020**; Oliveira et al., **2016**). Other reported biological activities include: anti-tumor, anti-inflammatory, anti-atherosclerotic, anti-adhesive, anti-peptic, anti-ulcerogenic, anti-lipidemic, and lubricity (Campo et al., **2009**; Jiao et al., **2011**; Ngo and Kim, **2013**; Toida et al., **2003**). These activities arise from discreet polysaccharide-protein interactions (*e.g.* anticoagulation) as well as coordination and storage of water molecules (*e.g.* lubricity). Furthermore, they deeply depend on the carbohydrate backbone composition, molecular mass, and, importantly, the position of sulfate group(s) and amount or degree of sulfation (Mestechkina and Shcherbukhin, **2010**).

Given the interesting and diverse biological activities of this class of biomacromolecules, in the last decades significant research efforts have been devoted to the development of methods to obtain chemically sulfated polysaccharides and to study structure-property-activity relationships (see also paragraph 1.3.3).

1.2.2. Glycosaminoglycans and Proteoglycans

GAGs are a family of complex polysaccharides ubiquitously distributed in the animal kingdom, where they play crucial roles in a plethora of biological events.

GAGs are present on the cell surface, inside the cell, and in the ECM usually conjugated to proteins. The resulting structures are called proteoglycans (PGs) and are generally constituted of a core protein and one or more GAG chains, covalently attached through their reducing ends to the side chains of serine —or more rarely threonine or asparagine— residues in the protein (Lindahl et al., **2015**). PGs are involved both in ECM structure, by governing its assembly and its physical properties, and in regulating signalling pathways by interacting with other ECM components, directing tissue growth and development, cell proliferation, adhesion, and motility. As a consequence, PGs possess key roles in several physiological and pathological processes, such as angiogenesis, cancer, immunity, and infectious diseases (Iozzo and Karamanos, **2010**). Interestingly, it has been very recently reported the role of GAGs in SARS-CoV-2 infection: cell surface HS has been established as an assisting factor for ACE2-mediated cell entry of SARS-Cov and CoV-2 (Clausen et al., **2020**; Zhang et al., **2020**).

GAGs have been also found as bacterial cell wall components in some pathogenic microorganisms; the surface exposed GAGs are expected to serve as a virulence factor and their resemblance with the host glycans results in very limited or no response of the hosts' immune system (Raedts et al., **2011**).

From a structural point of view, GAGs are highly negatively charged heteropolysaccharides, consisting of a linear sequence of disaccharide repeating units, each composing of an amino sugar (glucosamine or galactosamine) and a hexose (galactose) or an uronic (D-glucuronic or L-iduronic) acid. The saccharide backbone can be decorated with acetyl groups on the nitrogen atoms of the aminosugars, and sulfate groups on aminosugar nitrogen atoms and/or on the hydroxyl oxygen atoms of both aminosugar and uronic acid moieties.

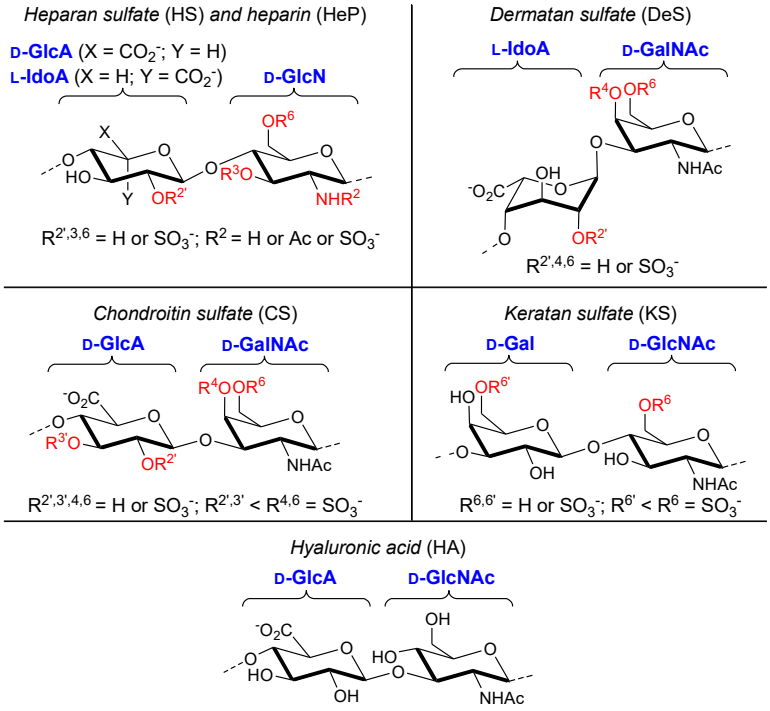

Figure 1.1. Repeating unit structures of GAGs.

GAGs can be distinguished into six main different types: HA, CS, DeS, KS, HeP, and HS (Figure 1.1). Except for HA, the only GAG that is non-sulfated and non-covalently linked to a protein core, the other GAG polysaccharides are extensively and variously decorated with sulfate groups. Theoretically, they can be distributed along the polymeric chain in a particularly high number of diverse combinations. This creates an enormous structural diversity and potential variation in biological activity. Nevertheless, sulfate group distribution, also referred as sulfation pattern, seems to be strictly regulated in *vivo*, is tissue- and age-specific, and also depends on the physiological or pathological state of the organism (Bedini et al., **2019**). It has been even suggested that the sulfation pattern sequence might be able to encode specific functional information; although this "GAG sulfation code" is still poorly understood, some details on its function in controlling blood clotting, guiding neuronal growth, and

controlling adhesion of pathogens, have been elucidated (Gama et al., **2006**; Martín et al., **2013**; Rogers et al., **2011**; Swarup et al., **2013**; Zhao et al., **2020**).

1.3. Synthetic Carbohydrate Chemistry and Polysaccharide Modifications

Though abundant in nature, glycans produced in biological systems are frequently heterogeneous; besides, the quantities that can be obtained from biological sources are often small. So, chemical synthesis can be a useful tool to the access to homogeneous structures in quantities larger than those available from natural sources.

Although carbohydrate chemistry has been largely explored in the last decades, the major attention has been focused on modification of mono- and short oligosaccharide derivatives, whereas the research of reactions for the manipulation of polysaccharide structures is still rather limited to few cases. This gap is due to some limitations linked to polysaccharide chemistry. First, most polysaccharide are generally poorly soluble in common organic solvents. To reach homogeneous reaction conditions, high boiling, polar solvents, such as formamide, DMF, DMSO and water, are often required (Table 1.2). Furthermore, new solvent systems have been developed and investigated; for example, multi-components solvents, consisting of a mixture of a polar aprotic solvent and a chaotropic salt (e.g. DMF/LiCl, DMAc/LiCl, or DMSO/TBAF), or ionic liquids have been proved to be particularly efficient in certain cases (Heinze et al., **2006b**; Silva et al., **2017**; Zhu et al., **2006**).

Further drawbacks concerning polysaccharide synthetic chemistry are related to the difficulties in achieving derivatization of the selected hydroxyl position(s) in each subunit of the polymeric chain, and at the same time the necessity to avoid harsh reaction conditions that might break the polymeric structure by cleaving

glycosidic linkages. Finally, any polysaccharide structure usually requires a difficult and long work for a complete characterization. In certain cases, these limitations have been overtaken by exploiting suitably developed protection/deprotection reaction sequences, together with advanced 2D-NMR and mass spectrometry techniques (Bedini et al., **2011**; Laezza et al., **2016**; Xu et al., **2012**; Zong et al., **2016**; Zou and Khor, **2009**).

1.3.1. Protecting Groups in Carbohydrate Chemistry

Carbohydrate synthesis is commonly characterized by the manipulation of various protecting groups, which mask reactive functionalities (hydroxyl, amino or carboxyl groups) on the saccharide skeleton and prevent them from reacting with other chemical reagents. Protecting groups are selectively added and removed from glycan structures, allowing for chemical alteration of the exposed functionalities. The choice of protecting groups and the order of their installation are essential for a synthetic route to be successful.

The protecting groups used in carbohydrate chemistry are the same as in the other areas of organic synthesis. Their insertion and removal, as well as their stability and orthogonality, often recall the reaction conditions already developed for non-carbohydrate molecules. In addition, several protecting groups developed *ad hoc* for sugar species have been reported (Wuts, **2014a**). The main difference in carbohydrate chemistry is the vast number of protecting groups needed and the continuous research for regioselective protections (Ghosh and Kulkarni, **2020**). Besides, protecting groups on saccharide structures can affect some chemical features of the molecule, enhancing or decreasing its reactivity, and they can participate in the reactions, influencing the regiochemical and/or stereochemical outcomes.

The most important protecting groups in carbohydrate chemistry are obviously the hydroxyl protecting groups. Amino- and carboxy- protecting groups for the

manipulation of structures containing aminosugars and uronic acid, respectively, are also of interest.

1.3.1.1. Hydroxyl Protecting Groups

Hydroxyl groups are the most present moieties in glycan structures and many chemical transformations involve their protection. In addition, it is often required to distinguish between two or more hydroxyl groups on the same structures, so the research for regioselective protection is continuously in progress. The distinction could be achieved considering the different nucleophilicity of the four hydroxyl types (hemiacetal, primary, secondary equatorial, secondary axial) on a carbohydrate structure. Their reactivity is tied to both steric and electronic effects and a general scale follows the order of primary OH > hemiacetal OH > equatorial OH > axial OH (Figure 1.2). Besides, in oligomeric structures, such as polysaccharides, a pronounced reactivity is observed for the OH group adjacent to the glycosidic linkage, due to electronic reasons. For example, for (1→4)- and (1→3)- linked polysaccharides. *e.g.* curdlan, starch and cellulose, the rate of esterification is usually in the order of OH–6 > OH–2 > OH–3(4) (Heinze et al., **2006c**). However, these scales of reactivity are rarely so clear, and consequently the differentiation of secondary hydroxyls based on their nucleophilicity is often difficult.

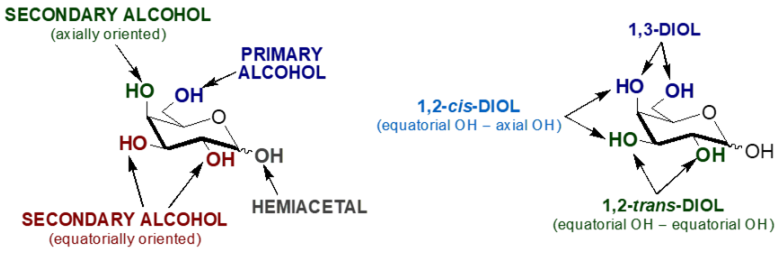

Figure 1.2. Different hydroxyl groups (left) and diols (right) on a *galacto*-configured monosaccharide.

Another alternative approach for regioselective protection of hydroxyls considers them not as single functionalities to be protected separately, but as couples, namely diols, that can be protected together with a cyclic group. On a simple monosaccharide structure (see Figure 1.3), only 1,2- and 1,3-diols are relevant for synthetic purposes, whereas the concomitant protection of OH groups at higher distances (for example 1,4-diols) is prevented because of the consequent formation of instable cycles. Among all the possible 1,3-diols, only positions 4 and 6 can be protected together with the same groups, generating sufficiently not-tensed cycles. The 1,2-diols involve positions 2 and 3 or positions 3 and 4 and, according to their stereochemistry, they can be distinguished in *trans* (*e.g.* two axial OHs or two equatorial OHs) and *cis* (*e.g.* an equatorial and an axial OH). Several kinds of protecting groups for diols in carbohydrates have been designed and developed and it is often possible to discriminate among the different diols with an accurate choice of the protecting groups.

The three macro-categories (ether, ester and acetal/ketal) of hydroxyl protecting groups will be discussed in the following paragraphs with a particular attention on their application for polysaccharide modifications.

Ethers

Ethers are among the most used protective groups in carbohydrate synthesis. They vary from the simplest, most stable methyl ether to the more elaborate, substituted, trityl or silyl ethers (Figure 1.3). They are formed and removed under a wide variety of conditions, which have been applied not only in the synthesis of oligosaccharides and glycoconjugates, but also for polysaccharide structural modifications.

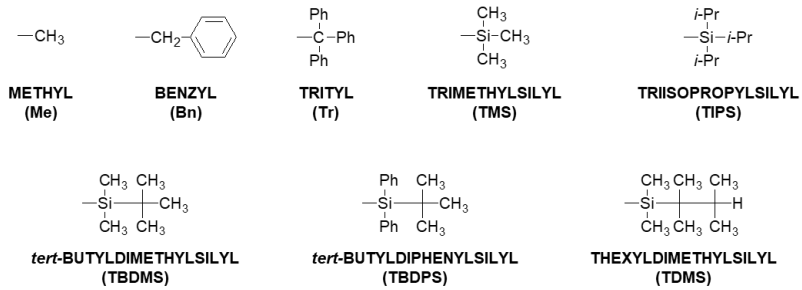

Figure 1.3. Commonly used ether protecting groups.

Simple alkyl groups can be introduced readily by alkylation. In the field of polysaccharide chemistry, their insertion have been extensively employed for the derivatization of unmodified cellulose in the presence of a suitable alkyl halides under basic conditions and in different solvent systems (*e.g.* DMI/LiCl, DMAc/LiCl, or SO_2/DEA/DMSO) yielding 2,3,6-tri-*O*-alkylated cellulose derivatives (Isogai et al., **1986**; McCormick and Callais, **1987**; Petruš et al., **1995**; Takaragi et al., **1999**).

Benzyl ether groups are among the widest employed permanent protections in glycan synthesis, thanks to their well-known stability together with a variety of selective cleavage reactions. They are usually introduced by a classic Williamson reaction, employing a benzyl halide and a strong base (*e.g.* NaH) in an aprotic polar solvent, though non-basic conditions —in the presence of benzyl trichloroacetimidate and an acid catalyst (usually TfOH)— have been developed too (Wessel et al., **1985**). Benzyl groups have been also employed for polysaccharide derivatization as reported for benzylation of chitin to give, depending on the reaction conditions, a perbenzylated or selectively *O*-6 protected polysaccharide (Somorin et al., **1979**; Umemura et al., **2012**). Benzyl groups are usually cleaved under catalytic hydrogenolysis conditions or by electron-transfer reduction using sodium in liquid ammonia (Iserloh et al., **2002**). Alternatively, they can be selectively removed under mild oxidative conditions

(Adinolfi et al., **1999**), which have been applied also on structurally modified polysaccharide derivatives (Laezza et al., **2015**).

Triphenylmethyl (trityl) and hindered organosilyl ethers are among the most effective protecting groups for the obtainment of regioselectively modified saccharide derivatives. Because of their steric demands, they can be easily introduced exclusively on primary hydroxyl positions; this property has been extensively exploited for polysaccharide modification.

Tritylation reactions in the presence of triphenylchloromethane (trityl chloride) have been reported to occur regioselectively towards *O*-6 position on several polysaccharides, such as cellulose (Hall and Horne, **1973**; Heinze et al., **1994**), chitin and chitosan (Nishimura et al., **1991**; Umemura et al., **2012**), curdlan (Chien and Iwata, **2018**), and even chondroitin (Zoppetti and Oreste, **2004**). The trityl group can be quantitatively removed using mild aqueous acid conditions. Furthermore, the employment of methoxy-substituted trityl moieties has resulted to be more efficient for protection of polysaccharides, increasing both the rate of conversion and the rate of deprotection step (Camacho Gömez et al., **1996**).

Silyl groups are typically introduced by reaction with the corresponding silyl chloride under less basic conditions (*e.g.* pyridine or imidazole) than alkyl ether insertion. These groups have been largely employed for polysaccharide derivatization, especially to convert alcohol moieties into more hydrophobic and, often, more reactive groups as reported for the synthesis of various cellulose derivatives (Baumann et al., **2000**; Cooper et al., **1981**; Richter and Klemm, **2003**; Schultz and Lüning, **2002**). Furthermore, TDMS group has reported to be selectively inserted on cellulose either at *O*-6 or both at *O*-2 and *O*-6, in dependence on the employed reaction conditions (Koschella et al., **2001**; Koschella and Klemm, **1997**; Petzold et al., **2003**). One of the properties that has made these groups so popular is the possibility to be easily and highly selectively cleaved by fluoride ion, thanks to its high affinity for silicon.

Esters

Ester protecting groups are often a useful and complementary alternative to ethereal protection. Some of the most common ester moieties are depicted in Figure 1.4.

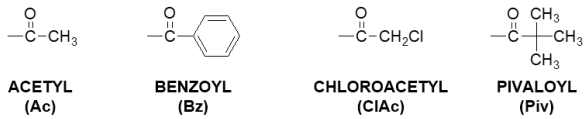

Figure 1.4. Commonly used ester protecting groups.

Standard conditions for esterification require the employment of the acyl chloride or the anhydride in pyridine or other tertiary amines, often with DMAP as a catalyst. In addition, the acetylation can be performed also in acid conditions using *in situ* generated HI for the activation of the acetic anhydride (Ravindranathan Kartha and Field, **1997**).

Interestingly, ester groups (especially acetates) tend to migrate both in acidic and basic conditions (Ekholm and Leino, **2018**). For instance, in *cis*-hydroxyls there is normally a preferred migration from the axial position to the equatorial one and in 4,6-diols the migration goes from *O*-4 to *O*-6 preferentially.

The normal ester-cleaving methods can be used for carbohydrate esters too, but because of solubility characteristics, alcoholic rather than aqueous solvents are commonly used as far as mono- and (short) oligosaccharides are concerned. Probably the most useful method for ester removal is the Zemplén procedure, consisting of a base-catalysed transesterification in anhydrous methanol with a trace amount of sodium methoxide (Pétursson, **1997**).

Esterification of polysaccharides has been a reliable and useful modification strategy, providing an easy access to a broad variety of bio-based materials with valuable properties. Ester protected polysaccharides have been prepared from starch (Grote and Heinze, **2005**) and cellulose (McCormick and Callais, **1987**) under basic conditions, obtaining in both cases an almost quantitative degree of

substitution; alginates have been also tested for hydroxyl protection by esterification (Pawar and Edgar, **2011**). Though polysaccharide esterification has been known for over a century, it remains very challenging to control the position of acylation on the glycan chain. Regioselective esterification at primary positions of polysaccharide structures has been investigated mainly on cellulose, displaying however a lower degree of substitution than ether protection (Fox et al., **2011**). An alternative and efficient approach for cellulose-6-*O*-esters is based on TBAF-catalysed regioselective deacylation at the secondary *O*-2 and *O*-3 positions of fully substituted cellulose esters (Xu and Edgar, **2012**). This method has also been tested on other glycan esters (amylose, curdlan, dextran, pullulan and glucomannan) observing a remarkably regioselective *O*-2/3 deacylation only with amylose triesters (Zhang et al., **2014**).

Cyclic Protecting Groups for Diols

As mentioned above, the simultaneous protection of two hydroxyl groups is a key issue in carbohydrate chemistry. This is often faced by the employment of cyclic protecting groups (Figure 1.5), among which the acetal benzylidene and the ketal isopropylidene are the oldest and still the most widely used ones.

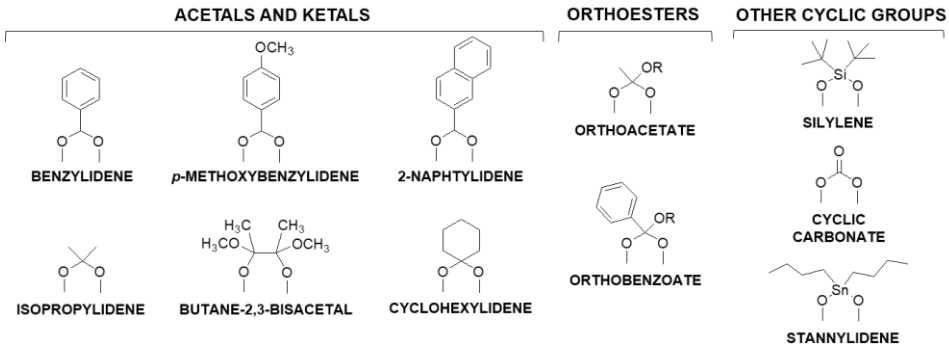

Figure 1.5. Common cyclic protecting groups for diols.

The standard conditions for the introduction of acetal/ketal moieties require the presence of the corresponding aldehyde/ketone or a suitable acetal/ketal reagent

with an acid catalyst. Under proper conditions, these groups have been installed also on polysaccharide structures; examples in this field have been reported for dextran (Cui et al., **2012**) and chondroitin (Bedini et al., **2011**).

The usefulness of these protecting groups lies in the possibility of tuning the regioselectivity of protection towards different diols by a careful choice of the protecting group. So, for example, benzylidene acetals are formed preferentially as six-membered dioxane cycles, reacting with 1,3-diols and forming 4,6-*O*-benzylidene derivatives; on the contrary, isopropylidene ketals are more stable as five-membered dioxolane rings, formed by reaction on 1,2-*cis*-diols.

The removal of acetal/ketal groups is usually performed under acid hydrolysis affording the free diol, though, especially in the case of the benzylidene group, several other methods for the regioselective opening have been developed (Ohlin et al., **2011**). These approaches rely on the employment of reductive conditions with a combination of a hydride reagent and a Lewis (or a proton) acid. By carefully choosing the reagent system combination, 6-*O*-benzyl or 4-*O*-benzyl ethers can be selectively prepared over the corresponding regioisomer from 4,6-*O*-benzylidene-hexopyranoside (Daragics and Fügedi, **2009**; Debenham and Toone, **2000**; Sakagami and Hamana, **2000**; Shie et al., **2005**; Tanaka et al., **2008**; Tani et al., **2007**; Wang et al., **2002**; Zinin et al., **2007**). All the reductive methods, however, suffer for a high sensitivity towards the employed reaction conditions (*e.g* solvent, temperature, reagent concentration) and the structure of the substrate, with sometimes a dramatic influence on regioselectivity and yields. Finally, benzylidene acetals can be also cleaved under oxidative conditions, using sodium bromate/sodium dithionite in a biphasic mixture (Adinolfi et al., **1999**). Interestingly, it has been reported that the cleavage of six-membered 4,6-*O*-benzylidine cycles occurs in a non-regioselective way giving a mixture of 6-*O*- and 4-*O*-benzoyl regioisomers, whereas on five-membered benzylidene cycles the cleavage occur with a high regioselectivity towards a

single isomer. Furthermore, these conditions have been revealed sufficiently mild and efficient to be applied also on some polysaccharide structures (Bedini et al., **2011**; Laezza et al., **2016**), contrary to reductive opening where no example of application on any polysaccharides has been reported so far.

1.3.1.2. Amino Protecting Groups

Amino functional groups are very common among glycan structures and a great variety of glycoconjugates and biologically relevant oligosaccharides are comprised of 2-amino-2-deoxysugars. Considerably, the second most abundant polysaccharide after cellulose, chitin, is a linear polymer mainly composed of β-(1→4)-linked D-GlcNAc, which constitutes a major components of the exoskeletons of crustaceans, insects, and the cell walls of fungi (Elieh-Ali-Komi and Hamblin, **2016**). Chitin, together with its deacetylated derivative, chitosan, has been largely employed in synthetic strategies for its chemical transformation, including *N*-selective modifications, aimed to the obtainment of novel materials with enhanced solubility in aqueous media, with respect to the starting product, and new bioactivity properties (Carvalho et al., **2016**).

In glycan synthesis, amino functionalities are often temporarily converted into an electron-withdrawing amide, carbamate or imide in order to decrease the reactivity of the amino group (Figure 1.6). It is worth noting that the amine protecting group for *C*-2 of aminosugars can directly influence the stereochemical outcome of a glycosylation reaction, when employing the aminosugar as donor (for a detailed discussion see paragraph 1.3.2).

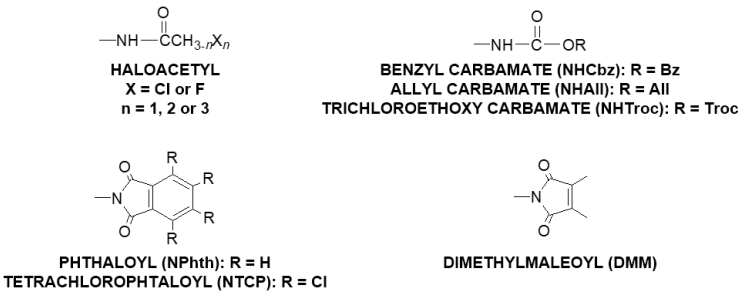

Figure 1.6. Commonly employed amino protecting groups.

Among amide-type protecting groups, acetyl ones are usually discarded, though many naturally occurring aminosugars are *N*-acetylated. This is due to the high nucleophilicity of the lone pair electrons on nitrogen atom of the acetamido group, which can attract electrophilic species, eventually involved in a reaction, often resulting in a decreased reactivity and/or additional by-products. Additionally, *N*-acetylated sugars show a very low reactivity in glycosylation reactions, above all when employed as glycosyl donors since they often form a relatively unreactive oxazoline intermediate which remains as a major by-product (Banoub et al., **1992**; Bongat and Demchenko, **2007**). Conversely, 2-haloacetamido-2-deoxyglycopyranosyl derivatives have been extensively used and they proved to be excellent donors in glycosylation reaction (Blatter et al., **1994**; Bongat and Demchenko, **2007**). Haloacetyl groups, including chloroacetyl, di-/trichloroacetyl, and trifluoroacetyl, are generally introduced by reaction with the corresponding acyl chloride or anhydride and can be hydrolysed by heating in strongly acidic or basic solutions (Wuts, **2014b**).

Carbamate groups, including benzyl carbamate (NHCbz), allyl carbamate (NHAlloc), and trichloroethyl carbamate (NHTroc), are also very common for amine protection thanks to their ease of formation and the orthogonality or chemoselectivity of *N*-deprotection (Banoub et al., **1992**). Protection is usually accomplished by condensation of the free amine and the appropriate chloroformate in the presence of a mild base (Boullanger et al., **1990**).

Conditions for removal, however, depend on the protecting group, for example catalytic hydrogenolysis for NHCbz cleavage, Pd-catalyzed isomerization for NHAlloc removal, and acidic hydrolysis or reduction with Zn for NHTroc cleavage (Wuts, **2014b**). Other carbamates, for example, *N*-methoxycarbonyl (Adamski-Werner et al., **2004**; Liu et al., **2002**; Nishiyama et al., **2004**), *N*-(*tert*-butyl)oxycarbonyl (Boullanger et al., **1990**) and *N*-(*p*-nitrobenzyl)oxycarbonyl (Liao et al., **2000**) have been used in oligosaccharide synthesis.

Alternatively, amino function can be blocked with bivalent cyclic groups, among which the phtalimido group is the first to be developed and still widely employed (Bongat and Demchenko, **2007**). Preparation of 2-deoxy-2-phthalimido glycopyranosyl derivatives is usually accomplished by treatment of the corresponding 2-amino-2-deoxy sugar precursor with phthalic anhydride in the presence of a base. Deprotection of the phthaloyl group can be achieved under strongly basic conditions (hydrazine, hydroxylamine or alkyldiamine) at high temperature; this constitutes the biggest drawbacks for the employment of this protecting group in target synthesis, especially when base-sensitive groups exist. To overcome this limitation, other phtaloyl-based protecting groups, such as tetrachlorophtalimides (TCP) (Debenham et al., **1996**) and dimethylmaleoides (DMM) (Aly et al., **1998**) were developed: they can be installed under similar conditions as phthaloyl group but require less demanding basic conditions for their removal.

Bivalent cyclic groups are widely used also in polysaccharide chemistry for chitosan selective *N*-modifications. *N*-Phthaloylation of chitosan is used to attain chito-derivatives with improved solubility in organic solvents while possessing a chromophore that allows easy monitoring of subsequent modifications. Phthaloyl group can be quantitatively inserted on chitosan by using phthalic anhydride in DMF/water mixture, avoiding a concomitant *O*-6 phthaloylation (Kurita et al., **2007**); alternatively, *N*-phthaloylation of chitosan was achieved

with phthalic anhydride by reaction in an aqueous acetic acid solution (Ifuku et al., **2011**). A similar procedure was also applied for the preparation of *N*-(4-bromophthaloyl) chitosan, which has an higher solubility in common solvents compared to phthaloylated chitosan (Ifuku et al., **2012**).

Finally, the amine functionality can be masked as an azido group, which is particularly useful when a non-participating group at *C*-2 is required in glycosylation step. The azido group can be introduced through a diazo-transfer reaction using triflyl azide (Titz et al., **2006**; Yan et al., **2005**) or imidazole-1-sulfonyl azide hydrochloride (Goddard-Borger and Stick, **2007**) and is converted into the free amine under hydrogenolysis conditions. 2-Azidation has revealed particularly useful also in chitosan chemistry since 2-azido chito-derivatives are functional precursor for click chemistry transformations (Kulbokaite et al., **2009**). The transformation of the amine group on chitosan into an azide moiety can be performed by using sodium azide or by diazo transfer analogously to monosaccharide case (Kulbokaite et al., **2009**; Zhang et al., **2008**).

1.3.1.3. Carboxyl Protecting Groups

Some natural occurring glycans present uronic acid residues, so their synthesis or chemical manipulation can require the employment of suitable protecting groups for the carboxylic moieties.

The most common way to mask a carboxylic function is, also in carbohydrate chemistry, by formation of esters. The carboxyl group can react as an electrophile, being activated under strongly acid conditions, then the reaction with a suitable alcohol gives the ester. This method could be not particularly appropriate for polysaccharide chemistry, since the acidic conditions can cause an undesirable cleavage of the glycosidic chain, although this inconvenient has been overcome with proper expedients in the esterification reaction of certain polysaccharide substrates (Laezza et al., **2015**). Alternatively, the carboxylic

acid reacts as a nucleophile and it is transformed in a carboxylate ion, which is alkylated by the desired alkylating agent. Also this approach has been employed for esterification of uronic acids in polysaccharides, as reported for alginates (Pawar and Edgar, **2013**; Pelletier et al., **2000**) and pectins (Pappas et al., **2004**).

1.3.2. Glycosidic Bond Formation

Arguably, the most important reaction in the field of glycochemistry is the glycosylation reaction, which allows the formation of inter-glycosidic bond. This is a key step for the obtainment of oligo- or polymeric structures from shorter saccharide moieties, glycoconjugates and glycosides. Moreover, glycosylation reaction could be also a useful tool for the introduction of saccharide branches on linear polysaccharides, with the obtainment of new, potentially bioactive molecules. Examples in this field are reported for chitin and chitosan (Kurita et al., **2003**, **1998**), for chitin-cellulose hybrids (Ishimaru et al., **2014**) and for curdlan, where the introduction of aminosugars moieties gave new immunomodulating and anti-tumour properties (Kurita et al., **2011**).
Glycosidic bond formation is generally achieved by condensing a fully protected glycosyl donor, bearing a potential leaving group (LG) at its anomeric centre, with a suitably protected glycosyl acceptor, a sugar residue possessing often only one free hydroxyl group (Scheme 1.1).

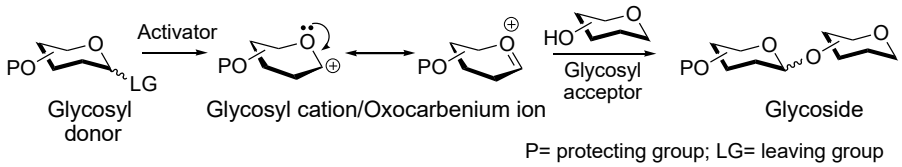

Scheme 1.1. Basic glycosylation reaction mechanism.

Commonly, a glycosylation reaction can be considered as a nucleophilic substitution, where the glycosyl acceptor acts as the nucleophile replacing the

leaving group on the electrophilic position, namely the anomeric carbon, of the glycosyl donor. In most cases, an activator, added in catalytic or stoichiometric amounts, assists the departure of the anomeric leaving group. This results in the formation of a glycosyl cation, which is stabilized by resonance from the endocyclic oxygen to give an oxocarbenium ion. Since there is a planar geometry around the anomeric carbon of both resonance contributors, the nucleophilic attack could occur from either the top (leading to a β-linkage for the D series) or the bottom (leading to a α-linkage for the D series) face of the ring. Various factors such as temperature, protecting groups, conformation, solvent, promoter, steric hindrance or leaving groups may influence the glycosylation outcome (Das and Mukhopadhyay, **2016**; Zhu and Schmidt, **2009**).

In addition to the apparent complexity of the glycosylation process, other competing reactions (elimination, substitution, cyclization, migration) can compromise the yields of the glycosylation products. A common example is the hydrolysis at the anomeric centre of the glycosyl donor with the consequent formation of the corresponding hemiacetal; this can be prevented by addition of proper desiccants (*e.g.* zeolites in the form of molecular sieves), which act as water molecules scavengers.

1.3.2.1. Stereoselectivity of Glycosylation

One of the most challenging aspects in the glycosidic bond formation is the stereocontrol of the newly formed linkage. Two stereochemical outcomes are possible and, according to the orientation of the substituent at the neighbouring *C*-2 atom, the glycosidic bonds can be classified as 1,2-*trans* or 1,2-*cis* (Figure 1.7).

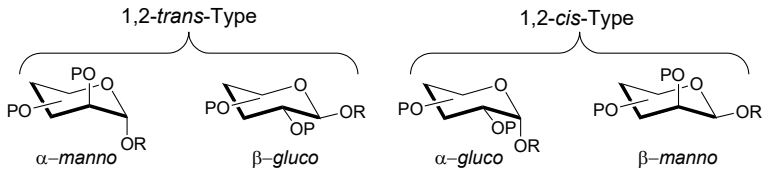

Figure 1.7. Four different stereochemical types of glycosidic bonds.

In general, the anomeric effect favours α-glycoside formation (1,2-*cis*- for D-*gluco* series, 1,2-*trans* for D-*manno* series). However, the role of the anomeric effect is not so determining, and other factors often come to the fore.

The most powerful impact on the stereoselectivity is produced from a neighbouring group at *C*-2. A 1,2-*trans* glycosidic linkage can be stereoselectively formed with the use of anchimeric assistance of a neighbouring participating group, such as an acyl moiety (*e.g. O*-acetyl or *O*-benzoyl). In these cases, the reaction proceeds primarily *via* a bicyclic intermediate, the dioxolenium ion (Scheme 1.2), resulted from an intramolecular stabilization of the glycosyl cation. Hence, the attack of an external nucleophile can only occur from the top face of the ring, therefore allowing stereoselective formation of a 1,2-*trans* glycoside (pathway *a*, Scheme 1.2). A drawback in the use of a participating protecting group is the possible competing formation of an orthoester from the dioxolenium ion (pathway *b* Scheme 1.2).

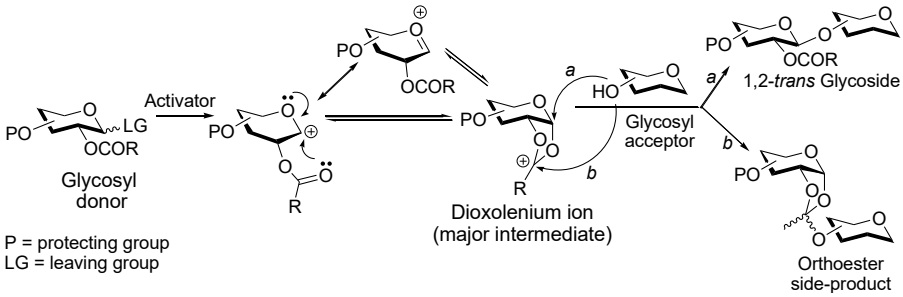

Scheme 1.2. General mechanism of neighbouring group participation in glycosylation reactions.

Another important factor for the stereoselectivity control is the choice of the reaction solvent. The so-called participating solvents, such as acetonitrile and diethyl ether, are the typical cases for the preferential formation of β-D- and α-D-glucosides, respectively. If the reaction is performed in acetonitrile, the nitrilium cation formed *in situ* exclusively adopts the kinetically controlled axial orientation, allowing stereoselective formation of equatorially substituted glycosides (Scheme 1.3, pathway *b*). This approach revealed to be a useful way for the obtainment of 1,2-*trans* glucosides with good stereoselectivity even with glycosyl donors bearing a non-participating substituent. Ether-type solvents, such as diethyl ether, THF or dioxane, can also participate in the glycosylation process, but, differently from nitrile solvents, an equatorially oriented intermediate is preferentially formed, leading to the axial glycosidic bond formation (Scheme 1.3, pathway *a*). More recently, also DMF, employed as reaction additive or co-solvent, has been reported to promote the formation of 1,2-*cis* α-glycosidic bonds (Lu et al., **2011**).

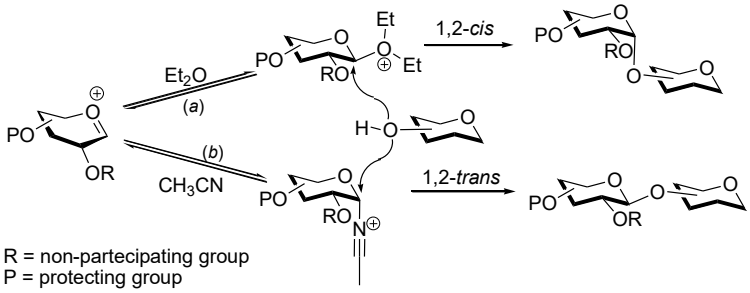

Scheme 1.3. Solvent effect in glycosylation reaction (a: nitrile-type solvent; b: ether-type solvent).

Whereas the neighbouring-group participation is sufficient to warrant stereoselective 1,2-*trans* glycosylation, the synthesis of 1,2-*cis* glycosides with a comparable high stereoselectivity is still challenging. As mentioned above, the selection of a proper solvent could help to reach a good stereoselectivity. Other

strategies for 1,2-*cis*-stereoselective glycosylation have been reported, *e.g.*, intramolecular aglycon delivery (IAD) (Ishiwata et al., **2010**), conformationally restrained methods (Crich, **2011**; Elferink et al., **2016**; Hashimoto et al., **2016**; Manabe et al., **2006**), six-membered ring neighbouring group participation (Kim et al., **2005b**, **2005a**), hydrogen-bond-mediated aglycon delivery (HAD) (Yasomanee and Demchenko, **2012**), and remote participation (Hahm et al., **2016**; Li et al., **2011**).

1.3.2.2. Glycosyl Donors and Activation Conditions

Glycosyl donors are usually classified according to the kind of leaving group place at the anomeric positions. Both their number and activation conditions are continuously in progress. Here the most common and used glycosyl donors will be discussed only: glycosyl halides, thioglycosides, trichloro- and *N*-phenyltrifluoroacetimidates, whose structures are depicted in Figure 1.8.

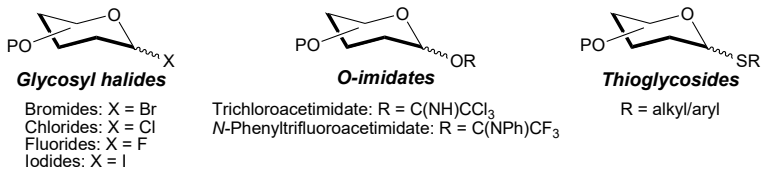

Figure 1.8. Structure of most common glycosyl donors.

The first glycosyl donors to be described were glycosyl bromides and chlorides. The original procedure for their employment is credited to Knoenigs and Knorr and required Ag_2CO_3, which primarily acted as an acid scavenger (Igarashi, **1977**). A wide variety of heavy metal promoter have been developed over the years, such as other silver(II) compounds (Garegg et al., **1982**; Wulff and Röhle, **1974**) or mercury(II) salts (Schroeder and Green, **1966**). Besides, Lewis acids, such as $SnCl_4$, $BF_3{\cdot}OEt_2$ or $ZnCl_2$, have been also employed as promoters (Higashi et al., **1990**; Ogawa and Matsui, **1976**).

Among the other halides, glycosyl fluoride and iodides were not considered as glycosyl donors for a long time, being the former unreactive under the Knoenigs-Knorr conditions, and the latter too unstable to be synthetically useful. Glycosyl fluorides were introduced as donors in the early 80s when Mukaiyama and co-workers demonstrated that these compounds could be activated with $AgClO_4/SnCl_2$ (Mukaiyama et al., **1981**). Several other methods for their activation have been reported since then, with the commonly used systems being $BF_3{\cdot}OEt_2$ (Kunz and Sager, **1985**; Nicolaou et al., **1984**), $Cp_2MCl_2–AgClO_4$ (M=Hf, Zr) (Matsumoto et al., **1988**; Suzuki et al., **1989**), and $Cp_2HfCl_2–AgOTf$ (Nicolaou et al., **1992**). As regards glycosyl iodides, only in the early 2000's it was shown that they could offer some advantages respect to glycosyl bromides and chlorides in terms of time, efficiency and selectivity (Adinolfi et al., **2003b**; Miquel et al., **2004**; van Well et al., **2005**).

O-Imidate glycosyl donors —in particular, trichloroacetimidates (Schmidt and Michel, **1980**) and *N*-phenyltrifluoroacetimidates (Yu and Tao, **2001**)— are probably the most common glycosyl donors used in glycosylation reactions. This can be attributed to the employment of a catalytic amount of promoter for their activation, contrary to most glycosyl donors, including glycosyl halides. Typically, TMSOTf (Schmidt and Grundler, **1982**) and $BF_3{\cdot}OEt_2$ (Schmidt and Michel, **1980**) are involved in the activation of both kinds of donors. In addition to that, several other promoters have been developed, including protic and Lewis acids (Fügedi, **1987**; Urban et al., **1990**), metal triflates (Adinolfi et al., **2006**, **2001**, **2000**; Castro-Palomino and Schmidt, **1995**; Yamada and Hayashi, **2002**), acid molecular sieves (Adinolfi et al., **2003a**), and combined systems, such as I_2/Et_3SiH (Adinolfi et al., **2002**). Although glycosyl *N*-phenyltrifluoroacetimidates can be activated in the same ways as trichloroacetimidates, they often require stronger conditions to react; however,

their relatively higher stability and the less amount of by-products than the latter could be ascribed to their great diffusion.

Thioglycosyl donors are also very common in carbohydrate chemistry; an unquestionable advantage in their use is the stability of the thio-alkyl(aryl) group on the anomeric position under a wide range of reaction conditions, thus acting itself as a temporary protecting group. Nevertheless, they can be activate using mild thiophilic reagents, usually soft electrophiles; this leads to a sulfonium ion, which is a better leaving group than the thio-alkyl(aryl) moiety and the oxonium ion is rapidly formed (Scheme 1.4).

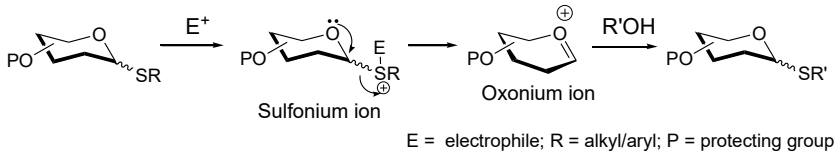

Scheme 1.4. Activation of thioglycosides.

The standard activation method for this kind of donors involves the employment of *N*-iodosuccinimide with a catalytic amount of TfOH, to generate *in situ* the electrophilic iodonium ions (Veeneman et al., **1990**). Other Lewis acid have been also employed as catalysts and many variants have been developed (Codée et al., **2003**; Konradsson et al., **1990**). Even though the versatility of thioglycosides is very well documented, their employment poses some drawbacks, among which the possibility of side-products, due to the stoichiometric amounts of electrophile-source reagent, is the most relevant.

1.3.3. Sulfation Decoration of Polysaccharides

Given the interesting and diverse biological activities of sulfated polysaccharides (see also Paragraph 1.2.1), significant research efforts have been focused on their obtainment through chemical or chemoenzymatic methods.

The synthesis of sulfated polysaccharides *via* the stepwise addition of sugars is extremely challenging due to the large number of stereocenters, the presence of similar functional groups, and the need to preserve the orientation of the glycosidic linkages. Therefore, from a chemical synthesis perspective, polymeric sulfated structures can be obtained by sulfating either natural polysaccharides or their polymeric analogues.

Sulfation is usually performed under non regioselective conditions, thus affording derivatives showing sulfate groups randomly distributed on the polysaccharide backbone. A wide variety of sulfating agents have been developed and used to this aim (Figure 1.9). Traditionally, sulfation of polysaccharides was accomplished using sulfuric acid or chlorosulfuric acid to generate an active sulfur trioxide reagent (Yoshida et al., **1995**). Variants of this methods includes the employment of chlorosulfuric acid–pyridine reagent (Mähner et al., **2001**), piperidine-*N*-sulfonic acid (Nagasawa et al., **1972**), and sulfamic acid–pyridine reagent (Zhou et al., **2014**). However, they all cause significant depolymerization by breakage of the glycosidic linkages of the polysaccharides. Currently, the most widely employed method requires sulfur trioxide–amine (or amide) complexes in a highly polar organic solvent, such as DMF or DMAc; the advantages of these reagents include their relatively stability, ease of handling and compatibility with highly polar solvent, aiding in the solubility of polysaccharides.

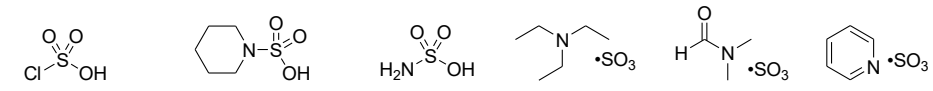

Figure 1.9. Structures of different sulfation reagents.

Although randomly sulfated polysaccharides show interesting biological activities, few information on the influence of the sulfation pattern in the

biological processes can be deduced in this way. For this reason, in the last twenty years, enzymatic or chemical methods for the regioselective insertion of sulfate groups on polysaccharide structures have been developed. The enzymatic approaches are highly regioselective and have produced some outstanding results in the recent years (Sugiura et al., **2012**; Xu et al., **2017**, **2014**). However, they still present some limitations linked to the often scarce availability and high costs of the enzymes (sulfotransferases) and their almost exclusive applicability on structures that correspond, or are very similar, to the natural substrate of these enzymes. Hence, even though chemical approach does not often allow to gain the same high regioselectivities displayed by enzymatic methods, it has proven to be a valid alternative thanks to its applicability to structurally different polysaccharides. In this approach, sulfation reactions are usually embedded in multi-step sequences of protection/deprotection reactions involving the employment of suitable protecting groups. For example, bulky pivaloyl esters were selectively introduced on primary hydroxyl positions of curdlan (Gao et al., **1997**) and carrageenan (De Araújo et al., **2013**) affording, after sulfation and global deprotection, polysaccharides composed of a 2,4-*O*-disulfated glucose repeating unit in the former case and 2,4-*O*-disulfated galactose and 2,4,6-*O*-trisulfated galactose together with 2-*O*-sulfated anhydrogalactose in the latter. In addition to pivaloyl, other ester groups, such as benzoyl and trifluoroacetyl, have been used for the selective protection of primary hydroxyl alcohols on polysaccharide structures to be then sulfated, as reported for hyaluronic acid (Becher et al., **2010**) and cellulose (Baumann et al., **2000**; Klemm et al., **1995**; Zhang et al., **2013**).

Some multi-step sequences exploited also trityl ethers and congeners (MMTr and DMTr) as protecting groups for primary hydroxyls, in protection-sulfation-deprotection sequences applied on cellulose (Heinze et al., **2000**), guar gum (Wang et al., **2013**) and chitosan (Nishimura et al., **1998**).

Probably, the longest and most elaborated multi-step sequences, developed so far, for regioselective sulfation have been aimed to the obtainment of differently sulfated CS (Bedini et al., **2012**, **2011**; Bianchi et al., **2012**; Laezza et al., **2014**; Vessella et al., **2019a**) and fCS (Bedini et al., **2016**; Laezza et al., **2015**; Vessella et al., **2019b**) polysaccharides. Some of the latest advances in this field will be discussed in detail in the following chapters.

1.4. Aim of the Thesis

In this thesis work, the development of new site-selective procedures giving an accurate control on polysaccharide structural manipulations will be discussed. Indeed, despite their high natural abundance, the development of tailored reactions aiming to regioselective modifications of polysaccharide structures is still limited to few examples on not many derivatives. Thus, this project could also help to fill the gap between polysaccharide and mono-/oligosaccharide chemistry, which, instead, has been largely explored, as also discussed in the previous paragraphs of this chapter.

The research work will focus on high available, non-animal sourced polysaccharides, that will be subjected to proper strategies to obtain their corresponding sulfated derivatives with a well-defined and reproducible sulfation pattern. As touched upon, natural sulfated polysaccharides show diverse and interesting biological activities, however their employment is limited by several factors, including, for example, production costs, batch standardization, immunogenicity, and degradability. The artificial sulfation of polysaccharides can overcome these challenges and allow the obtainment of derivatives, potentially with novel or enhanced properties compared to their natural sulfated counterparts, thus revealing new possibilities for their use in biomaterials, drug delivery vehicles, and more. In addition, by obtaining well-

defined structures, such derivatives could show tuned biological activities, contributing to the elucidation of structure–function relationships.

The main topics will be divided as follows:

- Chapter 2 discusses the semi-synthetic strategies for the transformation of *E. coli* O5:K4:H4 sourced chondroitin polysaccharide into structurally well-defined CS and fCS derivatives by regioselective sulfation and/or insertion of L-fucose branches.
- Chapter 3 deals with a preliminary SAR study on some of the semi-synthetic CS derivatives, obtained during this work, and on marine-sourced CS species. The investigation, carried out in collaboration with the BioGlycoChem group of the Institute of General Organic Chemistry of the Spanish National Research Council, can help to decipher the effect of the different sulfate-bearing motifs within CS chain on its binding capacity to growth factors.
- Chapter 4 examines the research for new semi-synthetic strategies for regioselective sulfation of naturally occurring, unsulfated polysaccharides (*i.e.* curdlan, M-rich alginic acid, a marine-sourced bacterial exopolysaccharide), with the final aim to gain GAG-mimicking structures, potentially with analogous or enhanced bioactivities with respect to the natural products.

References

Adamski-Werner, S.L., Yeung, B.K.S., Miller-Deist, L.A., Petillo, P.A., **2004**. *Carbohydr. Res. 339*, 1255–1262.

Adinolfi, M., Barone, G., Guariniello, L., Iadonisi, A., **1999**. *Tetrahedron Lett. 40*, 8439–8441.

Adinolfi, M., Barone, G., Guariniello, L., Iadonisi, A., **2000**. *Tetrahedron Lett. 41*, 9005–9008.

Adinolfi, M., Barone, G., Iadonisi, A., Mangoni, L., Schiattarella, M., **2001**. *Tetrahedron Lett. 42*, 5967–5969.

Adinolfi, M., Barone, G., Iadonisi, A., Schiattarella, M., **2002**. *Synlett* 269–270.

Adinolfi, M., Barone, G., Iadonisi, A., Schiattarella, M., **2003a**. *Org. Lett. 5*, 987–989.

Adinolfi, M., Iadonisi, A., Ravidà, A., Schiattarella, M., **2003b**. *Tetrahedron Lett. 44*, 7863–7866.

Adinolfi, M., Iadonisi, A., Ravidà, A., Valerio, S., **2006**. *Tetrahedron Lett. 47*, 2595–2599.

Aly, M.R.E., Castro-Palomino, J.C., Ibrahim, E.-S.I., El-Ashry, E.-S.H., Schmidt, R.R., **1998**. *Eur. J. Org. Chem. 1998*, 2305–2316.

De Araújo, C.A., Noseda, M.D., Cipriani, T.R., Gonçalves, A.G., Duarte, M.E.R., Ducatti, D.R.B., **2013**. *Carbohydr. Polym. 91*, 483–491.

Banoub, J., Boullanger, P., Lafont, D., **1992**. *Chem. Rev. 92*, 1167–1195.

Baumann, H., Richter, A., Klemm, D.O., Faust, V., **2000**. *Macromol. Chem. Phys. 201*, 1950–1962.

Becher, J., Möller, S., Weiss, D., Schiller, J., Schnabelrauch, M., **2010**. *Macromol. Symp. 296*, 446–452.

Bedini, E., De Castro, C., De Rosa, M., Di Nola, A., Iadonisi, A., Restaino, O.F., Schiraldi, C., Parrilli, M., **2011**. *Angew. Chem., Int. Ed. 50*, 6160–6163.

Bedini, E., De Castro, C., De Rosa, M., Di Nola, A., Restaino, O.F., Schiraldi, C., Parrilli, M., **2012**. *Chem. - Eur. J. 18*, 2123–2130.

Bedini, E., Corsaro, M.M., Fernández-Mayoralas, A., Iadonisi, A., **2019**. Chondroitin, Dermatan, Heparan, and Keratan Sulfate: Structure and Functions, in: Cohen, E., Merzendorfer, H. (Eds.), *Extracellular Sugar-Based Biopolymers Matrices*. Springer Nature Switzerland, Cham, Switzerland, pp. 187–233.

Bedini, E., Laezza, A., Iadonisi, A., **2016**. *Eur. J. Org. Chem. 2016*, 3018–3042.

Bianchi, D., Valetti, M., Bazza, P., Miraglia, N., Valoti, E., **2012**. Biotechnological sulphated chondroitin sulphate at position 4 or 6 on the same polysaccharide chain, and process for the preparation thereof. WO2012/152872.

Blatter, G., Beau, J.M., Jacquinet, J.C., **1994**. *Carbohydr. Res. 260*, 189–202.

Bongat, A.F.G., Demchenko, A. V., **2007**. *Carbohydr. Res. 342*, 374–406.

Boullanger, P., Jouineau, M., Bouammali, B., Lafont, D., Descotes, G., **1990**. *Carbohydr. Res. 202*, 151–164.

Van Breedam, W., Pöhlmann, S., Favoreel, H.W., de Groot, R.J., Nauwynck, H.J., **2014**. *FEMS Microbiol. Rev. 38*, 598–632.

Brown, G.M., Levy, H.A., **1965**. *Science 147*, 1038–1039.

Brown, J.R., Crawford, B.E., Esko, J.D., **2007**. *Crit. Rev. Biochem. Mol. Biol. 42*, 481–515.

Camacho Gömez, J.A., Erler, U.W., Klemm, D.O., **1996**. *Macromol. Chem. Phys. 197*, 953–964.

Campo, V.L., Kawano, D.F., Silva, D.B. da, Carvalho, I., **2009**. *Carbohydr. Polym. 77*, 167–180.

Carvalho, L.C.R., Queda, F., Santos, C.V.A., Marques, M.M.B., **2016**. *Chem. - Asian J. 11*, 3468–3481.

Castro-Palomino, J.C., Schmidt, R.R., **1995**. *Tetrahedron Lett. 36*, 5343–5346.

Casu, B., Petitou, M., Provasoli, M., Sinaÿ, P., **1988**. *Trends Biochem. Sci. 13*, 221–225.

Chien, C.Y., Iwata, T., **2018**. *Carbohydr. Polym. 181*, 300–306.

Clausen, T.M., Sandoval, D.R., Spliid, C.B., Pihl, J., Perrett, H.R., Painter, C.D., Narayanan, A., Majowicz, S.A., Kwong, E.M., McVicar, R.N., Thacker, B.E., Glass, C.A., Yang, Z., Torres, J.L., Golden, G.J., Bartels, P.L., Porell, R.N., Garretson, A.F., Laubach, L., Feldman, J., Yin, X., Pu, Y., Hauser, B.M., Caradonna, T.M., Kellman, B.P., Martino, C., Gordts, P.L.S.M., Chanda, S.K., Schmidt, A.G., Godula, K., Leibel, S.L., Jose, J., Corbett, K.D., Ward, A.B., Carlin, A.F., Esko, J.D., **2020**. *Cell 183*, 1043–1057.

Codée, J.D.C., Litjens, R.E.J.N., Den Heeten, R., Overkleeft, H.S., Van Boom, J.H., Van Der Marel, G.A., **2003**. *Org. Lett. 5*, 1519–1522.

Cooper, G.K., Sandberg, K.R., Hinck, J.F., **1981**. *J. Appl. Polym. Sci. 26*, 3827–3836.

Crich, D., **2011**. *J. Org. Chem. 76*, 9193–9209.

Cui, L., Cohen, J.L., Chu, C.K., Wich, P.R., Kierstead, P.H., Fréchet, J.M.J., **2012**. *J. Am. Chem. Soc. 134*, 15840–15848.

Daragics, K., Fügedi, P., **2009**. *Tetrahedron Lett. 50*, 2914–2916.

Das, R., Mukhopadhyay, B., **2016**. *ChemistryOpen 5*, 401–433.

Debenham, J.S., Debenham, S.D., Fraser-Reid, B., **1996**. N-tetrachlorophthaloyl (TCP) for ready protection/deprotection of amino sugar glycosides, in: *Bioorganic and Medicinal Chemistry*. Pergamon, pp. 1909–1918.

Debenham, S.D., Toone, E.J., **2000**. *Tetrahedron: Asymmetry 11*, 385–387.

Ekholm, F.S., Leino, R., **2018**. Acyl Migrations in Carbohydrate Chemistry, in: Vidal, S. (Ed.), *Protecting Groups: Strategies and Applications in Carbohydrate Chemistry*. Wiley, pp. 227–241.

Elferink, H., Mensink, R.A., White, P.B., Boltje, T.J., **2016**. *Angew. Chem., Int. Ed. 55*, 11217–11220.

Elieh-Ali-Komi, D., Hamblin, M.R., **2016**. *Int. J. Adv. Res. 4*, 411–427.

Fox, S.C., Li, B., Xu, D., Edgar, K.J., **2011**. *Biomacromolecules 12*, 1956–1972.

Fügedi, P., **1987**. *J. Carbohydr. Chem. 6*, 377–398.

Gama, C.I., Tully, S.E., Sotogaku, N., Clark, P.M., Rawat, M., Vaidehi, N., Goddard, W.A., Nishi, A., Hsieh-Wilson, L.C., **2006**. *Nat. Chem. Biol. 2*, 467–473.

Gama, M., Nader, H.B., de Oliveira Rocha, H.A. (Eds.), **2015**. Sulfated Polysaccharides, *Biochemistry and Molecular Biology in the Post Genomic Era Series*. Nova Science Publishers, Inc.

Gao, Y., Fukuda, A., Katsuraya, K., Kaneko, Y., Mimura, T., Nakashima, H., Uryu, T., **1997**. *Macromolecules 30*, 3224–3228.

Garegg, P.J., Johansson, R., Samuelsson, B., **1982**. *Acta Chem. Scand. 36B*, 249–250.

Ghosh, B., Kulkarni, S.S., **2020**. *Chem. - Asian J. 15*, 450–462.

Goddard-Borger, E.D., Stick, R. V., **2007**. *Org. Lett. 9*, 3797–3800.

Grote, C., Heinze, T., **2005**. *Cellulose 12*, 435–444.

Hahm, H.S., Hurevich, M., Seeberger, P.H., **2016**. *Nat. Commun. 7*, 1–8.

Hall, D.M., Horne, J.R., **1973**. *J. Appl. Polym. Sci. 17*, 2891–2896.

Hashimoto, Y., Tanikawa, S., Saito, R., Sasaki, K., **2016**. *J. Am. Chem. Soc. 138*, 14840–14843.

Heinze, T., Liebert, T., Koschella, A., **2006a**. Esterification of Polysaccharides, 1st ed. Springer-Verlag Berlin Heidelberg, Germany.

Heinze, T., Liebert, T., Koschella, A., **2006b**. New Paths for the Introduction of Organic Ester Moieties, in: *Esterification of Polysaccharides*. Springer-Verlag Berlin Heidelberg, Germany, pp. 53–116.

Heinze, T., Liebert, T., Koschella, A., **2006c**. Polysaccharide Esters with Defined Functionalisation Pattern, in: *Esterification of Polysaccharides*. Springer-Verlag Berlin Heidelberg, Germany, pp. 169–180.

Heinze, T., Röttig, K., Nehls, I., **1994**. *Macromol. Rapid Commun. 15*, 311–317.

Heinze, T., Viera, M., Heinze, U., **2000**. *Lenzinger Ber. 79*, 39–44.

Higashi, K., Nakayama, K., Soga, T., Shioya, E., Uoto, K., Kusama, T., **1990**. *Chem. Pharm. Bull. 38*, 3280–3282.

Hudak, J.E., Bertozzi, C.R., **2014**. *Chem. Biol. 21*, 16–37.

Ifuku, S., Miwa, T., Morimoto, M., Saimoto, H., **2011**. *Green Chem. 13*, 1499–1502.

Ifuku, S., Wada, M., Morimoto, M., Saimoto, H., **2012**. *Carbohydr. Polym. 90*, 1182–1186.

Igarashi, K., **1977**. The Koenigs-Knorr Reaction, in: Tipson, R.S., Horton, D. (Eds.), *Advances in Carbohydrate Chemistry and Biochemistry*. Academic Press, Inc., New York (NY), pp. 243–283.

Iozzo, R. V., Karamanos, N., **2010**. *FEBS J. 277*, 3863–3863.

Iserloh, U., Dudkin, V., Wang, Z.G., Danishefsky, S.J., **2002**. *Tetrahedron Lett. 43*, 7027–7030.

Ishimaru, M., Nagatsuka, M., Masubuchi, A., Okazaki, J.I., Kurita, K., **2014**. *Polym.*

Bull. 71, 301–313.

Ishiwata, A., Lee, Y.J., Ito, Y., **2010**. *Org. Biomol. Chem. 8*, 3596–3608.

Isogai, A., Ishizu, A., Nakano, J., **1986**. *J. Appl. Polym. Sci. 31*, 341–352.

Jiao, G., Yu, G., Zhang, J., Ewart, H., **2011**. *Mar. Drugs 9*, 196–223.

Kim, J.H., Yang, H., Boons, G.J., **2005a**. *Angew. Chem., Int. Ed. 44*, 947–949.

Kim, J.H., Yang, H., Park, J., Boons, G.J., **2005b**. *J. Am. Chem. Soc. 127*, 12090–12097.

Klemm, D.O., Heinze, T., Stein, A., Liebert, T., **1995**. *Macromol. Symp. 99*, 129–140.

Knutsen, S.H., Myslabodski, D.E., Larsen, B., Usov, A.I., **1994**. *Bot. Mar. 37*, 163–170.

Konradsson, P., Udodong, U.E., Fraser-Reid, B., **1990**. *Tetrahedron Lett. 31*, 4313–4316.

Koschella, A., Heinze, T., Klemm, D.O., **2001**. *Macromol. Biosci. 1*, 49–54.

Koschella, A., Klemm, D.O., **1997**. *Macromol. Symp. 120*, 115–125.

Kulbokaite, R., Ciuta, G., Netopilik, M., Makuska, R., **2009**. *React. Funct. Polym. 69*, 771–778.

Kunz, H., Sager, W., **1985**. *Helv. Chim. Acta 68*, 283–287.

Kurita, K., Akao, H., Yang, J., Shimojoh, M., **2003**. *Biomacromolecules 4*, 1264–1268.

Kurita, K., Ikeda, H., Shimojoh, M., Yang, J., **2007**. *Polym. J. 39*, 945–952.

Kurita, K., Matsumura, Y., Takahara, H., Hatta, K., Shimojoh, M., **2011**. *Biomacromolecules 12*, 2267–2274.

Kurita, K., Shimada, K., Nishiyama, Y., Shimojoh, M., Nishimura, S.I., **1998**. *Macromolecules 31*, 4764–4769.

Laezza, A., De Castro, C., Parrilli, M., Bedini, E., **2014**. *Carbohydr. Polym. 112*, 546–555.

Laezza, A., Iadonisi, A., De Castro, C., De Rosa, M., Schiraldi, C., Parrilli, M., Bedini, E., **2015**. *Biomacromolecules 16*, 2237–2245.

Laezza, A., Iadonisi, A., Pirozzi, A.V.A., Diana, P., De Rosa, M., Schiraldi, C., Parrilli, M., Bedini, E., **2016**. *Chem. - Eur. J. 22*, 18215–18226.

Lahaye, M., Robic, A., **2007**. *Biomacromolecules 8*, 1765–1774.

Li, Z., Zhu, L., Kalikanda, J., **2011**. *Tetrahedron Lett. 52*, 5629–5632.

Liao, W., Piskorz, C.F., Locke, R.D., Matta, K.L., **2000**. *Bioorganic Med. Chem. Lett. 10*, 793–795.

Lindahl, U., Couchman, J., Kimata, K., Esko, J.D., **2015**. Proteoglycans and Sulfated Glycosaminoglycans, in: Varki, A., Cummings, R.D., Esko, J.D., Stanley, P., Hart, G.W., Aebi, M., Darvill, A.G., Kinoshita, T., Packer, N.H., Prestegard, J.H., Schnaar, R.L., Seeberger, P.H. (Eds.), *Essentials of Glycobiology*. Cold Spring Harbor Laboratory Press, Cold Spring Harbor (NY).

Liu, J., Huang, C.Y., Wong, C.H., **2002**. *Tetrahedron Lett. 43*, 3447–3448.

Loth, F., **2012**. Industrial gums: Polysaccharides and their derivatives, 3rd ed. Academic Press, Inc., San Diego/New York/Boston/London/Sidney/Tokyo/Toronto.

Lu, S.-R., Lai, Y.-H., Chen, J.-H., Liu, C.-Y., Mong, K.-K.T., **2011**. *Angew. Chem., Int.*

Ed. 50, 7315–7320.

Mähner, C., Lechner, M.D., Nordmeier, E., **2001**. *Carbohydr. Res. 331*, 203–208.

Manabe, S., Ishii, K., Ito, Y., **2006**. *J. Am. Chem. Soc. 128*, 10666–10667.

Marszalek, P.E., Oberhauser, A.F., Pang, Y.P., Fernandez, J.M., **1998**. *Nature 396*, 661–664.

Martín, R., Martín, C., Escobedo, S., Suárez, J.E., Quirós, L.M., **2013**. *BMC Microbiol. 13*, 210.

Matsumoto, T., Maeta, H., Suzuki, K., Gen-ichi, I., **1988**. *Tetrahedron Lett. 29*, 3567–3570.

McCormick, C.L., Callais, P.A., **1987**. *Polymer 28*, 2317–2323.

Mestechkina, N.M., Shcherbukhin, V.D., **2010**. *Appl. Biochem. Microbiol. 46*, 267–273.

Mettu, R., Chen, C.Y., Wu, C.Y., **2020**. *J. Biomed. Sci. 27*, 9–31.

Miquel, N., Vignando, S., Russo, G., Lay, L., **2004**. *Synlett* 341–343.

Moremen, K.W., Tiemeyer, M., Nairn, A. V., **2012**. *Nat. Rev. Mol. Cell Biol. 13*, 448–462.

Mukaiyama, T., Murai, Y., Shoda, S.-I., **1981**. *Chem. Lett. 10*, 431–432.

Nagasawa, K., Harada, H., Hayashi, S., Misawa, T., **1972**. *Carbohydr. Res. 21*, 420–426.

Ngo, D.H., Kim, S.K., **2013**. *Int. J. Biol. Macromol. 62*, 70–75.

Nicolaou, K.C., Chucholowski, A., Dolle, R.E., Randall, J.L., **1984**. *J. Chem. Soc., Chem. Commun.* 1155–1156.

Nicolaou, K.C., Hummel, C.W., Iwabuchi, Y., **1992**. *J. Am. Chem. Soc. 114*, 3126–3128.

Nishimura, S.I., Kai, H., Shinada, K., Yoshida, T., Tokura, S., Kurita, K., Nakashima, H., Yamamoto, N., Uryu, T., **1998**. *Carbohydr. Res. 306*, 427–433.

Nishimura, S.I., Kohgo, O., Kurita, K., Kuzuhara, H., **1991**. *Macromolecules 24*, 4745–4748.

Nishiyama, T., Ichikawa, Y., Isobe, M., **2004**. *Synlett 2004*, 89–92.

O'Neill, M.A., Moon, R.J., York, W.S., Darvill, A.G., **2015**. Glycans in Bioenergy and Materials Science, in: Varki, A., Cummings, R.D., Esko, J.D., Stanley, P., HArt, G.W., Aebi, M., Darvil, A.G., Kinoshita, T., Packer, N.H., Pregard, J.H., Schanaar, R.L., Seeberger, P.H. (Eds.), *Essentials of Glycobiology*. Cold Spring Harbor Laboratory Press, Cold Spring Harbor (NY).

Ogawa, T., Matsui, M., **1976**. *Carbohydr. Res. 51*, C13–C18.

Ohlin, M., Johnsson, R., Ellervik, U., **2011**. *Carbohydr. Res. 346*, 1358–1370.

Oliveira, R.C.R., Almeida, R.R., Goncalves, T.A., **2016**. *J. Dev. Drugs 5*, 166–168.

Pappas, C.S., Malovikova, A., Hromadkova, Z., Tarantilis, P.A., Ebringerova, A., Polissiou, M.G., **2004**. *Carbohydr. Polym. 56*, 465–469.

Pawar, S.N., Edgar, K.J., **2011**. *Biomacromolecules 12*, 4095–4103.

Pawar, S.N., Edgar, K.J., **2013**. *Carbohydr. Polym. 98*, 1288–1296.

Pelletier, S., Hubert, P., Lapicque, F., Payan, E., Dellacherie, E., **2000**. *Carbohydr. Polym. 43*, 343–349.

Penadés, S., Davis, B.G., Seeberger, P.H., **2015**. Glycans in Nanotechnology, in: Varki, A., Cummings, R.D., Esko, J.D., Stanley, P., HArt, G.W., Aebi, M., Darvil, A.G., Kinoshita, T., Packer, N.H., Pregard, J.H., Schanaar, R.L., Seeberger, P.H. (Eds.), *Essentials of Glycobiology*. Cold Spring Harbor Laboratory Press, Cold Spring Harbor (NY).

Petruš, L., Gray, D.G., BeMiller, J.N., **1995**. *Carbohydr. Res. 268*, 319–323.

Pétursson, S., **1997**. *J. Chem. Educ. 74*, 1297–1303.

Petzold, K., Koschella, A., Klemm, D.O., Heublein, B., **2003**. *Cellulose 10*, 251–269.

Pomin, V.H., **2009**. *Biopolymers 91*, 601–609.

Pomin, V.H., Mourão, P.A.S., **2008**. *Glycobiology 18*, 1016–1027.

Raedts, J., Kengen, S.W.M., Van Der Oost, J., **2011**. *Glycoconjugate J. 28*, 57–66.

Rao, V.S.R., Qasba, P.K., Balaji, P. V., Chandrasekaran, R., **1998**. Conformation of Carbohydrates, 1st ed. Harwood Academic Publishers, Reading (UK).

Ravindranathan Kartha, K.P., Field, R.A., **1997**. *Tetrahedron 53*, 11753–11766.

Richter, A., Klemm, D.O., **2003**. *Cellulose 10*, 133–138.

Rogers, C.J., Clark, P.M., Tully, S.E., Abrol, R., Garcia, K.C., Goddard, W.A., Hsieh-Wilson, L.C., **2011**. *Proc. Natl. Acad. Sci. U.S.A 108*, 9747–9752.

Sakagami, M., Hamana, H., **2000**. *Tetrahedron Lett. 41*, 5547–5551.

Schmidt, R.R., Grundler, G., **1982**. *Angew. Chem. Int. Ed. Engl. 21*, 781–782.

Schmidt, R.R., Michel, J., **1980**. *Angew. Chem. Int. Ed. Engl. 19*, 731–732.

Schnaar, R.L., **2016**. *J. Leukocyte Biol. 99*, 825–838.

Schroeder, L.R., Green, J.W., **1966**. *J. Chem. Soc. C* 530–531.

Schultz, P., Lüning, U., **2002**. *Macromol. Chem. Phys. 203*, 961–967.

Seeberger, P.H., **2015**. Monosaccharide Diversity, in: Varki, A., Cummings, R.D., Esko, J.D., Stanley, P., Hart, G.W., Aebi, M., Darvill, A.G., Kinoshita, T., Packer, N.H., Prestegard, J.H., Schnaar, R.L., Seeberger, P.H. (Eds.), *Essentials of Glycobiology*. Cold Spring Harbor Laboratory Press, Cold Spring Harbor (NY).

Shie, C.R., Tzeng, Z.H., Kulkarni, S.S., Uang, B.J., Hsu, C.Y., Hung, S.C., **2005**. *Angew. Chem., Int. Ed. 44*, 1665–1668.

Silva, S.S., Mano, J.F., Reis, R.L., **2017**. *Green Chem. 19*, 1208–1220.

Somorin, O., Nishi, N., Tokura, S., Noguchi, J., **1979**. *Polym. J. 11*, 391–396.

Sugiura, N., Shioiri, T., Chiba, M., Sato, T., Narimatsu, H., Kimata, K., Watanabe, H., **2012**. *J. Biol. Chem. 287*, 43390–43400.

Suzuki, K., Maeta, H., Matsumoto, T., **1989**. *Tetrahedron Lett. 30*, 4853–4856.

Swarup, V.P., Hsiao, T.W., Zhang, J., Prestwich, G.D., Kuberan, B., Hlady, V., **2013**. *J. Am. Chem. Soc. 135*, 13488–13494.

Takaragi, A., Minoda, M., Miyamoto, T., Liu, H.Q., Zhang, L.N., **1999**. *Cellulose 6*, 93–102.

Tanaka, N., Ogawa, I., Yoshigase, S., Nokami, J., **2008**. *Carbohydr. Res. 343*, 2675–2679.

Tani, S., Sawadi, S., Kojima, M., Akai, S., Sato, K. ichi, **2007**. *Tetrahedron Lett. 48*, 3103–3104.

Titz, A., Radic, Z., Schwardt, O., Ernst, B., **2006**. *Tetrahedron Lett. 47*, 2383–2385.

Toida, T., Chaidedgumjorn, A., Linhardt, R.J., **2003**. *Trends Glycosci. Glycotechnol. 15*, 29–46.

Umemura, T., Hirakawa, M., Yoshida, Y., Kurita, K., **2012**. *Polym. Bull. 69*, 303–312.

Urban, F.J., Moore, B.S., Breitenbach, R., **1990**. *Tetrahedron Lett. 31*, 4421–4424.

van Well, R., Ravindranathan Kartha, K.P., Field, R.A., **2005**. *J. Carbohydr. Chem. 24*, 463–474.

Varki, A., **2011**. *Cold Spring Harbor Perspect. Biol. 3*, 1–14.

Varki, A., Gagneux, P., **2015**. Biological Functions of Glycans, in: Varki, A., Cummings, R.D., Esko, J.D., Stanley, P., HArt, G.W., Aebi, M., Darvil, A.G., Kinoshita, T., Packer, N.H., Pregard, J.H., Schanaar, R.L., Seeberger, P.H. (Eds.), *Essentials of Glycobiology*. Cold Spring Harbor Laboratory Press, Cold Spring Harbor (NY).

Veeneman, G.H., van Leeuwen, S.H., van Boom, J.H., **1990**. *Tetrahedron Lett. 31*, 1331–1334.

Vessella, G., Traboni, S., Cimini, D., Iadonisi, A., Schiraldi, C., Bedini, E., **2019a**. *Biomacromolecules 20*, 3021–3030.

Vessella, G., Traboni, S., Pirozzi, A.V.A., Laezza, A., Iadonisi, A., Schiraldi, C., Bedini, E., **2019b**. *Mar. Drugs 17*, 655–670.

Wang, C.C., Luo, S.Y., Shie, C.R., Hung, S.C., **2002**. *Org. Lett. 4*, 847–849.

Wang, J., Niu, S., Zhao, B., Wang, X., Yao, J., Zhang, J., Zhao, W., Zhao, Y., **2013**. *Int. J. Biol. Macromol. 62*, 734–740.

Wessel, H.P., Iversen, T., Bundle, D.R., **1985**. *J. Chem. Soc., Perkin Trans. 1* 2247–2250.

Wulff, G., Röhle, G., **1974**. *Angew. Chem. Int. Ed. Engl. 13*, 157–170.

Wuts, P.G.M., **2014a**. Protection for the hydroxyl group, including 1,2- and 1,3-diols, in: *Greene's Protective Groups in Organic Synthesis*. John Wiley & Sons, Inc., Hoboken, New Jersey, pp. 654–659.

Wuts, P.G.M., **2014b**. Protection for the amino group, in: *Greene's Protective Groups in Organic Synthesis*. John Wiley & Sons, Inc., Hoboken, New Jersey, pp. 895–1193.

Xu, D., Edgar, K.J., **2012**. *Biomacromolecules 13*, 299–303.

Xu, D., Voiges, K., Elder, T., Mischnick, P., Edgar, K.J., **2012**. *Biomacromolecules 13*, 2195–2201.

Xu, Y., Cai, C., Chandarajoti, K., Hsieh, P.-H., Li, L., Pham, T.Q., Sparkenbaugh, E.M., Sheng, J., Key, N.S., Pawlinski, R., Harris, E.N., Linhardt, R.J., Liu, J., **2014**. *Nat. Chem. Biol. 10*, 248–250.

Xu, Y., Chandarajoti, K., Zhang, X., Pagadala, V., Dou, W., Moorman Hoppensteadt, D., Sparkenbaugh, E.M., Cooley, B., Daily, S., Key, N.S., Severynse-Stevens, D., Fareed, J., Linhardt, R.J., Pawlinski, R., Liu, J., **2017**. *Sci. Transl. Med. 9*, eaan5954.

Yamada, H., Hayashi, T., **2002**. *Carbohydr. Res. 337*, 581–585.

Yan, R.B., Yang, F., Wu, Y., Zhang, L.H., Ye, X.S., **2005**. *Tetrahedron Lett. 46*, 8993–8995.

Yasomanee, J.P., Demchenko, A. V., **2012**. *J. Am. Chem. Soc. 134*, 20097–20102.

Yoshida, T., Yasuda, Y., Mimura, T., Kaneko, Y., Nakashima, H., Yamamoto, N., Uryu, T., **1995**. *Carbohydr. Res. 276*, 425–436.

Yu, B., Tao, H., **2001**. *Tetrahedron Lett. 42*, 2405–2407.

Zhang, F., Bernet, B., Bonnet, V., Dangles, O., Sarabia, F., Vasella, A., **2008**. *Helv. Chim. Acta 91*, 608–617.

Zhang, K., Fischer, S., Geissler, A., Brendler, E., Gebauer, K., **2013**. *Cellulose 20*, 2069–2080.

Zhang, Q., Chen, C.Z., Swaroop, M., Xu, M., Wang, L., Lee, J., Wang, A.Q., Pradhan, M., Hagen, N., Chen, L., Shen, M., Luo, Z., Xu, X., Xu, Y., Huang, W., Zheng, W., Ye, Y., **2020**. *Cell Discovery 6*, 1–14.

Zhang, R., Zheng, X., Kuang, J., Edgar, K.J., **2014**. *Carbohydr. Polym. 113*, 159–165.

Zhao, J., Zhu, Y., Song, X., Xiao, Y., Su, G., Liu, X., Wang, Z., Xu, Y., Liu, J., Eliezer, D., Ramlall, T.F., Lippens, G., Gibson, J., Zhang, F., Linhardt, R.J., Wang, L., Wang, C., **2020**. *Angew. Chem., Int. Ed. 59*, 1818–1827.

Zhou, C.-L., Liu, W., Kong, Q., Song, Y., Ni, Y.-Y., Li, Q.-H., O'Riordan, D., **2014**. *Int. J. Food Sci. Technol. 49*, 508–514.

Zhu, S., Wu, Y., Chen, Q., Yu, Z., Wang, C., Jin, S., Ding, Y., Wu, G., **2006**. *Green Chem. 8*, 325–327.

Zhu, X., Schmidt, R.R., **2009**. *Angew. Chem., Int. Ed. 48*, 1900–1934.

Zinin, A.I., Malysheva, N.N., Shpirt, A.M., Torgov, V.I., Kononov, L.O., **2007**. *Carbohydr. Res. 342*, 627–630.

Zong, C., Huang, R., Condac, E., Chiu, Y., Xiao, W., Li, X., Lu, W., Ishihara, M., Wang, S., Ramiah, A., Stickney, M., Azadi, P., Amster, I.J., Moremen, K.W., Wang, L., Sharp, J.S., Boons, G.J., **2016**. *J. Am. Chem. Soc. 138*, 13059–13067.

Zoppetti, G., Oreste, P., **2004**. Process for the Preparation of Chondroitin sulfates from K4 Polysaccharide and Obtained Products. US Patent 6,777,398.

Zou, Y., Khor, E., **2009**. *Carbohydr. Polym. 77*, 516–525.

CHAPTER 2
NEW SEMI-SYNTHETIC PATHWAYS TOWARDS STRUCTURALLY WELL-DEFINED (FUCOSYLATED) CHONDROITIN SULFATE POLYSACCHARIDES

2
NEW SEMI-SYNTHETIC PATHWAYS TOWARDS STRUCTURALLY WELL-DEFINED (FUCOSYLATED) CHONDROITIN SULFATE POLYSACCHARIDES

2.1. Introduction

2.1.1. CS and fCS: Structure and Activity

CS is one of the major and widespread sulfated GAGs, widely distributed in animals, both vertebrates and invertebrates, and in some bacteria. In mammals, CS is a key constituent of the ECM, where several saccharide chains are covalently anchored to proteins forming large PGs, and it is also abundant in bones, cartilages, skin, and nerve tissues (Mikami and Kitagawa, **2013**).

Its saccharide backbone is composed of D-GlcA and D-GalNAc residues, linked together through alternating β-1→3 and β-1→4 glycosidic bonds. The resulting disaccharide repeating unit can be variously sulfated and, according to the sulfation pattern, several subunits (commonly identified by a letter) can be defined (Figure 2.1) (Pomin, **2013**). Interestingly, sulfate group distribution on chondroitin polysaccharides seems to be a result of the evolution, to let CS play key roles in complex biological processes typical of higher animals (*e.g.* central nervous system development). Indeed, simple and evolutionary more ancient organisms, such as bacteria and nematodes, possess only or mostly unsulfated chondroitin (Yamada et al., **2007**). On the contrary, from arthropods up to mammals, chondroitin can be found in one or more of its sulfated variants: in CSs from terrestrial animals, sulfation concerns almost exclusively position *C*-4 and/or *C*-6 of GalNAc, whereas CSs found in marine species, including for example

shark, ray, octopus, and shrimp, can be sulfated also at *C*-2 and/or *C*-3 of GlcA (Cavalcante et al., **2018**; Higashi et al., **2015**; Takeda et al., **2016**). Finally, sulfation pattern can be subjected to variations also depending on tissue source and, in higher animals, on different physio-pathological conditions, such as aging, inflammation and tumour formation (Collin et al., **2017**).

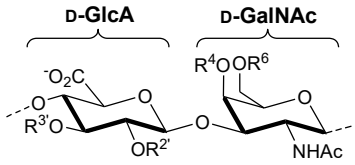

	0	A	C	U	V	B	D	E	K	L	R	M	S	S'	T
$R^{2'}$	H	H	H	S	H	S	S	H	H	H	S	H	S	S	S
$R^{3'}$	H	H	H	H	S	H	H	H	S	S	S	S	S	S	H
R^4	H	S	H	H	H	S	H	S	S	H	H	S	S	H	S
R^6	H	H	S	H	H	H	S	S	H	S	H	S	H	S	S

S = SO_3^-

Figure 2.1. CS structure and sulfate group distribution.

In biological systems, CS interacts with a plethora of key elements, such as growth factors, cytokines, chemokines, adhesion molecules and lipoproteins (Djerbal et al., **2017**; Mizumoto et al., **2013**); these interactions regulate several physiological processes, including neurite outgrowth, axonal regeneration, wound healing, and growth factors signalling (Malavaki et al., **2008**). In addition, a biosynthetic imbalance of CS-PGs is often associated with some diseases, such as cancer or osteoarthritis (Bara et al., **2012**; Pudełko et al., **2019**). In the case of osteoarthritis, the administration of exogenous CS-A,C represent a first-line therapy, where the efficiency is also due to an anti-inflammatory effect of this sulfated GAG (Bishnoi et al., **2016**). Other potential therapeutic applications of CS have been proposed, including antiviral, antimalarial, anticancer and as tissue regeneration factor (Yamada and Sugahara, **2008**).

In the last decades, some CS structural variants, with neutral or negatively charged mono- or disaccharide branches, have been found in some marine invertebrates (Higashi et al., **2016**; Kinoshita-Toyoda et al., **2004**). Among these branched CS polysaccharides, fCS, isolated up to now exclusively from the body wall of sea

cucumbers (*Echinodermata*, *Holothuroidea*), has been attracted much attention due to its interesting biological properties.

In fCS structure, the chondroitin core bears not only sulfate groups but also variously sulfated L-Fuc (6-deoxy-L-galactose) branches. Structural variants of fCS have been found in different species of sea cucumbers, also depending on diverse seasonal and habitat features (Chen et al., **2011**); the structural variations are generally related to type, amount and position of branches, as well as to degree and pattern of sulfation on both backbone and branches (Ustyuzhanina et al., **2019**). Mainly, the repeating blocks present sulfated L-Fuc monosaccharide residues α-glycosidically linked at *O*-3 site of GlcA units (Mou et al., **2018**; Myron et al., **2014**; Ustyuzhanina et al., **2016b**). Alternative structures show variously sulfated L-Fuc oligosaccharide branches (from two up to nine moieties) at *O*-3 of GlcA residues (Santos et al., **2015**; Soares et al., **2018**; Ustyuzhanina et al., **2017a**; Yin et al., **2021**) or, rarely, fucosyl branches at *O*-4 and/or *O*-6 of GalNAc units (Li et al., **2018**; Qiu et al., **2020**; Ustyuzhanina et al., **2017b**; Yang et al., **2018**). Sulfate group distribution on Fuc branching is particularly variable, and both monosulfation, generally at *O*-3 or *O*-4 sites, and disulfation, commonly at *O*-2,4 or *O*-3,4 sites, have been described (Mourão et al., **1996**; Wu et al., **2012**). Finally, sulfate groups can be located at *O*-4 and/or *O*-6 of GalNAc, though the presence of some 3-*O*-sulfated GlcA units in fCS structures has been detected in some cases (Ustyuzhanina et al., **2016a**; Vieira et al., **1991**). A schematic representation of fCS structural variability found up to now is depicted in Figure 2.2. Notably, in most fCSs studied so far, the presence of two or even more structurally different repeating units has been detected.

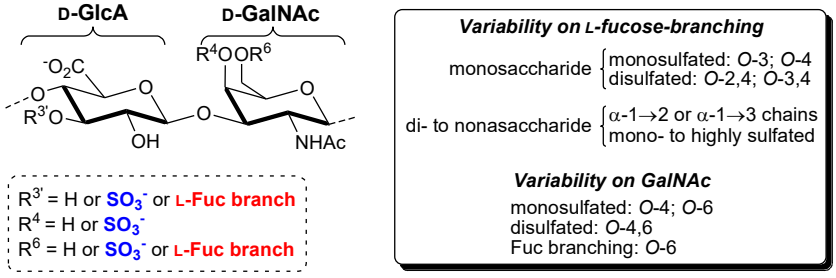

Figure 2.2. Structural variability of fCS from sea cucumbers.

fCS polysaccharides exhibit a wide spectrum of biological properties, including anticoagulant, antithrombotic, anti-inflammatory, anticancer, antiviral, and pro-angiogenic activities, and beneficial effects in hemodialysis, cellular growth modulation, fibrosis and hyperglycemia (Pomin, **2014**). The anticoagulant and antithrombotic actions are strictly related to the presence of sulfated L-Fuc branches, as demonstrated by the loss of activity shown by partially defucosylated and desulfated derivatives (Monteiro-Machado et al., **2015**; Mourão et al., **1998**, **1996**). As for heparin, one of the most widely used anticoagulant drugs, fCS anticoagulant actions are mediated by plasma protease inhibitors (serpins), namely AT and HCII, thus inhibiting essential factors for the coagulation cascade, such as factor Xa and thrombin (Mourão et al., **1996**). Interestingly, differently from heparin, fCS retains its activity also in serpins-depleted plasmas, by inhibiting the intrinsic tenase and prothrombinase complexes, which are critical for factor Xa and thrombin generation (Glauser et al., **2008**). Figure 2.3 summarizes the main target sites for fCS on the coagulation system; blue arrows on the right of the Figure indicate the anticoagulant effects.

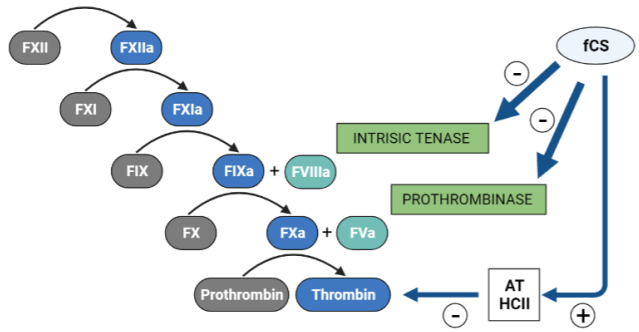

Figure 2.3. Major target sites for fCS activity on the coagulation system. (+) indicates activation and (-) indicated inhibitory effects.

The possibility to exploit an alternative mechanism of action, distinct from those of heparin, is a key aspect in the research for new and safer antithrombotic drugs (Mourão, **2015**). For this reason, fCS has been considered an interesting antithrombotic drug candidate, also thanks to the possibility to be orally deliverable; indeed it can be digested neither during its adsorption in the gastrointestinal tract nor by intestinal bacterial enzyme (Fonseca et al., **2017**; Fonseca and Mourão, **2006**).

2.1.2. CS and fCS: Synthetic and Semi-Synthetic Approaches

As extensively described above, naturally occurring CS and fCS polysaccharides very often show highly heterogeneous structures. This limits their therapeutic applications since the structural variability hampers detailed structure–activity relationship studies and can potentially lead to unspecific, unknown and even dangerous side effects. Notably, the molecular weight is another parameter to be considered for clinical uses since it also affects the biological activities of these sulfated GAGs. High molecular weight sulfated polysaccharides usually have low solubility and poor absorption by digestive system, besides their administration can cause some adverse effects such as platelet aggregation, hypotension, and bleeding (Fonseca et al., **2010**; Yan et al., **2017**). Depolymerization has been

considered as an effective method to address these issues, maintaining at the same time the biological activities, as demonstrated by the employment of low molecular weight CS as pharmaceutical and dietary supplements (Adebowale et al., **2000**). Finally, the supply chain of (f)CS also presents safety concerns. For commercial purposes, CS is commonly obtained from animal tissues (mainly porcine or bovine), thus it is highly susceptible to contamination by pathogenic agents, such as in the case of prion proteins causing spongiform encephalopathy, or by other sulfated GAGs, like KS (Pomin et al., **2012**). A particularly regrettable example of GAG contamination happened in 2007 as a consequence of a worldwide distribution of oversulfated CS contaminated heparin, which was associated with over 200 deaths in the United States (Guerrini et al., **2008**; Kishimoto et al., **2008**). This episode has also revealed the necessity of a strict regulation and control on the sulfation pattern of these animal-sourced polysaccharides.

For these reasons, the preparation of homogeneous (f)CS structures of appropriate molecular weight and defined sulfation and/or fucosylation pattern is highly desirable. Thus, several research groups have focused their attention on the production of (f)CS oligosaccharides and low molecular weight polysaccharides with well-defined structures. Chemical total-synthetic approaches for (f)CS oligosaccharides have been extensively pursued, despite the high demanding task linked to protecting group manipulation and glycosidic bond formation (He et al., **2019**; Macchione et al., **2014**; Matsushita et al., **2015**; Miyachi et al., **2015**; Poh et al., **2015**; Solera et al., **2016**; Tamura et al., **2013**; Ustyuzhanina et al., **2015**; Vinnitskiy et al., **2017**; Wakao et al., **2015**). Hence, during the last decade, (chemo)-enzymatic synthesis (Li et al., **2017**; Sugiura et al., **2012**; Zhang et al., **2020**) and semi-synthesis have emerged as alternative approaches. The latter relies on the employment of natural polysaccharides as starting material; for example, several semi-synthetic approaches are based on chemical or enzymatic

degradation of animal-sourced CS in order to obtain an unsulfated disaccharide, or even slightly longer oligosaccharides, that are in turn selectively modified by chemical methods to gain the desired sulfation and/or fucosylation pattern (Jacquinet et al., **2009**; H. Liu et al., **2018**; Lopin-Bon and Jacquinet, **2006**; Yao et al., **2018**; Zhang et al., **2018b**). A remarkable example in this field was recently accomplished by Li and co-workers and resulted in the obtainment of hexa- and nonasaccharide fCS structures starting from a CS enzymatic degradation (Zhang et al., **2018a**); notably, only the nonasaccharide displayed significant intrinsic pathway anticoagulation activity, in agreement with the concomitant finding of fCS octasaccharide as the minimum structural unit able to confer anticoagulant activity (Yin et al., **2018**). With the aim to avoid too many chemical reactions, partial depolymerization of natural polysaccharides has been also pursued, as in the obtainment of fCS oligosaccharides by deaminative cleavage (Guan et al., **2019**; Yan et al., **2017**; Zhao et al., **2015**) or β-eliminative degradation (Gao et al., **2015**; Shang et al., **2018**; Yin et al., **2018**). Finally, semi-synthetic approaches also include the chemical modification of polysaccharide structures through single regioselective reactions or multi-step procedures to afford polysaccharides with different, and often more well-defined, structures. Such approach allowed, for example, the obtainment of several semi-synthetic CS polysaccharides from already sulfated animal-sourced CSs (Bedini et al., **2016**; Benito-Arenas et al., **2018**; Han et al., **2018**). Furthermore, in the recent years, Bedini and co-workers have investigated an alternative semi-synthetic approach based on the employment, as starting polysaccharide material, of an unsulfated chondroitin derived from microbial sources (Bedini et al., **2012**, **2011**; Laezza et al., **2016**, **2015**). Although a conspicuous library of semi-synthetic (f)CS polysaccharides was achieved, only a partial control of their sulfation and/or fucosylation pattern was accomplished.

To overcome these limitations, alternative semi-synthetic strategies to non-animal sourced CS and fCS structures are here proposed with the aim to reach a more precise regiocontrol of their structural modifications. Furthermore, it is worth noting that a more detailed discussion on the syntheses and semi-syntheses of fCS structures already reported in literature can be found on a very recently published review paper, that has been developed during this Ph.D. work (Vessella et al., **2020**).

2.2. Results and Discussion

2.2.1. Regioselective Sulfation of Microbial Chondroitin

In this section, the strategies for the obtainment of a library of semi-synthetic CS polysaccharides with a well-defined sulfation pattern are discussed. The efforts have been focused on the research of appropriate regioselective synthetic procedures to access all the fourteen possible sulfation patterns in CS disaccharide repeating units (see Figure 2.4 and Table 2.1). In Table 2.1, for each subunit, its occurrence in natural and semi-synthetic CS polysaccharides is also shown. It is worth noting that natural CSs, as well as the semi-synthetic ones obtained so far, often show two or even more differently sulfated variants of the disaccharide repeating unit distributed along the same CS polysaccharide chain. On the contrary, the aim of this work is to open the access to CS products as much homogenous in structure as possible.

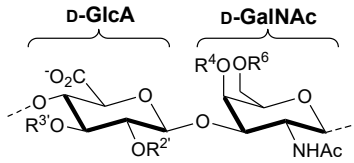

Figure 2.4. Disaccharide repeating unit of CS ($R^{2',3',4,6}$ = H or SO_3^-; see Table 2.1 for sulfation patterns found up to now in natural or semi-synthetic products).

Table 2.1. Sulfation pattern of natural and semi-synthetic CSs obtained so far.

	CS	R^4 GalNAc	R^6 GalNAc	$R^{2'}$ GlcA	$R^{3'}$ GlcA	Natural sourced [a,b]	Semi-synthetic [a,c,d]
Non-sulfated	**0**	H	H	H	H	*yes*	
Monosulfated	**A**	SO_3^-	H	H	H	*yes*	*yes*
	C	H	SO_3^-	H	H	*yes*	*yes*
	U	H	H	SO_3^-	H		
	V	H	H	H	SO_3^-		
Disulfated	**B**	SO_3^-	H	SO_3^-	H	*yes*	
	D	H	SO_3^-	SO_3^-	H	*yes*	*yes*
	E	SO_3^-	SO_3^-	H	H	*yes*	*yes*
	K	SO_3^-	H	H	SO_3^-	*yes*	*yes*
	L	H	SO_3^-	H	SO_3^-	*yes*	*yes*
	R	H	H	SO_3^-	SO_3^-		
Trisulfated	**M**	SO_3^-	SO_3^-	H	SO_3^-	*yes*	
	S	SO_3^-	H	SO_3^-	SO_3^-	*yes*	*yes*
	S′	H	SO_3^-	SO_3^-	SO_3^-	*yes*	*yes*
	T	SO_3^-	SO_3^-	SO_3^-	H	*yes*	*yes*
Persulfated		SO_3^-	SO_3^-	SO_3^-	SO_3^-		*yes*

[a] Disaccharide sulfation patterns present exclusively or in combination with other ones along the polysaccharide backbone. [b] See Malavaki et al., **2008**. [c] Synthetic oligosaccharides (degree of polymerization = DP ≤ 10) are not considered here. [d] See Bedini et al., **2017**, **2016**.

The employed semi-synthetic strategy involves the use, as starting material, of an unsulfated chondroitin-like polysaccharide produced by fed-batch fermentation of *Escherichia coli* O5:K4:H4; the subsequent downstream purification process allowed to obtain the desired chondroitin polysaccharide in high purity grade (89–94%) (Cimini et al., **2010**; Schiraldi et al., **2012**).

The general semi-synthetic approach relies on the development of protection/deprotection multi-step strategies, which include regioselective reactions and end with the sulfation of the free hydroxyl group(s) and the global deprotection. As regards the regioselective protection steps, a modular approach has been pursued; this consists in a combination of inter-residue differentiations —to distinguish the GalNAc diol from the GlcA one and *vice-versa*— and intra-residue differentiations —to discriminate between the two hydroxyl groups in each diol.

2.2.1.1. Semi-synthesis of CS-E, CS-A, and CS-C

We first focused the attention on the regioselective sulfation of the position 4 and/or 6 of GalNAc residues, leading to the natural-occurring CS polysaccharides with A, C and E sulfation patterns. Although most of the semi-synthetic efforts, developed up to now, has been focused on the obtainment of these products (Bedini et al., **2016**), they often exploited animal-derived CS polysaccharide as starting material or they did not achieve a high homogeneity in the sulfation pattern, as also discussed in the previous paragraph (Bedini et al., **2011**; Benito-Arenas et al., **2018**).

The possibility to access the CS-E sulfation pattern, showing sulfate group both on *O*-4 and *O*-6 of GalNAc, was first explored. To this aim, a differentiation between GalNAc and GlcA hydroxyls on microbial chondroitin was necessary; this can be easily done by protection of the diol on GalNAc units with a benzylidene ring, followed by acetylation of GlcA diol (Scheme 2.1). This two-step sequence has been demonstrated to work very well both on chondroitin in its acid form (**1**) and on its derivative with GlcA carboxyl units protected as methyl ester (**2**) (Bedini et al., **2011**; Laezza et al., **2016**).

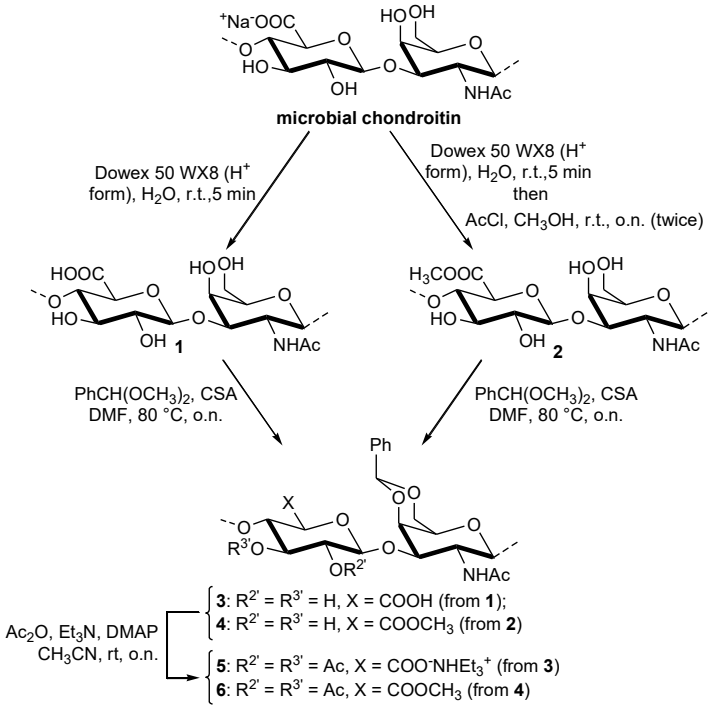

Scheme 2.1. Multi-step reaction sequence for GalNAc/GlcA hydroxyls differentiation on microbial chondroitin (Bedini et al., **2011**; Laezza et al., **2016**).

In our case, the fully protected chondroitin derivative **6** was selected as the best substrate in order both to increase the solubility of this polysaccharide in aprotic solvents and to have a protected carboxyl moiety that could instead interfere in the following steps. In order to restore the free *O*-4,6 diol to be subsequently sulfated for the obtainment of CS-E sulfation pattern, derivative **6** could be subjected to a chemoselective benzylidene ring cleavage. As discussed in Chapter 1, this reaction could be performed by employing different reaction conditions. For our purposes, oxidative and reductive benzylidene opening were not appropriate, both giving only a partial deprotection of the diol. Hence, our attention was focused on the reactions used in synthetic carbohydrate chemistry for the complete cleavage of benzylidene rings, such as hydrogenolysis and hydrolysis. The former was not considered further because it typically employs a

heavy metal, such as palladium, on an activated charcottal as catalyst, and it is therefore expensive, toxic and hard to be completely removed from a polysaccharide product. Moreover, this is a heterogeneous reaction that often gives low yield when —as for chondroitin derivative **6**— there is a high number of benzylidene rings to be removed and the saccharide substrate is complex and/or very long-chained such as a polysaccharide. On the contrary, hydrolytic cleavage of a benzylidene group is much easier, greener, and less expensive than hydrogenolysis, as it just requires aqueous acid solutions. Nonetheless, in the case of a polysaccharide, the reaction conditions must be finely tuned in order to achieve the removal of the benzylidene acetals with no significant breakage of the glycosidic bonds of the polysaccharide backbone.

To this aim, the stability of the native chondroitin polysaccharide chain to hydrolysis reactions under different temperature and pH conditions was preliminary studied. Weight-averaged molecular mass (M_w) and polydispersity — as ratio between M_w and number-averaged molecular mass (M_n)— were measured by HP-SEC combined with a triple detector array (TDA) (Bertini et al., **2005**; La Gatta et al., **2010**; Restaino et al., **2017**), on aliquots taken from the reaction mixtures at different times and then dialyzed (3.5 kDa cut-off) at low temperature (4 °C) before HP-SEC–TDA measurements (Figure 2.5). The data clearly showed that the temperature played an important effect in shortening the polysaccharide chain and increasing the polydispersity, with a threshold of 50 °C not to be surpassed in order to guarantee the integrity of the polymer.

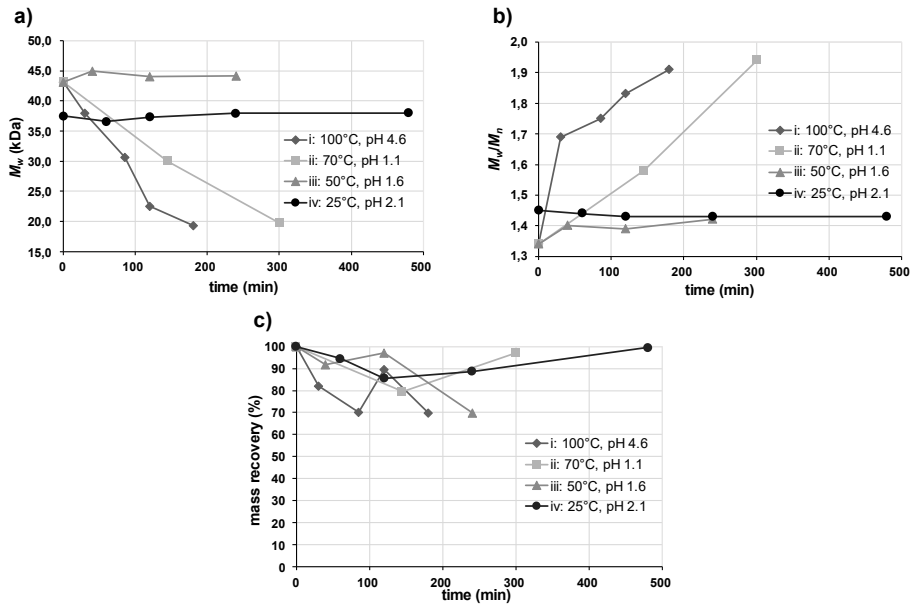

Figure 2.5. Stability data (a: molecular weight; b: polydispersity; c: percentage mass recovery) of chondroitin polysaccharide chain to hydrolysis reactions: *i*) AcOH in water, 100 °C, pH 4.6; *ii*) $HCl_{(aq)}$, 70 °C, pH 1.1; *iii*) $HCl_{(aq)}$, 50 °C, pH 1.6; *iv*) self-hydrolysis of chondroitin in its acid form, 25 °C, pH 2.1.

With this preliminary results in mind, the benzylidene acetal *vs*. glycosidic bond cleavage on chondroitin derivative **6** under hydrolytic conditions was monitored. In this case, the reaction conditions should be adapted to such water insoluble, fully protected polysaccharide, so two different reactions were conceived (Scheme 2.2). In the first one, a concentrate aqueous solution of acetic acid was employed (90% *v*/*v* AcOH in water, resulting in a solution with a protic activity approximately equal to that of reaction *iii* in Figure 2.5). Under similar conditions, the selective cleavage of 4,6-*O*-benzylidene rings on complex *N*-glycan oligosaccharide derivatives (Maki et al., **2016**) and, recently, also on chondroitin oligosaccharide derivatives (Zhang et al., **2019**) have been reported. In the second reaction, **6** was treated with an organic Brønsted acid, such as CSA, in acetonitrile in the presence of an acetal exchange reagent (DTT), according to a recently published methodology for the selective cleavage of acetals and ketals on complex

carbohydrate substrates (Y. Liu et al., **2018**). Aliquots were taken from both reaction mixtures at different times, dialyzed (3.5 kDa cut-off) at 4 °C and, after freeze-drying, mass recovery and the degree of benzylidene cleavage (DBC) were evaluated (Figure 2.6). The latter was estimated from the integral areas measured for the residual benzylidene ring and methine proton signals at δ_H 7.50–7.20 ppm and 5.45–5.35 ppm, respectively, and the *O*- and *N*-acetyl signals at δ_H 2.10–1.70 ppm in ^{1}H NMR spectrum, according to Equation 2.1 (see also Figure 2.29,2.30 in Paragraph 2.4.4).

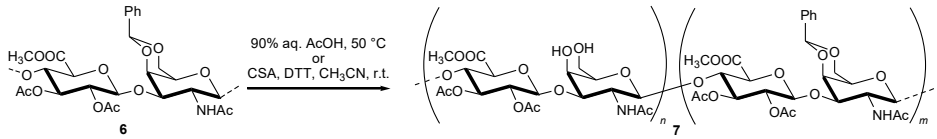

6 7

Scheme 2.2. Conversion of polysaccharide **6** into **7**. Reaction time was set according to Figure 2.6.

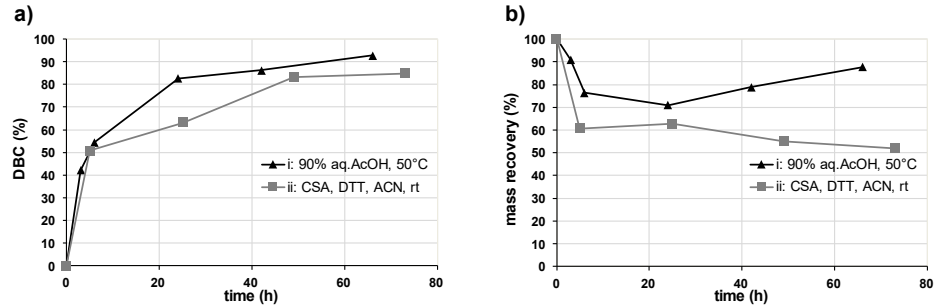

Figure 2.6. Conversion of polysaccharide **6** into **7** (a: percentage degree of benzylidene cleavage, DBC; b: percentage mass recovery) by: *i*) 90% *v*/*v* aq. AcOH, 50 °C; *ii*) CSA, DTT, ACN, 25 °C. (ACN: acetonitrile).

$$\mathrm{DBC} = \left(1 - \frac{\frac{I(\mathrm{PhCH})}{I(Ac)/9} + \frac{I(\mathrm{PhCH})/5}{I(Ac)/9}}{2}\right) \times 100 \qquad \text{(Eq. 2.1)}$$

The two reactions clearly afforded benzylidene cleavage with a very similar behaviour (Figure 2.6), nonetheless the method employing aqueous acetic acid

was preferred not only due to a slightly higher DBC and mass recovery, but also for its cheapness. In particular, derivative **7** with a percent degree of restored diol equal to 87% was obtained by treating **6** with 90% *v*/*v* aq. AcOH at 50 °C for 48 hours (Scheme 2.3).

Product **7** was directly subjected to sulfation of the free alcohols with SO_3·pyridine complex in DMF, followed by global deprotection under acid and then alkaline hydrolytic conditions to give, after purification by dialysis, semi-synthetic **CS-1** (Scheme 2.3).

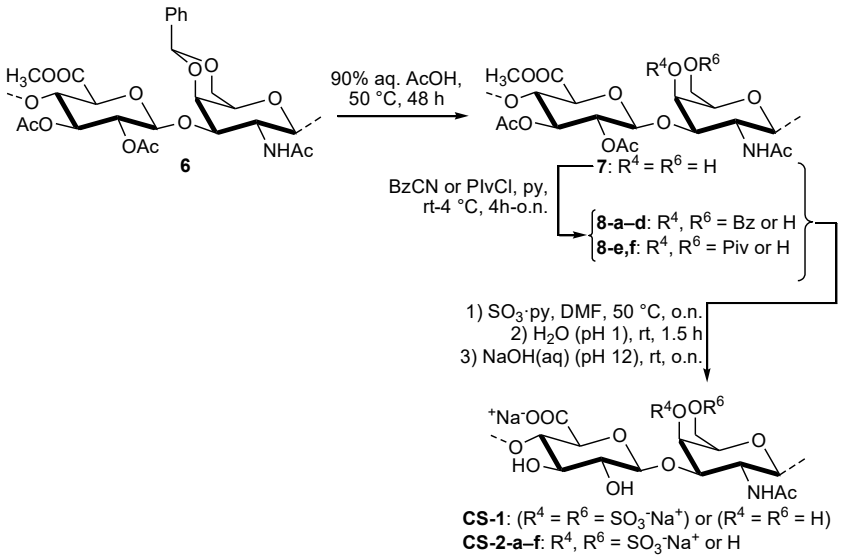

Scheme 2.3. Semi-synthesis of **CS-1** and **CS-2a–f** polysaccharides.

Structural characterization of **CS-1** was accomplished by 2D-NMR investigation. The anomeric CH region of $^{1}H,^{13}C$-DEPT-HSQC spectrum displayed two signals at $\delta_{H,C}$ 4.61/102.8 ppm and 4.47/105.1 ppm (Figure 2.7). The latter could be attributed to an unsulfated GlcA unit by means of COSY spectrum showing a correlation with the CH signal at $\delta_{H,C}$ 3.37/73.5 ppm, attributable to GlcA *CH*-2 in accordance with literature data (Mucci et al., **2000**). In addition, GlcA *CH*-1 signal was also connected, by TOCSY spectrum correlations, to typical signals of

an unsulfated GlcA unit (see Paragraph 2.4.4 for full NMR assignments) (Mucci et al., **2000**). The former anomeric signal ($\delta_{H,C}$ 4.61/102.8 ppm) was attributed to GalNAc *CH*-1, by means of COSY spectrum showing a correlation with the CH signal at $\delta_{H,C}$ 4.04/52.6 ppm, attributable to GalNAc *CH*-2. Besides, COSY and TOCSY allowed the identification of GalNAc proton sequence from *H*-1 to *H*-4 revealing the exclusive presence of 4,6-disulfated GalNAc *CH*-4 position ($\delta_{H,C}$ 4.79/77.4 ppm). However, the $^{1}H,^{13}C$-DEPT-HSQC spectrum revealed the presence of two signals in antiphase with respect to the other densities, attributable to sulfated ($\delta_{H,C}$ 4.24/68.9 ppm) and unsulfated ($\delta_{H,C}$ 3.77/62.3 ppm) carbinolic proton at position 6 of GalNAc units, respectively. The presence of unsulfated GalNAc units was ascribed to the non-exhaustive benzylidene ring cleavage, as expected by ^{1}H NMR of product **7**. The ratio between GalNAc4,6S (corresponding to the CS-E sulfation pattern) and GalNAc0S moieties was estimated by $^{1}H,^{13}C$-DEPT-HSQC 2D-NMR integration of the two kind of CH_2-6 signals, assuming that they displayed similar $^{1}J_{CH}$ coupling constants and that a difference of around 5−8 Hz from the experimental set value did not cause a substantial variation of the integrated peak volumes (Gargiulo et al., **2009**; Guerrini et al., **2005**). It was so possible to establish a 80:20 ratio between CS-E and CS-0 units in **CS-1**.

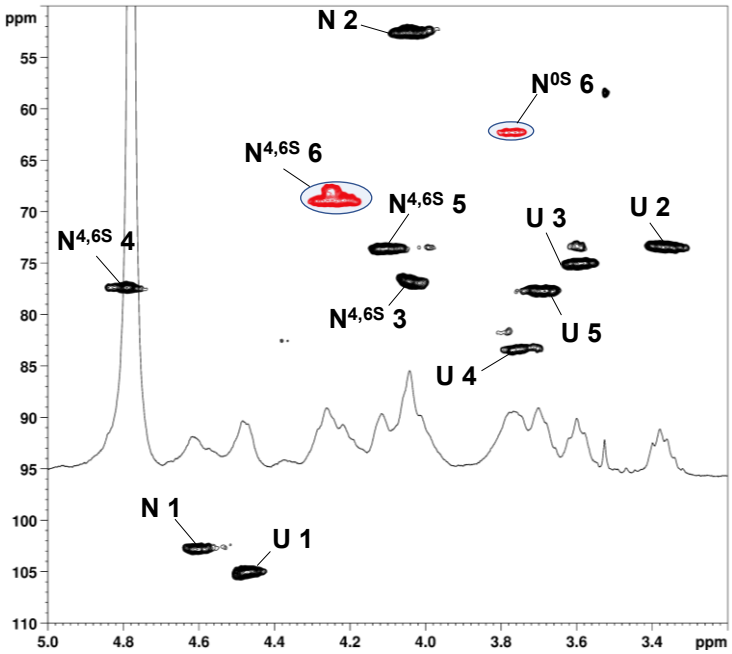

Figure 2.7. ^{1}H and $^{1}H,^{13}C$-DEPT-HSQC NMR spectra (400 MHz, D_2O, 298 K, zoom) of **CS-1**. Letter N is referred to both 4,6-di-*O*-sulfated and unsulfated GalNAc (if specified, superscripts 4,6S and 0S indicate the sulfation pattern on GalNAc). (Densities enclosed in the highlighted areas of the $^{1}H,^{13}C$-DEPT-HSQC spectrum were integrated for estimation of GalNAc4,6S and GalNAc0S percentage amounts).

Polysaccharide **7**, showing the free *O*-4,6 diol on GalNAc, was also a useful synthetic intermediate for the preparation of a CS-A polysaccharide, with a sulfate group exclusively at position 4 of GalNAc units. Indeed, under appropriate conditions, the regioselective protection of the primary OH-6 could be achieved, to obtain a derivative with a single free alcohol at position 4 suitable for a subsequent sulfation. Hence, polysaccharide **7** was subjected to test reactions for the selective acylation of primary positions (Scheme 2.3 and Table 2.2). The acylating agents BzCN and PivCl were selected in accordance with their use for the selective protection of primary *vs.* secondary alcohol functions on short chain chondroitin oligosaccharides or on other polysaccharide products (Gao et al., **1997**; Lopin-Bon and Jacquinet, **2006**). Different reaction conditions for the

acylation steps were tested, changing temperature, reaction time and acylating agent equivalents (Table 2.2).

Table 2.2. Optimization of regioselective acylating step conditions.

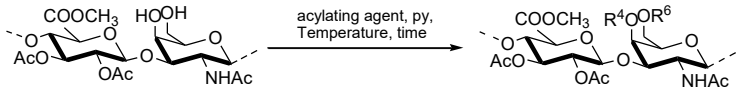

7

8-a–d: R^4, R^6 = Bz or H
8-e,f: R^4, R^6 = Piv or H

Entry	Acylating agent (equiv.)	Temperature, time	Product
a	BzCN (10)	r.t., o.n.	**8a**
b	BzCN (10)	4 °C, 4 h	**8b**
c	BzCN (5)	r.t., 4 h	**8c**
d	BzCN (2.5)	r.t., 4 h	**8d**
e	PivCl (5)	r.t., 4 h	**8e**
f	PivCl (5)	4 °C, 4 h	**8f**

The reaction regioselectivity on the polysaccharide could not be easily evidenced by NMR of the protected products because of the high complexity of the spectra and the absence of proper references. Therefore, products **8a–f**, recovered by precipitation from the reaction mixture, were directly subjected to sulfation under standard conditions, with SO_3·pyridine complex in DMF, followed by global deprotection under acid and then alkaline hydrolytic conditions to afford, after purification by dialysis, semi-synthetic **CS-2a–f** (Scheme 2.3).

All the obtained CS polysaccharides were then subjected to a deep structural characterization through 2D-NMR spectroscopy investigation. **CS-2a** and **CS-2b** displayed very similar $^{1}H,^{13}C$-DEPT-HSQC spectra (Figure 2.8A for **CS-2b**); in particular, it can be evidenced the presence of two signals, attributable to sulfated ($\delta_{H,C}$ 4.72/77.6 ppm) and unsulfated ($\delta_{H,C}$ 4.09/68.9 ppm) GalNAc *CH*-4 positions. The relative integration of these signals indicated a nearly equivalent percentage value of GalNAc4S and GalNAc0S units in both CS products (Table 2.3). This result could be explained considering a concomitant protection of *O*-4, together with *O*-6, by Bz group during the acylation step; this outcome could not be

avoided by decreasing both temperature and reaction time, as performed in the acylation step giving **8b** (see Table 2.2). **CS-2c** and **CS-2e** also displayed very similar $^{1}H,^{13}C$-DEPT-HSQC spectra (Figure 2.8B for **CS-2e**), and, again, the two signals attributable to sulfated ($\delta_{H,C}$ 4.71/77.7 ppm) and unsulfated ($\delta_{H,C}$ 4.08/68.9 ppm) GalNAc *CH*-4 positions could be revealed. However, in this case a high preponderance of GalNAc4S over GalNAc0S units was evaluated by the relative integration of the signals assigned to *CH*-4 of these two residues (Table 2.3). These results agreed with an increased regioselectivity towards *O*-6 *vs O*-4 in the acylation step, likely due to a decrease in the equivalent number of the acylating agent (see Table 2.2). Finally, **CS-2d** and **CS-2f** furnished more complicated $^{1}H,^{13}C$-DEPT-HSQC spectra (Figure 2.8C for **CS-2f**); indeed, together with the two signals related to sulfated ($\delta_{H,C}$ 4.76/77.6 ppm) and unsulfated ($\delta_{H,C}$ 4.11/69.0 ppm) GalNAc *CH*-4 positions, the presence of two different signals in antiphase with respect to the other densities was evidenced. These signals could be attributable to sulfated ($\delta_{H,C}$ 4.24/68.9 ppm) and unsulfated ($\delta_{H,C}$ 3.78/62.3 ppm) CH_2-6 positions in GalNAc units. The relative integration of the *CH*-4 and CH_2-6 signals allowed to evaluate 4-*O*- and 6-*O*-sulfation percentage, respectively (Table 2.3). The presence of sulfate groups on GalNAc *O*-6 sites in **CS-2d,2f** could be attributed to a non-quantitative protection of the primary alcohols under the acylation conditions employed to give **8d,f**. Comparing all the described results on **CS-2a–f** (Table 2.3), it could be assessed that the highest regioselectivity in *O*-6 protection was achieved in entry *e* (PivCl,5 eq, r.t., 4 h), allowing to obtain, after sulfation and global deprotection, a semi-synthetic CS polysaccharide with a CS-A,0 sulfation pattern in 86:14 ratio.

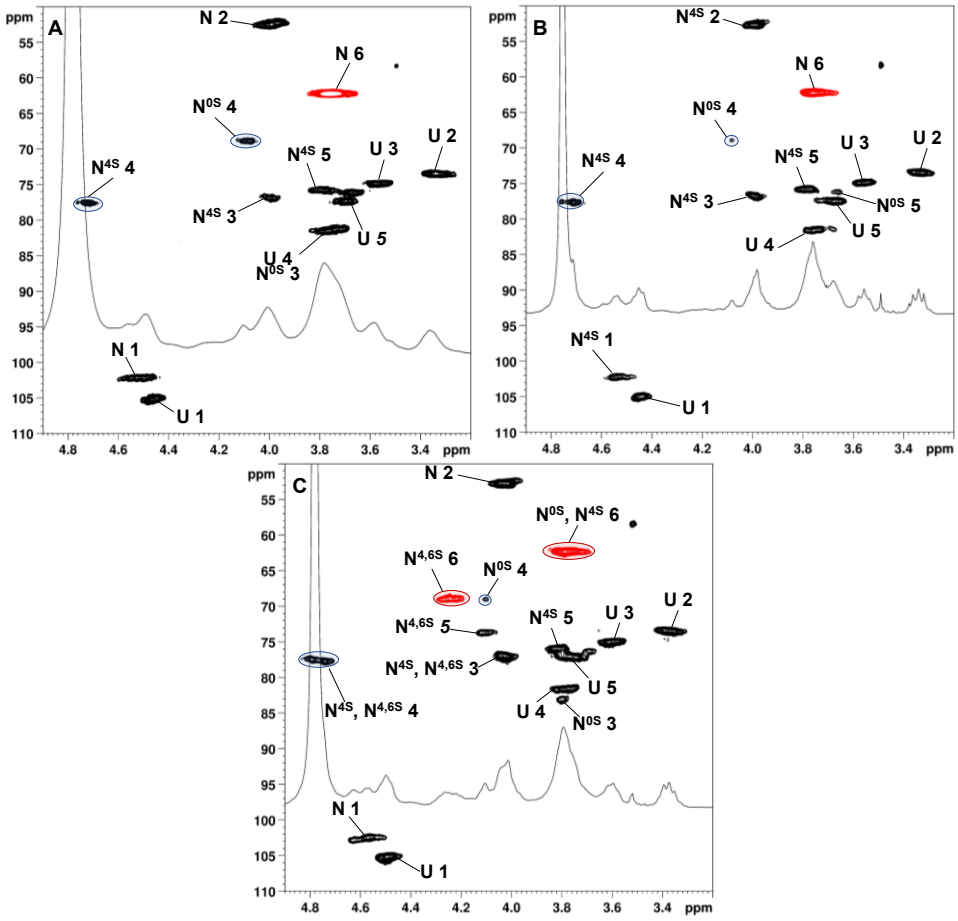

Figure 2.8. ^{1}H and $^{1}H,^{13}C$-DEPT-HSQC NMR spectra (600 MHz, D_2O, 298 K, zoom) of (A) **CS-2b**, (B) **CS-2e**, (C) **CS-2f**. Letter N is referred to 4,6-di-*O*-sulfated (if present), 4-*O*-sulfated and unsulfated GalNAc (when specified, superscripts 4,6S, 4S and 0S indicate the sulfation pattern on GalNAc). Densities enclosed in the highlighted areas of the HSQC-DEPT spectrum were integrated for estimation of 4S/4-OH (blue areas) and 6S/6-OH ratios (red areas). (See Paragraph 2.4.4 for full NMR assignments).

Table 2.3. Yield and structural features of semi-synthetic **CS-2a–f**.

Product	Acylating conditions	Yield [a]	4S/4-OH ratio [b]	6S/6-OH ratio [c]	CS-A	CS-0
CS-2a	BzCN (10 eq), rt, o.n.	45%	55:45	n.d. [d]	55%	45%
CS-2b	BzCN (10 eq), 4 °C, 4h	30%	53:47	n.d. [d]	53%	47%
CS-2c	BzCN (5 eq), rt, 4 h	53%	82:18	n.d. [d]	82%	18%
CS-2d	BzCN (2.5 eq), rt, 4 h	37%	90:10	13:87	n.a. [e]	n.a. [e]
CS-2e	PivCl (5 eq), rt, 4 h	19%	86:14	n.d. [d]	86%	14%
CS-2f	PivCl (5 eq), 4 °C, 4 h	40%	87:13	29:71	n.a. [e]	n.a. [e]

[a] Overall weight yield determined over 7 steps from product **2**. [b] Estimated as the percentage ratio between the integral of GalNAc4S *CH*-4 peak volumes and the integral of GalNAc0S *CH*-4 peak volume in the $^{1}H,^{13}C$-DEPT-HSQC spectrum. [c] Estimated as the percentage ratio between the integral of GalNAc6S CH_2-6 peak volumes and the integral of GalNAc0S and GalNAc4S CH_2-6 peak volume in the $^{1}H,^{13}C$-DEPT-HSQC spectrum. [d] not detected. [e] not assessable.

In order to complete all the possible sulfation patterns on GalNAc units, the preparation of a CS-C polysaccharide, showing the sulfate group on GalNAc *O*-6 position, was also accomplished. It is very well known in literature that the free *O*-6 position of GalNAc units on CS from different sources could be sulfated regioselectively by reacting their tri- or tetrabutylammonium salts with SO_3·DMF or SO_3·pyridine complex in DMF at 0–10 °C (Nagasawa et al., **1986**; Valoti et al., **2014**) or using the less reactive SO_3·NMe_3 complex in formamide (Cai et al., **2012**). Hence, microbial chondroitin was first converted into the corresponding tretrabutylammonium salt **9**, by adding some drops of a TBAOH solution (16% *w*/*v* TBAOH in water) to an aqueous solution of the polysaccharide in its acid form. This step allowed to obtain a polysaccharide derivative with an increased solubility in polar organic solvents with respect to the starting chondroitin polysaccharide. Then, derivative **9** was subjected to the sulfation step, under milder conditions with respect to the standard ones, *i.e.* with a solution of SO_3·pyridine complex in DMF for 1 hour at r.t. After neutralization and addition of an aqueous solution of NaCl, to allow the cation re-exchange, dialysis and freeze-drying gave product **CS-3** (Scheme 2.4).

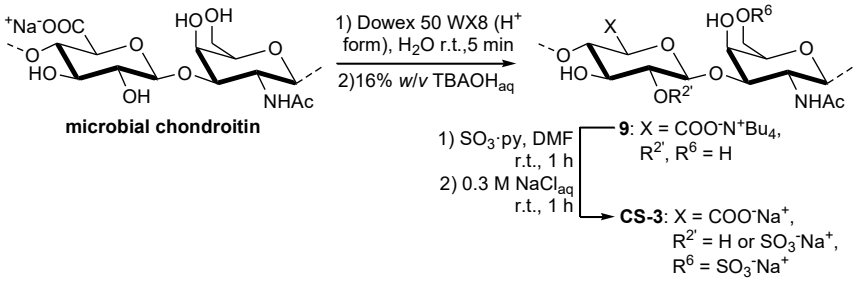

Scheme 2.4. Semi-synthesis of **CS-3** polysaccharide through a mild sulfation approach.

Structural characterization of **CS-3** by 2D-NMR investigation allowed to confirm the desired sulfation pattern with the presence of typical signals of 6-*O*-sulfated GalNAc units, in agreement with literature data (Figure 2.9, see Paragraph 2.4.4 for full NMR assignments) (Mucci et al., **2000**). Moreover, the additional presence of signals attributable to 2-*O*-sulfated GlcA units was detected and estimated to count for 43% of total GlcA residues in **CS-3**, as the percentage ratio between the integral of GlcA *CH*-2 peak volume and the sum of GlcA2S and GlcA *CH*-2 peak volumes in the $^{1}H,^{13}C$-DEPT-HSQC spectrum. This outcome was in agreement with the results reported by Valoti and co-workers, showing the concomitant 2-*O*-sulfation on GlcA units of a chondroitin polysaccharide under mild sulfation conditions (Valoti et al., **2014**).

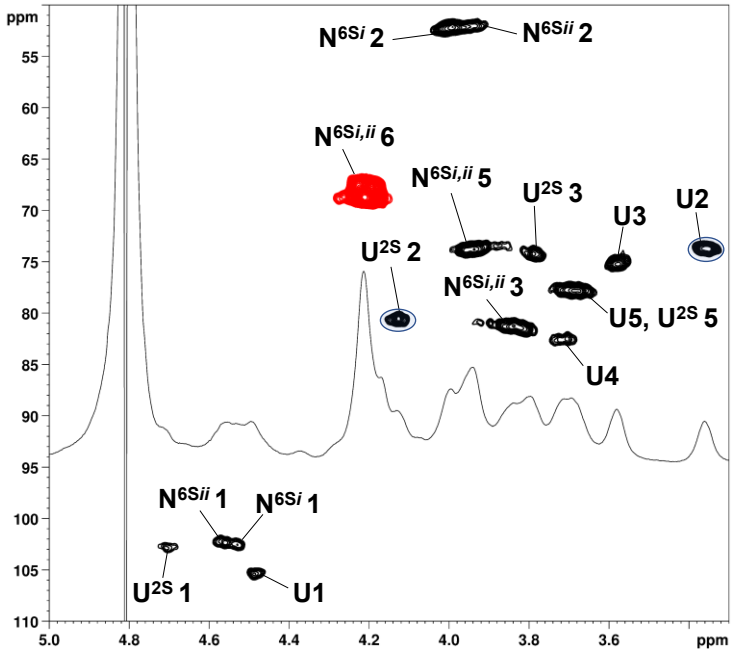

Figure 2.9. ^{1}H and ^{1}H,^{13}C-DEPT-HSQC NMR spectra (600 MHz, D_2O, 298 K, zoom) of **CS-3**. 2S and 6S superscripts represent the sulfated position in GlcA and GalNAc respectively; the superscripts *i* and *ii* represent the same residue type with different neighbouring residues. (Densities enclosed in the highlighted areas of DEPT-HSQC spectrum were integrated for estimation of GlcA2S percentage amount).

2.2.1.2. Semi-synthesis of CS-R, CS-V, and CS-U

Access to CS polysaccharides, bearing sulfate group(s) on GlcA units, has also been accomplished. In order to have a single sulfate group *per* disaccharide unit at GlcA *O*-2 or *O*-3 sites, the regioselective protection of either OH-2 or OH-3 of the GlcA 2,3-diol has been required. The difference in reactivity between such hydroxyls is subtler than between those at positions *C*-4 and *C*-6 of GalNAc moieties. Indeed, the latter diol is composed of a primary and a secondary, axially oriented alcohol, with the former hydroxyl much more nucleophilic toward a regioselective sulfation (Benito-Arenas et al., **2018**; Valoti et al., **2014**) or protection (Zoppetti and Oreste, **2004**), as also discussed above. On the contrary, the 2,3-*O*-β-*gluco*-configured diol of CS presents two secondary hydroxyls, both

displaying an equatorial orientation and also both flanked by equatorial glycosidic substituents. For these reasons, the regioselective protection of such secondary hydroxyl groups is still an unsolved problem and it is particularly troublesome also on β-Glc and β-GlcA monosaccharide structures (Chen et al., **2014**; Daly et al., **2013**; Ren et al., **2016**). Nonetheless, the differentiation between *O*-2 and *O*-3 in such diol was already accomplished on cellulose, for which a marked regioselective protection of *O*-2 (together with *O*-6) alcohol with respect to *O*-3 could be gained by silylation with bulky TDMSCl under homogeneous conditions in LiCl/DMAc or pyridine (Koschella and Klemm, **1997**). For our purposes, cellulose chemistry can be considered as a simplified model, since its →4)-β-Glc-(1→ repeating unit resembles quite well the β-1→4-linked GlcA residue of chondroitin.

Hence, we decided to investigate whether a regioselective silylation could be achieved also on the chondroitin backbone. To this aim, polysaccharide **4**, prepared according to the reaction sequence depicted in Scheme 2.1 (Laezza et al., **2016**), was subjected to a reaction with differently hindered trialkylsilyl chlorides (TBDMSCl, TDMSCl and TIPSCl) and imidazole as catalyst, in DMF (Scheme 2.5). Silyl ether installation regioselectivity on the polysaccharide could not be easily evidenced by NMR since no significant shift is usually observed for the ^{1}H and ^{13}C atom at the silylated position with respect to the unreacted one. Therefore, polysaccharides **10a–c**, recovered from the reaction mixture by precipitation, were directly subjected to sulfation of the free alcohols with SO_3·pyridine complex in DMF, followed by global deprotection under acid and then alkaline hydrolytic conditions to give, after purification by dialysis, semi-synthetic **CS-4a–c** (Scheme 2.5). A differentiation of *O*-2 and *O*-3 reactivity on GlcA residue was pursued also by acylation reactions, conducted under conditions recently shown to give a good regioselectivity on diols and polyols of monosaccharides and glycoconjugates, including the selective acylation of the

alcohol at the position 3 of β-configured Glc glycosides (Ren et al., **2018**, **2014**). In particular, a hydrogen-bond driven regioselective acetylation or benzoylation was attempted on polysaccharide **4**, by treatment with Ac_2O and TBAOAc (Ren et al., **2014**) or Bz_2O and DIPEA (Ren et al., **2018**), respectively (Scheme 2.5). After purification of the intermediate polysaccharides **10d**,**e** by precipitation from the crude reaction mixture, sulfation and global deprotection gave, after purification by dialysis, **CS-4d**,**e**. Finally, a further semi-synthetic CS (**CS-5**) was prepared by direct sulfation of polysaccharide **4**, followed by global deprotection (Scheme 2.5); **CS-5** should provide a standard for the unprecedented CS-R polysaccharide showing exclusively 2,3-disulfated GlcA residues.

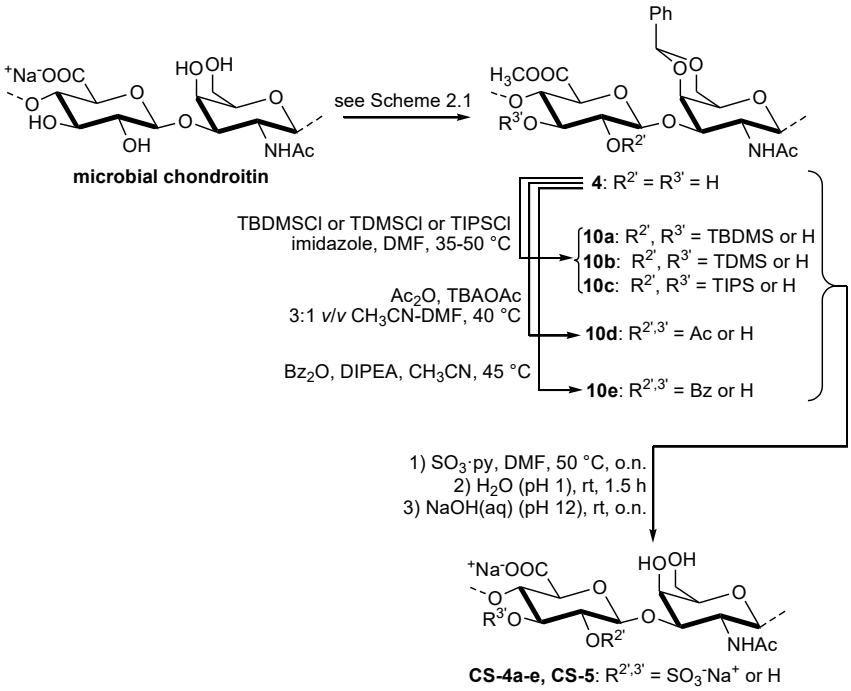

Scheme 2.5. Semi-synthesis of **CS-4a–e**, **CS-5** polysaccharides through GlcA 2,3-diol regioselective protection by silylation or acylation.

All the obtained CS polysaccharides were then subjected to a deep structural characterization through an extensive 2D-NMR spectroscopy investigation.

CS- 5 2D-NMR spectra were first studied. The anomeric CH region of the $^{1}H,^{13}C$-DEPT-HSQC spectrum displayed two signals at $\delta_{H,C}$ 5.04/102.4 and 4.65/104.7 ppm (Figure 2.10). The latter could be attributed to a non-sulfated GalNAc unit by means of a HSQC-TOCSY spectrum showing a correlation with the CH signal at $\delta_{H,C}$ 4.06/52.2 ppm, attributable to GalNAc *CH*-2, which in turn was connected to typical signals of a non-sulfated GalNAc residue (Mucci et al., **2000**) (see Paragraph 2.4.4 for full NMR signal assignments). The former anomeric signal ($\delta_{H,C}$ 5.04/102.4 ppm) could be correlated to a density at $\delta_{H,C}$ 4.47/79.0 ppm, which in turn was connected to the one at $\delta_{H,C}$ 5.12/77.0. The high downfield shift of all these three signals, with respect to the ones reported for non-sulfated GlcA units in CS (Mucci et al., **2000**), was indicative of a 2,3-disulfate decoration as expected for **CS-5**. Finally, minor signals clearly attributable to the GalNAc6S unit ($\delta_{H,C}$ 4.28/67.8 and 4.07/73.5 ppm for CH_2-6 and *CH*-5, respectively) could be found in the $^{1}H,^{13}C$-DEPT-HSQC spectrum. Their presence was hypothetically related to a slow cleavage of a minor amount of the benzylidene rings on **4** catalysed by the Lewis acidity of SO_3 during the sulfation reaction. The ratio between GalNAc and GalNAc6S units in **CS-5** was estimated to be 91:9 by $^{1}H,^{13}C$-DEPT-HSQC 2D-NMR integration of the CH_2-6 signals relative to the two kinds of residues.

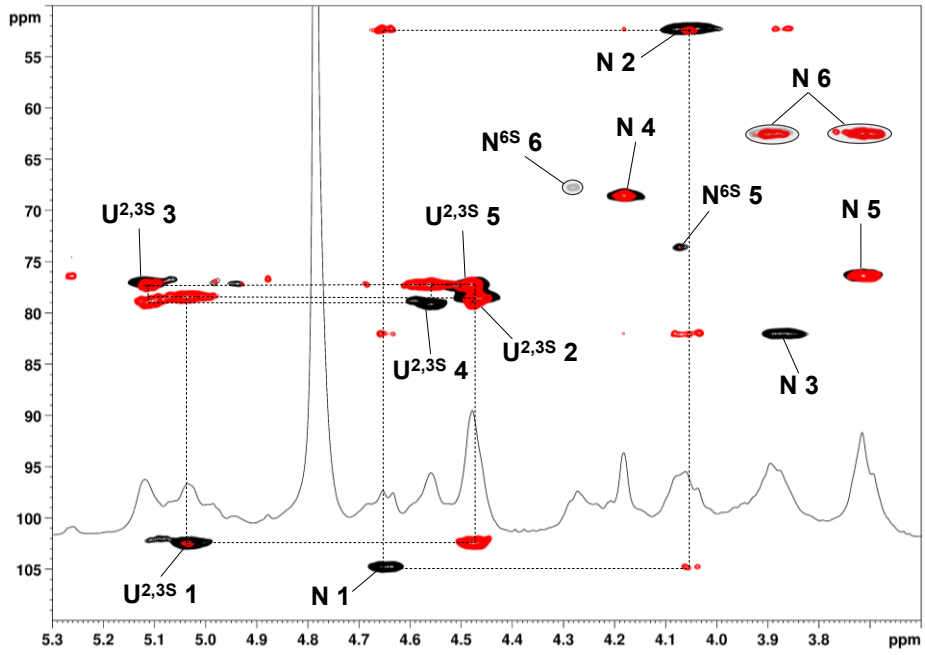

Figure 2.10. ^{1}H, DEPT-HSQC (black and grey), and HSQC-TOCSY (red) NMR spectra (400 MHz, D_2O, 298 K, zoom) of **CS-5** (= CS-R). 2,3S and 6S superscripts represent the sulfated position in GlcA and GalNAc, respectively. (Densities enclosed in the highlighted areas of ^{1}H,^{13}C-DEPT-HSQC spectrum were integrated for GalNAc/GalNAc6S ratio estimation; only some of the HSQC-TOCSY correlations are highlighted with dotted lines).

With the complete assignment of ^{1}H and ^{13}C NMR signals of the CS-R standard in hand, the study of **CS-4a–e** NMR spectra was then pursued. They furnished more complicated ^{1}H,^{13}C-DEPT-HSQC spectra with more than two signals displayed in the anomeric region. In particular, **CS-4a** showed anomeric signals at $\delta_{H,C}$ 5.05/102.4, 4.82/102.9, and 4.70/105.1 ppm, that, by the help of HSQC-TOCSY, COSY, and TOCSY correlations (see Figure 2.11 for ^{1}H,^{13}C-DEPT-HSQC and HSQC-TOCSY superimposition), could be assigned to GlcA2,3S, GlcA2S, and GlcA3S, respectively. The relative integration of the well-resolved signals assigned to *CH*-3 of these three residues in the ^{1}H,^{13}C-DEPT-HSQC spectrum indicated a slight preponderance of GlcA3S units over the other two

monosaccharides along the **CS-4a** polymer chain (Table 2.4). Under the highly realistic hypothesis that the sulfation reaction is not able to discriminate between the hydroxyls at positions 2 and 3 of GlcA units, the result obtained on **CS-4a** could be correlated with a slight preference of 2-*O*- *vs.* 3-*O*-protection in the TBDMS installation reaction, since GlcA2S, GlcA3S, and GlcA2,3S residues should derive from 3-*O*-, 2-*O*-, and not protected units in synthetic intermediate **10a**, respectively.

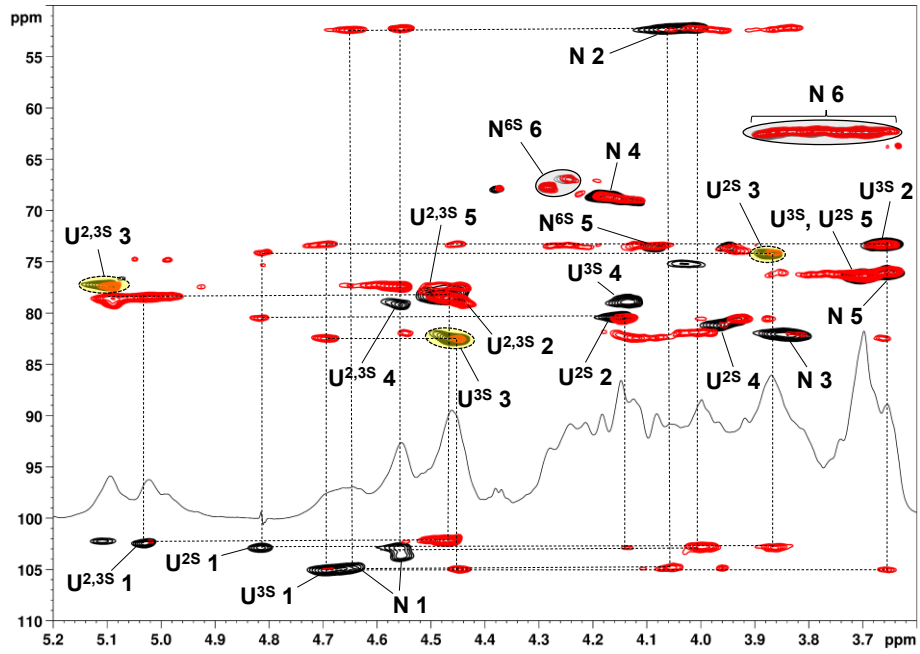

Figure 2.11. ^{1}H, ^{1}H,^{13}C-DEPT-HSQC (black and grey) and HSQC-TOCSY (red) NMR spectra (600 MHz, D_2O, 298 K, zoom) of **CS-4a**. 2S/3S/2,3S and 6S superscripts represent the sulfated position in GlcA and GalNAc, respectively. (Densities enclosed in the highlighted yellow and grey areas of the ^{1}H,^{13}C-DEPT-HSQC spectrum were integrated for GlcA2S/GlcA3S/GlcA2,3S and GalNAc/GalNAc6S ratio estimation, respectively; only some of the HSQC-TOCSY correlations are highlighted with dotted lines).

The 2-*O*/3-*O*-regioselectivity could be similarly estimated also for TDMS protection of **4** to **10b** (see Table 2.4) since the resulting polysaccharide **CS-4b**

showed a $^{1}H,^{13}C$-DEPT-HSQC NMR spectrum very similar to the **CS-4a** one (see Figure 2.31A in Paragraph 2.4.4).

An evident hindrance effect was observed in the case of the bulkiest TIPS group. Indeed, the $^{1}H,^{13}C$-DEPT-HSQC spectrum of **CS-4c** polysaccharide was very similar to the CS-R standard one (see Figure 2.31B in Paragraph 2.4.4), displaying almost exclusively densities related to 2,3-disulfated GlcA units that should derive from non-protected residues in **10c**. A DS_{TIPS} equal or slightly higher than zero could be therefore estimated for the semi-synthetic intermediate **10c**. Actually, **CS-4c** ^{1}H NMR spectrum clearly showed the presence of a small signal at δ 1.09 ppm (see Figure 2.31B in Paragraph 2.4.4), attributable to the six methyl groups of the residual TIPS group. Its presence is reasonably due to the much higher stability reported for such silyl ethers with respect to TBDMS one under both acidic and alkaline hydrolytic conditions (Cunico and Bedell, **1980**). A relative integration of this peak with the one at δ 2.05 ppm, assigned to the methyl group of GalNAc *N*-acetyl, returned a DS_{TIPS} = 0.06 for **CS-4c**; similarly, a residual DS_{TDMS} = 0.02 could be assigned for **CS-4b** by careful analysis of its ^{1}H NMR spectrum. As regards **CS-4d** and **CS-4e** polysaccharides obtained from partially acylated derivatives **10d** and **10e**, respectively (Scheme 2.5), a low regioselectivity of protection could be inferred also in this case. In particular, together with GlcA2S, GlcA3S, and GlcA2,3S as for **CS-4a–c** and **-4e**, also the presence of unsulfated GlcA residues along the polymer could be detected for **CS-4d** (Table 2.4, see also Figure 2.32A,B in Paragraph 2.4.4). This agrees with the possibility to have also 2,3-diprotected (di-*O*-acetylated) GlcA residues in **10d** due to a minor hindrance of Ac esters with respect to silyl ethers and Bz esters.

Table 2.4. Yield and structural features of semi-synthetic **CS-4a–e** and **CS-5**.

	CS-4a	**CS-4b**	**CS-4c**	**CS-4d**	**CS-4e**	**CS-5**
GlcA protecting group	TBDMS	TDMS	TIPS	Ac	Bz	--
%Weight yield (from **4**)	69%	35%	44%	82%	66%	88%
%GlcA2S [a]	26%	24%	n.d. [g]	25%	17%	n.d. [g]
%GlcA3S [b]	43%	32%	n.d. [g]	34%	6%	n.d. [g]
%GlcA2,3S [c]	31%	44%	100%	28%	77%	100%
%GlcA [d]	n.d. [g]	n.d. [g]	n.d. [g]	13%	n.d. [g]	n.d. [g]
GalNAc/GalNAc6S ratio [e]	78:22	87:13	88:12	89:11	91:9	91:9
2-*O*/3-*O* protection regioselectivity for 6a–e [f]	1.7	1.3	1.0	1.2	0.4	--

[a] Estimated as the percentage ratio between the integral of GlcA2S *CH*-3 peak volume and the sum of GlcA2S, GlcA3S, GlcA2,3S, and GlcA *CH*-3 peak volumes in the $^{1}H,^{13}C$-DEPT-HSQC spectrum. [b] Estimated as the percentage ratio between the integral of GlcA3S *CH*-3 peak volume and the sum of GlcA2S, GlcA3S, GlcA2,3S, and GlcA *CH*-3 peak volumes in the $^{1}H,^{13}C$-DEPT-HSQC spectrum. [c] Estimated as the percentage ratio between the integral of GlcA2,3S *CH*-3 peak volume and the sum of GlcA2S, GlcA3S, GlcA2,3S, and GlcA *CH*-3 peak volumes in the $^{1}H,^{13}C$-DEPT-HSQC spectrum. [d] Estimated as the percentage ratio between the integral of GlcA *CH*-3 peak volume and the sum of GlcA2S, GlcA3S, GlcA2,3S, and GlcA *CH*-3 peak volumes in the DEPT-HSQC spectrum. [e] Estimated as the ratio between the integral of GalNAc and GalNAc6S CH_2-6 peak volumes in the $^{1}H,^{13}C$-DEPT-HSQC spectrum. [f] Estimated as [%GlcA3S + %GlcA)]/[%GlcA2S + %GlcA] taking into account that GlcA2S, GlcA3S, and GlcA residues derive from a 3-*O*-, 2-*O*-, and 2,3-di-*O*-protected unit, respectively. [g] Not detected.

In the light of these unsatisfying results, it was necessary to change the approach and, looking at literature, we found a recently paper reporting the regioselective installation of a Bz ester at the position *O*-2 of the two or three GlcA residues in partially protected tetra- or hexasaccharide chondroitin derivatives, respectively, through a 3,6-lactonization/2-*O*-benzoylation/lactone opening one-pot sequence (Zhang et al., **2018a**). So, we decided to test whether this procedure could be extended from the tetra- and hexasaccharide cases to the polysaccharide structure. To this aim, chondroitin derivative **3**, prepared following the reaction sequence depicted in Scheme 2.1 (Bedini et al., **2011**), was treated with Bz_2O in DMF at 85 °C to form a 3,6-lactone on GlcA residues, followed by one-pot addition first of

DMAP and pyridine to allow 2-*O*-benzoylation and then of NaOAc and methanol to perform lactone opening and obtain derivative **11** with a free hydroxyl restored at the position 3 (Scheme 2.6). ^{1}H and ^{1}H,^{13}C-DEPT-HSQC NMR spectra clearly showed a homogeneous structure for derivative **11** (see Figure 2.12A and Paragraph 2.4.4 for full NMR signal assignments), with well resolved signals and a single downfield-shifted carbinol signal, which could be assigned to *CH*-2 of GlcA residues by means of COSY and TOCSY spectra, as expected by the 2-*O*-benzoylation.

By employing the same 3,6-lactonization reaction, but without the following benzoylation and lactone cleavages, it was possible to obtain derivative **12**, possessing a single hydroxyl at the position 2 of GlcA residues. Also in this case, the ^{1}H and ^{1}H,^{13}C-DEPT-HSQC NMR spectra displayed a homogeneous polysaccharide with well-resolved signals (see Figure 2.12B and Paragraph 2.4 for full NMR signal assignments) that could be assigned through COSY and TOCSY spectra. In addition, in the HMBC spectrum, a correlation between GlcA *CH*-3 signal at $\delta_{H,C}$ 4.76/73.1 ppm and a C=O signal δ_{C} 170.5 ppm (see Figure 2.33 in Paragraph 2.4.4) clearly demonstrated the presence of the 3,6-lactone ring on GlcA residues.

The two polysaccharide derivatives **11** and **12**, having a single hydroxyl per disaccharide repeating unit at positions 2 and 3 of the GlcA residue, respectively, were subjected to sulfation under standard conditions with SO_3·pyridine complex in DMF and then to a global deprotection under acidic and then alkaline hydrolytic conditions (Scheme 2.6). As regards the last step, an overnight treatment with aqueous NaOH solution (pH 12) allowed a complete de-*O*-acylation in the case of **12** to **CS-7** conversion, whereas Bz esters at *O*-2 proved to be rather recalcitrant to hydrolysis since after the same alkaline treatment a large amount of 2-*O*-acylated GlcA units remained unaffected (data not shown). A longer reaction time gave no increase in the extent of 2-*O*-acylation, whereas performing the reaction

at higher temperature (40 °C instead of r.t.) caused extensive polysaccharide depolymerization reasonably due to α,β-eliminative cleavage of 1→4 glycosidic bonds, with an almost total loss of the sample after dialysis purification. Finally, employment of an aqueous solution of lithium hydroperoxide (obtained *in situ* from LiOH and H_2O_2) followed by a treatment with aqueous NaOH at r.t. overnight (Tully et al., **2004**), allowed complete debenzoylation without a significant depolymerization and gave semi-synthetic **CS-6** after purification by dialysis (Scheme 2.6).

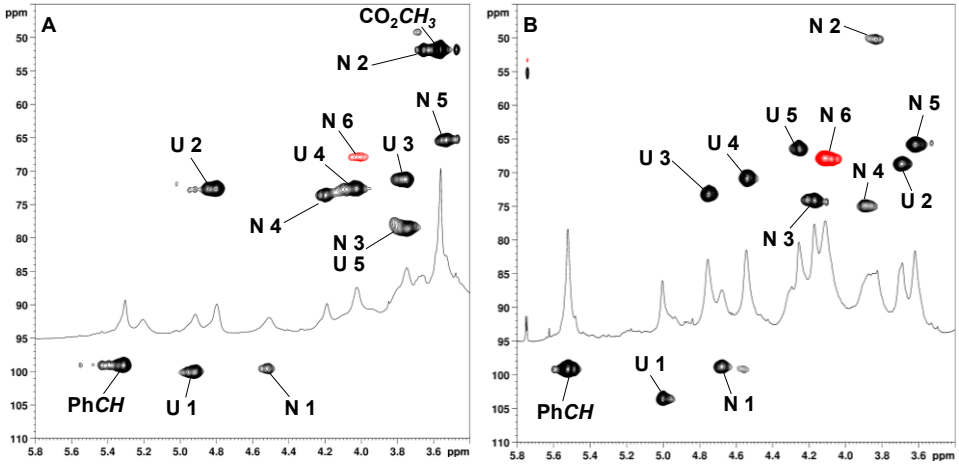

Figure 2.12. ^{1}H and $^{1}H,^{13}C$-DEPT-HSQC NMR spectra (600 MHz, DMSO-d_6, 298 K, zoom) of (A) **11** and (B) **12**.

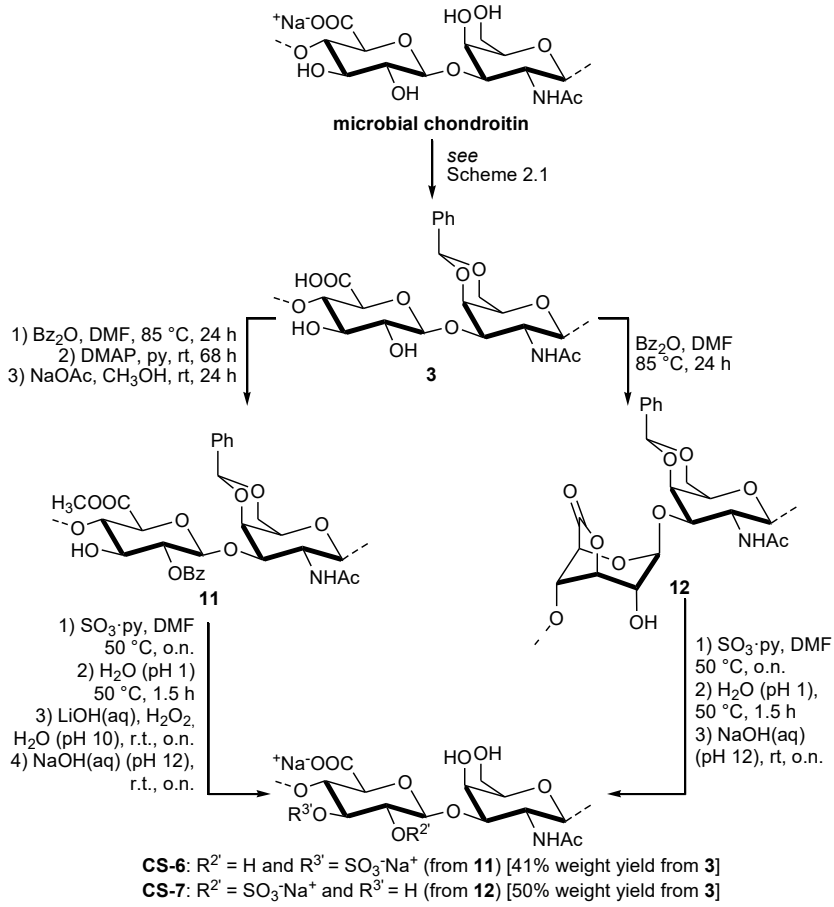

Scheme 2.6. Semi-synthesis of **CS-6,7** polysaccharides through GlcA regioselective protection by 3,6-lactonization.

Structural characterization of **CS-6** and **CS-7** by 2D-NMR analysis and comparison with data obtained for **CS-4-a–e** and **CS-5** confirmed the presence of a single sulfate group per disaccharide repeating unit at the GlcA *O*-2 position in **CS-7** and *O*-3 position in **CS-6** (see Figure 2.13 and Paragraph 2.4.4 for full NMR assignments). These sulfation patterns, obtained for the first time by a semi-synthetic strategy, are indicated as CS-U and CS-V, respectively. The presence of minor signals related to unsulfated GlcA unit, presumably due to a non-exhaustive sulfation, was also detected and estimated to count for 15% of total GlcA residues

in **CS-7**, as the percentage ratio between the integral of GlcA *CH*-2 peak volume and the sum of GlcA2S and GlcA *CH*-2 peak volumes in the $^{1}H,^{13}C$-DEPT-HSQC spectrum.

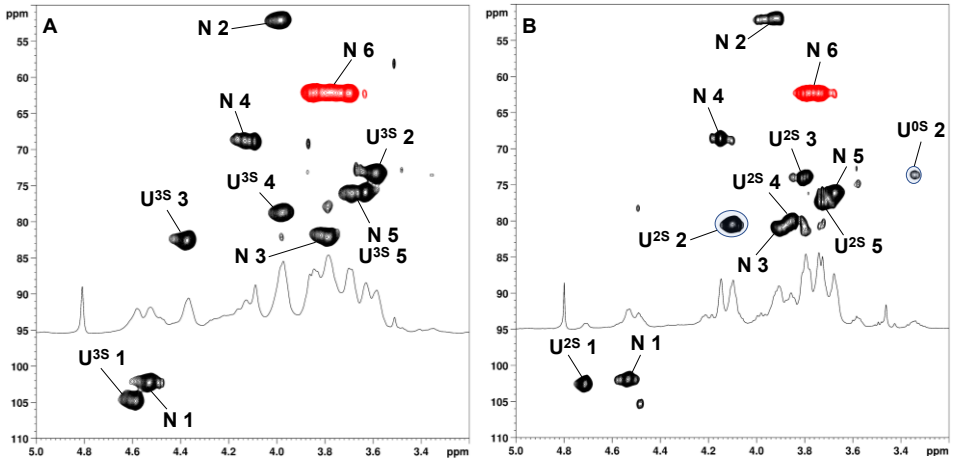

Figure 2.13. ^{1}H and $^{1}H,^{13}C$-DEPT-HSQC NMR spectra (600 MHz, D_2O, 298 K, zoom) of (A) **CS-6** (= CS-V) and (B) **CS-7** (= CS-U). 2S and 3S superscripts represent the sulfated position in GlcA. (Densities enclosed in the highlighted areas of the $^{1}H,^{13}C$-DEPT-HSQC spectrum were integrated for estimation of GlcA and GlcA2S percentage amount).

2.2.1.3 Semi-synthesis of CS-S′, CS-L, and CS-D

For the access to CS polysaccharides bearing sulfate groups both on GlcA and GalNAc positions in each subunit, a careful combination of the previously described regioselective steps could be carried out.

First of all, semi-synthetic **CS-5** (= CS-R), **CS-6** (= CS-V), and **CS-7** (= CS-U) could be employed for the preparation of chondroitin polysaccharide with CS-S′, CS-L and CS-D sulfation pattern, respectively, differencing from the first ones only for the presence of an additional sulfate group at the primary *O*-6 position of each GalNAc units. To this aim, the mild sulfation procedure, already used for the obtainment of **CS-3**, could be performed. Hence, **CS-5,6,7** were converted into the corresponding tetrabutylammonium salt to give products **13**, **14**, and **15**,

respectively, that were subjected to the regioselective sulfation step under the reaction conditions similar to the ones previously described for **CS-3**, affording **CS-8**, **CS-9**, and **CS-10**, respectively. In this case, to avoid a collateral sulfation at secondary positions, the reaction temperature was decreased at 4 °C (Scheme 2.7).

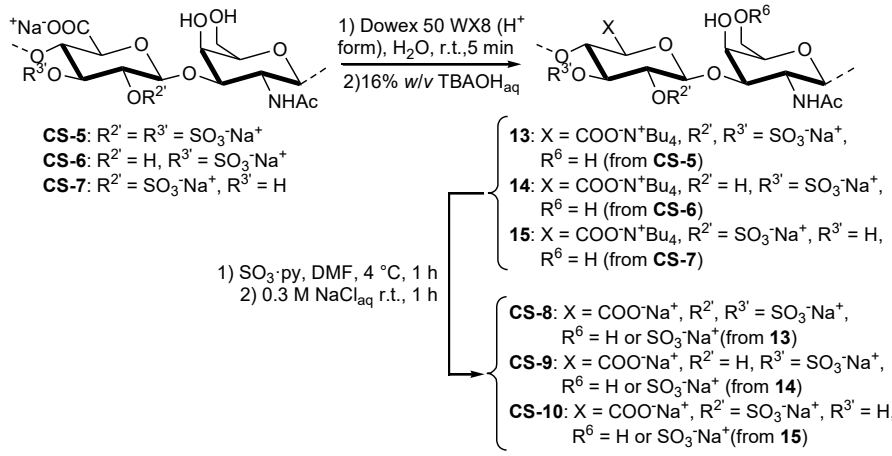

Scheme 2.7. Semi-synthesis of **CS-8,9,10** through mild sulfation approach.

Structural characterization of **CS-8**,**9**,**10** was accomplished by 2D-NMR analysis. Their $^{1}H,^{13}C$-DEPT-HSQC spectra were similar to those obtained for the corresponding starting semi-synthetic CSs, with, as expected, the additional presence of signals typical of 6-*O*-sulfated GalNAc units (Figure 2.14). In particular, in each $^{1}H,^{13}C$-DEPT-HSQC spectrum the presence of downfield shifted signals in antiphase with respect to the other densities ($\delta_{H,C}$ 4.20/67.6 ppm, 4.21/67.5 ppm, 4.21/68.6 ppm for **CS-8**, **CS-9** and **CS-10**, respectively), attributable to sulfated carbinolic protons at position 6 of GalNAc units, could be revealed. However, also the presence of other signals in antiphase could be evidenced in all the three $^{1}H,^{13}C$-DEPT-HSQC spectra; by comparison with data obtained for **CS-5**, **CS-6**, and **CS-7** these signals ($\delta_{H,C}$ 3.68–3.90/62.6 ppm, 3.67–3.88/62.4 ppm, 3.72 –3.80/62.4 ppm for **CS-8**, **CS-9** and **CS-10**, respectively)

could be easily assigned to unsulfated CH_2-6 position of GalNAc units (see Paragraph 2.4.4 for full NMR assignments). By $^{1}H,^{13}C$-DEPT-HSQC integration, the ratio between GalNAc6S and GalNAc0S units in **CS-8**, **CS-9**, **CS-10** was estimated to be 56:44, 23:77, 84:16, respectively. Under the highly realistic hypothesis that the GlcA sulfation pattern remains unaffected after the mild sulfation protocol, as also confirmed by 2D-NMR analysis, the GalNAc6S/GalNAc0S ratios is also an estimation of the percentage of CS-S′, CS-L or CS-D subunits along the whole polysaccharide chain (see Table 2.5).

Table 2.5. Disaccharide composition and sulfation pattern of semi-synthetic **CS-3**,**8–10**.

Entry	Product	Starting sulfation pattern	Final sulfation pattern	Ratio
i	**CS-3**	GlcA-GalNAc (**CS-0**)	GlcA-GalNAc6S/ GlcA2S-GalNAc6S (**CS-C,D**)	100
ii	**CS-8**	GlcA2,3S-GalNAc (**CS-R**)	GlcA2,3S-GalNAc6S/ GlcA2,3S-GalNAc (**CS-S′,R**)	56:44 [a]
iii	**CS-9**	GlcA3S-GalNAc (**CS-V**)	GlcA3S-GalNAc6S/ GlcA3S-GalNAc (**CS-L,V**)	23:77 [b]
iv	**CS-10**	GlcA2S-GalNAc (**CS-U**)	GlcA2S-GalNAc6S/ GlcA2S-GalNAc (**CS-D,U**)	84:16 [b]

[a] Estimated as the ratio between the integral of GalNAc6S *CH*-5 peak volume and the integral of GalNAc *CH*-5 peak volume in the $^{1}H,^{13}C$-DEPT-HSQC spectrum. [b] Estimated as the ratio between the integral of GalNAc6S CH_2-6 peak volume and the integral of GalNAc CH_2-6 peak volume in the DEPT-HSQC spectrum.

The data summarized in Table 2.5, including also **CS-3**, evidenced the different behaviour of the diverse starting compounds towards the mild sulfation reaction. Although a high regioselectivity towards the primary GalNAc *O*-6 position was confirmed, the GalNAc6S/GalNAc ratio was particularly variable depending on the starting CS polysaccharide, with a quantitative 6-*O*-sulfation only in entry *i* where the unsulfated microbial chondroitin was employed. In the other three cases, the lower amount of GalNAc6S units, and the lower degree of sulfation, could be due to the presence of one or more sulfate groups, already installed on

the polysaccharide chain, hampering the quantitative insertion of a further negatively charged group.

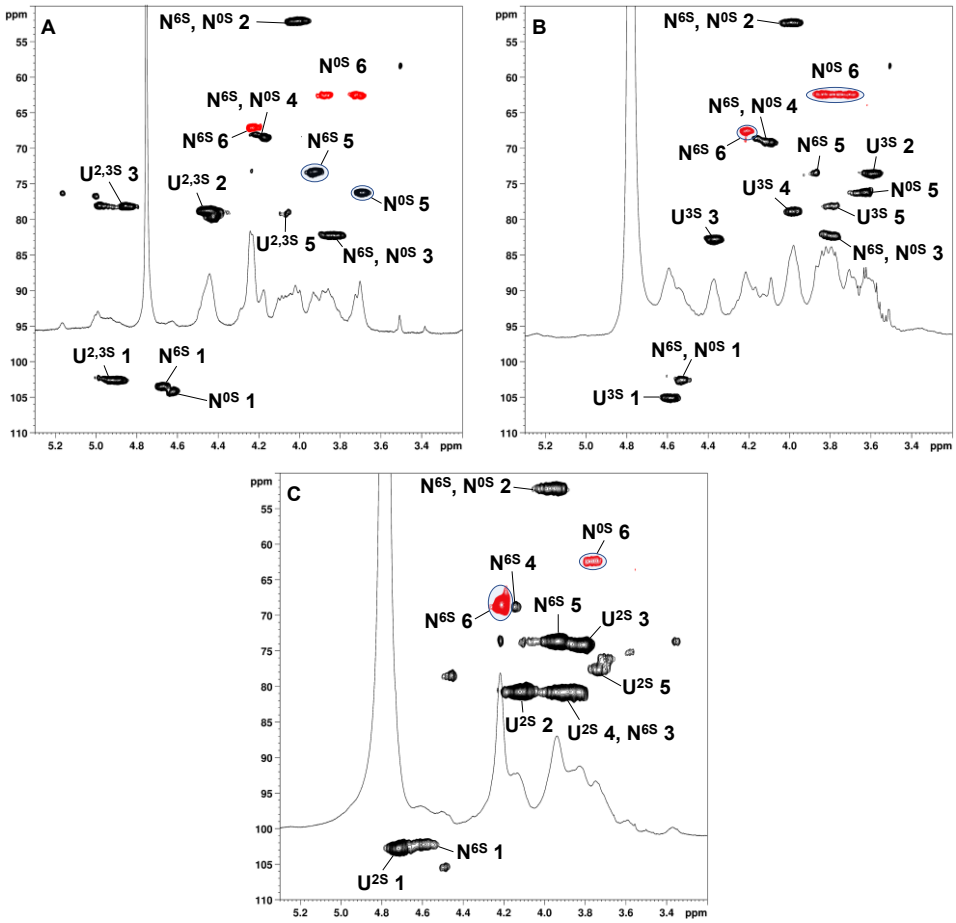

Figure 2.14. ^{1}H and $^{1}H,^{13}C$-DEPT-HSQC NMR spectra (400 MHz, D_2O, 298 K, zoom) of (A) **CS-8**, (B) **CS-9**, (C) **CS-10**. 2,3S/3S/2S and 6S/0S superscripts represent the sulfated position in GlcA and GalNAc, respectively. (Densities enclosed in the highlighted areas of the DEPT-HSQC spectra were integrated for GalNAc6S/GalNAc0S ratio estimation).

2.2.1.4. Semi-synthesis of CS-T and CS-M

A preliminary study for the obtainment of CS-T and CS-M sulfation patterns, showing sulfate group on GalNAc 4,6-diol and on GlcA *O*-2 or *O*-3, respectively,

was also attempted. Semi-synthetic CS polysaccharides with these sulfate group distribution could be prepared by sulfation of suitable protected CS polysaccharide intermediates, having a free *O*-2 or *O*-3 position on GlcA and the free GalNAc diol. Such derivatives could be obtained from the already prepared polysaccharides **11** and **12** by employing the benzylidene ring acid hydrolysis developed during this work.

To this aim, polysaccharides **11** and **12** were subjected to the same reaction conditions employed for benzylidene ring cleavage on **6** (90% aq. AcOH, 50 °C, 48 h, see Scheme 2.8,2.9). In the former case, a low degree of benzylidene cleavage (DBC = 31%) was estimated from ^{1}H NMR of **16-i** by relative integration of the methine proton signal at δ_H 5.30 ppm and the *N*-acetyl proton signals at δ_H 1.33–1.00 ppm (Figure 2.15). This behaviour was initially associated to the very low solubility of **11** in the reaction mixture, but even dissolving the polysaccharide in the minimum amount of DMF prior to aqueous acetic acid treatment, only a slight increase in the benzylidene ring removal was observed (product **16-ii**, DBC = 43%, see Scheme 2.8 and Figure 2.15). In the latter case, given the complexity of the ^{1}H NMR spectrum of polysaccharide product **17** (data not shown), no evaluation of the DBC could be accomplished, so **17** was directly subjected to sulfation under standard conditions with SO_3·pyridine complex in DMF and then to a global deprotection under acidic and then alkaline hydrolytic conditions giving **CS-11** (Scheme 2.9).

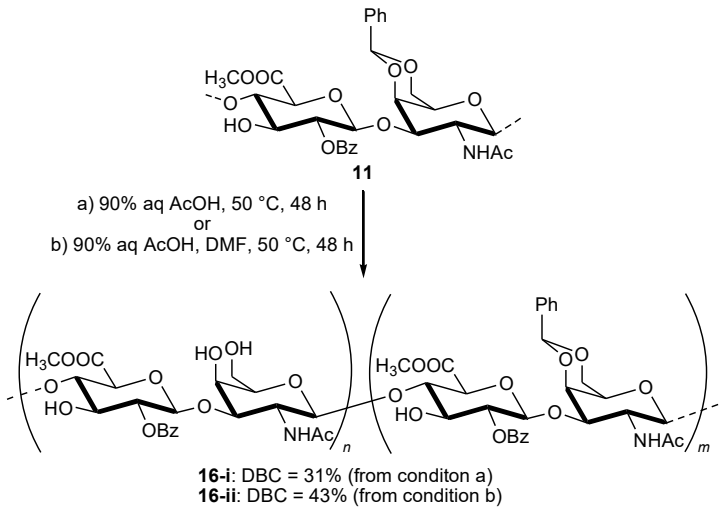

Scheme 2.8. Benzylidene ring opening tests on polysaccharide **11**.

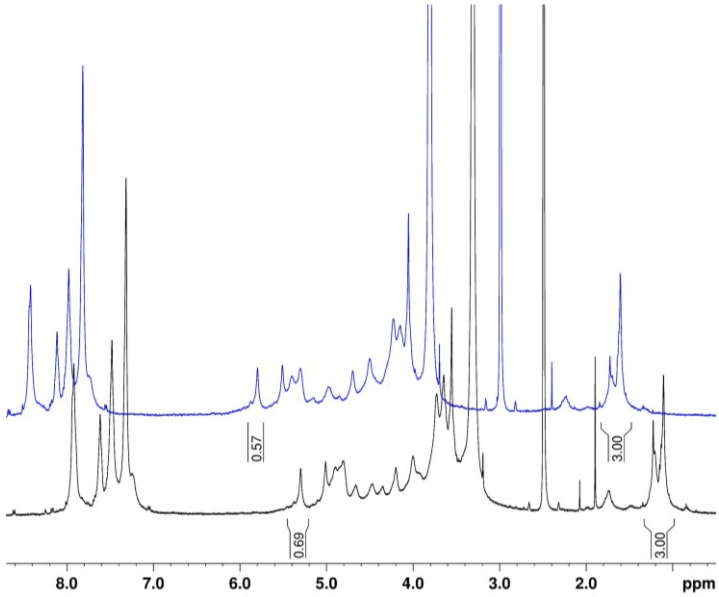

Figure 2.15. Stacked (with a $\Delta\delta$ = 0.25 ppm shift) ^{1}H NMR spectra (400 MHz, DMSO-d_6, 298 K) of **16-i** (black) and **16-ii** (blue).

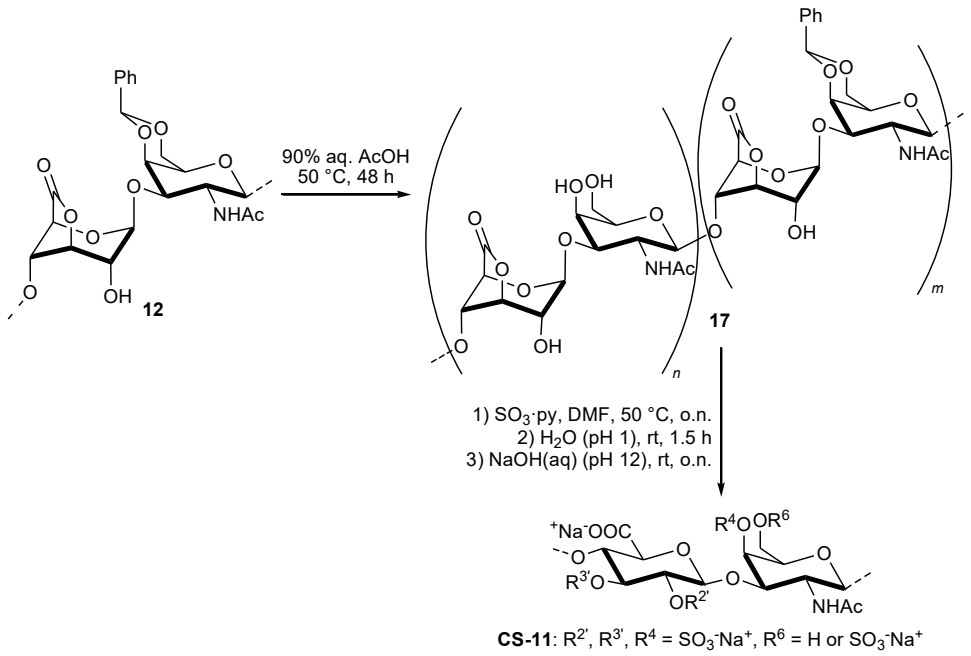

Scheme 2.9. Semi-synthesis of **CS-11**.

Structural characterization of **CS-11** by 2D-NMR analysis showed an unexpected sulfation pattern for this polysaccharide (Figure 2.16). In particular, by comparison with previous data (**CS-1** and **CS-5**), it was possible to assess the presence of sulfate groups at each hydroxyl position of **CS-11** (see Paragraph 2.4.4 for full NMR assignments). Particularly indicative were the signals attributed to *CH*-2 ($\delta_{H,C}$ 4.43/78.6 ppm) and *CH*-3 ($\delta_{H,C}$ 4.98/76.6) GlcA2,3S positions, which were high downfield shifted with respect both to monosulfated and unsulfated GlcA units. A minor sulfation pattern was also detected for GalNAc units by revealing the presence of additional antiphase signals ($\delta_{H,C}$ 3.90, 3.75/62.7 ppm), attributable to unsulfated CH_2-6 positions of GalNAc units. By $^{1}H,^{13}C$-DEPT-HSQC integration, it was possible to estimate that this minor sulfation pattern counted for 19% of the total GalNAc units. The per-sulfation on **CS-11** could be associated to an unexpected cleavage of the lactone ring on **12**, during the

benzylidene ring acid cleavage, likely due to a combination of the prolonged reaction time and the instability of the particularly strained lactone cycle.

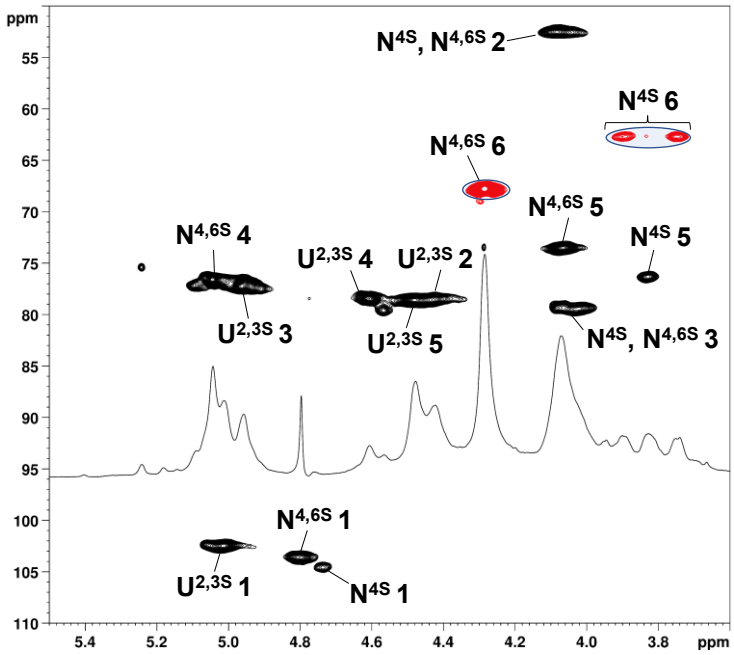

Figure 2.16. ^{1}H and $^{1}H,^{13}C$-DEPT-HSQC NMR spectrum (600 MHz, D_2O, 298 K, zoom) of **CS-11**. 2,3S and 4S/4,6S superscripts represent the sulfated position in GlcA and GalNAc, respectively. (Densities enclosed in the highlighted areas of the $^{1}H,^{13}C$-DEPT-HSQC spectra were integrated for estimation of GalNAc4S percentage amount).

It was so necessary to change the approach for the obtainment of CS-M and CS-T sulfation pattern, focusing the attention on the employment of a new cyclic protecting group for the GalNAc *O*-4,6 diol, that could be removed in a milder and/or different way. The *p*-methoxybenzylidene group was considered a good alternative since it is reported to undergo acid hydrolysis 10 times faster than the benzylidene group (Wuts, **2014**). So, the *p*-methoxybenzylidene group was installed on **1** under the same conditions optimized for benzylidene ring installation on chondroitin and employing *p*-methoxybenzaldehyde dimethyl acetal as the electrophilic reagent (Scheme 2.10). Product **18** was recovered by

precipitation and then analyzed by ^{1}H NMR; the presence of aromatic signals at δ_H 7.33, 6.91 ppm together with a broad peak centered at δ_H 5.46 ppm —the latter accounting for a benzylidene acetal hydrogen atom— confirmed the presence of the desired protecting group on the polysaccharide (Figure 2.17). Furthermore, a DS for the *p*-methoxybenzylidene group of 0.90 was evaluated from the integral areas measured for the aromatic ring (δ_H 7.33, 6.91 ppm) and methine (δ_H 5.46 ppm) proton signals and the *N*-acetyl (δ_H 1.76 ppm) signal in ^{1}H NMR spectrum, according to Equation 2.2. To the best of our knowledge, this was the first example of the *p*-methoxybenzylidene acetal formation on a polysaccharide structure with an almost quantitative DS.

$$\mathrm{DS} = \frac{\frac{\mathrm{I}(ArC\underline{H})}{\mathrm{I}(Ac)/3} + \frac{\sum \mathrm{I}(H\text{-}Ar)/5}{\mathrm{I}(Ac)/3}}{2} \qquad \text{(Eq. 2.2)}$$

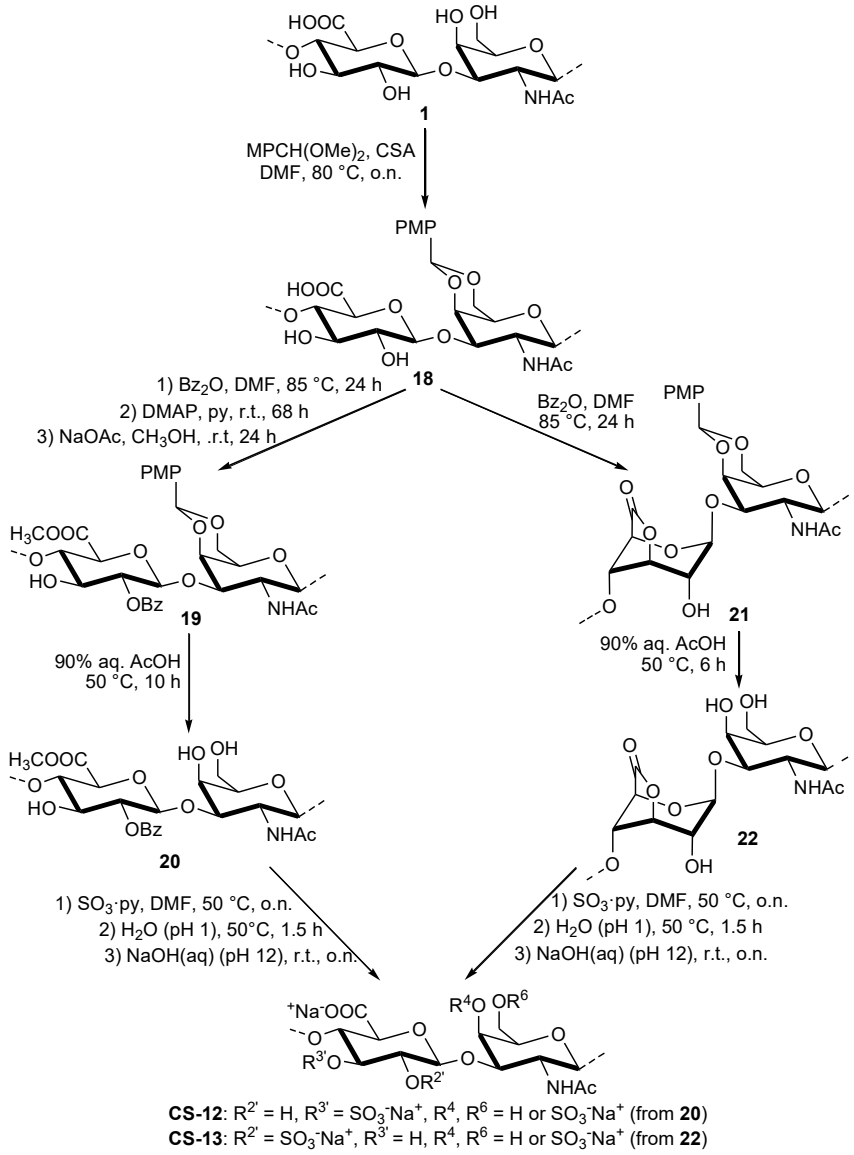

Scheme 2.10. Semi-synthesis of **CS-12** and **CS-13** polysaccharide through *p*-methoxybenzylidene approach.

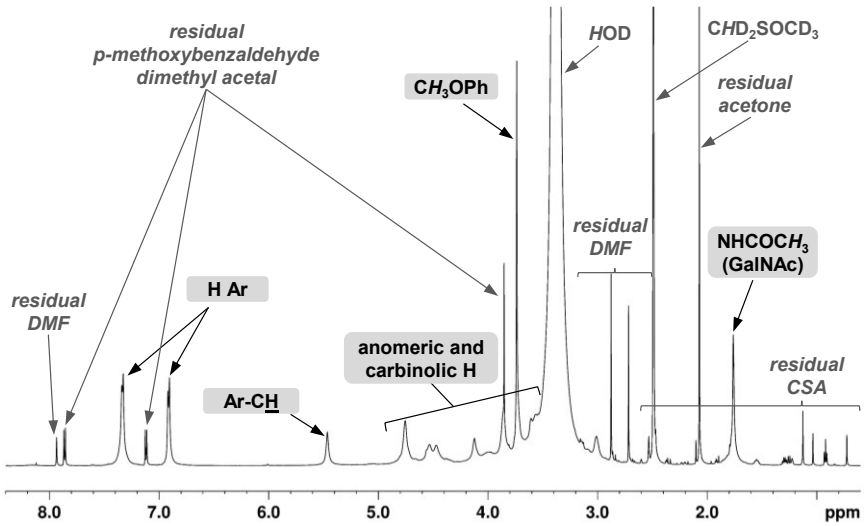

Figure 2.17. ^{1}H NMR spectrum (600 MHz, DMSO-d_6, 298 K) of derivative **18** (polysaccharide signal assignments are enclosed in rectangles).

Hence, product **18** was subjected to the 3,6-lactonization/2-*O*-benzoylation/lactone opening one-pot sequence, according to the same reaction conditions as previously described, to afford, after precipitation from the crude reaction mixture, product **19**. ^{1}H NMR spectrum of derivative **19** confirmed the installation of a benzoyl ester, as demonstrated by the presence of additional aromatic signals at δ 8.00–7.35 ppm, together with the downfield shift of the ring proton signals at δ 4.80–5.20 ppm due to the with-drawing benzoyl ester group (Figure 2.18). Then, the acid cleavage of the *p*-methoxybenzylidene group was performed, reducing the reaction time to 10 hours (instead of 48 hours as for product **6**, see Scheme 2.3), giving, after purification by dialysis, derivative **20**. NMR analysis confirmed a negligible amount of residual *p*-methoxybenzylidene rings on **20**, as detected by the very low intensity of the typical *p*-methoxybenzylidene signals at δ 7.30–6.80 and 5.45 ppm in the ^{1}H-NMR spectrum (Figure 2.19). Finally, product **20** was subjected to sulfation, under

standard conditions, and global deprotection under acid and then alkaline hydrolysis, to afford **CS-12** (Scheme 2.10).

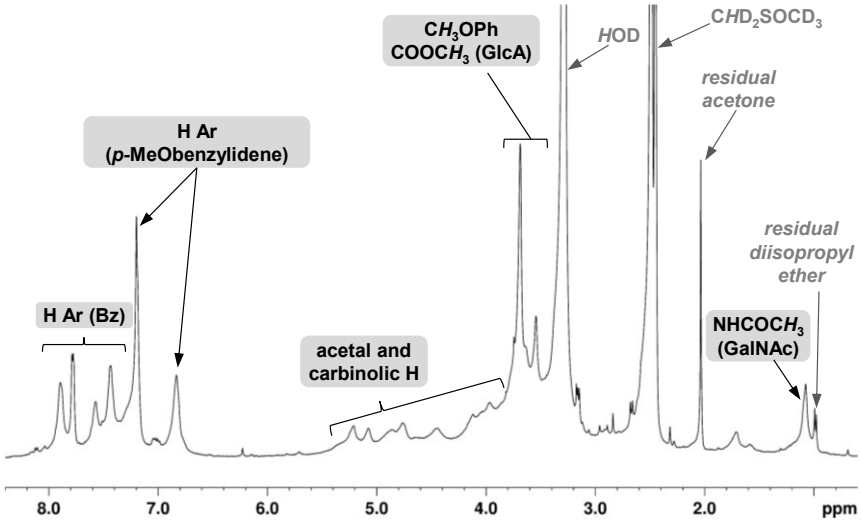

Figure 2.18. ^{1}H NMR spectrum (400 MHz, DMSO-d_6, 298 K) of derivative **19** (polysaccharide signal assignments are enclosed in rectangles).

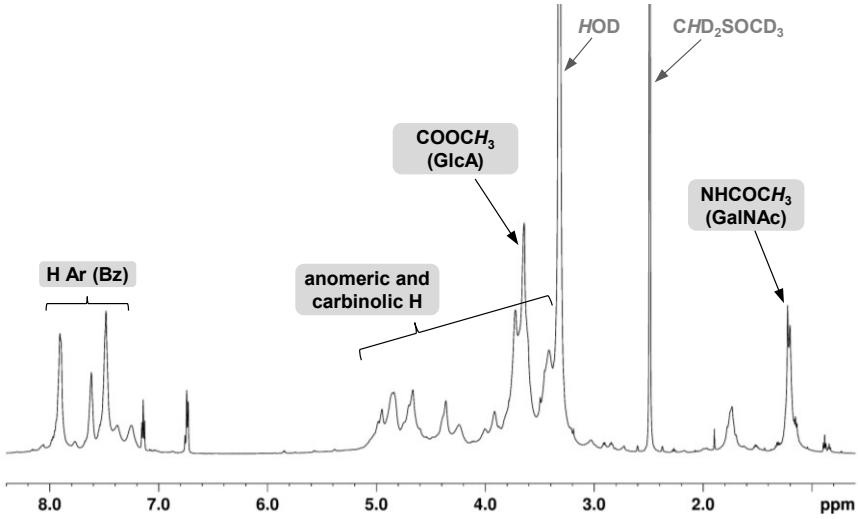

Figure 2.19. ^{1}H NMR spectrum (600 MHz, DMSO-d_6, 298 K) of derivative **20** (polysaccharide signal assignments are enclosed in rectangles).

In addition, by employing only the 3,6-lactonization reaction on **18** it was possible to obtain derivative **21** (see Figure 2.20 for ^{1}H NMR spectrum). Again, the acid hydrolysis on **21** was performed, further reducing the reaction to 6 hours in order to limit undesired collateral reactions. Products **22**, obtained after purification by dialysis of the crude reaction mixture and freeze-drying, could not be subjected to NMR analysis as it was insoluble in any deuterated solvent. So, sulfation and global deprotection were directly performed giving **CS-13**.

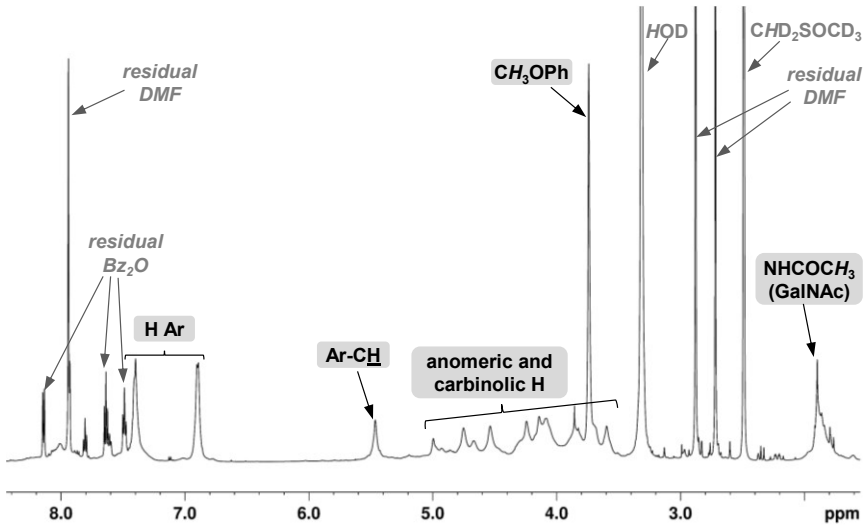

Figure 2.20. ^{1}H NMR spectrum (600 MHz, DMSO-d_6, 298 K) of derivative **21** (polysaccharide signal assignments are enclosed in rectangles).

^{1}H,^{13}C-DEPT-HSQC spectra of **CS-12**,**13** showed a substantial level of structural heterogeneity, particularly evidenced by very complex anomeric regions (Figure 2.21). This impeded a complete assignment, although some characteristic signals could be detected in both spectra. In the case of **CS-12** (Figure 2.21A), *CH*-4 ($\delta_{H,C}$ 4.84/77.1 ppm) and *CH*$_2$-6 ($\delta_{H,C}$ 4.26/68.6 ppm) signals of 4,6-di-*O*-sulfated GalNAc units were exclusively detected, thus evidencing an efficient cleavage of the *p*-methoxybenzilidene group. However, the presence of more than two densities attributable to *CH*-1 GalNAc positions evidenced the existence of

different type of GalNAc4,6S residues. Furthermore, densities relative to 3-*O*-sulfated GlcA units were detected (*e.g, CH*-3 4.33/77.9 and 4.40/82.3 ppm, *CH*-2 3.54/72.6 and 3.62/73.4 ppm) and, in this case, it is particularly evident the presence of, at least, two different types of GlcA3S units. The high heterogeneity of this spectrum could be hypothetically due to the presence of different conformers for the same kind of monosaccharide unit; indeed, it is reported that some residues in oversulfated CS chains can undergo conformational changes from a typical $^4C_1$ to other arrangements, leading to different chemical shifts for the corresponding CH positions (Maruyama et al., **1998**). An even higher heterogeneity was observed in **CS-13** spectrum (Figure 2.21B); also in this case, signals typical of 4,6-di-*O*-sulfated GalNAc units were detected, while no clear assignment was possible for GlcA positions, either by the aid of COSY and TOCSY spectra. Further NMR experiments will be necessary in order to allow a complete structural characterization for both products.

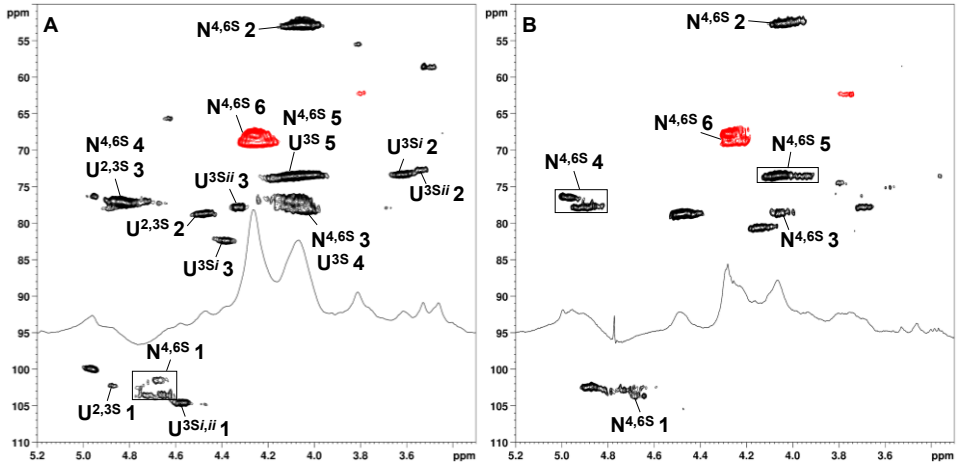

Figure 2.21. ^{1}H and ^{1}H,^{13}C-DEPT-HSQC NMR spectra (400 MHz, D_2O, 298 K, zoom) of (A) **CS-12** and (B) **CS-13**. 3S/2,3S and 4,6S superscripts represent the sulfated position in GlcA and GalNAc, respectively (only some of the signals were assigned).

2.2.1.5. Semi-synthesis of CS-S

Finally, the obtainment of the CS-S sulfation pattern, displaying sulfate groups only at the secondary positions of the disaccharide repeating unit, was also attempted. This sulfation pattern can be accessed from a persulfated CS, such as **CS-11**, through a regioselective de-*O*-sulfation involving the primary position. To this aim, we tested the use of silylating agents, such as BTSA or MSTFA, which are reported to successfully de-*O*-sulfate at primary positions several sulfated polysaccharides, including CS derivatives (Benito-Arenas et al., **2018**; Han et al., **2018**; Kariya et al., **2000**; Toida et al., **2000**). In these reactions, the silylating agent is able to selectively cleave sulfate groups at *O*-6 position of the polysaccharide, converting the released primary hydroxyl groups into trimethylsilyl ethers; then, the alcohol moieties are restored by silyl ether cleavage on aqueous work-up. So, **CS-11** was first converted into its pyridinium salt (**23**), then 6-de-*O*-sulfation with BTSA in pyridine at 70 °C was performed, obtaining **CS-14** (Scheme 2.11).

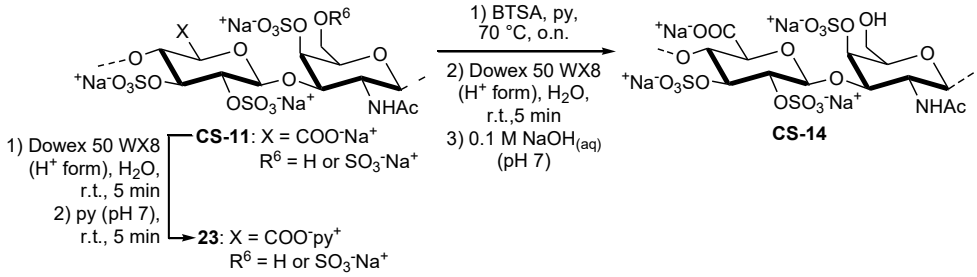

Scheme 2.11. Semi-synthesis of **CS-14** through 6-de-*O*-sulfation.

2D-NMR characterization of **CS-14** allowed to confirm a complete de-*O*-sulfation at the primary positions of GalNAc units, indeed only one kind of antiphase signals, attributable to unsulfated CH_2-6 position of GalNAc, was evidenced in the $^{1}H,^{13}C$-DEPT-HSQC spectrum of **CS-14** (Figure 2.22). In addition, typical signals of 2,3-di-*O*-sulfated GlcA and 4-*O*-sulfated GalNAc units could be

detected and assigned by COSY and TOCSY correlations (see Paragraph 2.4.4 for full NMR assignments). Finally, it was also possible to notice the presence of minor signals related to 3-*O*-sulfated GlcA units, derived from a concomitant 2-de-*O*-sulfation and counting for the 24% of the total GlcA, according to 2D-NMR integration.

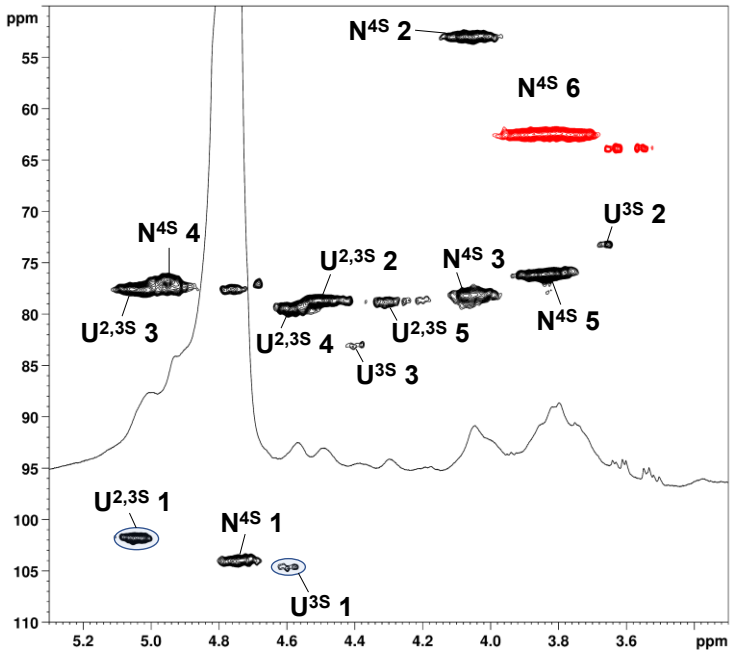

Figure 2.22. ^{1}H and $^{1}H,^{13}C$-DEPT-HSQC NMR spectra (400 MHz, D_2O, 298 K, zoom) of **CS-14**. 3S/2,3S and 4S superscripts represent the sulfated position in GlcA and GalNAc, respectively. (Densities enclosed in the highlighted areas of the DEPT-HSQC spectrum were integrated for estimation of GlcA2,3S and GlcA3S percentage amounts).

2.2.2. Regioselective Fucosylation of Microbial Chondroitin

In this section, the strategies for the obtainment of a library of semi-synthetic fCS polysaccharides with a strict regiocontrol of both sulfation pattern and fucose branch positions will be discussed.

Potentially, it could be possible to obtain all the regioisomers of natural fCS, displaying the Fuc branch in each of the four different positions of the

polysaccharide backbone (Figure 2.23). The Fuc branches can be differently sulfated and, in this study, four possibilities were considered (Figure 2.23), including 2-*O*-, 2,3-di-*O*-, 2,4-di-*O*- and 2,3,4-tri-*O*-sulfated branches. It is worth noting that the 2,4-di-*O*-sulfation pattern was chosen because it is one of the most commonly found in natural fCSs (Myron et al., **2014**; Ustyuzhanina et al., **2019**), and it has also been identified to give the strongest anticoagulant activity (Chen et al., **2013**, **2011**), although some results suggested the independence of the antithrombotic and anticoagulant action from the sulfation pattern on Fuc ramification in natural fCSs (Santos et al., **2015**). The other sulfation patterns were selected because they are very rare or, even, absent in natural fCSs, and therefore their obtainment could allow to enlarge the structure-activity relationship investigation.

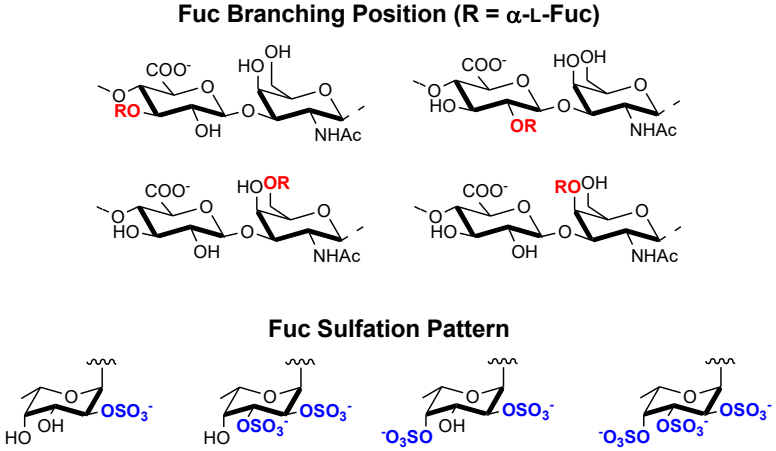

Figure 2.23. Fuc branching position and sulfation pattern variability in target fCSs.

The overall strategy requires first the realization of two sets of molecules: on one hand, a set of chondroitin polysaccharide glycosyl acceptors with a regular protection pattern, ideally displaying only one free hydroxyl group per repeating unit; on the other hand, a set of properly protected fucosyl donors. Then the components of these two sets could be combined through a glycosylation reaction

in order to allow the insertion of a Fuc branch on the linear polymer chain. Finally, further chemical derivatization, including sulfation as a key reaction, would allow to obtain the desired semi-synthetic fCS polysaccharides.

Before performing the semi-synthetic strategies, Fuc donors and polysaccharide acceptors were prepared. As for the donors, Fuc thioglycosides were selected thanks to their longer shelf-life with respect to other donors and also to their reported efficiency in glycosylation reactions on chondroitin polysaccharides (Laezza et al., **2016**, **2015**). The four donors were designed with different protecting group patterns, which correspond to different sulfate group distributions of the Fuc ramification on the final fCSs. In particular, two orthogonal protecting groups (Bn and Bz) were selected: Bn groups can be oxidatively cleaved before the sulfation step, whereas Bz groups can be removed at the end of the strategy. Thus, a per-*O*-benzylated Fuc donor could be used to obtain fCS polysaccharides with per-*O*-sulfated Fuc branches, whereas 2-*O*-Bn-3,4-di-*O*-Bz-Fuc, 2,3-di-*O*-Bn-4-*O*-Bz-Fuc and 2,4-di-*O*-Bn-3-*O*-Bz-Fuc donors could allow the access to fCSs with 2-*O*-sulfated, 2,3-di-*O*-sulfated or 2,4-di-*O*-sulfated Fuc branches, respectively. It is important to underline that the presence of a non-participating ether-type protecting group, such as a Bn one, at position 2 of all the Fuc donors is strictly required for a 1,2-*cis* stereoselectivity in the glycosylation reaction.

Therefore, thioglycosides **24**, **25**, **26**, **27** were selected as Fuc donors (Scheme 2.12). They were prepared from ethyl 1-thio-β-L-fucopyranoside **28**, which in turn could be obtained from commercially available L-fucose. Briefly, L-fucose was subjected to a peracetylation step, followed by iodination at the anomeric position, thioalkylation (Valerio et al., **2007**), and removal of the acetyl groups under classical Zemplén conditions to afford triol **28** (56% overall yield). The direct benzylation of the free alcohols on **28** gained per-*O*-benzylated fucosyl thioglycoside **24** (76% yield). To obtain donor **25**, triol **28** was subjected to a

three-step regioselective protection sequence (3-*O*-silylation, benzylation, and de-*O*-silylation) to give **29** (51% overall yield), which was then benzoylated to afford **25** in 67% yield. To obtain donors **26** and **27,** triol **28** was first subjected to a regioselective protection sequence including the installation of an isopropylidene ring at the *O*-3,4-diol, the benzylation of the free hydroxyl at *O*-2, and the isopropylidene ring acid-catalyzed cleavage to afford **30** (90% overall yield). Direct benzoylation on **30** gave donor **26** (85% yield), whereas tin complex-assisted 3-*O*-benzylation on **30**, followed by 4-OH benzoylation gave donor **27** (78% overall yield).

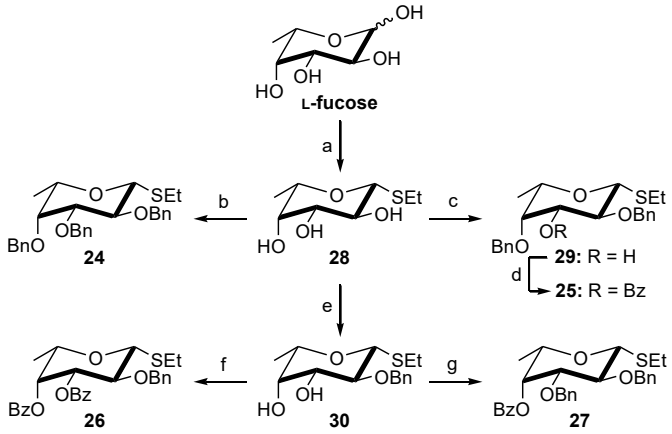

Scheme 2.12. Syntheses of Fuc donors **24**, **25**, **26**, **27**. (a) *i*) Ac_2O, py, r.t.; *ii*) I_2, Et_3SiH, CH_2Cl_2, reflux; *iii*) $(NH_2)_2CS$, CH_3CN, 60 °C; EtI, Et_3N, r.t., 56% (from L-fucose); *iv*) NaH, CH_3OH, r.t., 98%. (b) BnBr, NaH, DMF, 0 °C→r.t., 76%. (c) *i*) TBDMSCl, ImH, DMF, r.t., 70%; *ii*) BnBr, NaH, DMF, 0 °C→r.t., 82%; *iii*) TBAF·THF, THF, r.t., 89%. (d) BzCl, py, CH_2Cl_2, r.t., 67%. (e) *i*) $(CH_3)_2C(OCH_3)_2$, CSA, r.t.; *ii*) BnBr, NaH, DMF 0°C→r.t., 65% (over two steps); *iii*) 4:1 *v*/*v* TFA–H_2O, r.t., 90% (f) BzCl, py, CH_2Cl_2, r.t., 85%. (g) *i*) Bu_2SnO, C_6H_6/CH_3OH, 60°C; BnBr, Bu_4NI, 60°C, 95%; *ii*) BzCl, py, CH_2Cl_2, rt, 82%.

As for the polysaccharide acceptors, they could be accessed by chemical manipulation of the unsulfated chondroitin polysaccharide from *E. coli* O5:K4:H4, exploiting some of the protecting group strategies developed for CS polysaccharide semi-syntheses. Indeed, chondroitin derivatives with free

hydroxyl groups at position *O*-3, *O*-2 and *O*-4 (products **11**, **12** and **8a**,**c** respectively) were already prepared in the previously described work (see Paragraph 2.2.1), and they could be suitable polysaccharide acceptors for the fucosylation reactions.

Hence, in a first attempt, polysaccharide **11**, with a single free hydroxyl at position *O*-3 of GlcA, was tested as glycosyl acceptor in a glycosylation reaction with the per-*O*-benzylated donor **24** (Scheme 2.13). It is worth noting that this coupling would afford a semi-synthetic fCS polysaccharide very similar to the most common natural one in terms of the branching position. The reaction conditions for glycosylation were set in accordance with previous results on fucosylation of chondroitin polysaccharides (Laezza et al., **2016**, **2015**): NIS/TMSOTf as the typical thioglycoside activator system and 5:3 *v*/*v* CH_2Cl_2–DMF as solvent mixture, to exploit the reported α-stereodirecting modulation of DMF in glycosylations with 2-*O*-benzylated thioglycoside donors (Lu et al., **2011**), including 1,2-*cis*-glycosylation of polysaccharide acceptors (Laezza et al., **2016**, **2015**). The reaction temperature was set at −20 °C to make the benzylidene acid cleavage rate slow enough to avoid Fuc branching also on the GalNAc units. Furthermore, in order to test the possibility to increase the fucosylation degree on the final fCS product, the glycosylation reaction was also reiterated twice and thrice, employing 2.5 equivalent of donor in each step to reduce the likely formation of Fuc by-products. Glycosylation products **31-a**,**b**,**c** were recovered by precipitation from the reaction mixture, then an aliquot was preserved to continue the semi-synthetic strategy, while the remaining portion was subjected to the following glycosylation step. The complexity of the ^{1}H NMR spectra of **31-a,b,c** impeded a preliminary evaluation of the substitution degree for the fucosylation reaction. So, they were directly subjected to the following steps in order to convert them into fCS polysaccharides. First, acetylation with Ac_2O, Et_3N and DMAP in acetonitrile allowed to protect the (possible) unreacted hydroxyls on the GlcA

units (**32-a**,**b**,**c**). Then, the oxidative cleavage of both Bn and benzylidene groups, with $NaBrO_3$, $Na_2S_2O_3$ in H_2O/ethyl acetate mixture (Adinolfi et al., **1999**), furnished derivatives **33-a**,**b**,**c** with three free hydroxyls on the Fuc branches as well as at either *O*-4 or *O*-6 position of the GalNAc units. Finally, sulfation of the free alcohol moieties with SO_3·pyridine complex in DMF at 50 °C and subsequent hydrolysis of Ac, Bz, and methyl ester groups under alkaline aqueous conditions afforded **fCS-1a**,**1b**,**1c**.

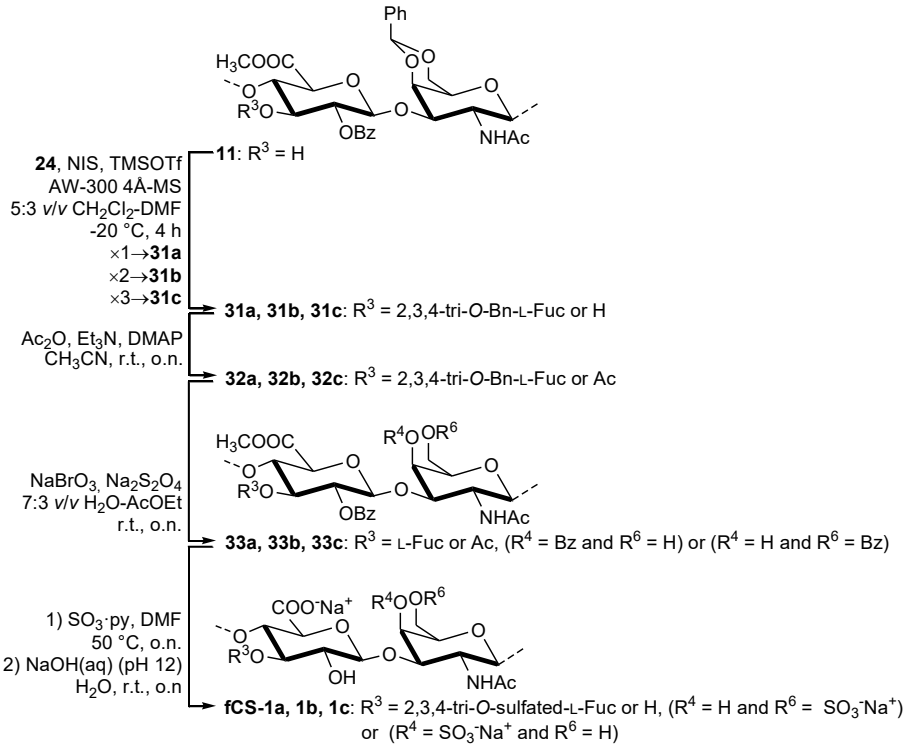

Scheme 2.13. Synthesis of **fCS-1a,1b,1c** from chondroitin acceptor **11** and fucosyl donor **24**.

^{1}H NMR spectra of semi-synthetic **fCS-1a**,**1b**,**1c** polysaccharides allowed the determination of their DF, as the ratio between the *H*-6 Fuc methyl signal (δ_H 1.20–1.43 ppm) and the acetyl signal (δ_H 1.90–2.15 ppm) integrations. The obtained values (0.65, 0.83, 0.90 for **fCS-1a**,**1b**,**1c**, respectively) indicated a

satisfying DF already for **fCS-1a**, gained by performing the glycosylation reaction once, although a significant increase in DF was observed in **fCS-1b**, after two glycosylation reactions. However, these DF values were overestimated because of the presence in the methyl proton region of other, sharper signals, probably related to traces of Fuc by-products. 2D-NMR analysis was so performed in order to achieve a better assessment of the structural parameters for **fCS-1a**,**1b**,**1c**. They showed very similar $^{1}H,^{13}C$-DEPT-HSQC spectra (see Figure 2.24 for **fCS-1b**), where it could be noticed at the highest ^{1}H chemical shift values the presence of one density ($\delta_{H/C}$ 5.64/98.0 ppm), assignable to the anomeric CH of α-linked sulfated Fuc units. This confirmed the presence of only one type of α-linked Fuc branch on the polysaccharide backbone. Another minor signal ($\delta_{H/C}$ 5.53/91.5 ppm) could be also detected in the anomeric region at lowest ^{13}C chemical shift with respect to the previous one; this density could be assigned to the anomeric CH of α-Fuc hemiacetal impurities, as also hypothesized by ^{1}H NMR spectra analysis. COSY, TOCSY and NOESY correlations allowed the identification of α-linked Fuc proton sequences from *H*-1 to *H*-4. Their downfield shifts (δ_H 4.5–5.0 ppm) revealed the exclusive presence of 2,3,4-trisulfated Fuc units, confirming a quantitative cleavage of Bn groups on Fuc branches under oxidative conditions (**32-a**,**b**,**c**→**33-a**,**b**,**c**), to restore the 2,3,4-triol that was then quantitively sulfated. Finally, NOESY spectra investigation allowed to assess the Fuc branch position in the three fCS products. Indeed, a correlation between Fuc anomeric signals (δ_H 5.64 ppm) and a cross-peak density at δ_H 3.64 ppm, corresponding to *H*-3 GlcA, as previously assigned by 2D-NMR spectroscopy (Laezza et al., **2016**), was revealed.

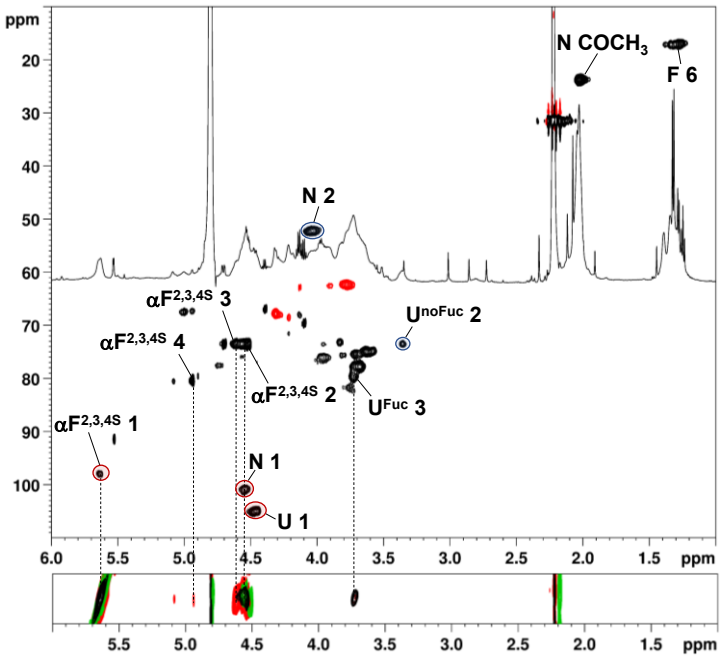

Figure 2.24. *Up*: ^{1}H and ^{1}H,^{13}C-DEPT-HSQC NMR spectra (600 MHz, D_2O, 298 K) of **fCS-1b**. *Down*: zoom of COSY (green), NOESY (black) and TOCSY (red) NMR spectra (600 MHz, D_2O, 298 K) of **fCS-1b**. 2,3,4S superscript represents the sulfated positions in Fuc units; Fuc/noFuc superscripts indicate the presence/absence of Fuc ramification on GlcA units. (Densities enclosed in the highlighted areas of ^{1}H,^{13}C-DEPT-HSQC spectrum were integrated for estimation of DF and DF$_\alpha$ values; only some of the assignments are shown, see Paragraph 2.4.4 for full NMR assignments).

With all these assignment in minds, the evaluation of the structural parameters for **fCS-1a**,**b**,**c** was performed. In particular, the DF values were estimated from the integral areas measured for *CH*-2 signal of non-fucosylated GlcA residues at $\delta_{H/C}$ 3.36/73.5 ppm and *CH*-2 signal of GalNAc units at $\delta_{H/C}$ 4.05/52.3 ppm, according to Equation 2.3:

$$\mathrm{DF} = 1 - \frac{\mathrm{I}(CH\text{-}2\ \mathrm{GlcA}^{\mathrm{noFuc}})}{\mathrm{I}(CH\text{-}2\ \mathrm{GalNAc})} \qquad \text{(Eq. 2.3)}$$

Hence, DF values of 0.41, 0.69, and 0.69 were estimated for **fCS-1a**,**1b**,**1c** (see Table 2.6), respectively, confirming an increment of Fuc branching in **fCS-1b**

obtained by performing glycosylation twice, while no increase in DF was observed with a further glycosylation reaction (**fCS-1c**). Furthermore, an estimation of the degree of α-fucosylation (DF_α) was also performed from the ratio between the integral area measured for the Fuc anomeric signals ($\delta_{H/C}$ 5.64/98.0 ppm) and the average between the integral areas of GalNAc and GlcA anomeric signals ($\delta_{H/C}$ 4.55/100.9 and 4.48/105.2 ppm, respectively), as previously assigned by 2D-NMR spectroscopy (Laezza et al., **2016**) (Equation 2.4):

$$DF_\alpha = \frac{I(CH\text{-}1\ \alpha\text{-Fuc})}{\frac{I(CH\text{-}1\ \text{GalNAc}) + I(CH\text{-}1\ \text{GlcA})}{2}} \qquad \text{(Eq. 2.4)}$$

fCS-1a,**1b**,**1c** had DF_α values of 0.24, 0.41, 0.39, respectively, confirming the same trend shown before for the increment of Fuc branching (see Table 2.6). As for the α/β stereochemical ratios of the Fuc glycosidic bonds, it could not be determined by integration of the α- and β-Fuc anomeric signals, because the latter could be not unambiguously detected even in 2D NMR spectra due to low intensity and/or overlap with other anomeric signals (Mulloy et al., **2000**). Hence, an indirect estimation of the α/β ratios for the three fCSs was performed by evaluating the β-Fuc branches amount as the difference between the DF and the DF_α values —as the former counts for both α- and β-linked Fuc units— according to Equation 2.5:

$$\alpha/\beta = \frac{DF_\alpha}{DF - DF_\alpha} \qquad \text{(Eq. 2.5)}$$

The α/β ratio was found to be rather similar for the three fCS products (Table 2.6), with a slight preponderance of the α-stereochemistry, as expected from the α-

stereodirecting effect of DMF in fucosylations (Laezza et al., **2015**; Lu et al., **2011**).

Table 2.6. Yield and structural parameters of **fCS-1a,1b,1c**.

Product	Yield [a]	DF [b]	DF_α [b]	α/β Ratio [b]
fCS-1a	30%	0.41	0.24	1.4
fCS-1b	20%	0.69	0.41	1.4
fCS-1c	24%	0.69	0.39	1.3

[a] Overall mass yield determined with respect to starting glycosyl acceptor **11**. [b] Estimated by $^{1}H,^{13}C$-DEPT-HSQC integration (see text for details).

With these results in mind, further glycosylation tests were performed in order to obtain fCS products with a different sulfation pattern and/or, by employing the other acceptors (**8a**, **8c** or **12**), different Fuc branching position (Table 2.7).

Table 2.7. Glycosylation reactions of chondroitin acceptors **8a**,**c**, **11**, **12** with fucosyl donors **24**–**27**.

Entry	Acceptor	Donor [a]	Reaction temperature	Product [b]
a [c]				**31a**
1 *b* [c]	**11**	**24**	−20 °C	**31b**
c [c]				**31c**
2 [c]	**11**	**26**	−20 °C	--
3 [c]	**11**	**27**	−20 °C	--
4 [c]	**12**	**24**	−20 °C	--
5 [d]	**8a**	**24**	r.t.	**34**
6 [d]	**8c**	**24**	r.t.	**35**
7 [d]	**8c**	**25**	r.t.	**36**
8 [d]	**8c**	**26**	r.t.	**37**

[a] 2.5 equivalent at each glycosylation step. [b] Postulated structures depicted in Scheme 2.13,2.14. [c] Conditions: NIS (2.75 eq), TMSOTf (0.75 eq), 5:3 *v*/*v* CH_2Cl_2–DMF, AW–300 4Å–MS, −20 °C, 4 h. [d] Conditions: NIS (2.75 eq), TMSOTf (0.75 eq), 5:3 *v*/*v* CH_2Cl_2–DMF, AW-300 4 Å-MS, r.t., 4 h.

Glycosylation reactions were performed twice under the same reaction conditions described above. Only the reaction temperature was changed in the case of the

fucosylation reactions with acceptors **8a** and **8c** (Table 2.7, entries *5–8*), by increasing it to room temperature, since no acid-cleavable benzylidene groups had to be preserved. Polysaccharide products obtained by precipitation with suitable solvents from the crude glycosylation mixtures showed very complex ^{1}H NMR spectra, except for the products of entries *2–4*. In this case, chondroitin acceptors **11** (entries *2, 3*) and **12** (entry *4*) were recovered unreacted, also after reiterating the glycosylation step twice. In the other cases, the complexity of the ^{1}H NMR spectra as well as the co-precipitation of part of Fuc by-products with the polysaccharide did not allow an exact evaluation of the fucosylation reactions' substitution degree. Hence, glycosylation products **34**, **35**, **36**, **37** were subjected to the subsequent reaction steps (acetylation, Bn oxidative cleavage, sulfation, and alkaline hydrolysis, see Scheme 2.14) for their transformation into **fCS-5**,**6**,**7**,**8**.

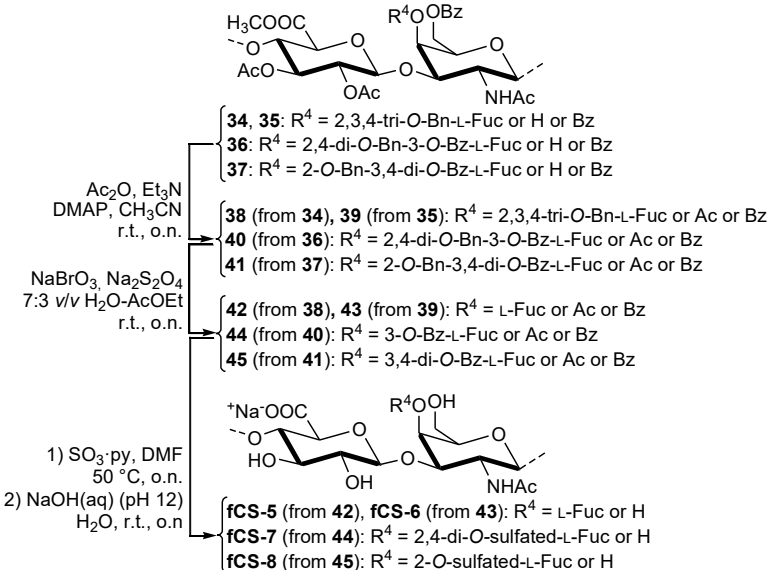

Scheme 2.14. Transformation of glycosylation products of Table 2.7 into fC(S)s.

A 2D NMR (COSY, TOCSY, NOESY, ^{1}H,^{13}C-DEPT-HSQC) analysis of the semi-synthetic polysaccharides was then conducted to investigate the regiochemistry of the Fuc branches and the sulfate group distribution (see Table

2.8). $^{1}H,^{13}C$-DEPT-HSQC spectrum of **fCS-5** (Figure 2.25A) showed at the highest ^{1}H chemical shift values the presence of one density ($\delta_{H/C}$ 5.38/100.5 ppm) which could be associated to the anomeric CH of α-linked Fuc units, thus confirming the presence of only one kind of α-linked Fuc branching on the polysaccharide chain. The analysis of the cross peaks related to this signal in the NOESY spectrum (Figure 2.25A) revealed a correlation with a density at δ_H 4.20 ppm, attributable to GalNAc *H*-4 by means of the other 2D NMR spectra and literature data (Laezza et al., **2016**, **2015**). The same approach for the assignment of the Fuc branching site was repeated for the other semi-synthetic fCSs (Figures 2.25B,C,D), confirming in all cases the expected regiochemistry of fucosylation.
NMR analysis allowed also to investigate the Fuc sulfation pattern expected from the position of orthogonally cleavable (Bn) and permanent (Bz) protecting groups on fucosyl donors **24**, **25**, **26** used in the glycosylation steps. As regards **fCS-7,8** (Figure 2.25C,D), the cross peaks related to the anomeric α-Fuc signals in the COSY, TOCSY and NOESY spectra confirmed the expected sulfation patterns for the α-Fuc residues. Indeed, α-Fuc branches of **fCS-7** (obtained from fucosylation reaction with 2,4-di-*O*-benzylated donor **25**) displayed *H*-2 and *H*-4 signals downfield shifted for *O*-sulfation (δ_H 4.43 and 4.69 ppm, respectively), whereas only *H*-2 signal showed a similar shift (δ_H 4.42 ppm) in **fCS-8** (deriving from fucosylation reaction with 2-*O*-benzylated donor **26**). An unexpected result was instead obtained for **fCS-5,6** (Figure 2.25A,B): indeed, in both cases *H*-2, *H*-3 and *H*-4 densities of α-Fuc branches, assigned by COSY, TOCSY and NOESY correlation from the anomeric α-Fuc signal, had lower chemical shifts values ranging from 3.75 ppm to 3.95 ppm, thus evidencing the absence of sulfate groups on Fuc branches. Considering that sulfation usually occurs quantitively even on Fuc branches with three free hydroxyls (see products **fCS-1a,1b,1c**), this outcome could be hypothetically due to a particular 3D-structure of polysaccharides **fCS-5,6**, where the free hydroxyl groups on the Fuc branches at GalNAc *O*-4 positions

could be involved in strong hydrogen bonds which prevent them to react during the sulfation step. However, this preliminary hypothesis should be validated by molecular dynamic calculation, that are currently in progress to investigate the actual 3D arrangement of the polysaccharide chain.

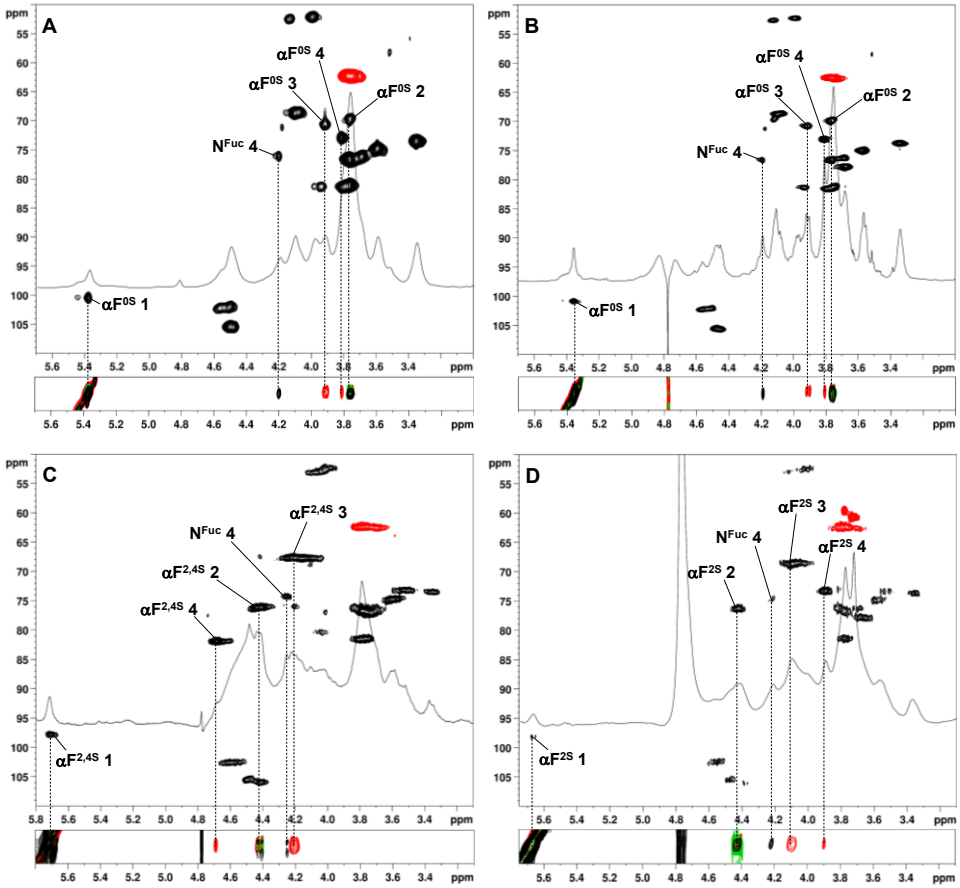

Figure 2.25. Zoom of ^{1}H and $^{1}H,^{13}C$-DEPT-HSQC NMR spectra (*up*) and zoom of COSY (green), NOESY (black) and TOCSY (red) NMR spectra (*down*) of (A) **fCS-5** (600 MHz, D_2O, 298 K), (B) **fCS-6** (600 MHz, D_2O, 298 K), (C) **fCS-7** (400 MHz, D_2O, 298 K), (D) **fCS-8** (400 MHz, D_2O, 298 K). 0S/2,4S/2S superscripts represent the sulfated positions in Fuc units; Fuc superscript indicate the presence of Fuc ramification on GalNAc units. (Only some of the assignments are shown, see Paragraph 2.4.4 for full NMR assignments).

Also in this case, 2D-NMR assignment allowed a preliminary estimation of the structural parameters (DF, DF_α, α/β) for **fCS-5–8**. In particular, the DF values were estimated from the integral areas measured for *CH*-2 signal of fucosylated and non-fucosylated GalNAc units, as assigned by 2D-NMR analysis with the aid of literature data (Laezza et al., **2016**) (see Equation 2.6), whereas for DF_α and α/β the previous described equation (Equation 2.4, 2.5) were employed.

$$DF = \frac{I(CH\text{-}2\ GalNac^{Fuc})}{I(CH\text{-}2\ GalNac^{Fuc}) - I(CH\text{-}2\ GalNac^{noFuc})} \qquad \text{(Eq. 2.6)}$$

No significant variations among the four fCS polysaccharides were observed, even if slightly lower DF values, with respect to the **fCS-1b**, were found (Table 2.8). Besides, a high α-Fuc content was detected in all cases, thus evidencing the efficacy of the α-stereodirecting solvent mixture for these glycosylation reactions.

Table 2.8. Yields and structural data of semi-synthetic fC(S) products.

Product	Yield [a]	Fuc branch position [b]	Fuc sulfation pattern [b]	DF [c]	DF_α [c]	α/β ratio [d]
fCS-5	13%	*O*-4 GalNAc	unsulfated	0.34	0.34	only α
fCS-6	10%	*O*-4 GalNAc	unsulfated	0.44	0.46	only α
fCS-7	60%	*O*-4 GalNAc	2,4-sulfated	0.43	0.50	only α
fCS-8	19%	*O*-4 GalNAc	2-sulfated	0.40	0.36	9.0

[a] Overall mass yield determined with respect to starting glycosyl acceptor (**8a**, **8c**). [b] Confirmed by 2D-NMR analysis. [c] Estimated from $^{1}H,^{13}C$-DEPT-HSQC integrations (see text for details).

Finally, a preliminary study for the access of fCS products bearing Fuc branched at *O*-6 position of GalNAc residues was performed.

In this case, no chondroitin derivative displaying only the free hydroxyl at the *O*-6 position, thus suitable as glycosyl acceptor, was already prepared. To fill this gap, we decided to test whether reductive conditions for benzylidene ring cleavage

could be applied on a polysaccharide derivative, such as the known product **6**. With a proper choice of the reductive conditions, it could be possible to obtain a derivative showing a free alcohol at position 6 of GalNAc units and a Bn ether protection at *O*-4. Thanks to their regioselective outcome, reductive opening methods are extensively employed in monosaccharide or (short) oligosaccharide synthetic chemistry, however, to the best of our knowledge, no example of their employment on polysaccharide structures has been reported up to now. Reaction conditions for reductive opening are generally based on borane- or silane-type reagents. Among the several reported variants (Wuts, **2014**), we focused our attention on those showing the following features, necessary for an application on chondroitin polysaccharide **6**: i) a high regioselectivity on *galacto*-configured sugars, and ii) the possibility to avoid very low temperatures (*e.g.* −78 °C) for gaining a satisfying regioselectivity in benzylidene opening. The latter feature is desirable because it is highly unlikely that polysaccharide **6** is soluble in any solvent at very low temperatures. The methods employing either a borane-type reagent such as BH_3·THF complex in THF under TMSOTf catalysis (Daragics and Fügedi, **2009**) or a silane-type reagent such as Et_3SiH in CH_3CN under BF_3·OEt_2 catalysis (Debenham and Toone, **2000**), were selected. They were tested on polysaccharide **6** under strict anhydrous conditions ensured by an Ar atmosphere and the presence of 3Å–MS in the reaction mixture (Scheme 2.15). Even if the selected methods are known to guarantee a high yielding benzylidene reductive opening to 4-benzylated derivatives on *galacto*-configured species, the resulting polysaccharides **46a** and **46b**, recovered by precipitation from the reaction mixture, showed in their ^{1}H NMR spectrum a residual signal related to the benzylidene methine proton at δ_H 5.45 ppm (see Figure 2.34 in Paragraph 2.4.4). Nonetheless degree and regioselectivity of modification could not be easily evidenced by NMR. Therefore, derivatives **46a** and **46b** were directly subjected to sulfation with SO_3·pyridine complex in DMF, followed by deprotection under

acid and then alkaline hydrolytic conditions, in order to confirm or invalidate the postulated regioselectivity of reductive benzylidene cleavage. Such semi-synthetic sequence should have given, after purification by dialysis, partially *O*-benzylated CS polysaccharides **CS-15a,15b**.

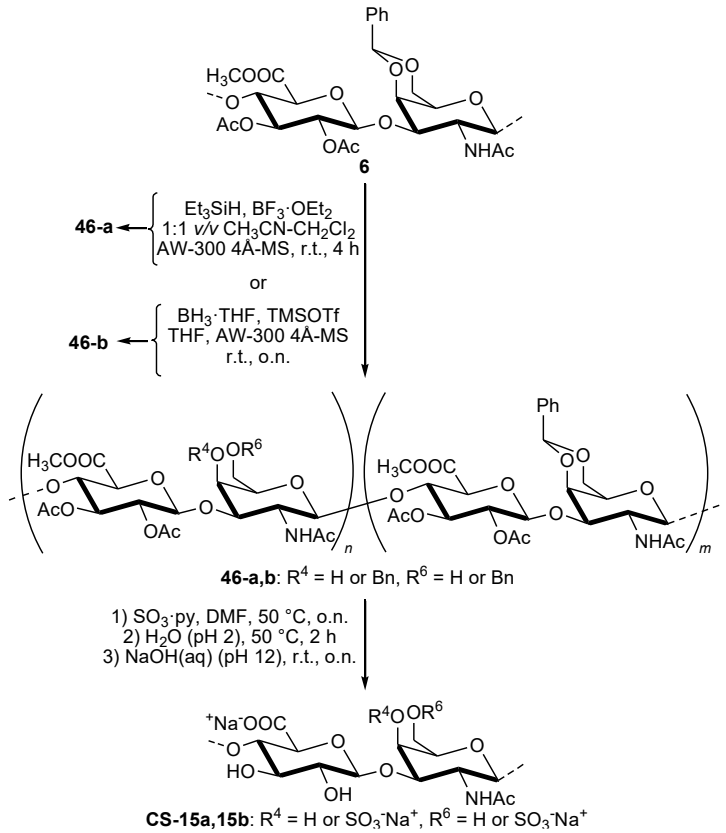

Scheme 2.15. Semi-synthesis of **CS-15a,15b** polysaccharides through benzylidene reduction approach.

On the contrary, 2D-NMR spectroscopy investigation on these products revealed, by comparison with literature data (Cai et al., **2012**; Mucci et al., **2000**), that signals of neither mono-sulfated disaccharide subunits (CS-A or CS-C having a single sulfate at position 4 or 6 of GalNAc units, respectively) nor benzyl ether moieties could be detected. Surprisingly, unsulfated (CS-0) and 4,6-di-*O*-sulfated

subunits (CS-E) were only found, in 68:32 and 97:3 ratios for **CS-15a,15b**, respectively, as measured by relative integration of GalNAc *O*-6 methylene signals for CS-0 and CS-E units (at $\delta_{H/C}$ 3.71/61.0 and 4.15–4.21/75.9 ppm, respectively) in $^{1}H,^{13}C$-DEPT-HSQC spectra (see Figure 2.35 in Paragraph 2.4.4). Unsulfated subunits could derive from the GalNAc residues of **46a** and **46b** still carrying a benzylidene ring, according to their residual presence detected in the ^{1}H NMR spectrum of **46a** and **46b**. The presence of minor CS-E subunits could be explained with a hydrolytic (instead of reductive) mechanism operating during the benzylidene cleavage reaction. This was supposedly due to the presence of residual water molecules entrapped in the 3D-structure of polysaccharide **6** that cannot be eliminated even after co-evaporation of the polysaccharide with dry toluene, a prolonged vacuum-desiccation and, finally, the use of molecular sieves in the reaction vessel.

In the light of these unsatisfying results, we decided to employ derivative **7**, with the free *O*-4,6-diol at GalNAc units and obtained from **6** by benzylidene ring acid cleavage, for testing reactions for the selective protection of the primary position of the diol. By properly choosing a selectively removable protecting group, after a subsequent protection of the position 4 with a permanent group (such as an Ac or Bz ester) it could be possible to obtain a derivative with a free primary alcohol *per* repeating unit, that might be suitable for single site Fuc branching of GalNAc units. In particular, the high steric demand and the ease of removal of DMTr ethers justify their wide use as protecting groups for primary hydroxyls not only on simple carbohydrates but also on polysaccharides (Bedini et al., **2017**). Unfortunately, the reaction of **7** with DMTrCl in the presence of pyridine using DMF or LiCl in DMAc as solvent system (Camacho Gömez et al., **1996**) gave no derivatization at all (Scheme 2.16). This was clearly indicated by the absence of aromatic signals in addition to the residual benzylidene ones in the ^{1}H NMR

spectrum of the polysaccharide recovered from the reaction mixture by precipitation (data not shown).

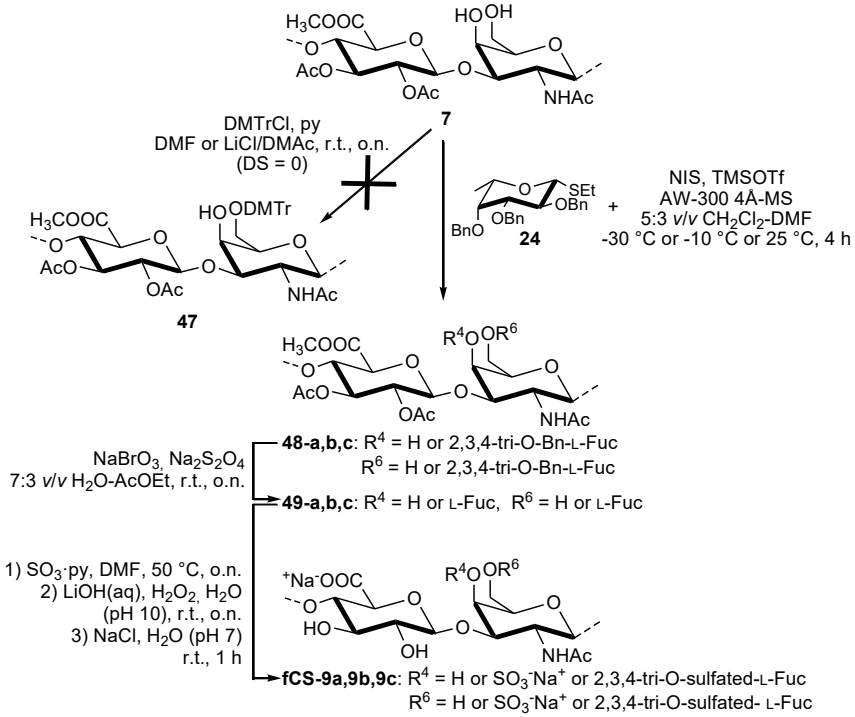

Scheme 2.16. Semi-synthesis of **fCS-9a–c** polysaccharides fucosylated on GalNAc units (DS = degree of substitution).

As an alternative strategy to Fuc branching at a single site of GalNAc units, polysaccharide **7** was employed directly in glycosylation reactions with the per-*O*-bezylated fucosyl donor **24** under different conditions. The hypothesis is that the primary hydroxyl of GalNAc 4,6-diol is much more nucleophilic than the secondary alcohol at position *C*-4. Furthermore, the latter has an axial orientation and the *cis* adjacent *C*-3 position is glycosylated. Both these features should be additional, sterically detrimental factors for its reactivity. Hence, glycosylation of **7** was tested with donor **24** at different temperatures ranging from −30 to 25 °C using NIS/TMSOTf as thioglycoside activator system and a 5:3 *v*/*v* CH_2Cl_2-DMF

as α-stereodirecting solvent mixture (Laezza et al., **2015**; Lu et al., **2011**), that also allowed to conduct the reaction under homogeneous conditions (Scheme 2.16). Polysaccharide products **48-a–c** obtained by precipitation with suitable solvents from the crude glycosylation mixtures showed rather complex ^{1}H NMR spectra that impeded any structural characterization. Therefore, they were directly transformed into the target fCSs by a sequence of additional steps, including: the oxidative cleavage of Bn protecting groups on putative Fuc branches (**49-a–c**), the sulfation under standard conditions (SO_3·pyridine, DMF, 50 °C) of the liberated alcohol moieties on Fuc branches together with the residual non-fucosylated GalNAc sites, followed by the alkaline hydrolysis of the ester protecting groups. Purification of the polysaccharides by dialysis, followed by freeze-drying, furnished semi-synthetic **fCS-9a–c** in 50%–58% weight yield (over five steps, calculated from **7**; see Table 2.9).

Table 2.9. Yield and structural parameters of **fCS-9i–iii**.

Product	Yield [a]	DF [b]	GalNAc *O*-6/*O*-4 branching site ratio [c]	α/β Fuc ratio [c]
fCS-9a	50%	0.21	only 6-*O* linked	0.33
fCS-9b	52%	0.20	9:1	9.0
fCS-9c	58%	0.29	4:1	19.0

[a] Overall mass yield determined with respect to starting glycosyl acceptor **7**. [b] Determined by ^{1}H NMR integration of Fuc methyl and GalNAc acetyl signals. [c] Estimated by DEPT-HSQC integration (see text for details).

Integration of the ^{1}H NMR spectra of semi-synthetic fCSs allowed the determination of some structural parameters such as degree of fucosylation (DF), 6-*O*/4-*O*-fucosylation ratio (glycosylation regioselectivity) and α-/β-linked Fuc ratio (glycosylation stereoselectivity). DF was evaluated from the ratio between the *H*-6 Fuc methyl (δ_H 1.35–1.20 ppm) and the *N*-acetyl signal (δ_H 2.10–1.95 ppm) integrations (see Table 2.9). By conducting the glycosylation at −30 °C, DF

of the final semi-synthetic **fCS-9a** was 0.21. This value did not change (0.20) for **fCS-9b**, obtained by a glycosylation at −10 °C, and only a slight enhancement was observed for **fCS-9c** (0.29), afforded by increasing the reaction temperature to 25 °C. Fuc branching regioselectivity between GalNAc *O*-4 and *O*-6 positions was measured by integration of $^{1}H,^{13}C$-DEPT-HSQC spectra of **fCS-9a–c** (Figures 2.26–2.28). In particular, it was calculated the ratio of the signals at $\delta_{H/C}$ 5.31/98.5 and 5.77/97.7 ppm, corresponding to 6-*O*- and 4-*O*-α-linked *CH*-1 Fuc atoms respectively, as previously assigned by 2D-NMR spectroscopy (Laezza et al., **2016**). The obtained data revealed a decrease in 6-*O* vs. 4-*O*-regioselectivity with the increase of the glycosylation temperature from −30 °C to 25 °C, even if in all cases the relative amount of 6-*O*-linked α-Fuc branches was much higher with respect to the 4-*O*-linked ones (see Table 2.9). Concerning Fuc branching stereochemistry, since the α/β ratio could not be determined directly by integration of the α- and β-Fuc anomeric signals, as also previously described, it was estimated by evaluating the β-Fuc branches amount as the difference between the CH_3-6 and the sum of 6-*O* and 4-*O*-linked α-Fuc *CH*-1 signal integrations—as the former counts for both α- and β-linked units—according to Equation 2.7:

$$\alpha/\beta = \frac{\sum \mathrm{I}(CH\text{-}1\ \alpha\text{-}Fuc)}{\frac{\mathrm{I}(CH_3\text{-}6\ Fuc)}{3} - \sum \mathrm{I}(CH\text{-}1\ \alpha\text{-}Fuc)} \qquad \text{(Eq. 2.7)}$$

The obtained data revealed a clear increase of α- over β-stereochemistry with the increase of glycosylation temperature (see Table 2.9). In particular, α-linked Fuc branches were almost exclusively found on **fCS-9b** and **fCS-9c**, as expected from the α-stereodirecting effect of DMF in fucosylations (Lu et al., **2011**), whereas β-stereochemistry surprisingly prevailed on polysaccharide **fCS-9a** obtained with a glycosylation at −30 °C.

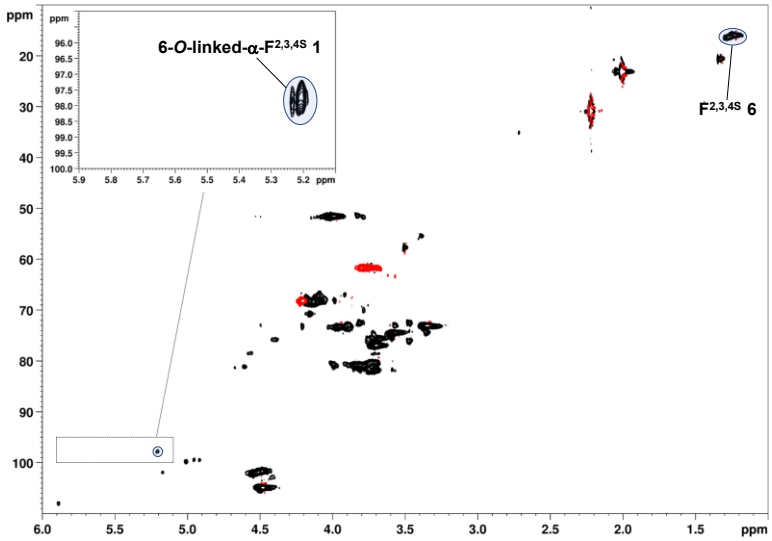

Figure 2.26. ^{1}H and ^{1}H,^{13}C-DEPT-HSQC NMR spectra (600 MHz, D_2O, 298 K) of **fCS-9a**. (F: Fuc; 2,3,4S superscript represents the sulfated positions in Fuc units. Densities enclosed in the highlighted areas were integrated for estimation of α/β Fuc ratio and GalNAc *O*-6/*O*-4 branching site ratio).

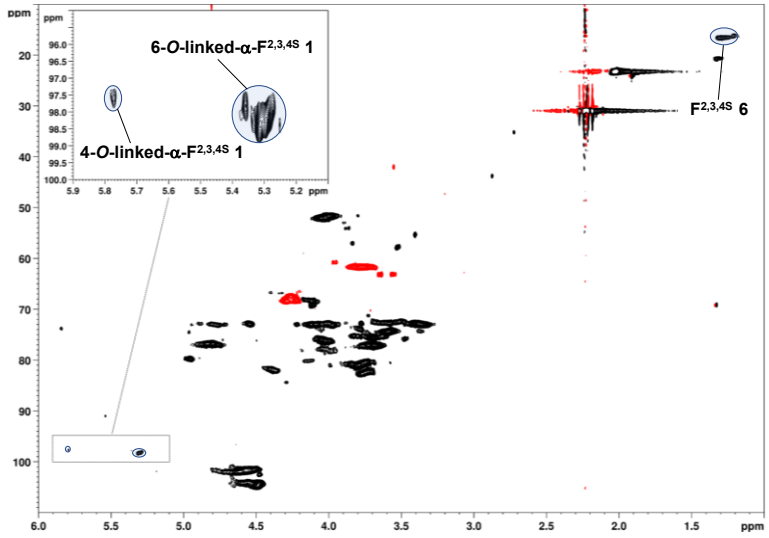

Figure 2.27. ^{1}H and ^{1}H,^{13}C-DEPT-HSQC NMR spectra (600 MHz, D_2O, 298 K) of **fCS-9b**. (F: Fuc; 2,3,4S superscript represents the sulfated positions in Fuc units. Densities enclosed in the highlighted areas were integrated for estimation of α/β Fuc ratio and GalNAc *O*-6/*O*-4 branching site ratio).

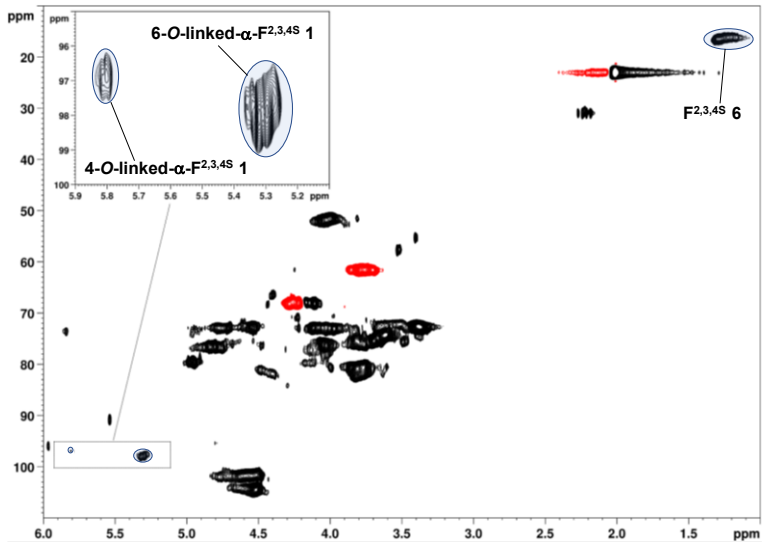

Figure 2.28. ^{1}H and $^{1}H,^{13}C$-DEPT-HSQC NMR spectra (600 MHz, D_2O, 298 K) of **fCS-9c**. (F: Fuc; 2,3,4S superscript represents the sulfated positions in Fuc units. Densities enclosed in the highlighted areas were integrated for estimation of α/β Fuc ratio and GalNAc *O*-6/*O*-4 branching site ratio).

2.3. Conclusions

In this chapter, the development of the semi-synthetic strategies for the chemical transformation of *E. coli* O5:K4:H4 sourced chondroitin into CS polysaccharides with a well-defined sulfation pattern were described. To this aim, a modular approach, including regioselective steps —for either an inter-residue (GalNAc diol *vs.* GlcA diol) or an intra-residue (*O*-4 *vs.* *O*-6, *O*-2 *vs.* *O*-3) differentiation— together with sulfation and global deprotection as last steps, was pursued.

First, the strategies for the regioselective sulfation of *O*-4 and/or *O*-6 positions of GalNAc residues were described, gaining the access to CS polysaccharides, predominantly composed of E-, A- or C-type disaccharide repeating units. CS-E and CS-A semi-syntheses were both based on a finely tuned chemoselective cleavage of benzylidene groups on GalNAc *C*-4,6-positions to restore the diol without a significant breakage of glycosidic bonds and, only for CS-A obtainment,

a carefully optimized regioselective acylation on *O*-6 site of the restored diol was also performed. On the contrary, a mild sulfation procedure was the key and only step applied for CS-C semi-synthesis.

In addition, the semi-syntheses of CS polysaccharides, carrying a single sulfate group regioselectively placed at either *O*-2 or *O*-3 position of the GlcA residues or at both sites, were developed, allowing the access, for the first time, to structurally homogenous CS-R, CS-U and CS-V polysaccharides. The successful strategies for regioselective sulfation of a single GlcA position relied both upon GlcA 3,6-*O*-lactonization as key regioselective step to give a chondroitin derivative showing a single hydroxyl group at position 2 of GlcA units or, after two one-pot additional steps, at the position 3 of the same residues.

Finally, properly combining the already known and the newly developed regioselective steps, the semi-synthetic strategies for CS polysaccharides bearing sulfate group at specific position of both GalNAc and GlcA units were preliminary designed, leading to six CS polysaccharides with semi-homogenous structures in terms of their sulfation pattern.

The whole obtained library of semi-synthetic CSs will allow more detailed and complete structure–activity relationship investigations of CS biological functions and biomedical applications. In this context, some of the described CS products have been included in a preliminary study aimed to decipher the effect of different sulfate-bearing motifs on CS binding to growth factor. This work, performed in collaboration with the BioGlycoChem group of the Institute of General Organic Chemistry of the Spanish National Research Council (CSIC), will be discussed in the following chapter.

Table 2.10. Semi-synthetic CS polysaccharides.

Product	Disaccharide Units	Ratio	Weight Yield [a]
CS-1	GlcA-GalNAc(4,6S)/GlcA-GalNAc	80:20	84%
CS-2c	GlcA-GalNAc(4S)/GlcA-GalNAc	82:18	45%
CS-2e	GlcA-GalNAc(4S)/GlcA-GalNAc	86:14	16%
CS-3	GlcA-GalNAc(6S)/GlcA(2S)-GalNAc(6S)	57:43	70%
CS-5	GlcA(2,3S)-GalNAc/GlcA(2,3S)-GalNAc(6S)	91:9	105% (quant.)
CS-6	GlcA(3S)-GalNAc	100	54%
CS-7	GlcA(2S)-GalNAc/GlcA-GalNAc	85:15	66%
CS-8	GlcA(2,3S)-GalNAc(6S)/GlcA(2,3S)-GalNAc	56:44	116% (quant.)
CS-9	GlcA(3S)-GalNAc(6S)/GlcA(3S)-GalNAc	23:77	60%
CS-10	GlcA(2S)-GalNAc(6S)/GlcA(2S)-GalNAc	84:16	72%
CS-12	GlcA(3S)-GalNAc(4,6S)/GlcA(3S)-GalNAc[b]	n.a.[c]	178% (quant.)
CS-13	GlcA(2S)-GalNAc(4,6S)/GlcA(2S)-GalNAc [b]	n.a. [c]	172% (quant.)
CS-14	GlcA(2,3S)-GalNAc(4S)/GlcA(3S)-GalNAc(4S)	76:24	131% (quant.)

[a] Overall weight yield form microbial chondroitin. [b] Expected sulfation pattern according to the semi-synthetic strategy. [c] not assessable.

In addition to that, the production of a library of fC(S) polysaccharides, with a different and strictly regulated Fuc sulfation pattern and Fuc branch position, was described in this work. The whole approach relied upon the employment of a set of polysaccharide glycosyl acceptors, accessed by chemical modification of *E. coli* O5:K4:H4 unsulfated chondroitin (also exploiting some of the protecting group strategies developed for CS polysaccharide semi-syntheses), and a set of properly protected fucosyl donors, prepared from commercially available L-Fuc according to already reported synthetic routes. The semi-synthetic strategy involved the modular use of five different reactions: glycosylation of a suitably protected chondroitin acceptors with a proper Fuc donor, acetylation, selective cleavage of orthogonal protecting groups (Bn ethers and benzylidene), sulfation and global deprotection. An optimization of the glycosylation step was also performed in order to increase the Fuc branching contents in the final polymer chains. Hence, three fCS polysaccharides, all bearing per-*O*-sulfated Fuc branches at *O*-3 position of GlcA, but with different DF values, were obtained by

performing the glycosylation step once, twice, or thrice. It is noteworthy that these fCS structures were similar to the most common natural one in terms of the branching position, while showing an unnatural Fuc sulfation pattern. Moreover, four other fC(S) polysaccharides with unsulfated, 2-*O*-, or 2,4-*O*-sulfated Fuc branches placed at the unnatural *O*-4 position of GalNAc were prepared. Finally, the access to fCS polysaccharides carrying per-*O*-sulfated Fuc branches at position *O*-6 of GalNAc units was also attempted. 2D-NMR spectroscopic analysis allowed a full characterization of all the obtained fC(S) products, confirming the Fuc branching at the expected position according to the designed strategy. A single, well-defined sulfation pattern was found for Fuc branches in all the semi-synthesized fCS polysaccharides, contrary to the natural ones studied up to now, which display two or even more different sulfation patterns within the same polymer chain.

Table 2.11. Semi-synthetic fCS polysaccharides.

Product	Yield [a]	Fuc Branching Position	Fuc Sulfation Pattern	DF	α/β ratio
fCS-1a	30%	*O*-3 GlcA	2,3,4-*O*-sulfated	0.41	1.4
fCS-1b	20%	*O*-3 GlcA	2,3,4-*O*-sulfated	0.69	1.4
fCS-1c	24%	*O*-3 GlcA	2,3,4-*O*-sulfated	0.69	1.3
fCS-5	13%	*O*-4 GalNAc	unsulfated	0.34	only α
fCS-6	10%	*O*-4 GalNAc	unsulfated	0.44	only α
fCS-7	60%	*O*-4 GalNAc	2,4-*O*-sulfated	0.43	only α
fCS-8	19%	*O*-4 GalNAc	2-*O*-sulfated	0.40	9.0
fCS-9a	50%	*O*-6 GalNAc	2,3,4-*O*-sulfated	0.21	0.33
fCS-9b	52%	*O*-6/*O*-4 GalNAc (9:1)	2,3,4-*O*-sulfated	0.20	9.0
fCS-9c	58%	*O*-6/*O*-4 GalNAc (4:1)	2,3,4-*O*-sulfated	0.29	19.0

[a] Overall weight yield from corresponding polysaccharide glycosyl acceptor.

Future research will be aimed to the completion of the library of semi-synthetic fC(S) polysaccharides, in order to perform wider and more accurate structure–activity relationship studies with respect to those achieved so far, involving only

naturally-occurring heterogenous structures. In this frame, a preliminary screening of the biological activities of the semi-synthetic fC(S) products, combined with the three-dimensional structure characterization through NMR and computational techniques, has been recently launched. The results will drive further research efforts aimed at the development of an effective, safe and non-animal sourced antithrombotic drug candidate.

2.4. Experimental Section

2.4.1. General Methods

Unsulfated chondroitin sodium salt was obtained at the laboratories of Prof. Chiara Schiraldi group (Department of Experimental Medicine, Università della Campania Luigi Vanvitelli) by fed-batch fermentation of *Escherichia coli* O5:K4:H4 followed by down-stream purification processes performed as already reported (Cimini et al., **2010**; Schiraldi et al., **2012**).

Commercial grade reagents and solvents were used without further purification, except where differently indicated. The term "deionized water" refers to water purified by a Millipore Milli-Q Gradient system. Centrifugations were performed with an Eppendorf Centrifuge 5804 R instrument at 4 °C (3500 rpm, 5 min). Dialyses were conducted on Spectra/Por 3.5 kDa cut-off membranes at 4 °C. Freeze-dryings were performed with a 5Pascal Lio 5P 4K freeze dryer.

NMR spectra were recorded on a Bruker DRX-400 (^{1}H: 400 MHz, ^{13}C: 100 MHz), or on a Bruker Avance-III HD (^{1}H: 600 MHz, ^{13}C: 150 MHz) instrument equipped with a cryo probe, in D_2O (acetone as internal standard, ^{1}H: $(CH_3)_2CO$ at δ 2.22 ppm; ^{13}C: $(CH_3)_2CO$ at δ 31.5 ppm), $CDCl_3$ (^{1}H: $CHCl_3$ at δ 7.26 ppm; ^{13}C: $CDCl_3$ at δ 77.0 ppm) or DMSO-*d*$_6$ (^{1}H: CHD_2SOCD_3 at δ 2.49 ppm; ^{13}C: CD_3SOCD_3 at δ 39.5 ppm). Data were processed using the data analysis packages integrated with Bruker TopSpin® 4.0.5 software. Gradient-selected COSY, NOESY and TOCSY

experiments were performed using spectral widths of 6000 Hz in both dimensions, using data sets of 2048 × 256 points. TOCSY and NOESY mixing times were set to 120 and 200 ms, respectively. $^{1}H,^{13}C$-DEPT-HSQC experiments were measured in the ^{1}H-detected mode via single quantum coherence with proton decoupling in the ^{13}C domain, using data sets of 2048 × 512 points and typically 100 increments. As for HSQC-TOCSY and HMBC, data sets of 2048 × 256 points were used, with 120 increments, and the mixing time for HSQC-TOCSY was set to 120 ms.

2.4.2. Synthetic Procedures for CS Polysaccharides

Preparation of chondroitin acid form (1) from chondroitin sodium salt. A solution of chondroitin sodium salt (5.184 g, 12.92 mmol RU) in deionized water (154 mL) was passed through a Dowex 50 WX8 column (H^+ form, 20–50 mesh, approx. 190 cm^3). Elution with deionized water was continued until a neutral pH of the eluate was detected. Freeze-drying of the collected eluate gave chondroitin **1** (4.823 g, 93% weight yield).

Chondroitin methyl ester 2. Chondroitin **1** (2.050 g, 5.404 mmol RU) was manually chopped and then suspended under an Ar atmosphere in dry CH_3OH (250 mL). After overnight stirring at r.t., a 0.56 M methanolic solution of AcCl (102 mL, 57.7 mmol) was added *via* cannula and stirring was continued overnight at r.t. The reaction was then quenched by neutralization with 1 M $NaHCO_{3(aq)}$. The mixture was concentrated by rotoevaporation and then freeze-dried. The protocol was repeated to give, after dialysis and freeze-drying, chondroitin methyl ester **2** (1.896 g, 92% weight yield) as a white waxy solid.

General procedure of benzylidene/*p*-methoxybenzylidene ring installation. Polysaccharide **1** (or **2**) (433 mg, 1.14 mmol RU) was dried under vacuum and then dry DMF (16 mL) was added. After overnight (or 90 min in the case of reaction on **2**) stirring at 80 °C, a homogeneous suspension was obtained. It was

cooled to r.t. and then treated with α,α-dimethoxytoluene (or *p*-methoxybenzaldehyde dimethyl acetal) (1.7 mL, 11.4 mmol), freshly dried over 4Å–MS. Finally, a 0.41 M solution of CSA in dry DMF (700 μL, 0.285 mmol) was added. After overnight stirring at 80 °C, the obtained clear, yellowish solution was cooled to r.t. and treated with cold acetone (or diisopropyl ether in the case of reaction on **2**) (25 mL). The obtained whitish precipitate was collected by centrifugation and dried under vacuum overnight. Derivative **3** (or **4** from **2**, or **18** from **1** with *p*-methoxybenzaldehyde dimethyl acetal) (615 mg, 140% weight yield) was obtained as a yellowish amorphous solid.

General procedure of acetylation reaction. Polysaccharide **4** (or **3**) (722 mg, 1.50 mmol RU) was treated with Et_3N (4.2 mL, 30.0 mmol) and then with dry CH_3CN (14.3 mL). After vigorous stirring and sonication, a suspension was obtained and Ac_2O (9.9 mL, 105 mmol) and DMAP (67.3 mg, 600 μmol) were added. After overnight stirring at r.t., the obtained clear solution was treated with diisopropyl ether (60 mL). The obtained yellowish precipitate was collected by centrifugation and then dried under vacuum to afford derivative **6** (or **5**) (839 mg, 116% weight yield).

Study of benzylidene acetal *vs.* glycosidic bond cleavage on derivative 6. Polysaccharide **6** (100 mg, 177 μmol RU) was dissolved in 9:1 *v*/*v* AcOH–H_2O (3.0 mL) and the obtained solution was stirred at 50 °C. At different times, 500 μL aliquots were collected, cooled to r.t., diluted with deionized water (10 mL) and dialyzed. After freeze-drying, the obtained solid residues were weighted and subjected to ^{1}H NMR analysis in DMSO-d_6.

Alternatively, derivative **6** (92.7 mg, 164 μmol RU) was dissolved in CH_3CN (1.8 mL) and then treated with DTT (127 mg, 820 μmol) and CSA (47.6 mg, 205 μmol). The solution was stirred at r.t. At different times, 400 μL aliquots were collected, cooled to r.t., diluted with deionized water (10 mL) and dialyzed. After

freeze-drying, the obtained solid residues were weighted and subjected to ^{1}H NMR analysis in DMSO-d_6.

General procedure of benzylidene/*p*-methoxybenzylidene ring acid hydrolysis. Derivative **6** (or **11**, **12**, **19** and **21**) (816 mg, 1.44 mmol RU) was treated with 9:1 *v*/*v* AcOH–H_2O (19 mL). The resultant brownish mixture was stirred at 50 °C for 50 h (10 h and 6 h in the case of reactions on **19** and **21**, respectively). The solution was then cooled to r.t., diluted with deionized water (30 mL) and dialyzed to give, after freeze-drying, derivative **7** (or **16-i**, **17**, **20**, **22**) (457 mg, 56% weight yield), as a yellowish waxy solid.

The same procedure was applied for the obtainment of derivative **16-ii**, but in that case starting product **11** was first dissolved in the minimum amount of DMF before the aqueous acetic acid treatment.

Study of regioselective acylation reaction on polysaccharide 7. A solution of polysaccharide **7** (39.9 mg, 83.6 μmol RU) in pyridine (1.7 mL) was treated with the acylating reagent (see Table 2.12). After stirring at r.t. (or 4 °C see Table 2.12) for 4 h (or overnight, see Table 2.12), the reaction was quenched by addition of CH_3OH (700 μL) and then the mixture was treated with cold diisopropyl ether (10 mL). The obtained precipitate was collected by centrifugation and then dried under vacuum overnight to afford the crude polysaccharide products **8a–f** in the weight yields indicated in Table 2.12.

Table 2.12. Regioselective reaction conditions for O-6 protection of GalNAc units.

Entry	Acylating agent (eq)	Temperature, time	Product	Weight yield
a	BzCN (10)	r.t., o.n.	**8a**	119%
b	BzCN (10)	4 °C, 4 h	**8b**	95%
c	BzCN (5)	r.t., 4 h	**8c**	119%
d	BzCN (2.5)	r.t., 4 h	**8d**	98%
e	PivCl (5)	r.t., 4 h	**8e**	200%
f	PivC (5)	4 °C, 4 h	**8f**	210%

General procedure for silylation. Polysaccharide **4** (67.5 mg, 140 μmol RU) was dissolved in DMF (2.5 mL), which was freshly dried over 4Å–MS, and treated with TBDMSCl (106 mg, 703 μmol), TDMSCl (138 μL, 702 μmol), or TIPSCl (150 μL, 701 μmol). Imidazole (143 mg, 2.10 mmol) was then added. The resulting yellowish solution was stirred at 50 °C (35 °C in the case of reaction with TDMSCl) overnight, then cooled to r.t., and treated with diisopropyl ether (12 mL). The obtained precipitate was collected by centrifugation and then dried under vacuum overnight. Crude derivative **10a** (135 mg, 200% weight yield) was obtained as a yellowish amorphous solid [**10b** (160 mg, 237% weight yield) as a yellowish oil; **10c** (42.5 mg, 75% weight yield) as a white amorphous solid].

Polysaccharide derivative 10d. Polysaccharide **4** (69.3 mg, 144 μmol RU) was suspended in 3:1 *v*/*v* CH_3CN–DMF (3.6 mL), which were freshly dried over 4Å–MS, treated with Ac_2O (30 μL, 0.32 mmol), and heated to 40 °C. To the yellowish suspension, a 0.37 M solution of TBAOAc in freshly dried CH_3CN (233 μL, 86.4 μmol) was finally added. The mixture was stirred at 40 °C for 44 h, then cooled to r.t., and treated with diisopropyl ether (13 mL). The obtained precipitate was collected by centrifugation and then dried under vacuum overnight. Crude derivative **10d** (57.5 mg, 83% weight yield) was obtained as a white amorphous solid.

Polysaccharide derivative 10e. A mixture of polysaccharide **4** (40.1 mg, 83.4 μmol RU) and Bz_2O (20.7 mg, 91.7 μmol) was suspended under an Ar atmosphere in 3:1 *v*/*v* CH_3CN–DMF (1.3 mL), which were freshly dried over 4Å–MS. The mixture was then treated with DIPEA (17.4 μL, 100 μmol). After 90 min stirring at r.t., the mixture was heated to 45 °C and stirred for additional 24 h, then cooled to r.t., and treated with diisopropyl ether (8 mL). The obtained precipitate was collected by centrifugation and then dried under vacuum overnight. Crude derivative **10e** (39.5 mg, 99% weight yield) was obtained as a white amorphous solid.

General procedure of 3,6-lactonization/2-*O*-benzoylation/lactone opening one-pot sequence. Polysaccharide **3** (or **18**) (192 mg, 410 μmol RU) was dissolved under an Ar atmosphere in dry DMF (8.6 mL). The solution was treated with Bz_2O (2.77 g, 12.3 mmol) and then heated to 85 °C. After 26 h stirring at 85 °C, the solution was cooled to r.t. and treated with pyridine (7.3 mL) and DMAP (100 mg, 819 μmol). The yellowish solution was stirred at r.t. for 68 h and then CH_3OH (7.3 mL) and NaOAc (50.4 mg, 614 μmol) were added. After 26 h stirring at r.t., the solution was treated with CH_3OH (16 mL), concentrated by rotoevaporation to approximately 15 mL in volume and then treated with cold diisopropyl ether (25 mL). The obtained white precipitate was collected by centrifugation, then dissolved in DMSO (7 mL), and precipitated again with 2:1 *v*/*v* acetone–diisopropyl ether (30 mL). The white solid was collected by centrifugation and dried under vacuum overnight to give crude derivative **11** (or **19**) (200 mg, 104% weight yield).

General procedure of 3,6-lactonization. Polysaccharide **3** (or **18**) (204 mg, 436 μmol RU) was dissolved under an Ar atmosphere in dry DMF (9.0 mL). The solution was treated with Bz_2O (2.956 g, 13.07 mmol) and then heated to 85 °C. After 26 h stirring at 85 °C, the reaction mixture was cooled to r.t. and treated with cold diisopropyl ether (50 mL). The obtained white precipitate was collected by centrifugation and dried under vacuum overnight. Crude derivative **12** (or **21**) (123 mg, 60% weight yield) was obtained as a yellowish powder.

General procedure of sulfation and global deprotection to CS derivatives. Polysaccharide **7** (42.4 mg, 88.8 μmol RU) was dissolved in dry DMF (1.4 mL), and then treated with a 1.22 M solution of SO_3·py in dry DMF (1.5 mL, 1.78 mmol). After overnight stirring at 50 °C, a saturated NaCl solution in acetone (4 mL) was added at r.t. The obtained yellowish precipitate was collected by centrifugation and then suspended in deionized water (3.0 mL). The acid mixture (pH ≈ 1–2) was heated to 50 °C and stirred for 2 h to give a yellowish solution

that was cooled to r.t. and then treated with 4 M $NaOH_{(aq)}$ to adjust pH to 12. The solution was stirred overnight at r.t., and then 1 M $HCl_{(aq)}$ was added until neutralization. Dialysis and subsequent freeze-drying yielded polysaccharide **CS-1** (46.3 mg, 109% weight yield) as a white amorphous solid.

CS-2a–f, **CS-4a–e**, **CS-5**, **CS-7** and **CS-11–13** were obtained according to the above-mentioned procedure from the corresponding polysaccharide derivatives (**8a–f→CS-2a–f**, **10a–e→CS-4a–e**, **4→CS-5**, **12→CS-7**, **17→CS-11**, **20→CS-12**, **22→CS-13**). To obtain **CS-6**, an additional alkaline hydrolytic reaction was performed by treating a solution of the obtained solid (28.6 mg in 2.4 mL of deionized water) first with 2:1 *v/v* 1 M $LiOH_{(aq)}$–30% H_2O_2 (1.8 mL, pH ≈ 10) at r.t. overnight and then with 4 M $NaOH_{(aq)}$ to adjust pH to 12. The obtained solution was stirred at r.t. overnight, then neutralized with 4 M $HCl_{(aq)}$, and finally, treated with 1 M $NaCl_{(aq)}$ (3.6 mL). After 1 h stirring at r.t., the solution was dialyzed and subsequently freeze-dried to yield polysaccharide **CS-6** (22.2 mg, 31% weight yield from **11**) as a white amorphous solid.

General procedure of mild sulfation. CS-5 (or chondroitin sodium salt, or **CS-6**,**7**) (35.9 mg, 59.3 μmol RU) was dissolved in deionized water (550 μL) and passed through a short Dowex 50 WX8 column (H^+ form, 20–50 mesh, approx. 4 cm^3). Elution with deionized water was continued until pH of the eluate was neutral. The obtained eluate was treated with a few drops of an aqueous solution of TBAOH (16% *w/v* TBAOH in H_2O) to neutralize the solution. Freeze-drying of the collected eluate gave product **13** (or **9**, **14**, **15**) (68.1 mg), that was then dissolved in dry DMF (800 μL). The obtained solution was cooled to 4° C (r.t. was set in the case of reaction on chondroitin sodium salt) and treated with a 0.46 M solution of SO_3·py in dry DMF (540 μL, 244 μmol). After 1 h stirring at 4 °C (or r.t.), some drops of 1 M $NaHCO_{3(aq)}$ were added at r.t. to adjust pH to 7. Then 0.3 M $NaCl_{(aq)}$ (7.3 mL) was added keeping the same temperature and the stirring was continued for 1 h. The obtained solution was dialyzed for one day and

subsequently passed through a short Dowex 50 WX8 column (H^+ form, 20-50 mesh, approx. 4 cm^3). Elution with deionized water was continued until pH of the eluate was neutral. The eluate was treated with some drops of 1 M $NaOH_{(aq)}$ to adjust pH to 7. Dialysis and subsequent freeze-drying yielded polysaccharide **CS-8** (or **CS-3**, **CS-9**, **CS-10**) (39.8 mg, 111% weight yield).

6-de-*O*-sulfation procedure (CS-14). A solution of **CS-11** (35.8 mg) in deionized water (1.0 mL) was passed through a short Dowex 50 WX8 column (H^+ form, 20–50 mesh, approx. 4 cm^3) at r.t., the eluate was neutralized with pyridine, and freeze-dried. The obtained pyridinium salt **23** (39.1 mg) was dissolved in dry pyridine (1.7 ml) and BTSA (380 μL, 1.56 mmol) was added. The mixture was kept overnight stirring at 70 °C to give a clear yellowish solution, then deionized water (3 mL) was added at r.t. to the mixture, with the simultaneous appearance of whitish turbidity. After 10 min stirring at r.t., the mixture was dialyzed for 3 days; the dialysate was treated with Dowex 50 WX8 resin (H^+ form, 20-50 mesh), until pH 3 was reached, filtered and pH was adjusted to 7 with 0.1 M $NaOH_{(aq)}$. Dialysis and freeze-drying gave **CS-14** (15.4 mg, 43% weight yield).

2.4.3. Synthetic Procedures for fCS Polysaccharides

Ethyl 1-thio-β-L-fucopyranoside (28). Commercially available L-fucose (5.017 g, 30.55 mmol) was suspended in pyridine (11.5 mL) and treated with Ac_2O (11.5 mL, 122 mmol). After overnight stirring at r.t., the obtained solution was diluted with CH_2Cl_2 (60 mL) and washed with 0.5 M $HCl_{(aq)}$ (60 mL). The organic phase was dried over anhydrous Na_2SO_4, filtered and concentrated to afford 1,2,3,4-tetra-*O*-acetyl-L-fucopyranoside (9.717 g, 96%, α/β 35:65) as a yellow oil. ^1H NMR (600 MHz, $CDCl_3$): δ 6.24 (d, *J* 3.1 Hz, 1H, H-$1^{\alpha\text{-anomer}}$), 5.68 (d, *J* 8.3 Hz, 1H, H-$1^{\beta\text{-anomer}}$), 5.29–5.23 (m, 6H, H-$2^{\alpha\text{-anomer}}$, H-$3^{\alpha\text{-anomer}}$, H-$4^{\alpha\text{-anomer}}$, H-$2^{\beta\text{-anomer}}$, H-$3^{\beta\text{-anomer}}$, H-$4^{\beta\text{-anomer}}$), 5.08 (dd, *J* 10.4, 3.4 Hz, 1H , H-$3^{\beta\text{-anomer}}$) 4.27 (q, *J* 6.4 Hz,

1H, H-5$^{\alpha\text{-anomer}}$), 3.95 (q, *J* 6.4 Hz, 1H, H-5$^{\beta\text{-anomer}}$), 2.20 (s, 3H, OCOCH$_3^{\beta\text{-anomer}}$), 2.18 (s, 3H, OCOCH$_3^{\alpha\text{-anomer}}$), 2.15 (s, 3H, OCOCH$_3^{\alpha\text{-anomer}}$), 2.12 (s, 3H, OCOCH$_3^{\beta\text{-anomer}}$), 2.04 (s, 3H, OCOCH$_3^{\beta\text{-anomer}}$), 2.02 (s, 3H, OCOCH$_3^{\alpha\text{-anomer}}$), 2.00 (s, 3H, OCOCH$_3^{\alpha\text{-anomer}}$), 1.99 (s, 3H, OCOCH$_3^{\beta\text{-anomer}}$), 1.23 (d, *J* 6.0 Hz, 3H, H-6$^{\beta\text{-anomer}}$), 1.16 (d, *J* 6.4 Hz, 3H, H-6$^{\alpha\text{-anomer}}$). A solution of 1,2,3,4-tetra-*O*-acetyl-L-fucopyranoside (9.717 g, 29.24 mmol) in CH_2Cl_2 (30.0 mL), was treated with I_2 (10.391 g, 40.94 mmol), and Et_3SiH (6.54 mL, 40.9 mmol). After stirring for 3 h at reflux, the mixture was then cooled to r.t., diluted with CH_2Cl_2 (100 mL) and washed with 1:1 *v*/*v* 1 M $NaHCO_{3(aq)}$–10% $Na_2S_2O_{3(aq)}$ (100 mL). The organic phase was dried over anhydrous Na_2SO_4, filtered, and concentrated obtaining crude product 2,3,4-tri-*O*-acetyl-1-iodo-α-L-fucopyranoside as an oil, contaminated by the presence of siloxanes. ^{1}H NMR (400 MHz, $CDCl_3$): δ 7.10 (d, *J* 3.9 Hz, 1H, H-1), 5.34 (d, *J* 2.4 Hz, 1H, H-4), 5.29 (dd, *J* 10.2, 3.2 Hz, 1H, H-3), 4.44 (m, 1H, H-2), 4.28 (q, *J* 6.4 Hz, 1H, H-5), 2.17 (s, 3H, $OCOCH_3$), 2.11 (s, 3H, $OCOCH_3$), 2.00 (s, 3H, $OCOCH_3$), 1.23 (d, *J* 6.4 Hz, 3H, H-6). A suspension of 2,3,4-tri-*O*-acetyl-1-iodo-α-L-fucopyranoside in dry CH_3CN (30 mL) was treated with $(NH_2)_2CS$ (3.339 g, 43.86 mmol) and stirred for 1 h at 60 °C. The mixture was cooled to r.t., then C_2H_5I (4.70 mL, 58.5 mmol) and Et_3N (16.3 mL, 117 mmol) were added. After stirring for 2 h at r.t., the yellowish solution was concentrated by rotoevaporation, then diluted with CH_2Cl_2 (100 mL) and washed with 0.1 M $HCl_{(aq)}$ (100 mL). The organic phase was dried over anhydrous Na_2SO_4, filtered and concentrated. The obtained residue was purified by column chromatography (5:1–3:1 *v*/*v* petroleum ether–ethyl acetate) to afford pure ethyl 2,3,4-tri-*O*-acetyl-1-thio-β-L-fucopyranoside (5.688 g, 58% over two steps from 1,2,3,4-tetra-*O*-acetyl-L-fucopyranoside) as a yellowish oil. ^{1}H NMR (400 MHz, $CDCl_3$): δ 5.28 (d, *J* 3.2 Hz, 1H, H-4), 5.23 (t, *J* 10.0 Hz, 1H, H-2), 5.05 (dd, *J* 10.0, 3.2 Hz, 1H, H-3), 4.46 (d, *J* 9.9 Hz, 1H, H-1), 3.83 (q, *J* 6.3 Hz, 1H, H-5), 2.74 (m, 2H, S*CH*$_2$CH$_3$), 2.22 (s, 3H, $OCOCH_3$), 2.07 (s, 3H, $OCOCH_3$),

1.99 (s, 3H, $OCOCH_3$), 1.29 (t, *J* 7.4 Hz, 3H, SCH_2CH_3), 1.23 (d, *J* 6.4 Hz, 3H, H-6). A suspension of ethyl 2,3,4-tri-*O*-acetyl-1-thio-β-L-fucopyranoside (5.685 g, 17.00 mmol) in dry CH_3OH (30.0 mL) was treated with a 5.0 M solution of $Na_{(s)}$ in dry CH_3OH (2.0 mL, 10.2 mmol). The yellow solution was stirred for 3 h at r.t., neutralized with Dowex 50 WX8 resin (H^+ form, 20-50 mesh), filtered and concentrated to afford pure product **28** (3.465 g, 98%) as a yellowish amorphous solid. ^{1}H NMR (400 MHz, $CDCl_3$): δ 4.30 (d, *J* 9.4 Hz, 1H, H-1), 3.80 (s, 1H, H-4), 3.68 (q, *J* 6.5 Hz, 1H, H-5), 3.63 (m, 2H, H-2, H-3), 2.75 (m, 2H, SCH_2CH_3), 1.35 (d, *J* 6.4 Hz, 3H, H-6), 1.32 (t, *J* 7.2 Hz, 3H, SCH_2CH_3).

Ethyl 2,3,4-tri-*O*-benzyl-1-thio- β-L-fucopyranoside (24). A solution of **28** (647 mg, 3.11 mmol) in dry DMF (4.8 mL) was cooled to 0 °C and treated with BnBr (1.33 mL, 11.2 mmol) and then NaH (60% dispersion in mineral oil, 447.5 mg, 18.65 mmol). After 20 min stirring at 0 °C, the solution was warmed up to r.t. and stirred for 3 h further. The reaction was then quenched by careful addition in small aliquots of deionized water (20 mL) at 0 °C, then CH_2Cl_2 (15 mL) was added. The organic layer was collected, dried over anhydrous Na_2SO_4, filtered and concentrated. The obtained residue was subjected to column chromatography (15:1–8:1 *v*/*v* *n*-hexane–ethyl acetate) to afford pure product **24** (1.131 g, 76%) as a yellowish amorphous solid. ^{1}H NMR (400 MHz, $CDCl_3$): δ 7.41–7.22 (m, 15H, Ar H), 5.01 (d, *J* 11.8 Hz, 1H, OC*H*HPh), 4.92 (d, *J* 10.2 Hz, 1H, OC*H*HPh), 4.82 (d, *J* 10.2 Hz, 1H, OC*H*HPh), 4.78 (d, *J* 10.2 Hz, 1H, OC*H*HPh), 4.76 (d, *J* 11.8 Hz, 1H, OC*H*HPh), 4.71 (d, *J* 11.8 Hz, 1H, OC*H*HPh), 4.41 (d, *J* 9.6 Hz, 1H, H-1), 3.85 (t, *J* 9.4 Hz, 1H, H-2), 3.64 (d, *J* 2.1 Hz, 1H, H-4), 3.58 (dd, *J* 9.2, 2.7 Hz, 1H, H-3), 3.50 (q, *J* 6.4, 1H, H-5), 2.76 (m, 2H, SCH_2CH_3), 1.33 (t, *J* 7.2 Hz, 3H, SCH_2CH_3), 1.25 (d, *J* 6.4 Hz, 3H, H-6).

Ethyl 2,4-di-*O*-benzyl-1-thio-β-L-fucopyranoside (29). A solution of **28** (341 mg, 1.64 mmol) in DMF (2.8 mL) was cooled to 0 °C and treated with imidazole (280 mg, 4.11 mmol) and TBDMSCl (150 mg, 1.89 mmol). After 15 min stirring

at 0 °C, the temperature was raised to r.t. and stirring was continued for additional 4 h. The solution was then diluted with ethyl acetate (20 mL) and washed with deionized water (20 mL). The organic phase was collected, dried over anhydrous Na_2SO_4, filtered, and concentrated. The obtained residue was purified by column chromatography (10:1–6:1 *v*/*v* *n*-hexane–ethyl acetate) to afford pure ethyl 3-*O*-*tert*-butyldimethylsilyl-1-thio-β-L-fucopyranoside (370 mg, 70%). ^{1}H NMR (600 MHz, $CDCl_3$): δ 4.24 (d, *J* 9.3 Hz, 1H, H-1), 3.64–3.57 (m, 4H, H-2, H-3, H-4, H-5), 2.74 (m, 2H, SC*H*$_2$CH$_3$), 1.36 (d, *J* 6.5 Hz, 3H, H-6), 1.30 (t, *J* 7.4 Hz, 3H, SCH$_2$C*H*$_3$), 0.92 (s, 9H, SiC(C*H*$_3$)$_3$), 0.16 (s, 3H, SiC*H*$_3$), 0.13 (s, 3H, SiC*H*$_3$). A solution of ethyl 3-*O*-*tert*-butyldimethylsilyl-1-thio-β-L-fucopyranoside (364 mg, 1.13 mmol) in DMF (3.3 mL) was cooled to 0 °C and treated with BnBr (325 μL, 2.71 mmol) and then NaH (60% dispersion in mineral oil, 108 mg, 4.52 mmol). After 10 min stirring at 0 °C, the temperature was raised to r.t. and stirring was continued for additional 2 h. The reaction was then quenched by careful addition in small aliquots of deionized water (20 mL) at 0 °C, then CH_2Cl_2 (30 mL) was added. The organic layer was collected, dried over anhydrous Na_2SO_4, filtered, and concentrated to give a residue that was subjected to column chromatography (12:1–8:1 *v*/*v* *n*-hexane–ethyl acetate) to afford pure ethyl 2,4-di-*O*-benzyl-3-*O*-*tert*-butyldimethylsilyl-1-thio-β-L-fucopyranoside (466 mg, 82%). ^{1}H NMR (400 MHz, $CDCl_3$): δ 7.43–7.27 (m, 10H, Ar H), 5.09 (d, *J* 11.5 Hz, 1H, OC*H*HPh), 4.87 (d, *J* 10.8 Hz, 1H, OC*H*HPh), 4.74 (d, *J* 10.1 Hz, 1H, OC*H*HPh), 4.62 (d, *J* 12.1 Hz, 1H, OC*H*HPh), 4.38 (d, *J* 9.4 Hz, 1H H-1), 3.75 (dd, *J* 9.3, 2.3 Hz, 1H, H-3), 3.67 (t, *J* 9.4 Hz, 1H, H-2), 3.55 (m, 1H, H-5), 3.45 (d, *J* 2.0 Hz, 1H, H-4), 2.73 (m, 2H, SC*H*$_2$CH$_3$), 1.32–1.22 (m, 6H, SCH$_2$C*H*$_3$, H-6), 0.96 (s, 9H, SiC(C*H*$_3$)$_3$), 0.13 (s, 3H, SiC*H*$_3$), 0.08 (s, 3H, SiC*H*$_3$). A solution of ethyl 2,4-di-*O*-benzyl-3-*O*-*tert*-butyldimethylsilyl-1-thio-β-L-fucopyranoside (460 mg, 915 μmol) in THF (6.2 mL) was treated with a 1.0 M solution of TBAF in THF (2.3 mL). After 3 h stirring at r.t., the reaction mixture was concentrated by

rotoevaporation and the obtained residue was subjected to column chromatography (10:1–4:1 *v*/*v* *n*-hexane–ethyl acetate) to afford pure **29** (316 mg, 89%). ^{1}H NMR (400 MHz, $CDCl_3$): δ 7.42–7.30 (m, 10H, Ar H), 4.95 (d, *J* 10.8 Hz, 1H, OC*H*HPh), 4.76 (s, 2H, OCH_2Ph), 4.69 (d, *J* 10.8 Hz, 1H, OC*H*HPh), 4.38 (d, *J* 9.6 Hz, 1H, H-1), 3.67 (dd, *J* 9.1, 3.0 Hz, 1H, H-3), 3.61 (d, *J* 3.5 Hz, 1H, H-4), 3.58–3.52 (m, 2H, H-2, H-5), 2.76 (m, 2H, SCH_2CH$_3$), 1.33–1.28 (m, 6H, SCH$_2$CH_3, H-6).

Ethyl 3-*O*-benzoyl-2,4-di-*O*-benzyl-1-thio-β-L-fucopyranoside (25). A solution of **29** (310 mg, 798 μmol) in 1:1 *v*/*v* CH_2Cl_2 /pyridine (4.9 mL) was treated with BzCl (140 μL, 1.20 mmol). After 3 h stirring at r.t., the reaction was quenched by adding CH_3OH (600 μL). The solution was diluted with CH_2Cl_2 (20 mL) and washed with 0.1 M $HCl_{(aq)}$ (20 mL). The organic layer was dried over anhydrous Na_2SO_4, filtered, and concentrated to give a residue that was subjected to column chromatography (12:1–8:1 *v*/*v* *n*-hexane–ethyl acetate) to afford pure **25** (263 mg, 67%) as a white powder. ^{1}H NMR (400 MHz, $CDCl_3$): δ 8.01 (d, *J* 7.2, 2H, H$_{ortho}$-Bz), 7.59 (t, *J* 7.6 Hz, 1H, H$_{para}$-Bz), 7.44 (t, *J* 7.6 Hz, 2H, H$_{meta}$-Bz), 7.25–7.15 (m, 15H, Ar H), 5.22 (dd, *J* 9.8, 3.2 Hz, 1H, H-3), 4.87 (d, *J* 10.8 Hz, 1H, OC*H*HPh), 4.71 (d, *J* 11.8 Hz, 1H, OC*H*HPh), 4.67 (d, *J* 10.9 Hz, 1H, OC*H*HPh), 4.57 (d, *J* 11.6 Hz, 1H, OC*H*HPh), 4.53 (d, *J* 9.6 Hz, 1H, H-1), 3.98 (t, *J* 9.7 Hz, 1H, H-2), 3.86 (d, *J* 3.1 Hz, 1H, H-4), 3.74 (q, *J* 6.5 Hz, 1H, H-5), 2.79 (m, 2H, SCH_2CH$_3$), 1.32 (t, *J* 7.4 Hz, 3H, SCH$_2$CH_3), 1.26 (d, *J* 6.4 Hz, 3H, H-6).

Ethyl 2-*O*-benzyl-1-thio-β-L-fucopyranoside (30). Compound **28** (1.251 g, 6.015 mmol) was treated with $(CH_3)_2C(OCH_3)_2$ (6.7 mL, 54 mmol) and with CSA (348.3 mg, 1.500 mmol). After 5 h stirring at r.t., the solution was diluted with CH_2Cl_2 (20 mL) and then washed with 1 M $NaHCO_{3(aq)}$ (20 mL). The organic phase was dried over anhydrous Na_2SO_4, filtered and concentrated to afford crude ethyl 3,4-*O*-isopropylidene-1-thio-β-L-fucopyranoside (1.223 g, 82%) as a

yellowish oil. ^{1}H NMR (600 MHz, $CDCl_3$, δ): 4.20 (d, *J* 10.2 Hz, 1H, H-1), 4.05 (dd, *J* 5.5, 2.2 Hz, 1H, H-4), 4.03 (dd, *J* 6.8, 5.5 Hz, 1H, H-3), 3.87 (quartet of doublets, *J* 6.6, 2.2 Hz, 1H, H-5), 3.54 (dd, *J* 10.2, 6.8 Hz 1H, H-2), 2.74 (m, 2H, SCH_2CH_3), 1.53 (s, 3H, CCH_3), 1.40 (d, *J* 6.4 Hz, 3H, H-6), 1.36 (s, 3H, CCH_3), 1.31 (t, *J* 7.4 Hz, 3H, SCH_2CH_3). A solution of ethyl 3,4-*O*-isopropylidene-1-thio-β-L-fucopyranoside (1.214 g, 4.888 mmol) in dry DMF (9.9 mL) was cooled to 0 °C and treated with BnBr (700 μL, 5.86 mmol) and then with NaH (60% dispersion in mineral oil, 234 mg, 9.78 mmol). After 10 min stirring at 0 °C, the mixture was cooled to r.t. and stirred for 1 h further. The reaction was quenched by careful addition in small aliquots of deionized water (10 mL) at 0 °C, then CH_2Cl_2 (20 mL) was added. The organic layer was collected, dried over anhydrous Na_2SO_4, filtered and concentrated. The obtained residue was subjected to column chromatography (12:1–7:1 *v*/*v* *n*-hexane–ethyl acetate) to afford pure ethyl 2-*O*-benzyl-3,4-*O*-isopropylidene-1-thio-β-L-fucopyranoside (1.307 g, 79%) as a yellowish powder. ^{1}H NMR (600 MHz, $CDCl_3$): δ 7.43-7.26 (m, 5H, Ar H), 4.84 (d, *J* 11.4 Hz, 1H, OC*H*HPh), 4.76 (d, *J* 11.4 Hz, 1H, OC*H*HPh), 4.38 (d, *J* 9.7 Hz, 1H, H-1), 4.19 (dd, *J* 6.7, 5.6 Hz, 1H, H-3), 4.05 (dd, *J* 5.6, 2.1 Hz, 1H, H-4), 3.81 (quartet of doublets, *J* 6.6, 2.2 Hz, 1H, H-5), 3.44 (dd, *J* 9.8, 6.7 Hz, 1H, H-2), 2.71 (m, 2H, SCH_2CH_3), 1.45 (s, 3H, CCH_3), 1.39 (d, *J* 6.5 Hz, 3H, H-6), 1.36 (s, 3H, CCH_3), 1.29 (t, *J* 7.43 Hz, 3H, SCH_2CH_3). A suspension of ethyl 2-*O*-benzyl-3,4-*O*-isopropylidene-1-thio-β-L-fucopyranoside (1.300 g, 3.347 mmol) in 4:1 *v*/*v* TFA–H_2O (10.6 mL) was stirred for 1 h at r.t. The mixture was then diluted with deionized water (70 mL) and washed with CH_2Cl_2 (70 mL). The organic phase was washed with 1 M $NaHCO_{3(aq)}$ (70 mL), then dried over anhydrous Na_2SO_4, filtered and concentrated affording product **30** (898.7 mg, 90%) as a yellowish oil. ^{1}H NMR (600 MHz, $CDCl_3$): δ 7.43–7.30 (m, 5H, Ar H), 4.97 (d, *J* 11.2 Hz, 1H, OC*H*HPh), 4.69 (d, *J* 11.1 Hz, 1H, OC*H*HPh), 4.40 (d, *J* 9.7 Hz, 1H, H-1), 3.75 (d, *J* 3.0 Hz, 1H, H-4), 3.64–3.60 (m, 2H, H-3, H-5), 3.45

(t, *J* 9.4 Hz, 1H, H-2), 2.67 (m, 2H, SC*H*$_2$CH$_3$), 1.35–1.25 (m, 6H, SCH$_2$C*H*$_3$, H-6).

Ethyl 3,4-di-*O*-benzoyl-2-*O*-benzyl-1-thio-β-L-fucopyranoside (26). Compound **30** (697 mg, 2.33 mmol) was dissolved in dry CH_2Cl_2 (14 mL) and then treated with BzCl (1.14 mL, 9.81 mmol) and pyridine (3.5 mL). After 2 h stirring at r.t., the solution was diluted with CH_2Cl_2 (50 mL) and washed with 1 M $HCl_{(aq)}$ (50 mL). The organic phase was dried over anhydrous Na_2SO_4, filtered and concentrated. The obtained residue was purified through column chromatography (12:1–10:1 *v*/*v* toluene–ethyl acetate), to afford pure compound **26** (1.005 g, 85%) as a yellowish solid. ^{1}H NMR (400 MHz, $CDCl_3$): δ 8.18–7.14 (m, 15H, Ar H), 5.65 (d, *J* 3.3 Hz, 1H, H-4), 5.42 (dd, *J* 9.6, 3.4 Hz, 1H, H-3), 4.85 (d, *J* 10.4 Hz, 1H, OC*H*HPh), 4.66 (d, *J* 9.7 Hz, 1, H-1), 4.63 (d, *J* 10.4 Hz, OC*H*HPh), 3.99 (quartet of doublets, *J* 14.2, 7.1 Hz, 1H, H-5), 3.91 (t, *J* 9.7 Hz, 1H, H-2), 2.85 (m, 2H, SC*H*$_2$CH$_3$), 1.40–1.20 (m, 6H, SCH$_2$C*H*$_3$, H-6).

Ethyl 4-*O*-benzoyl-2,3-di-*O*-benzyl-1-thio-β-L-fucopyranoside (27). A mixture of **30** (1.741 g, 6.128 mmol) and Bu_2SnO (1.830 g, 7.354 mmol) was suspended in 10:1 *v*/*v* C_6H_6–CH_3OH (35.2 mL) and stirred at 60 °C. After 3 h, the solution was cooled to r.t., concentrated and then, under an Ar atmosphere, Bu_4NBr (1.975 g, 6.128 mmol), dry toluene (17.9 mL) and BnBr (728 μL, 6.13 mmol) were added. After overnight stirring at 65 °C, the solution was cooled to r.t., concentrated and the residue was purified through column chromatography (6:1–1:4 *v*/*v* *n*-hexane–ethyl acetate) affording pure ethyl 2,3-di-*O*-benzyl-1-thio-β-L-fucopyranoside (2.715 g, 95%). ^{1}H NMR (600 MHz, $CDCl_3$): δ 7.41–7.28 (m, 10H, Ar H), 4.88 (d, *J* 10.2 Hz, 1H, OC*H*HPh), 4.76 (d, *J* 10.2 Hz, 1H, OC*H*HPh), 4.72–4.70 (m, 2H, OC*H*HPh, OC*H*HPh), 4.39 (d, *J* 9.7 Hz, 1H, H-1), 3.82 (s, 1H, H-4), 3.62 (t, *J* 9.6 Hz, 1H, H-2), 3.56-3.52 (m, 2H, H-3, H-5), 2.75 (m, SC*H*$_2$CH$_3$, 2H), 1.34 (d, *J* 6.4 Hz, 3H, H-6), 1.31 (t, *J* 7.4 Hz, 3H, SCH$_2$C*H*$_3$). A suspension of ethyl 2,3-di-*O*-benzyl-1-thio-β-L-fucopyranoside (2.131 g, 5.492 mmol) in dry

CH_2Cl_2 (24.0 mL) was treated with BzCl (958 μL, 8.25 mmol) and pyridine (6.0 mL). After 2h stirring at r.t., the solution was diluted with CH_2Cl_2 (50.0 mL) and washed with 1.0 M $HCl_{(aq)}$ (50.0 mL). The organic phase was collected, dried over anhydrous Na_2SO_4, filtered and concentrated affording a residue that was purified through column chromatography (12:1–6:1 *v*/*v* *n*-hexane–ethyl acetate), to afford pure compound **27** (2.216 g, 82%). ^{1}H NMR (600 MHz, $CDCl_3$): δ 8.14–7.24 (m, 15H, HAr), 5.63 (d, *J* 2.9 Hz, 1H, H-4), 4.85–4.81 (m, 2H, OC*H*HPh, OC*H*HPh), 4.77 (d, *J* 10.26 Hz, 1H, OC*H*HPh), 4.57 (d, *J* 11.7 Hz, 1H, OC*H*HPh), 4.50 (d, *J* 9.70 Hz, 1H, H-1), 3.77 (q, *J* 6.40 Hz, 1H, H-5), 3.73 (dd, *J* 9.17 Hz, *J* 3.21 Hz, 1H, H-3), 3.69 (t, *J* 9.7 Hz, 1H, H-2), 2.81 (m, SC*H*$_2$CH$_3$, 2H), 1.35 (t, *J* 7.4 Hz, 3H, SCH_2CH_3), 1.29 (d, *J* 6.4 Hz, 3H, H-6).

Polysaccharide derivative 46a. Polysaccharide **6** (40.1 mg, 71.0 μmol RU) was co-evaporated three times with dry toluene (4 mL each). The residue was further dried under vacuum for 2 h and then mixed with AW–300 4Å–MS under an Ar atmosphere. The mixture was treated with 1:1 *v*/*v* CH_2Cl_2–CH_3CN (4.2 mL), that were freshly dried over AW–300 4Å–MS. The polysaccharide was completely dissolved in few minutes. The mixture was cooled to 0 °C and then treated with Et_3SiH (136 μL, 852 μmol) and $BF_3{\cdot}OEt_2$ (18.0 μL, 142 μmol). After 4 h stirring at r.t., the reaction was worked up by neutralization with Et_3N; the molecular sieves were then removed by decantation and the mixture was poured in ethyl acetate (15 mL). The obtained precipitate was collected by centrifugation and then dried under vacuum overnight to afford crude derivative **46a** (19.2 mg, 48% weight yield) as a yellowish powder.

Polysaccharide derivative 46b. Polysaccharide **6** (44.3 mg, 78.3 μmol RU) was co-evaporated three times with dry toluene (3 mL each). The residue was further dried under vacuum for 2 h and then mixed with AW–300 4Å–MS under an Ar atmosphere. The mixture was treated with freshly dried THF (2.0 mL). The polysaccharide was finely suspended after 4 h stirring at 50 °C. The mixture was

then cooled to r.t. and treated with a 1.0 M solution of BH_3·THF complex in THF (783 μL, 783 μmol) and a 0.55 M solution of TMSOTf in freshly dried THF (46 μL, 25.5 μmol). After overnight stirring at r.t., the reaction was worked up by neutralization with Et_3N and then addition of CH_3OH (3 mL). The solution obtained by mechanical separation from the molecular sieves was concentrated by rotoevaporation. The residue was dissolved in DMSO (1 mL) and then treated with acetone (8 mL) to obtain a precipitate that was collected by centrifugation and then dried under vacuum overnight. Crude derivative **46b** (22.0 mg, 50% weight yield) was afforded as a brownish amorphous solid.

Example of glycosylation reaction. A mixture of polysaccharide acceptor **11** (125 mg, 214 μmol) and fucosyl donor **24** (313 mg, 534 μmol) was co-evaporated three times with dry toluene (5 mL each). The residue was dried under vacuum and then mixed, under an Ar atmosphere, with AW–300 4Å–MS. DMF (5.6 mL) and CH_2Cl_2 (9.3 mL), which were freshly dried over AW–300 4Å–MS, were added to the solid mixture. The mixture was stirred at −20 °C (or at r.t. for glycosylation on **8a** and **8c**) for 10 min, and then treated under an Ar atmosphere with NIS (132 mg, 587 μmol) and a 0.37 M solution of TMSOTf in freshly dried CH_2Cl_2 (29 μL, 160 μmol). After 4 h stirring at r.t., a few drops of Et_3N were added to quench the reaction. Then, the molecular sieves were removed by decantation and the mixture was poured in cold diisopropyl ether (30 mL). The obtained brownish precipitate was collected by centrifugation and dried under vacuum overnight. The product was then subjected to a second glycosylation step, reiterating the same procedure, and affording **31b** (73.8 mg, 59% weight yield).

Glycosylation products **34**, **35**, **36**, **37** were prepared according to the procedure described above. Glycosylation product **31a** was prepared without repeating the fucosylation step. Glycosylation product **31c** was prepared repeating three times the procedure described above.

The same procedure (without reiteration) was also applied in the case of glycosylation reactions of polysaccharide acceptor **7** with fucosyl donor **24**, performing the reaction at −30 °C or −10 °C or r.t., and giving products **48a**, **48b** and **48c**.

Example of acetylation. Derivative **31b** (72.9 mg) was treated with Et_3N (350 μL) and CH_3CN (2.4 mL); the suspension was then treated with Ac_2O (825 μL) and DMAP (6 mg). After stirring overnight at r.t., a clear solution was obtained. It was treated with diisopropyl ether (20 mL) to give a precipitate that was collected by centrifugation and then dried under vacuum overnight to afford derivative **32b** (70.9 mg, 97% weight yield). The same procedure was applied for acetylation of **31a** (**31a → 32a**), **31c** (**31c → 32c**), **34** (**34 → 38**), **35** (**35 → 39**), **36** (**36 → 40**), **37** (**37 → 41**).

Example of benzyl (and benzylidene) oxidative cleavage. Derivative **32b** (69.3 mg) was suspended in ethyl acetate (2.0 mL) and then treated with a 0.34 M solution of $NaBrO_3$ in deionized water (2.45 mL). A 0.27 M solution of $Na_2S_2O_4$ in deionized water (2.3 mL) was added portion wise over a period of 10 min. The triphasic mixture was vigorously stirred at r.t. overnight under visible light irradiation. A yellowish precipitate was collected by centrifugation and dried under vacuum overnight affording **33b** (50.9 mg, 73% weight yield).

The same procedure was applied on **32a** (**32a → 33a**), **32c** (**32c → 33c**), **38** (**38 → 42**), **40** (**40 → 44**). In the case of reactions on **39**, **41**, **48a,b,c**, the supernatant obtained after centrifugation was diluted with ethyl acetate (30 mL) and deionized water (30 mL) and partitioned in a separatory funnel. The aqueous phase was dialyzed and, after freeze-drying, mixed with the previously obtained precipitate to afford products **43**, **45**, **49a,b,c**.

Example of sulfation and global deprotection. A solution of **33b** (50.9 mg) in dry DMF (800 μL) was treated with a 1.0 M solution of SO_3·py in dry DMF (1.3 mL) and then stirred overnight at 50 °C. A saturated NaCl solution in acetone (15

mL) was then added to give a precipitate that was collected by centrifugation and then suspended in deionized water (3.2 mL). The suspension was treated with 4 M $NaOH_{(aq)}$ to adjust pH to 12. After overnight stirring at r.t., 4 M $HCl_{(aq)}$ was added to the suspension until neutralization. Dialysis and subsequent freeze-drying gave **fCS-1b** (38.8 mg, 76% weight yield). The same procedure was applied on **33a** (**33a → fCS-1a**), **33c** (**33ac→ fCS-1c**), **42** (**42→ fCS-5**), **43** (**43→ fCS-6**), **44 (44→ fCS-7**), **45** (**45→ fCS-8**). In the case of reaction on **49a** (or **49b** or **49c**) (34.6 mg), the precipitate obtained after the sulfation step was suspended in deionized water (2.7 mL), then treated with 2:1 *v/v* 1 M $LiOH_{(aq)}$–30% $H_2O_{2(aq)}$ (4.7 mL, pH ≈ 10) and stirred overnight at r.t. The resulting solution was then neutralized with 4 M aqueous $HCl_{(aq)}$ and treated with 1 M aqueous NaCl (9.5 mL). After 1 h stirring at r.t., the solution was dialyzed and freeze-dried, affording **fCS-9a** (or **fCS-9b**, or **fCS-9c**) (23.0 mg, 66% weight yield).

2.4.4. ^{1}H and ^{13}C NMR Chemical Shifts Attributions and 1D and 2D NMR Spectra

Table 2.13. ^{1}H (plain) and ^{13}C (italic) chemical shift attribution of **CS-1**, **CS-2b**. [a]

	GalNAc						*GlcA*					*Other*
	1	**2**	**3**	**4**	**5**	**6**	**1**	**2**	**3**	**4**	**5**	*signals*
CS-1[b]	4.61 *102.8*	4.04 *52.6*	4.04 *76.8* 4,6S n.d.[d]	4.79 *77.4* 4,6S n.d.[d]	4.11 *73.7* 4,6S n.d.[d]	4.24 *68.9* 4,6S 3.77 *62.3* 0S	4.47 *105.1*	3.37 *73.5*	3.60 *75.1*	3.77 *83.5*	3.69 *77.8*	NAc 2.02 *23.8*
CS-2b[c]	4.56 *102.2* 4S 4.50 *102.2* 0S	4.02 *52.5* 4S 3.98 *52.3* 0S	4.01 *76.9* 4S 3.79 *81.4* 0S	4.74 *77.5* 4S 4.09 *68.8* 0S	3.81 *75.8* 4S 3.68 *76.2* 0S	3.78 *62.2*	4.49 *105.1*	3.35 *73.2*	3.59 *74.8*	3.75 *81.2*	3.78 76.4	NAc 2.00 *23.7*

[a] Chemical shifts are expressed in δ relative to internal acetone (^{1}H: $(CH_3)_2CO$ at δ = 2.22 ppm; ^{13}C: $(CH_3)_2CO$ at δ = 31.5 ppm). [b] NMR experiments conducted in D_2O (400 MHz, 298 K). [c] NMR experiments conducted in D_2O (600 MHz, 298 K).

Table 2.14. ^{1}H (plain) and ^{13}C (italic) chemical shift attribution of **CS-2e,f**, **CS-3**. [a]

	GalNAc						*GlcA*					*Other*
	1	**2**	**3**	**4**	**5**	**6**	**1**	**2**	**3**	**4**	**5**	*signals*
CS-2e[b]	4.58 *102.3* 4S	3.99 *52.7* 4S	3.99 *76.8* 4S	4.71 *77.7* 4S	3.79 *75.8* 4S	3.76 *62.3*	4.44 *105.0*	3.34 *73.4*	3.56 *74.6*	3.68 *81.4*	3.68 *77.5*	NAc 2.00 *23.7*
	4.49 *102.3* 0S	3.95 *52.3* 0S	3.76 *81.6* 0S	4.08 *68.9* 0S	3.66 *76.2* 0S							
CS-2f[c]	4.52/62 *102.4/8*	3.98– 4.07 *52.7*	4.03 *77.0* 4,6S/4S	4.74/79 *77.2/4* 4,6S/4S	4.10 *73.7* 4,6S 3.81 *75.9* 4S	4.22/27 *69.0* 4,6S 3.71/84 *62.3* 4S/0S	4.50 *105.1*	3.38 *73.4*	3.60 *75.0*	3.80 *75.0*	3.80 *81.6*	NAc 1.97–2.06 23.8
			3.80 *83.0* 0S	4.10 *69.0* 0S	3.69 *76.3* 0S							
CS-3[b]	4.53 *102.6* 6S^{i}	3.99 *52.1* 6S^{i}	3.80/87 *83.3/6*	n.d.[d]	3.91/97 *73.6/9*	4.16/26 *66.5– 69.6*	4.49 *105.5* 0S	3.36 *73.7* 0S	3.58 *75.2* 0S	3.71 *82.6*	3.68 *77.8*	NAc 1.99–2.06 *24.1*
	4.56 *102.4* 6S^{ii}	3.94 *52.0* 6S^{ii}					4.71 *102.9* 2S	4.13 *80.6* 2S	3.79 *74.2* 2S			

The superscripts *i* and *ii* represent the same residue type with different neighbouring residues. [a] Chemical shifts are expressed in δ relative to internal acetone (^{1}H: $(CH_3)_2CO$ at δ = 2.22 ppm; ^{13}C: $(CH_3)_2CO$ at δ = 31.5 ppm). [b] NMR experiments conducted in D_2O (600 MHz, 298 K). [c] NMR experiments conducted in D_2O (400 MHz, 298 K). [d] not detected.

Table 2.15. ^{1}H (plain) and ^{13}C (italic) chemical shift attribution of derivative **11**, **12**[a,b].

	GalNAc						*GlcA*					*Other signals*
	1	**2**	**3**	**4**	**5**	**6**	**1**	**2**	**3**	**4**	**5**	
11	4.51 *99.5*	3.65 *51.7*	3.76 *79.2*	4.19 *73.5*	3.53 *65.4*	4.01 *67.9*	4.92 *99.9*	4.81 *72.5*	3.76 *71.1*	4.02 *72.6*	3.76 *79.2*	NAc: 1.11/*21.5* Ph*CH*: 5.32/*98.9* Ar: 7.32/*127.6* OCH_3: 3.56/*51.7*
12	4.68 *98.9*	3.84 *50.2*	4.17 *74.0*	3.89 *75.0*	3.62 *65.8*	4.11 *67.8*	5.00 *103.5*	3.70 *68.6*	4.76 *73.1*	4.55 *70.8*	4.26 *66.5*	NAc: 1.90/*22.4* Ph*CH*: 5.52/*99.2* Ar: 7.35/*127.6* CO_2: *170.5*

[a] NMR experiments conducted in DMSO-d_6 (600 MHz, 298 K). [b] Chemical shift expressed in δ relative to isotopic impurity of DMSO-d_6 (^{1}H: CHD_2SOCD_3 at δ = 2.49 ppm) in DMSO-d_6 (^{13}C: CD_3SOCD_3 at δ = 39.5 ppm).

Table 2.16. ^{1}H (plain) and ^{13}C (italic) chemical shift attribution of **CS-5-7** [a,b].

	GalNAc						*GlcA*					*Other signals*
	1	**2**	**3**	**4**	**5**	**6**	**1**	**2**	**3**	**4**	**5**	
CS-5	4.65 *104.7*	4.06 *52.2*	3.88 *82.0*	4.19 *68.5*	3.66 *76.6*	3.90,3.70 *62.4*	5.04 *102.4*	4.47 *78.3*	5.12 *77.0*	4.56 *79.0*	4.48 *77.0*	NAc: 2.08/*23.7*
CS-6	4.53 *102.2*	3.99 *52.1*	3.79 *81.8*	4.09 *68.8*	3.63 *75.8*	3.85,3.70 *62.0*	4.59 *104.8*	3.59 *73.3*	4.37 *82.5*	3.98 *78.9*	3.70 *76.1*	NAc: 2.01/*23.8*
CS-7	4.54 *101.8*	3.92 *51.9*	3.91 *80.9*	4.15 *68.4*	3.68 *75.2*	3.77 *62.1*	4.72 *102.5*	4.10 *80.6*	3.81 *73.9*	3.86 *80.0*	3.72 *77.2*	NAc: 2.03/*23.8*

[a] NMR experiments conducted in D_2O (600 MHz, 298 K). [b] Chemical shift expressed in δ relative to internal acetone (^{1}H: $(CH_3)_2CO$ at δ = 2.22 ppm; ^{13}C: $(CH_3)_2CO$ at δ = 31.5 ppm).

Table 2.17. ^{1}H (plain) and ^{13}C (italic) chemical shift attribution of **CS-8-10** [a,b].

	GalNAc						*GlcA*					*Other signals*
	1	**2**	**3**	**4**	**5**	**6**	**1**	**2**	**3**	**4**	**5**	
CS-8	4.68 *103.5* 6S 4.63 *104.2* 0S	4.02 *52.1*	3.84 *82.2*	4.22 *68.0* 6S 4.17 *68.4* 0S	3.93 *73.3* 6S 3.70 *76.2* 0S	4.23 *67.1* 6S 3.72,3.88 *62.6* 0S	4.89 *102.6*	4.45 *78.9*	4.86 *78.1*	4.43 *78.7*	4.06 *79.1*	NAc 2.08 *23.7*
CS-9	4.53 *102.5*	3.98 *52.3*	3.80 *82.3*	4.16 *68.6* 6S 4.09 *69.1* 0S	3.87 *73.4* 6S 3.63 *76.2* 0S	4.20 *67.5* 6S 3.68–3.86 *62.4* 0S	4.59 *105.1*	3.59 *73.5*	4.37 *82.8*	3.98 *78.9*	3.79 *78.0*	NAc 2.01 *23.9*
CS-10	4.60 *102.2* 6S n.d.[c]	3.91/99 *52.1*	3.93 *80.8* 6S n.d.[c]	4.15 *68.6* 6S n.d.[c]	3.93 *73.6* 6S n.d.[c]	4.21 *68.5* 6S 3.77 *62.4* 0S	4.72 *102.7*	4.12 *80.7*	3.81 *74.1*	3.84 *80.7*	3.73 *77.6*	NAc 2.03 *23.8*

[a] NMR experiments conducted in D_2O (400 MHz, 298 K). [b] Chemical shift expressed in δ relative to internal acetone (^{1}H: $(CH_3)_2CO$ at δ = 2.22 ppm; ^{13}C: $(CH_3)_2CO$ at δ = 31.5 ppm). [c] not detected.

Table 4.18. ^{1}H (plain) and ^{13}C (italic) chemical shift attribution of **CS-11,14**. [a,b]

	GalNAc						*GlcA*					*Other*
	1	**2**	**3**	**4**	**5**	**6**	**1**	**2**	**3**	**4**	**5**	*signals*
CS-11	4.80 *103.6* 4,6S	4.09 *52.4* 4,6S	4.04 *79.4* 4,6S	5.05 *76.7*	4.07 *73.4* 4,6S	4.26 *67.8* 4,6S	5.02 *102.6*	4.43 *78.6*	4.98 *76.6*	4.61 *78.5*	4.49 *78.6*	NAc 2.12 *24.0*
	4.74 *104.5* 4S	4.07 *52.6* 4S	4.01 *79.4* 4S		3.83 *70.4* 4S	3.75,3.90 *62.7* 4S						
CS-14	4.74 *104.0*	4.06 *52.9*	4.07 *78.3*	4.95 *76.8*	3.83 *76.0*	3.75–3.88 *62.5*	5.04 *101.8* 2,3S	4.51 *78.6* 2,3S	5.04 *77.4* 2,3S	4.59 *79.4* 2,3S	4.32 *78.8* 2,3S	NAc 2.07 *23.9*
							4.59 *10.6* 3S	3.65 *73.1* 3S	4.40 *83.1* 3S	n.d.[c]	n.d.[c]	

[a] NMR experiments conducted in D_2O (400 MHz, 298 K). [b] Chemical shift expressed in δ relative to internal acetone (^{1}H: $(CH_3)_2CO$ at δ = 2.22 ppm; ^{13}C: $(CH_3)_2CO$ at δ = 31.5 ppm). [c] not detected.

Table 2.19. ^{1}H (plain) and ^{13}C (italic) chemical shift attribution of **fCS-1b, fCS-5,6**. [a,b]

		1	**2**	**3**	**4**	**5**	**6**	*Other signals*
fCS-1b	*GalNAc*	4.55 *100.9*	4.04 *52.2*	3.95 *76.0* 4S	4.75 *77.6* 4S	3.83 *73.1* 4S	3.72/82 *62.3* 4S	NAc 1.98–2.06 23.8
				3.73 *81.7* 6S	4.10 *69.7* 6S	3.96 *73.6* 6S	4.32 *67.9* 6S	
	GlcA^{Fuc}	4.47 *104.9*	3.64 *74.9*	3.73 *79.9*	3.68 *77.8*	3.80 *75.6*	---	---
	GlcA^{noFuc}		3.36 *73.5*	3.59 *74.8*	3.74 *81.9*			
	α-Fuc2,3,4S-(1→3)-GlcA	5.64 *98.0*	4.53 *73.5*	4.62 *73.5*	4.94 *80.4*	5.01 *67.4*	1.31/34 *17.2*	---
fCS-5 **fCS-6**	*GalNAc^{Fuc}*	4.56 *102.2*	4.13 *52.7*	3.94 *81.4*	4.20 *76.7*	3.76 *76.6*	3.68/82 *62.5*	NAc 2.00–2.06 23.8
	GalNAc^{noFuc}	4.50 *102.2*	3.99 *52.5*	3.78 *81.5*	4.10 *68.7*	3.69 *76.3*		
	GlcA	4.46 *105.8*	3.34 *73.7*	3.57 *75.1*	3.75 *79.7*	3.68 *78.0*	---	---
	α-Fuc-(1→4)-GalNAc	5.38 *100.5*	3.76 *69.8*	3.92 *70.9*	3.81 *73.1*	4.08 *68.7*	1.18/27 *16.6*	---

[a] Chemical shifts are expressed in δ relative to internal acetone (^{1}H: $(CH_3)_2CO$ at δ = 2.22 ppm; ^{13}C: $(CH_3)_2CO$ at δ = 31.5 ppm). [b] NMR experiments conducted in D_2O (600 MHz, 298 K).

Table 2.20. ^{1}H (plain) and ^{13}C (italic) chemical shift attribution of **fCS-7,8.** [a,b]

		1	**2**	**3**	**4**	**5**	**6**	*Other signals*
fCS-7	*GalNAc^{Fuc}*	4.61 *102.9*	4.07 *53.2*	4.03 *80.6*	4.26 *74.5*	3.75 *76.8*	3.66/84 *62.4*	NAc 1.94–2.05 *23.8*
	GalNAc^{noFuc}	4.54 *102.6*	3.99 *52.5*	3.80 *81.8*	n.d.[d]			
	GlcA^{i}	4.49 *105.7*	3.35 *73.6*	3.61 *74.9*	3.76 *81.7*	3.79 *76.7*	---	---
	GlcA^{ii}	4.42 *106.0*	3.50 *73.3*					
	α-Fuc2,4S-(1→4)-GalNAc	5.71 *98.0*	4.43 *76.4*	4.19 *67.8*	4.69 *82.1*	4.06 *68.0*	1.21/36 *17.0*	---
fCS-8	*GalNAc^{Fuc}*	4.52/59 *102.4*	3.98– 4.12 *52.5/8*	n.d.[d]	4.22 *74.6*	3.78 *76.8*	3.71/83 *62.4*	NAc 1.99–2.06 *23.7*
	GalNAc^{noFuc}			3.79 *81.4*	4.01 *68.6*	n.d.[d]		
	GlcA^{i}	4.48 *105.6*	3.36 *73.8*	3.58 *75.1*	3.75 *81.5*	3.67 *77.9*	---	---
	GlcA^{ii}	4.38 *106.1*	3.53 *73.6*	3.64 *77.9*	n.d.[d]	n.d.[d]		
	α-Fuc2S-(1→4)-GalNAc	5.67 *98.2*	4.42 *76.3*	4.10 *68.8*	3.90 *73.2*	4.05 *68.5*	1.19/26 *16.4*	---

The superscripts *i* and *ii* represent the same residue type with different neighbouring residues. [a] Chemical shifts are expressed in δ relative to internal acetone (^{1}H: $(CH_3)_2CO$ at δ = 2.22 ppm; ^{13}C: $(CH_3)_2CO$ at δ = 31.5 ppm). [b] NMR experiments conducted in D_2O (400 MHz, 298 K). [d] not detected.

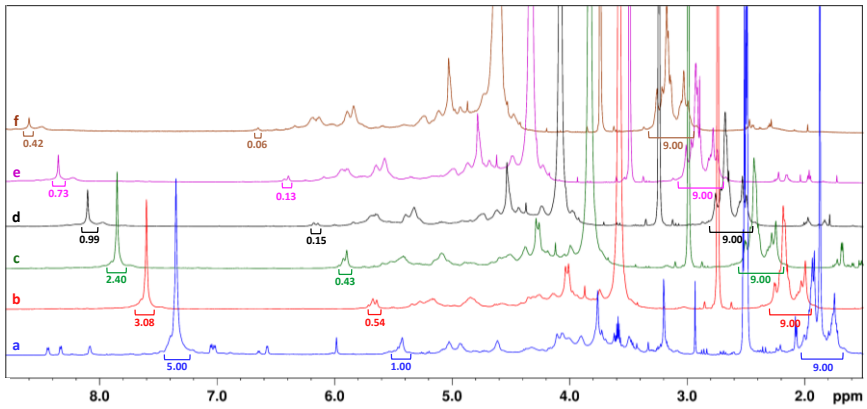

Figure 2.29. Stacked (Δδ = 0.25 ppm) ^{1}H-NMR spectra (600 MHz, DMSO-d_6, 298 K) of aliquots taken at different times (a: 0, b: 3, c: 6, d: 24, e: 42, f: 66 hours) from reaction **6→7** with 90% *v*/*v* aq. AcOH. Integration values are relative to signals, from left to right, of benzylidene ring protons at δ_H 7.50–7.20 ppm, of benzylidene methine proton at δ_H 5.45–5.35 ppm, and of *O*- and *N*-acetyl methyl protons at δ_H 2.10–1.70 ppm [integration of *O*- and *N*-acetyl signal for t = 0 hours spectrum was taken from literature (Laezza et al., **2016**) due to superimposition with other peaks].

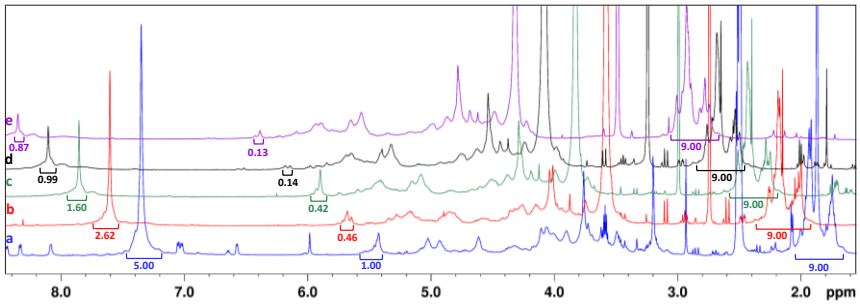

Figure 2.30. Stacked (with a Δδ = 0.25 ppm shift) ^{1}H-NMR spectra (600 MHz, DMSO-*d*$_6$, 298 K) of aliquots taken at different times (a: 0, b: 5, c: 25, d: 49, e: 73 hours) from hydrolysis reaction **6**⟶**7** with DTT and CSA. Integration values are relative to signals, from left to right, of benzylidene ring protons at δ_H 7.50–7.20 ppm, of benzylidene methine proton at δ_H 5.45–5.35 ppm, and of *O*- and *N*-acetyl methyl protons at δ_H 2.10–1.70 ppm [integration of signals for t = 0 hours spectrum was imposed from literature (Laezza et al., **2016**) due to superimposition with other peaks].

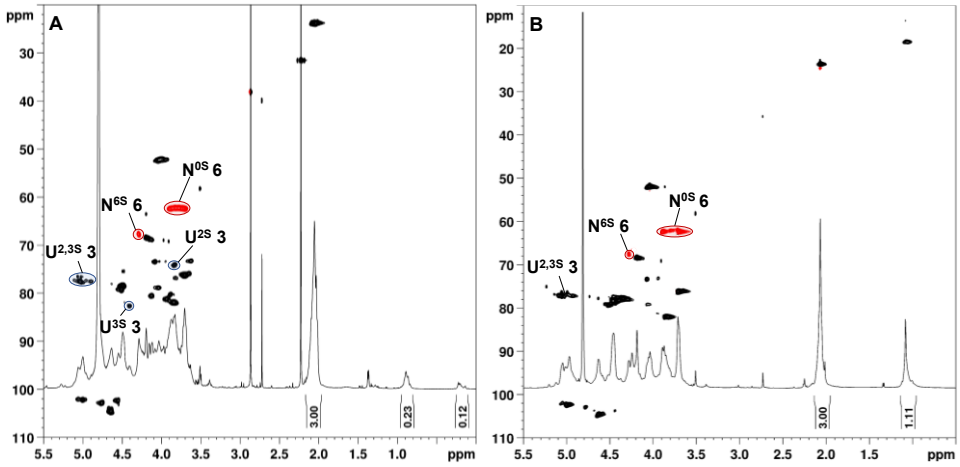

Figure 2.31. ^{1}H and DEPT-HSQC NMR spectra (600 MHz, D_2O, 298 K) of (A) **CS-4b**, (B) **CS-4c**. 2,3S/2S/3S/0S and 6S/0S superscripts represent the sulfated position in GlcA and GalNAc, respectively. Densities enclosed in the highlighted areas of the HSQC-DEPT spectra were integrated for GlcA2,3S-GlcA3S-GlcA2S (blue areas) and GalNAc-GalNAc6S (red areas) ratio estimations.

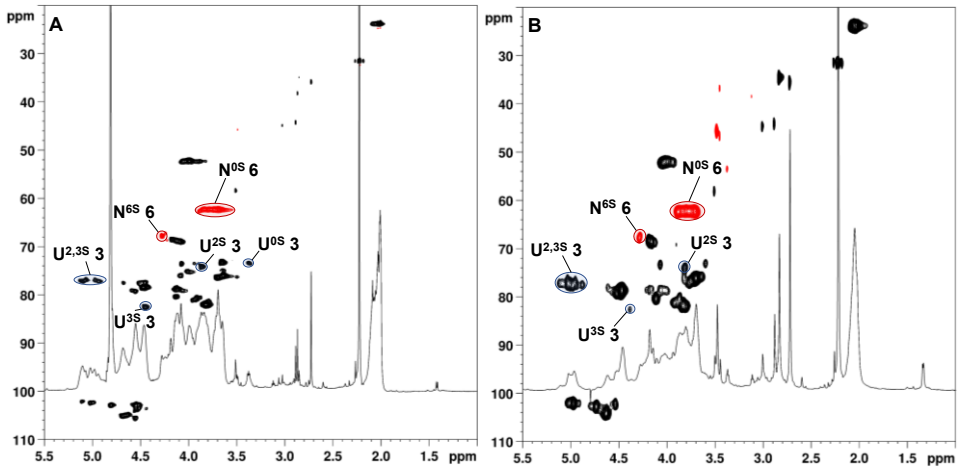

Figure 2.32. [1]H and DEPT-HSQC NMR spectra (600 MHz, D_2O, 298 K) of (A) **CS-4d**, (B) **CS-4e**. 2,3S/2S/3S/0S and 6S/0S superscripts represent the sulfated position in GlcA and GalNAc, respectively. Densities enclosed in the highlighted areas of the HSQC-DEPT spectra were integrated for GlcA2,3S-GlcA3S-GlcA2S (blue areas) and GalNAc-GalNAc6S (red areas) ratio estimations.

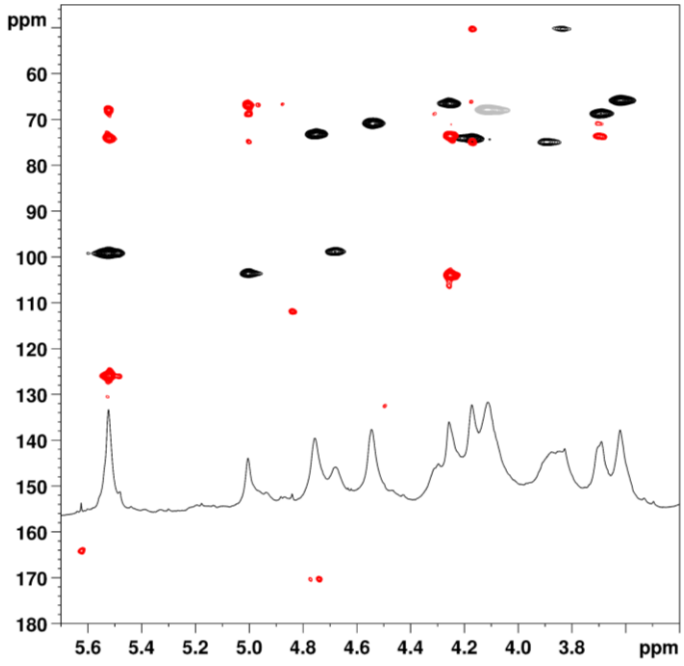

Figure 2.33. [1]H, DEPT-HSQC (black and grey) and HMBC (red) NMR spectra (600 MHz, DMSO-d_6, 298 K, zoom) of **12**.

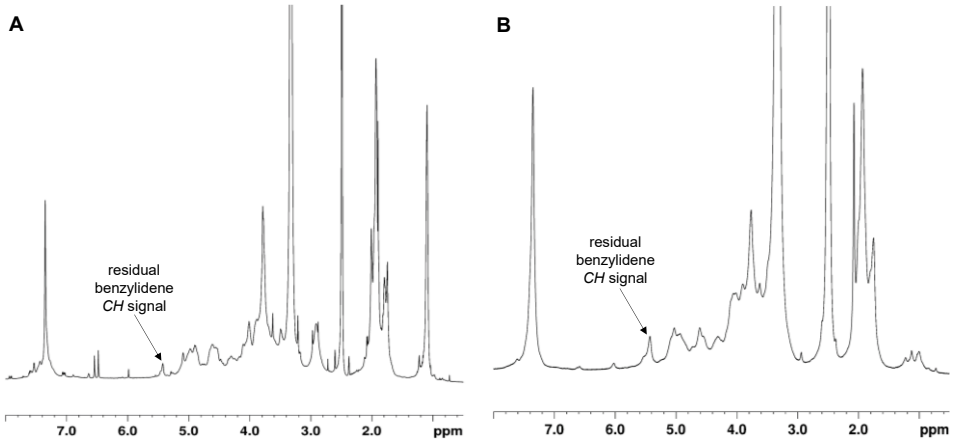

Figure 2.34. ^{1}H NMR spectra (600 MHz, DMSO-d_6, 298 K) of (A) **46a**, (B) **46b**.

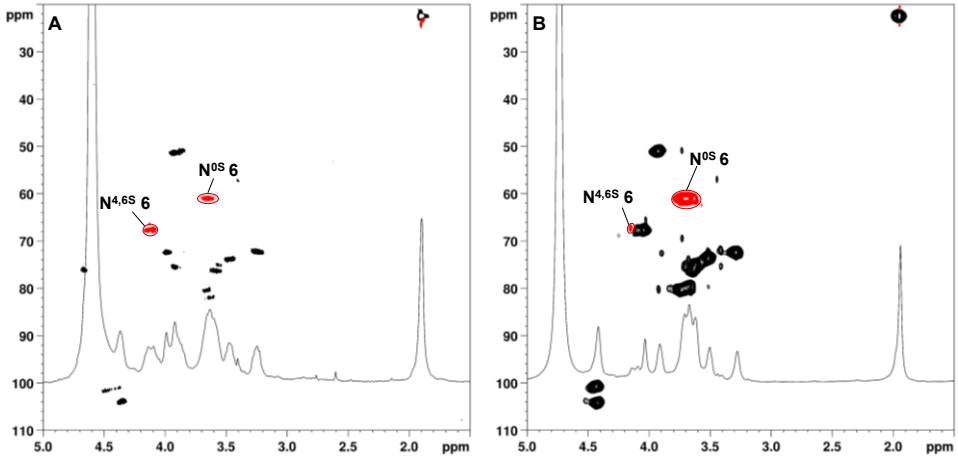

Figure 2.35. ^{1}H, DEPT-HSQC NMR spectra of (A) **CS-15a** (400 MHz, DMSO-d_6, 298 K), (B) **CS-15b** (600 MHz, DMSO-d_6, 298 K). 4,6S/0S superscripts represent sulfated position in GalNAc. (Densities enclosed in the highlighted areas of the HSQC-DEPT spectrum were integrated for CS-0/CS-E ratio estimation).

References

Adebowale, A.O., Cox, D.S., Liang, Z., Eddington, N.D., **2000**. *J. Am. Nutraceutical Assoc. 3*, 37–44.

Adinolfi, M., Barone, G., Guariniello, L., Iadonisi, A., **1999**. *Tetrahedron Lett. 40*, 8439–8441.

Bara, J.J., Johnson, W.E.B., Caterson, B., Roberts, S., **2012**. *Connect. Tissue Res. 53*, 220–228.

Bedini, E., De Castro, C., De Rosa, M., Di Nola, A., Iadonisi, A., Restaino, O.F., Schiraldi, C., Parrilli, M., **2011**. *Angew. Chem., Int. Ed. 50*, 6160–6163.

Bedini, E., De Castro, C., De Rosa, M., Di Nola, A., Restaino, O.F., Schiraldi, C., Parrilli, M., **2012**. *Chem. - Eur. J. 18*, 2123–2130.

Bedini, E., Laezza, A., Iadonisi, A., **2016**. *Eur. J. Org. Chem. 2016*, 3018–3042.

Bedini, E., Laezza, A., Parrilli, M., Iadonisi, A., **2017**. *Carbohydr. Polym. 174*, 1224–1239.

Benito-Arenas, R., Doncel-Pérez, E., Fernández-Gutiérrez, M., Garrido, L., García-Junceda, E., Revuelta, J., Bastida, A., Fernández-Mayoralas, A., **2018**. *Carbohydr. Polym. 202*, 211–218.

Bertini, S., Bisio, A., Torri, G., Bensi, D., Terbojevich, M., **2005**. *Biomacromolecules 6*, 168–173.

Bishnoi, M., Jain, A., Hurkat, P., Jain, S.K., **2016**. *Glycoconjugate J. 33*, 693–705.

Cai, C., Solakyildirim, K., Yang, B., Beaudet, J.M., Weyers, A., Linhardt, R.J., Zhang, F., **2012**. *Carbohydr. Polym. 87*, 822–829.

Camacho Gömez, J.A., Erler, U.W., Klemm, D.O., **1996**. *Macromol. Chem. Phys. 197*, 953–964.

Cavalcante, R.S., Brito, A.S., Palhares, L.C.G.F., Lima, M.A., Cavalheiro, R.P., Nader, H.B., Sassaki, G.L., Chavante, S.F., **2018**. *Carbohydr. Polym. 183*, 192–200.

Chen, I.-H., Kou, K.G.M., Le, D.N., Rathbun, C.M., Dong, V.M., **2014**. *Chem. - Eur. J. 20*, 5013–5018.

Chen, S., Li, G., Wu, N., Guo, X., Liao, N., Ye, X., Liu, D., Xue, C., Chai, W., **2013**. *Biochim. Biophys. Acta, Gen. Subj. 1830*, 3054–3066.

Chen, S., Xue, C., Yin, L., Tang, Q., Yu, G., Chai, W., **2011**. *Carbohydr. Polym. 83*, 688–696.

Cimini, D., Restaino, O.F., Catapano, A., De Rosa, M., Schiraldi, C., **2010**. *Appl. Microbiol. Biotechnol. 85*, 1779–1787.

Collin, E.C., Carroll, O., Kilcoyne, M., Peroglio, M., See, E., Hendig, D., Alini, M., Grad, S., Pandit, A., **2017**. *Signal Transduction Targeted Ther. 2*, 17049–17056.

Cunico, R.F., Bedell, L., **1980**. *J. Org. Chem. 45*, 4797–4798.

Daly, R., McCabe, T., Scanlan, E.M., **2013**. *J. Org. Chem. 78*, 1080–1090.

Daragics, K., Fügedi, P., **2009**. *Tetrahedron Lett. 50*, 2914–2916.

Debenham, S.D., Toone, E.J., **2000**. *Tetrahedron: Asymmetry 11*, 385–387.

Djerbal, L., Lortat-Jacob, H., Kwok, J., **2017**. *Glycoconjugate J. 34*, 363–376.

Fonseca, R.J.C., Mourão, P.A.S., **2006**. *Thromb. Haemostasis 96*, 822–829.

Fonseca, R.J.C., Oliveira, S.N.M.C.G., Pomin, V.H., Mecawi, A.S., Araujo, I.G., Mourão, P.A.S., **2010**. *Thromb. Haemostasis 103*, 994–1004.

Fonseca, R.J.C., Sucupira, I.D., Oliveira, S.N.M.C.G., Santos, G.R.C., Mourão, P.A.S., **2017**. *Thromb. Haemostasis 117*, 662–670.

Gao, N., Lu, F., Xiao, C., Yang, L., Chen, J., Zhou, K., Wen, D., Li, Z., Wu, M., Jiang, J., Liu, G., Zhao, J., **2015**. *Carbohydr. Polym. 127*, 427–437.

Gao, Y., Fukuda, A., Katsuraya, K., Kaneko, Y., Mimura, T., Nakashima, H., Uryu, T., **1997**. *Macromolecules 30*, 3224–3228.

Gargiulo, V., Lanzetta, R., Parrilli, M., De Castro, C., **2009**. *Glycobiology 19*, 1485–1491.

La Gatta, A., De Rosa, M., Marzaioli, I., Busico, T., Schiraldi, C., **2010**. *Anal. Biochem. 404*, 21–29.

Glauser, B.F., Pereira, M.S., Monteiro, R.Q., Mourão, P.A.S., **2008**. *Thromb. Haemostasis 100*, 420–428.

Guan, R., Peng, Y., Zhou, L., Zheng, W., Liu, X., Wang, P., Yuan, Q., Gao, N., Zhao, L., Zhao, J., **2019**. *Mar. Drugs 17*, 195–207.

Guerrini, M., Beccati, D., Shriver, Z., Naggi, A., Viswanathan, K., Bisio, A., Capila, I., Lansing, J.C., Guglieri, S., Fraser, B., Al-Hakim, A., Gunay, N.S., Zhang, Z., Robinson, L., Buhse, L., Nasr, M., Woodcock, J., Langer, R.S., Venkataraman, G., Linhardt, R.J., Casu, B., Torri, G., Sasisekharan, R., **2008**. *Nat. Biotechnol. 26*, 669–675.

Guerrini, M., Naggi, A., Guglieri, S., Santarsiero, R., Torri, G., **2005**. *Anal. Biochem. 337*, 35–47.

Han, W., Li, Q., Lv, Y., Wang, Q.C., Zhao, X., **2018**. *Carbohydr. Res. 460*, 8–13.

He, H., Chen, D., Li, X., Li, C., Zhao, J.H., Qin, H., **2019**. *Org. Biomol. Chem. 17*, 2877–2882.

Higashi, K., Okamoto, Y., Mukuno, A., Wakai, J., Hosoyama, S., Linhardt, R.J., Toida, T., **2015**. *Carbohydr. Polym. 134*, 557–565.

Higashi, K., Takeda, K., Mukuno, A., Okamoto, Y., Masuko, S., Linhardt, R.J., Toida, T., **2016**. *Biochem. J. 473*, 4145–4158.

Jacquinet, J.C., Lopin-Bon, C., Vibert, A., **2009**. *Chem. - Eur. J. 15*, 9579–9595.

Kariya, Y., Kyogashima, M., Suzuki, K., Isomura, T., Sakamoto, T., Horie, K., Ishihara, M., Takano, R., Kamei, K., Hara, S., **2000**. *J. Biol. Chem. 275*, 25949–25958.

Kinoshita-Toyoda, A., Yamada, S., Haslam, S.M., Khoo, K.H., Sugiura, M., Morris, H.R., Dell, A., Sugahara, K., **2004**. *Biochemistry 43*, 11063–11074.

Kishimoto, T.K., Viswanathan, K., Ganguly, T., Elankumaran, S., Smith, S., Pelzer, K., Lansing, J.C., Sriranganathan, N., Zhao, G., Galcheva-Gargova, Z., Al-Hakim, A., Bailey, G.S., Fraser, B., Roy, S., Rogers-Cotrone, T., Buhse, L., Whary, M., Fox, J.,

Nasr, M., Dal Pan, G.J., Shriver, Z., Langer, R.S., Venkataraman, G., Austen, K.F., Woodcock, J., Sasisekharan, R., **2008**. *N. Engl. J. Med. 358*, 2457–2467.

Koschella, A., Klemm, D.O., **1997**. *Macromol. Symp. 120*, 115–125.

Laezza, A., Iadonisi, A., De Castro, C., De Rosa, M., Schiraldi, C., Parrilli, M., Bedini, E., **2015**. *Biomacromolecules 16*, 2237–2245.

Laezza, A., Iadonisi, A., Pirozzi, A.V.A., Diana, P., De Rosa, M., Schiraldi, C., Parrilli, M., Bedini, E., **2016**. *Chem. - Eur. J. 22*, 18215–18226.

Li, J., Su, G., Liu, J., **2017**. *Angew. Chem., Int. Ed. 56*, 11784–11787.

Li, Q., Cai, C., Chang, Y., Zhang, F., Linhardt, R.J., Xue, C., Li, G., Yu, G., **2018**. *Carbohydr. Polym. 181*, 1160–1168.

Liu, H., Zhang, X., Wu, M., Li, Z., **2018**. *Carbohydr. Res. 467*, 45–51.

Liu, Y., Zeng, J., Sun, J., Cai, L., Zhao, Y., Fang, J., Hu, B., Shu, P., Meng, L., Wan, Q., **2018**. *Org. Chem. Front. 5*, 2427–2431.

Lopin-Bon, C., Jacquinet, J.C., **2006**. *Angew. Chem., Int. Ed. 45*, 2574–2578.

Lu, S.R., Lai, Y.H., Chen, J.H., Liu, C.Y., Mong, K.K.T., **2011**. *Angew. Chem., Int. Ed. 50*, 7315–7320.

Macchione, G., Maza, S., Mar Kayser, M., de Paz, J.L., Nieto, P.M., **2014**. *Eur. J. Org. Chem. 2014*, 3868–3884.

Maki, Y., Okamoto, R., Izumi, M., Murase, T., Kajihara, Y., **2016**. *J. Am. Chem. Soc. 138*, 3461–3468.

Malavaki, C., Mizumoto, S., Karamanos, N., Sugahara, K., **2008**. *Connect. Tissue Res. 49*, 133–139.

Maruyama, T., Toida, T., Imanari, T., Yu, G., Linhardt, R.J., **1998**. *Carbohydr. Res. 306*, 35–43.

Matsushita, K., Nakata, T., Tamura, J.-I., **2015**. *Carbohydr. Res. 406*, 76–85.

Mikami, T., Kitagawa, H., **2013**. *Biochim. Biophys. Acta, Gen. Subj. 1830*, 4719–4733.

Miyachi, K., Wakao, M., Suda, Y., **2015**. *Bioorganic Med. Chem. Lett. 25*, 1552–1555.

Mizumoto, S., Fongmoon, D., Sugahara, K., **2013**. *Glycoconjugate J. 30*, 619–632.

Monteiro-Machado, M., Tomaz, M.A., Fonseca, R.J.C., Strauch, M.A., Cons, B.L., Borges, P.A., Patrão-Neto, F.C., Tavares-Henriques, M.S., Teixeira-Cruz, J.M., Calil-Elias, S., Cintra, A.C.O., Martinez, A.M.B., Mourão, P.A.S., Melo, P.A., **2015**. *Toxicon 98*, 20–33.

Mou, J., Li, Q., Qi, X., Yang, J., **2018**. *Carbohydr. Polym. 185*, 41–47.

Mourão, P.A.S., **2015**. *Mar. Drugs 13*, 2770–2784.

Mourão, P.A.S., Guimarães, M.A.M., Mulloy, B., Thomas, S., Gray, E., **1998**. *Br. J. Haematol. 101*, 647–652.

Mourão, P.A.S., Pereira, M.S., Pavo, M.S.G., Mulloy, B., Tollefsen, D.M., Mowinckel, M.C., Abildgaard, U., **1996**. *J. Biol. Chem. 271*, 23973–23984.

Mucci, A., Schenetti, L., Volpi, N., **2000**. *Carbohydr. Polym. 41*, 37–45.

Mulloy, B., Mourão, P.A.S., Gray, E., **2000**. *J. Biotechnol. 77*, 123–135.

Myron, P., Siddiquee, S., Al Azad, S., **2014**. *Carbohydr. Polym. 112*, 173–178.

Nagasawa, K., Uchiyama, H., Wajima, N., **1986**. *Carbohydr. Res. 158*, 183–190.

Poh, Z.W. e., Gan, C.H. en., Lee, E.J., Guo, S., Yip, G.W., Lam, Y., **2015**. *Sci. Rep. 5*, 14355–14362.

Pomin, V.H., **2013**. Chondroitin Sulfate: Structure, Uses and Health Implications, 1st ed. Nova Science Publishers, New York (NY).

Pomin, V.H., **2014**. *Mar. Drugs 12*, 232–254.

Pomin, V.H., Piquet, A.A., Pereira, M.S., Mourão, P.A.S., **2012**. *Carbohydr. Polym. 90*, 839–846.

Pudełko, A., Wisowski, G., Olczyk, K., Koźma, E.M., **2019**. *FEBS J. 286*, 1815–1837.

Qiu, P., Wu, F., Yi, L., Chen, L., Jin, Y., Ding, X., Ouyang, Y., Yao, Y., Jiang, Y., Zhang, Z., **2020**. *Carbohydr. Polym. 240*, 116337.

Ren, B., Gan, L., Zhang, L., Yan, N., Dong, H., **2018**. *Org. Biomol. Chem. 16*, 5591–5597.

Ren, B., Rahm, M., Zhang, X., Zhou, Y., Dong, H., **2014**. *J. Org. Chem. 79*, 8134–8142.

Ren, B., Ramström, O., Zhang, Q., Ge, J., Dong, H., **2016**. *Chem. - Eur. J. 22*, 2481–2486.

Restaino, O.F., Finamore, R., Diana, P., Marseglia, M., Vitiello, M., Casillo, A., Bedini, E., Parrilli, M., Corsaro, M.M., Trifuoggi, M., De Rosa, M., Schiraldi, C., **2017**. *Anal. Chim. Acta 958*, 59–70.

Santos, G.R.C., Glauser, B.F., Parreiras, L.A., Vilanova, E., Mourão, P.A.S., **2015**. *Glycobiology 25*, 1043–1052.

Schiraldi, C., Alfano, A., Cimini, D., De Rosa, M., Panariello, A., Restaino, O.F., Rosa, M. De, **2012**. *Biotechnol. Prog. 28*, 1012–1018.

Shang, F., Gao, N., Yin, R., Lin, L., Xiao, C., Zhou, L., Li, Z., Purcell, S.W., Wu, M., Zhao, J., **2018**. *Eur. J. Med. Chem. 148*, 423–435.

Soares, P.A.G., Ribeiro, K.A., Valente, A.P., CapillCrossed D'Sign, N. V., Oliveira, S.N.M.C.G., Tovar, A.M.F., Pereira, M.S., Vilanova, E., Mourão, P.A.S., **2018**. *Glycobiology 28*, 565–579.

Solera, C., Macchione, G., Maza, S., Kayser, M.M., Corzana, F., de Paz, J.L., Nieto, P.M., **2016**. *Chem. - Eur. J. 22*, 2356–2369.

Sugiura, N., Shioiri, T., Chiba, M., Sato, T., Narimatsu, H., Kimata, K., Watanabe, H., **2012**. *J. Biol. Chem. 287*, 43390–43400.

Takeda, N., Horai, S., Tamura, J.-I., **2016**. *Carbohydr. Res. 424*, 54–58.

Tamura, J.-I., Tanaka, H., Nakamura, A., Takeda, N., **2013**. *Tetrahedron Lett. 54*, 3940–3943.

Toida, T., Suzuki, A., Nakajima, K., Chaidedgumjorn, A., Imanari, T., **2000**. *Glycoconjugate J. 17*, 393–399.

Tully, S.E., Mabon, R., Gama, C.I., Tsai, S.M., Liu, X., Hsieh-Wilson, L.C., **2004**. *J. Am. Chem. Soc. 126*, 7736–7737.

Ustyuzhanina, N.E., Bilan, M.I., Dmitrenok, A.S., Nifantiev, N.E., Usov, A.I., **2017a**. *Carbohydr. Polym. 164*, 8–12.

Ustyuzhanina, N.E., Bilan, M.I., Dmitrenok, A.S., Shashkov, A.S., Kusaykin, M.I., Stonik, V.A., Nifantiev, N.E., Usov, A.I., **2016a**. *Glycobiology 26*, 449–459.

Ustyuzhanina, N.E., Bilan, M.I., Dmitrenok, A.S., Shashkov, A.S., Nifantiev, N.E., Usov, A.I., **2017b**. *Carbohydr. Polym. 165*, 7–12.

Ustyuzhanina, N.E., Bilan, M.I., Dmitrenok, A.S., Tsvetkova, E.A., Shashkov, A.S., Stonik, V.A., Nifantiev, N.E., Usov, A.I., **2016b**. *Carbohydr. Polym. 153*, 399–405.

Ustyuzhanina, N.E., Bilan, M.I., Nifantiev, N.E., Usov, A.I., **2019**. *Pure Appl. Chem. 91*, 1065–1071.

Ustyuzhanina, N.E., Fomitskaya, P., Gerbst, A., Dmitrenok, A.S., Nifantiev, N.E., **2015**. *Mar. Drugs 13*, 770–787.

Valerio, S., Iadonisi, A., Adinolfi, M., Ravidà, A., **2007**. *J. Org. Chem. 72*, 6097–6106.

Valoti, E., Miraglia, N., Bianchi, D., Valetti, M., Bazza, P., **2014**. Shark-like chondroitin sulphate and process for the preparation thereof. US 8,664,196.

Vieira, R.P., Mulloy, B., Mourão, P.A.S., **1991**. *J. Biol. Chem. 266*, 13530–13536.

Vinnitskiy, D.Z., Ustyuzhanina, N.E., Dmitrenok, A.S., Shashkov, A.S., Nifantiev, N.E., **2017**. *Carbohydr. Res. 438*, 9–17.

Wakao, M., Obata, R., Miyachi, K., Kaitsubata, Y., Kondo, T., Sakami, C., Suda, Y., **2015**. *Bioorganic Med. Chem. Lett. 25*, 1407–1411.

Wu, M., Huang, R., Wen, D., Gao, N., He, J., Li, Z., Zhao, J., **2012**. *Carbohydr. Polym. 87*, 862–868.

Wuts, P.G.M., **2014**. Protection for the hydroxyl group, including 1,2- and 1,3-diols, in: *Greene's Protective Groups in Organic Synthesis*. John Wiley & Sons, Inc., Hoboken, New Jersey, pp. 654–659.

Yamada, S., Morimoto, H., Fujisawa, T., Sugahara, K., **2007**. *Glycobiology 17*, 886–894.

Yamada, S., Sugahara, K., **2008**. *Curr. Drug Discovery Technol. 5*, 289–301.

Yan, L., Li, J., Wang, D., Ding, T., Hu, Y., Ye, X., Linhardt, R.J., Chen, S., **2017**. *Carbohydr. Polym. 178*, 180–189.

Yang, L., Wang, Y., Yang, S., Lv, Z., **2018**. *Int. J. Biol. Macromol. 108*, 710–718.

Yao, W., Zhu, Y., Zhang, X., Sha, M., Meng, X., Li, Z., **2018**. *J. Org. Chem. 83*, 14069–14077.

Yin, R., Zhou, L., Gao, N., Li, Z., Zhao, L., Shang, F., Wu, M., Zhao, J., **2018**. *J. Biol. Chem. 293*, 14089–14099.

Yin, R., Zhou, L., Gao, N., Lin, L., Sun, H., Chen, D., Cai, Y., Zuo, Z., Hu, K., Huang, S., Liu, J., Zhao, J., **2021**. *Biomacromolecules 22*, 1244–1255.

Zhang, X., Lin, L., Huang, H., Linhardt, R.J., **2020**. *Acc. Chem. Res. 53*, 335–346.

Zhang, X., Liu, H., Lin, L., Yao, W., Zhao, J., Wu, M., Li, Z., **2018a**. *Angew. Chem., Int. Ed. 57*, 12880–12885.

Zhang, X., Liu, H., Yao, W., Meng, X., Li, Z., **2019**. *J. Org. Chem. 84*, 7418–7425.

Zhang, X., Yao, W., Xu, X., Sun, H., Zhao, J., Meng, X., Wu, M., Li, Z., **2018b**. *Chem. - Eur. J. 24*, 1694–1700.

Zhao, L., Wu, M., Xiao, C., Yang, L., Zhou, L., Gao, N., Li, Z., Chen, Jun, Chen, Jianchao, Liu, J., Qin, H., Zhao, J., **2015**. *Proc. Natl. Acad. Sci. U.S.A 112*, 8284–8289.

Zoppetti, G., Oreste, P., **2004**. Process for the Preparation of Chondroitin sulfates from K4 Polysaccharide and Obtained Products. US Patent 6,777,398.

CHAPTER 3
PRELIMINARY STUDY ON DECIPHERING STRUCTURAL DETERMINANTS IN CHONDROITIN SULFATE BINDING TO GROWTH FACTORS

3
PRELIMINARY STUDY ON DECIPHERING STRUCTURAL DETERMINANTS IN CHONDROITIN SULFATE BINDING TO GROWTH FACTORS

3.1. Introduction

In biological system, CS plays key roles in the control of numerous biological processes, such as cell migration, growth, differentiation, guidance, and development (see also Paragraph 2.1.1 in Chapter 2). Many of these functions arises from its ability to interact with various positively charged signalling proteins (*e.g.* growth factors, receptors and guidance molecules) mainly through electrostatic forces driven by the sulfate groups attached to the polysaccharide chain. In addition, the sulfate group distribution along the CS chain seems to be crucial in determining such interactions, thus encoding specific functional information (Gama et al., **2006**; Kjellén and Lindahl, **2018**; Swarup et al., **2013**). A notable example is the ability of a specific CS sulfation motif, CS-E, to inhibit axon regeneration after central nervous system injury through its interactions with specific cell-surface receptors (Brown et al., **2012**; Dickendesher et al., **2012**).
However, the remarkable structural heterogeneity of natural CS polysaccharides, particularly in terms of their sulfation pattern (Figure 3.1), hampers a complete understanding of the molecular basis of CS–protein interactions (for a detailed description of CS structural features see Paragraph 2.1.1 in Chapter 2). Thus, several chemical or chemoenzymatic approaches have been developed for the obtainment of CS oligo- or polysaccharides with well-defined structures to be used for the elucidation of the effects of their structural parameters (length, sulfation pattern, etc.) on the recognition by signalling molecules (Ji et al., **2020**).

In this frame, during the last decade semi-synthetic methods, relying on chemical/chemoenzymatic manipulation of naturally occurring and/or commercially available polysaccharides, have emerged as a valid alternative to the expensive and time-consuming bottom-up syntheses (see also Paragraph 2.1.2 in Chapter 2). These strategies have not only afforded CS species with a well-defined sulfation distribution, but also new polysaccharides with rare or unprecedented sulfation profiles (Bedini et al., **2012**, **2011**; Vessella et al., **2019**).

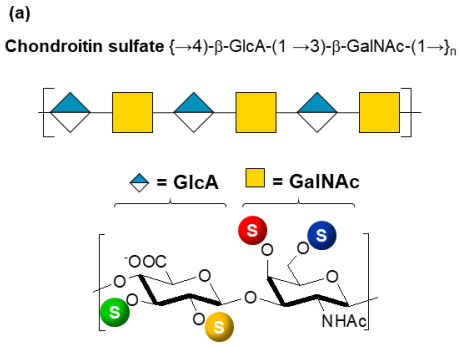

(b)

Disaccharide sulfation pattern

Type	Disaccharide subunit
CS-A	GlcA-GalNAc4S
CS-C	GlcA-GalNAc6S
CS-B	GlcA2S-GalNAc4S
CS-D	GlcA2S-GalNAc6S
CS-E	GlcA-GalNAc4,6S
CS-K	GlcA3S-GalNAc4S
CS-L	GlcA3S-GalNAc6S
CS-M	GlcA3S-GalNAc4,6S
CS-S	GlcA2,3S-GalNAc4S
CS-S′	GlcA2,3S-GalNAc6S
CS-T	GlcA2S-GalNAc4,6S

Figure 3.1. (a) Structure of chondroitin sulfate chain (*top*); chemical structure of typical disaccharide units found in CS chain (*bottom*). Letter "S" enclosed by circles indicates the various position(s) that can be sulfated. (b) Disaccharide sulfation pattern of natural CSs.

In addition to that, due to the large number of binding partners and diverse GAG structures, the development of new approaches enabling to look more rapidly and more globally across protein families and GAG structures is becoming even more crucial (Joffrin and Hsieh-Wilson, **2020**). Very recently, a new "holistic approach" has been proposed, aimed to a comprehensive look at how a specific sulfate distribution within the CS disaccharide subunits directs the CS binding to growth factors (Benito-Arenas et al., **2018**). In particular, it has been observed that this disposition affects the surface charge of the polysaccharides' 3D-structure, that, in turn, has a considerable influence on their capacity to bind to growth factors and, consequently, on their functional effects.

In the light of these statements, it could be proposed that a detailed understanding of the physico-chemical properties of CS polysaccharides and how these relate to their protein binding would lead to an enhanced predictability of their biological functions. Such proposal arises from the question whether CS structures can be customized in terms of their disaccharide sulfation motifs in such a way that they are able to induce desired functions without causing unwanted ones. However, the control on CS activities for a complete exploitation of its potential requires a more thorough comprehension of how the particular sulfation pattern can impact on CS biological functions.

In this study, the structure-activity relationships of several CS polysaccharides have been systematically analysed, trying to isolate the effect of different sulfate-bearing motifs. To this aim, a binding affinity screening was performed using SPR analysis and the zeta potential as the physico-chemical indicative parameter, in accordance to the above-mentioned holistic approach (Benito-Arenas et al., **2018**). As an example of target protein, fibroblast growth factor 2 (FGF-2) was selected. Like other FGF family members, FGF-2 is involved in a large number of biological processes in a GAG cofactor-assisted manner (Turnbull et al., **2001**; Xu and Esko, **2014**); moreover, an increasing amount of evidences has shown that CS participates and regulates FGF-2 binding to its receptor (FGFR) (Smock and Meijers, **2018**).

3.2. Results and Discussion

Herein, a binding affinity study of a library of CSs, with the FGF-2 growth factor, is described. To systematize the analysis, five natural CSs (**CS-16**, **CS-17**, **CS-18**, **CS-19**, **CS-20**), differing from each other in one of their sulfated disaccharide topological motifs were first selected. Furthermore, a commercially available, animal-sourced LMW-CS (**CS-21**) and nine semi-synthetic CSs (**CS-1**, **CS-5**, **CS-**

6, **CS-7**, **CS-8**, **CS-9**, **CS-10**, **CS-22**, **CS-23**) were analysed to recapitulate individually the effect of these motifs (Figure 3.2). Noteworthy, five of the semi-synthetic CSs (**CS-5**, **CS-6**, **CS-7**, **CS-8**, **CS-9**) carry rare sulfation pattern with sulfate groups at *C*-2 and/or *C*-3 positions of GlcA units, alone or in combination with the *C*-6 sulfation on GalNAc residues, in order to perform a more comprehensive analysis (Figure 3.2).

The final aim was to complete the panel of disaccharide epitopes with very rare or non-natural sulfated motifs with respect to their recognition by target proteins. It is worth noting that, despite actual knowledge is scarce, recent works have demonstrated that CS polysaccharides with rare K subunits, displaying 3-*O*-sulfated GlcA residues, show a neurite outgrowth activity comparable to natural CS-E species (Higashi et al., **2015**).

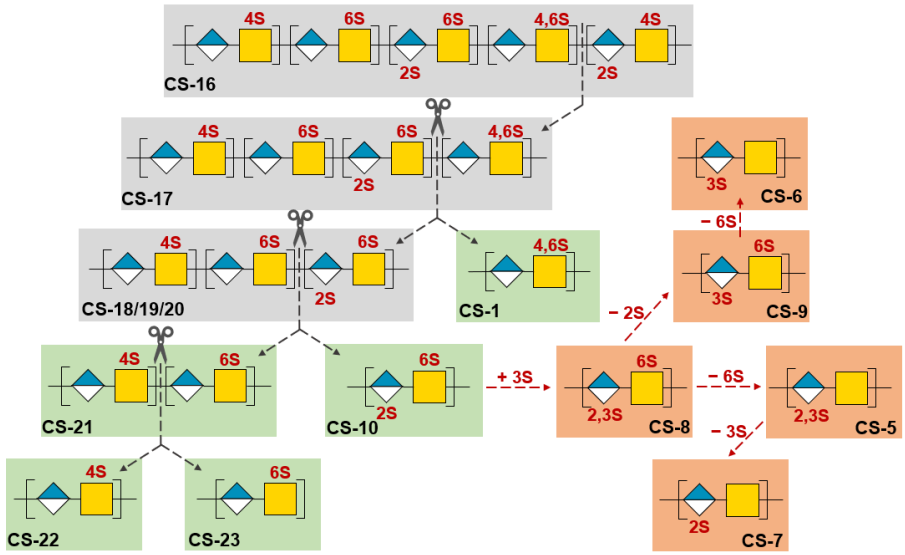

Figure 3.2. Schematic representation of CS polysaccharides analysed in this study. Natural CSs are highlighted with a grey background; the grey dashed lines indicate differences in term of disaccharide motifs among natural CSs. These motifs were isolated in the polysaccharides highlighted with a green background. A red background represents polysaccharides found to recapitulate rare or unnatural sulfation pattern in GlcA; differences among these polysaccharides are shown over the red dashed arrows.

The five marine-sourced CS compounds (molecular weight ranging between 45 to 70 kDa) were first examined. As evidenced by disaccharide composition analysis, performed by chondroitinase ABC digestion and subsequent separation by HPLC (Novoa-Carballal et al., **2017**; Volpi, **2000**), three polysaccharides (**CS-18–20**) displayed sulfate groups at positions *C*-6, *C*-4 and *C*-2,6 in different proportions, while the other two (**CS-16**, **CS-15**) possess also lower amounts of other sulfation motifs, namely at *C*-4,6 and *C*-2,4 (Table 3.1). This latter feature also gave the possibility to profile the possible effect of minority sulfation patterns on binding preferences to FGF-2.

Table 3.1. Disaccharide composition and DS values (average number of sulfate groups per disaccharide unit) of marine-sourced CS species.

	C. monstrosa **(CS-16)**	***G. melastomus*** **(CS-17)**	***P. glauca*** **(CS-18)**	***S. canicula*** **(CS-19)**	***R. clavata*** **(CS-20)**
GlcA-GalNAc4S [a]	22.1 ± 0.3	23.8 ± 0.1	10.1 ± 0.1	31.5 ± 0.6	16.0 ± 0.1
GlcA-GalNAc6S [a]	52.7 ± 0.1	54.9 ± 0.4	64.2 ± 0.4	32.4 ± 0.1	55.9 ± 0.1
GlcA-GalNAc [a]	4.4 ± 0.2	4.2 ± 0.5	16.3 ± 0.6	22.5 ± 1.4	19.5 ± 0.1
GlcA2S-GalNAc6S [a]	17.4 ± 0.1	15.0 ± 0.1	9.3 ± 0.2	16.3 ± 0.2	8.6 ± 0.1
GlcA-GalNAc4,6S [a]	2.4 ± 0.1	1.5 ± 0.0	n.o.[b]	n.o.[b]	n.o.[b]
GlcA2S-GalNac4S [a]	1.0 ± 0.0	0.6	n.o.[b]	n.o.[b]	n.o.[b]
DS	1.16	1.13	0.93	0.96	0.89
4S/6S ratio	0.33	0.35	0.14	0.65	0.25

[a] Results expressed as mean % ± standard deviation (n = 2); [b] not observed.

In order to establish a correlation between CS sulfation pattern and its 3D-structure, the dependence of the surface charge on the DS and the effect of different sulfate group arrangements were examined. To this aim, zeta potential, a physico-chemical parameter indicative of polysaccharide surface charge, was measured, and CD spectra were recorded. As can be observed in Figure 3.3, no dependence of the surface charge on the sulfation degree seemed to exist. Notably, polysaccharide **CS-19** displayed an unexpected decrease in the zeta-potential value, despite its similar DS to **CS-18**.

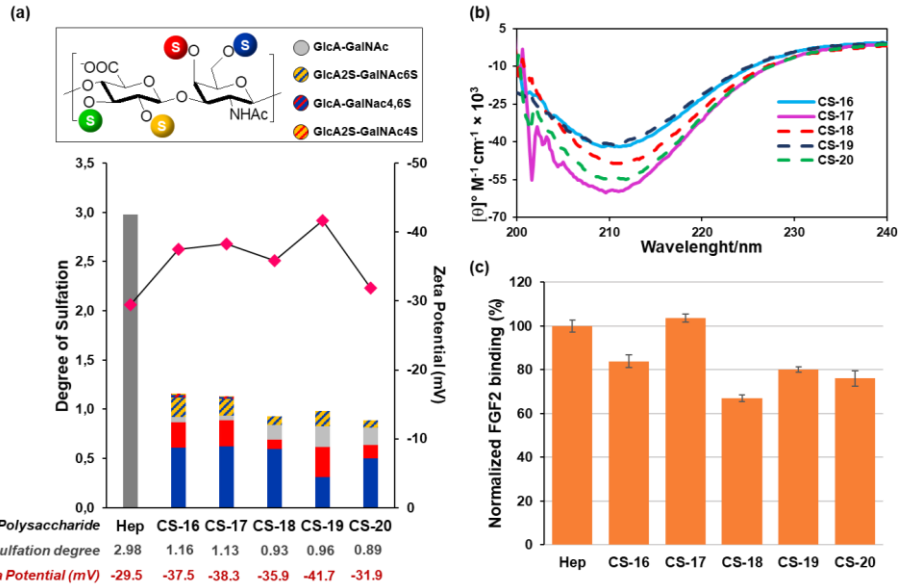

Figure 3.3. (a) Degree of sulfation of polysaccharides (numerical values indicated at the bottom, in grey). The pink points indicate the zeta-potential values (numerical values indicated at the bottom in red). The sulfated-disaccharide composition of each polysaccharide is shown in colours (for interpretation, see figure legend). (b) CD spectra of polysaccharides. (c) Bar graphs of normalized FGF-2 binding. The concentrations of polysaccharides were 0.5 mg/mL. Heparin (Hep) was employed as reference.

Recently, it has been proposed that 6-*O*-sulfated disaccharide subunits within CS backbone favour the arrangement of sulfate groups on the surface, whereas 4-*O*-sulfated repeating units have the opposite effect (Benito-Arenas et al., **2018**). However, it is important to underline that the polysaccharides examined in this previous study displayed only 6S- and/or 4S- sulfated residues. On the contrary, in the marine polysaccharide analysed herein, other sulfation motifs were present, and they could have notable effects on zeta-potential values. An evident example of such possible effect was the important decrease of zeta-potential value observed for polysaccharide **CS-19** (−41.7 mV). In this case, according to the abovementioned previous study, the higher 4S/6S ratio should involve a significant increase in zeta-potential value due to the effect of 4-*O*-sulfated disaccharide units in the arrangement of sulfates on the surface. The unexpected

low value could enable to outline an unknown effect of minor sulfated disaccharides along CS backbone in the arrangement of sulfates on the helical 3D-structure of the polysaccharides. Indeed, all the CD spectra, including those of polysaccharides with rare sulfate distributions, showed the negative band at 210 nm, that has been previously described for polysaccharide rich in helix content (Kreisman et al., **2007**; Lim et al., **2018**) (Figure 3.3).

To validate the initial hypothesis that this arrangement directs the binding of CSs to growth factors, SPR experiments were carried out. The SPR response units for the various compounds correlated well with the surface charge, even for **CS-19**, being indicative of the important role that minor sulfated disaccharide epitopes may play not only in the arrangement of sulfate groups on the surface, but also in the binding process to growth factors. Additionally, titration experiments were performed with a selected set of natural CSs (**CS-16**, **CS-17**, **CS-19**); the titration curves (for an example see Figure 3.7 in Paragraph 3.4) fitted well with a two-state binding model, and K_D values were determined (Table 3.2). These results could be rationalized considering a model in which the CS chain first forms a weak complex with the protein, which then matures to a tight binding (Zong et al., **2017**). Besides, the shape of the sensograms of **CS-16**–, **CS-17**–, and **CS-19**–FGF-2 interactions seemed to be similar and to have a comparable K_D, suggesting the importance of the minor sulfated-disaccharide epitopes in the binding to growth factors.

Table 3.2. K_D values of marine CSs–FGF-2 interactions.

Polysaccharide	K_{D1} (M)	K_{D2} (M)
CS-16 [a]	1.8×10^{-5}	8.6×10^{-8}
CS-17	7.4×10^{-6}	2.1×10^{-8}
CS-19	3.4×10^{-6}	6.8×10^{-9}

[a] For titration curves see Figure 3.7 in Paragraph 3.4.

With these results in mind, and to gain insights in the role of different disaccharide epitopes, the library of semi-synthetic polysaccharides, showing defined sulfation patterns, was analysed. In this case, polysaccharide molecular weights ranged between 7 and 10 kDa, thus also mimicking the dimension of possible domains. Disaccharide composition evaluation was performed through 2D-NMR spectroscopy. For polysaccharides **CS-1,5**–**10**, 2D-NMR integrations were employed as previously described in Chapter 2. As for **CS-21–23**, literature data from NMR analyses were considered (Benito-Arenas et al., **2018**). The results are summarized in Table 3.3. It can be noticed that, according to their sulfation profile, the semi-synthetic CSs can be divided in three types: with sulfo group(s) (one or two) placed at GalNAc residues (**CS-1**, **CS-21**, **CS-22**, **CS-23**), at GlcA units (**CS-5**, **CS-6**, **CS-7**) and at both GalNAc and GlcA (**CS-8**, **CS-9**, **CS-10**).

Table 3.3. Disaccharide composition and DS values (average number of sulfate groups per disaccharide unit) of semi-synthetic CS species.

Polysaccharide	Disaccharide Units	Ratio	DS
CS-1	GlcA-GalNAc4,6S/GlcA-GalNAc	80:20	1.60
CS-5	GlcA2,3S-GalNAc	100	2.00
CS-6	GlcA3S-GalNAc	100	1.00
CS-7	GlcA2S-GalNAc	100	1.00
CS-8	GlcA2,3S-GalNAc/ GlcA2,3S-GalNAc6S	44:56	2.56
CS-9	GlcA3S-GalNAc/ GlcA3S-GalNAc6S	77:23	1.23
CS-10	GlcA2S-GalNAc/ GlcA2S-GalNAc6S	16:84	1.84
CS-21 [a]	GlcA-GalNAc6S/ GlcA-GalNAc4S/ GlcA-GalNAc	25:72:3	0.97
CS-22	GlcA-GalNAc4S/ GlcA-GalNAc	75:25	0.75
CS-23	GlcA-GalNAc6S/ GlcA-GalNAc	86:14	0.86

[a] Provided by Creative Biomart.

Also for these semi-synthetic compounds, zeta-potential and CD spectra were measured. When GalNAc was modified, the zeta-potential data were similar to those previously observed for semi-synthetic CS with A- and C-type sulfation patterns (Benito-Arenas et al., **2018**). Thus, 6-*O*-sulfated moieties (**CS-23**) again seemed to induce the sulfate groups to point outside the 3D-structure, while the

presence of 4-*O*-sulfated motifs (**CS-22**), even with a small proportion of 6-*O*-sulfated ones (**CS-21**), led to an arrangement of the sulfate group inside the 3D-structure, as evidenced by their zeta-potential values (−21.3 mV for **CS-23** *vs.* −16.8, −16.4 mV for **CS-21** and **CS-22**, respectively) (Figure 3.4a). These differences affected the recognition by FGF-2, which prefers **CS-23**, having a more negatively charged surface, over **CS-21** or **CS-22** (Figure 3.4c).

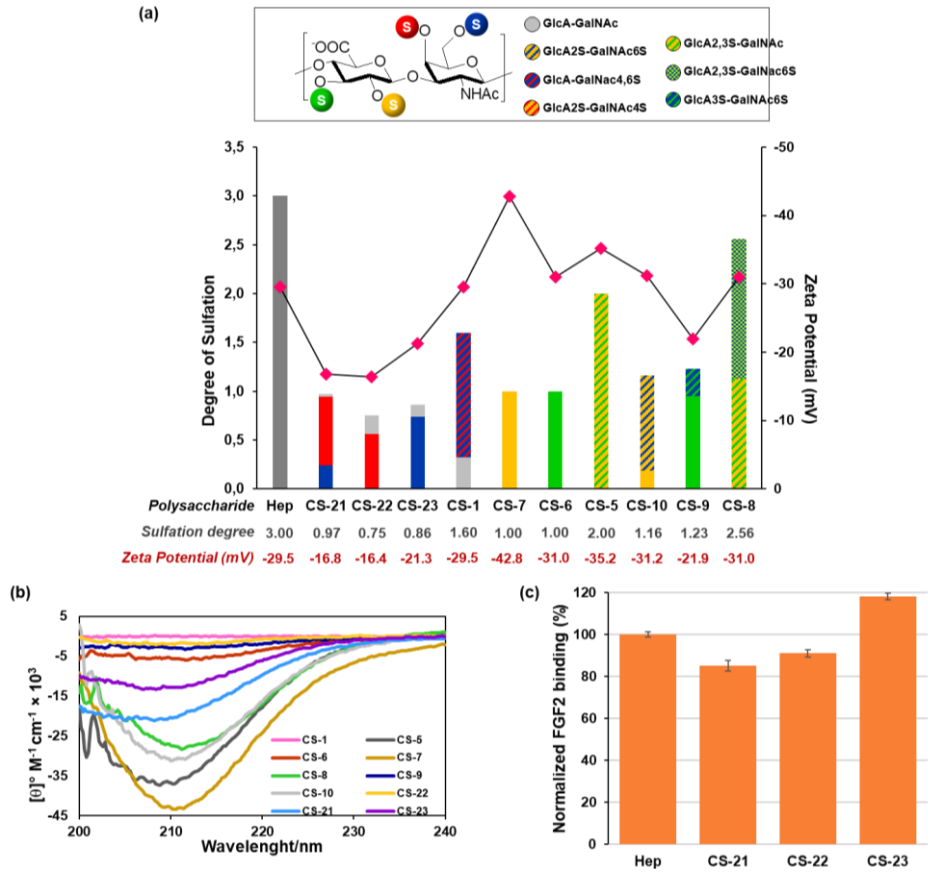

Figure 3.4. (a) Degree of sulfation of polysaccharides (numerical values indicated at the bottom, in grey). The pink points indicate the zeta-potential values (numerical values indicated at the bottom, in red). Sulfated-disaccharide composition of each polysaccharide is shown in colours (for interpretation, see figure legend). (b) CD spectra of polysaccharides. (c) SPR binding of immobilized FGF-2 to GalNAc sulfated derivatives (**CS-21**, **CS-22** and **CS-23**) (0.5 mg/mL) normalized against heparin.

On the other hand, CS compounds having sulfate groups at GlcA residues showed a very different behaviour depending on the sulfation pattern. For instance, the very low zeta-potential value displayed by **CS-7** (−42.8 mV) suggested that 2-*O*-sulfated motifs particularly favour the arrangement of the negatively charged sulfate group on the helical surface. This behaviour was further supported by comparing the zeta-potential value of **CS-6** (−31.0 mV), an isomer sulfated at *C*-3 position of the same saccharide ring (Figure 3.4a).

As expected, this zeta-potential variation resulted in important differences in binding affinity to FGF-2. Hence, a much higher affinity was observed for 2-*O*-sulfated CS (**CS-7**) than for 3-*O*-sulfated one (**CS-6**) (Table 3.4 entries *5* and *4*, respectively). Indeed, the only K_D observed for **CS-6** (6.6 μM) suggested that it formed a weak, non-specific complex with the protein, without showing the subsequent tight binding. In addition, as it could be observed from **CS-5**, the negative effect of *C*-3 sulfation at GlcA moieties could be countered in part by 2-*O*-sulfated position in the same units, thus further supporting the relevance of sulfation at such position. In this case, besides the slight decrease in zeta-potential value with respect to **CS-6**, it is worth noting the effect that 2-*O*-sulfation produces on 3D-structure, rising the helix content to levels like those of **CS-7** (Figure 3.4b). This structural feature could be the origin of the large increase in binding affinity showed by **CS-5** (K_{D1} = 8.6 μM, K_{D2} = 33.7 nM) (Table 3.4 entry *3*). A similar trend was observed in the case of **CS-8**, a polysaccharide obtained by partial sulfation (~50%) at the *C*-6 position of GalNAc units of **CS-5**. Surprisingly, the binding affinity of this polysaccharide to FGF-2 (K_{D1} = 1.33 μM, K_{D2} = 4.75 nM) (Table 3.4 entry *6*) was even higher than **CS-5**, though a slight increase in zeta-potential was observed (−31.0 mV for **CS-8** *vs.* −35.2 mV for **CS-5**), corroborating again the importance of the overall molecular architecture in the binding process.

Contrarily, when **CS-6** and **CS-7** were sulfated at *C*-6 positions of GalNAc to afford **CS-9** and **CS-10**, respectively, a different behaviour was observed. In both cases, SPR results indicated that these polysaccharides displayed diverse binding preferences with respect to the other compounds, in accordance with a model in which a strong binding to FGF-2 occurs first, followed by a weak interaction. These results could be in consonance with the previously observed effect that 6-*O*-sulfated GalNAc residues have on the binding capacity and on the specificity of CSs binding to growth factors (Pudełko et al., **2019**). Nevertheless, more studies are needed to elucidate the mechanism of action.

Table 3.4. K_D values of semi-synthetic CSs–FGF-2 interactions.

Entry	Polysaccharide	K_{D1} (M)	K_{D2} (M)
1	**CS-21**[a]	1.37×10^{-4}	1.08×10^{-6}
2	**CS-1**	1.31×10^{-6}	3.88×10^{-9}
3	**CS-5**	8.61×10^{-6}	3.37×10^{-8}
4	**CS-6**	6.6×10^{-6}	-
5	**CS-7**	3.67×10^{-6}	7.77×10^{-9}
6	**CS-8**	1.33×10^{-6}	4.75×10^{-9}
7	**CS-9**	4.0×10^{-8}	2.9×10^{-6}
8	**CS-10**	1.75×10^{-8}	2.56×10^{-6}

[a] For titration curves see Figure 3.8 in Paragraph 3.4.

Lastly, a peculiar effect was observed when **CS-1,** a disulfated polysaccharide possessing predominantly an E-type sulfation pattern (GalNAc4,6S), was analysed. Surprisingly, despite the total loss of helical structural motifs, as proved by the absence of the band at 210 nm in its CD spectrum (Figure 3.4b), this polysaccharide displayed a good responsiveness when interacting with FGF-2 (K_{D1} = 1.31 μM, K_{D2} = 3.88 nM) (Table 3.4 entry *2*). This result was particularly remarkable since CSs studied so far exhibited a clear helical structure; moreover, many previous studies reported the importance of recognizing such molecular architecture in terms of the defined periodic spacing between sulfate moieties and

their helical layout (Nagel et al., **2017**; Raman et al., **2003**). In particular, it has been showed that spinal cord CS (mainly composed of 4S- and 6S- monosulfated residues) binds to FGF-2 with a greater affinity that the more highly sulfated CS-E of natural origin (composed of a mixture of different disaccharides with over 50% of E-type units) (Deepa et al., **2002**; Liu et al., **2010**).

To gain an insight into this unexpected result, an SPR solution/surface competition assay was performed to examine the effect of helical structure on the FGF-2–polysaccharide interaction. To this aim, **CS-1** and **CS-7** were selected being two polysaccharides that exhibited a similar responsiveness against FGF-2 (see entries *2* and *5* in Table 3.4), although possessing completely different 3D-structures (Figure 3.4b). As displayed in Figure 3.5 for FGF-2–**CS-1** interaction, no competition effect was detected when different concentrations of **CS-7** were added. On the contrary, binding signals considerably raised when **CS-7** was present in **CS-1** solution, and an increase in **CS-7** concentration resulted in a greater responsiveness.

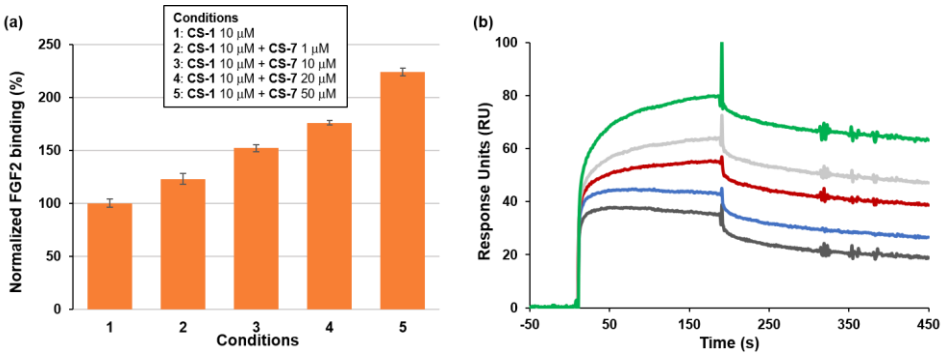

Figure 3.5. (a) Bar graph of normalized **CS-1** binding preference to surface FGF-2 by competing with different concentrations of **CS-7**. (**b**) SPR sensograms for binding-affinity measurements. The concentration of **CS-1** was, in all cases, 10 µM, and concentrations of **CS-7** were (from top to bottom): 50 µM, 20 µM, 10 µM,, 1 µM and 0 µM.

These results suggested that FGF-2 could recognize simultaneously **CS-1** and **CS-7**, so tolerating derivatives with or without a defined 3D-structures. On the basis

on these and previous results (Doncel-Pérez et al., **2018**; Revuelta et al., **2020**), it could be hypothesized that the helical layout of the CS chain would allow a productive binding mode. This could be connected to the binding between growth factor–growth factor receptor and CS, which would act as co-receptor, leading to an enhanced signal transduction across the plasma membrane. On the contrary, non-structured polysaccharides would sequester the protein, protecting it from proteolysis or locally blocking its active site (Figure 3.6).

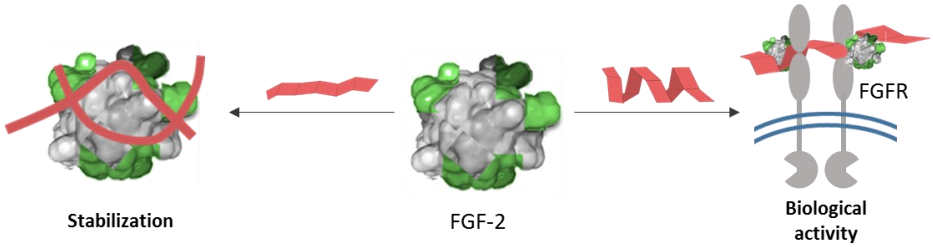

Figure 3.6. Dual function of chondroitin sulfates in their binding to FGF-2 as mediators of growth factor signalling to cells (*right*) or as providers of storage sites, protecting and stabilization the protein (*left*).

However, in order to validate this hypothesis, a deep insight into the influence of the 3D-helical structure in the selectivity of the binding to a specific region of the protein as well as its consequence in biological function is required.

3.3. Conclusions

In this work, different natural CSs of marine origin, as well as semi-synthetic ones, were analysed, isolating the effects of their rare sulfate-bearing motifs in the binding to FGF-2.

The results highlighted that the particular sulfate distribution within the disaccharide repeating units plays a key role in the binding of FGF-2, modulating the surface charge of the 3D-structure that, according with our hypothesis, has a significant influence on the binding capacity. Furthermore, the collected data

revealed that rare sulfated epitopes and even unnatural ones may have a similar, if not better, effect in the binding affinity to growth factors than 4-*O*- and 6-*O*-sulfated CS isomers, the most abundant disaccharide units in natural CS polysaccharides. Finally, we have observed that although sulfation profiles provide the primary basis for modulating interactions with growth factors, the presence of the helical layout of sulfate charges could be determinative in terms of the specificity of the binding epitope, which could have important biological consequences. These results were included in a very recently paper published during this Ph.D. work (Vessella et al., **2021**).

3.4. Experimental Section

Materials. Commercial grade reagents and solvents were used without further purification. The term "deionized water" refers to water purified by a Millipore Milli-Q gradient system. **CS-21** was purchased from Creative Biomart and was dialysed with a Spectra/Por 3.5 kDa cut-off membrane against deionized water before use. For disaccharide compositional analysis of natural CSs, chondroitinase ABC was purchased from Sigma-Aldrich (EC 4.2.2.4, 1.66 U mg^{-1}, product number C2905), and unsaturated disaccharide standards were obtained from GrampEnz; an Agilent 1260 HPLC system (Agilent Technologies, Inc.) was used for separation. A Viscotek instrument (Malvern) was used to determine molecular mass data of semi-synthetic CSs. SPR measurements were performed on a BIAcore X100 system (Cytiva). Recombinant human FGF-2 was purchased from PeproTech.

Production and disaccharide composition of CSs from marine sources. Highly purified CSs were obtained at the laboratories of Dr. Jesús Valcárcel group (Group of Recycling and Valorization of Waste Material, Marine Research Institute, *Consejo Superior de Investigaciones Científicas*–CSIC) using cartilage

waste from *Chimaera monstrosa* (**CS-16**), *Galeus melastomus* (**CS-17**), *Prionace glauca* (**CS-18**), *Scyliorhinus canicula* (**CS-19**), and *Raja clavata* (**CS-20**), in accordance with reported procedures (Blanco et al., **2015**; Vázquez et al., **2019**, **2018**, **2016**). Disaccharide composition was determined by SAX-HPLC (Vázquez et al., **2018**; Volpi, **2000**), after enzymatic digestion with chondroitinase ABC from *Proteus vulgaris* at 0.2 U mg^{-1} of CS, according to a previously described procedure (Vázquez et al., **2018**).

Preparation of semi-synthetic CSs. CS-1,5–10 were prepared starting from *Escherichia coli* O5:K4:H4 sourced chondroitin following the multi-step procedures developed by us and described in Chapter 2 (see Paragraphs 2.2.1.1, 2.2.1.2, 2.2.1.3 for a detailed discussion and Paragraph 2.4.2 for the experimental methods). **CS-22** and **CS-23** were prepared at the laboratories of Dr. Julia Revuelta (BioGlycoChem Group, Institute of General Organic Chemistry, *Consejo Superior de Investigaciones Científicas*–CSIC) starting from **CS-21** according to two previously described procedures (Benito-Arenas et al., **2018**).

Determination of molecular mass (CS-5, CS-6, CS-7). The molecular weight analyses of the CS samples (**CS-5, CS-6, CS-7**) were performed by a high-performance size-exclusion chromatographic system (Viscotek, Malvern), equipped with an integrated gel permeation chromatography system (GPCmax VE 2001, Viscotek, Malvern) and a triple detector array module (TDA 305, Viscotek, Malvern) including a RI detector, a four-bridge VIS, and a laser detector made of a RALS detector and a LALS one. Two gel-permeation columns (TSK-GEL GMPWXL, 7.8 × 300 mm, Tosoh Bioscience), equipped with a guard column (TSK-GEL GMPWXL, 6.0 × 40 mm, Tosoh Bioscience), were set in series to perform the analyses. An OmniSEC software (Viscotek, Malvern) program was used for the acquisition and analysis of the data. Samples were analysed at concentrations ranging from 0.3 to 4 g L^{-1} to have a column load for each analysis (injection volume × sample concentration × intrinsic viscosity) of approximately

0.2 dL and, at the same time, appreciable LALS and VIS signals when analysing low-molecular-mass fragments. Elution was performed in isocratic conditions with 0.1 M $NaNO_3$ at pH 7.0, at a flow rate of 0.6 ml min^{-1}, at 40 °C in 50 min runs. The calibration of the instrument was performed by using a PEO standard (22 kDa PolyCAL, Viscotek, Malvern). The fragment molecular weight distribution, the molecular size distribution, the polydispersity were calculated by the data of the sample concentration, the molecular weight and the intrinsic viscosity that the system simultaneously determined, according to previously reported formulas (La Gatta et al., **2010**). The refractive index increment (dn dc^{-1}) used for the samples was referred to the literature value for CS: 0.147 mL g^{-1} (Swann et al., **1984**).

Molecular weight of natural CSs. Molecular weight analyses of natural CSs were performed a GPC/SEC system (Agilent Technologies), according to recently described analytical methods (Vázquez et al., **2018**). The eluent was 1% acetic acid in deionized water (pH = 3.7). Elution was conducted at r.t.

Table 4.5. Representative molecular weights of CSs.

Polysaccharide	M_w (kDa) [a]	M_n (kDa) [b]	M_w/M_n [a,b]
CS-5	9.7 ± 0.1	7.40 ± 0.4	1.31
CS-6	7.3 ± 0.2	5.57 ± 0.3	1.31
CS-7	8.2 ± 0.9	6.12 ± 0.5	1.34
CS-15	70 ± 5	51 ± 4	1.37
CS-16	69 ± 5	55 ± 5	1.25
CS-17	60 ± 6	51 ± 5	1.17
CS-18	45 ± 4	34 ± 3	1.32
CS-19	44 ± 5	34 ± 4	1.29
CS-20	7.05 ± 0.2	6.7 ± 0.1	1.05
CS-21	6.13 ± 0.3	5.9 ± 0.4	1.03
CS-22	6.80 ± 0.2	6.53 ± 0.1	1.04

[a] M_w: weight-averaged molecular weight. [b] M_n: number-averaged molecular weight.

Zeta potential analysis. Zeta potential measurements were performed on a Malvern Zetasizer Nano ZS (Malvern Instrument). The polysaccharides were dissolved (1 mg/mL) in 0.01 mM $NaCl_{(aq)}$. Each experiment was performed in triplicate.

Circular dichroism. CD spectra were acquired using a Jasco-815 dichrograph (JASCO International Co. Ltd.), previously calibrated with CSA. Measurements were performed at 25 °C in quartz cuvettes (path length 1 cm, Hellma GmbH & Co. KG). For all samples, total polysaccharide concentration in the cuvette was 1 mg/mL in HEPES buffer (2.5 mM, pH 7.4). UV-CD spectra were recorded between 200 and 240 nm with a step size of 1 nm and bandwidth of 1 nm at 25 °C.

Determination of binding affinity of polysaccharides with FGF-2 through SPR. The surface of a CM5 sensor chip (Cytiva) was activated using freshly mixed 1:1 *v*/*v* 100 mM $NHS_{(aq)}$–400 mM $EDC_{(aq)}$. Then, a solution of FGF-2 (50 µg/mL) in 10 mM $NaOAc_{(aq)}$ buffer (pH 5.0) was passed over the surface until a ligand density of 7000 RUs. Quenching of the remaining active esters was accomplished by passing aqueous ethanolamine (1.0 M, pH 8.5) over the surface of the chip. The control flow cell was activated with NHS and EDC, which was then treated with ethanolamine. HBS-EP buffer (0.01 M HEPES, 150 mM NaCl, 3 mM EDTA, 0.05% polysorbate 20; pH 7.4) was employed as the running buffer for immobilization, binding and affinity analysis. Serial dilutions of each compound in HBS-EP buffer at a flow rate of 30 µL/min was employed for association and dissociation at a temperature of 25 °C. One 30 s injections of 2.0 M $NaCl_{(aq)}$ at flow rate of 30 µL/min was employed for regeneration to achieve baseline status. Affinity data were fitted, except for **CS-6**, to a two sites affinity model, yielding two K_D values (for an example see Figure 3.7-3.8). The competition experiments were prepared with samples containing a fixed concentration of **CS-1** (10 µM) and a series of concentrations of the

polysaccharide **CS-7** which range from 1 to 50 µM in HBS-EP. The regeneration conditions were similar to the binding experiments described above. The evaluation was made using a BIAcore X100 Evaluation Software (Cytiva).

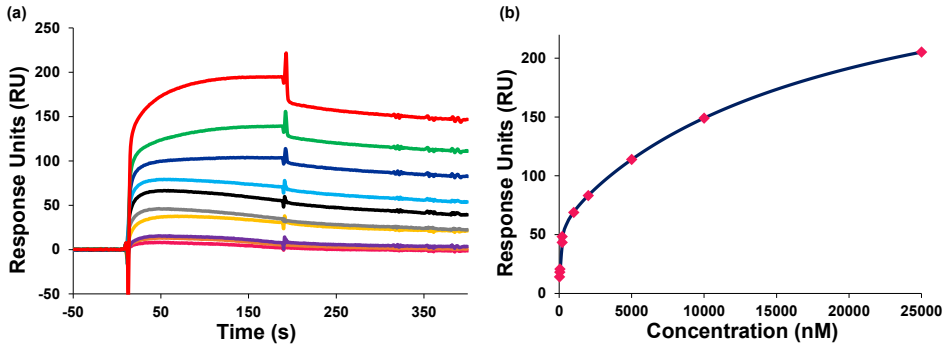

Figure 3.7. (a) SPR sensograms for binding affinity measurements for FGF-2/**CS-16** interactions. Concentrations of **CS-16** (from bottom to top) were: 20 nM, 35 nM, 50 nM, 200 nM, 500 nM, 1000 nM, 2000 nM, 5000 nM, 10000 nM, and 25000 nM. (b) Representation of SPR values at the steady state against polysaccharide concentration in the dissociation phase.

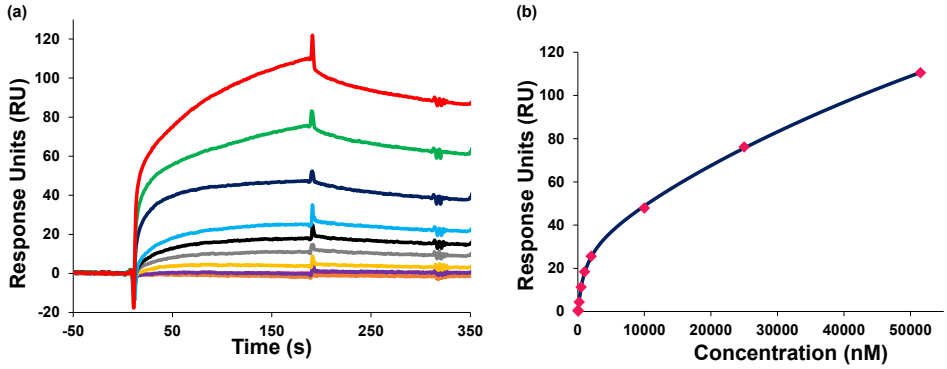

Figure 3.8. (a) SPR sensograms for binding affinity measurements for FGF-2/**CS-21** interactions. Concentrations of CS-21 (from bottom to top) were: 20 nM, 35 nM, 50 nM, 200 nM, 500 nM, 1000 nM, 2000 nM, 10000 nM, 25000, 51500 nM. (b) Representation of SPR values at the steady state against polysaccharide concentration in the dissociation phase

References

Bedini, E., De Castro, C., De Rosa, M., Di Nola, A., Iadonisi, A., Restaino, O.F., Schiraldi, C., Parrilli, M., **2011**. *Angew. Chem., Int. Ed. 50*, 6160–6163.

Bedini, E., De Castro, C., De Rosa, M., Di Nola, A., Restaino, O.F., Schiraldi, C., Parrilli, M., **2012**. *Chem. - Eur. J. 18*, 2123–2130.

Benito-Arenas, R., Doncel-Pérez, E., Fernández-Gutiérrez, M., Garrido, L., García-Junceda, E., Revuelta, J., Bastida, A., Fernández-Mayoralas, A., **2018**. *Carbohydr. Polym. 202*, 211–218.

Blanco, M., Fraguas, J., Sotelo, C., Pérez-Martín, R., Vázquez, J., **2015**. *Mar. Drugs 13*, 3287–3308.

Brown, J.M., Xia, J., Zhuang, B.Q., Cho, K.S., Rogers, C.J., Gama, C.I., Rawat, M., Tully, S.E., Uetani, N., Mason, D.E., Tremblay, M.L., Peters, E.C., Habuchi, O., Chen, D.F., Hsieh-Wilson, L.C., **2012**. *Proc. Natl. Acad. Sci. U.S.A 109*, 4768–4773.

Deepa, S.S., Umehara, Y., Higashiyama, S., Itoh, N., Sugahara, K., **2002**. *J. Biol. Chem. 277*, 43707–43716.

Dickendesher, T.L., Baldwin, K.T., Mironova, Y.A., Koriyama, Y., Raiker, S.J., Askew, K.L., Wood, A., Geoffroy, C.G., Zheng, B., Liepmann, C.D., Katagiri, Y., Benowitz, L.I., Geller, H.M., Giger, R.J., **2012**. *Nat. Neurosci. 15*, 703–712.

Doncel-Pérez, E., Aranaz, I., Bastida, A., Revuelta, J., Camacho, C., Acosta, N., Garrido, L., Civera, C., García-Junceda, E., Heras, A., Fernández-Mayoralas, A., **2018**. *Carbohydr. Polym. 191*, 225–233.

Gama, C.I., Tully, S.E., Sotogaku, N., Clark, P.M., Rawat, M., Vaidehi, N., Goddard, W.A., Nishi, A., Hsieh-Wilson, L.C., **2006**. *Nat. Chem. Biol. 2*, 467–473.

La Gatta, A., De Rosa, M., Marzaioli, I., Busico, T., Schiraldi, C., **2010**. *Anal. Biochem. 404*, 21–29.

Higashi, K., Okamoto, Y., Mukuno, A., Wakai, J., Hosoyama, S., Linhardt, R.J., Toida, T., **2015**. *Carbohydr. Polym. 134*, 557–565.

Ji, Y., Zhang, S., Qiao, M., Jiao, R., Li, J., Song, P., Zhang, X., Huang, H., **2020**. *Carbohydr. Polym. 248*, 116796–116806.

Joffrin, A.M., Hsieh-Wilson, L.C., **2020**. *J. Am. Chem. Soc. 142*, 13672–13676.

Kjellén, L., Lindahl, U., **2018**. *Curr. Opin. Struct. Biol. 50*, 101–108.

Kreisman, L.S.C., Friedman, J.H., Neaga, A., Cobb, B.A., **2007**. *Glycobiology 17*, 46–55.

Lim, T.C., Cai, S., Huber, R.G., Bond, P.J., Siew Chia, P.X., Khou, S.L., Gao, S., Lee, S.S., Lee, S.G., **2018**. *Chem. Sci. 9*, 7940–7947.

Liu, Z., Masuko, S., Solakyildirim, K., Pu, D., Linhardt, R.J., Zhang, F., **2010**. *Biochemistry 49*, 9839–9847.

Nagel, Y.A., Raschle, P.S., Wennemers, H., **2017**. *Angew. Chem., Int. Ed. 56*, 122–126.

Novoa-Carballal, R., Pérez-Martín, R., Blanco, M., Sotelo, C.G., Fassini, D., Nunes, C., Coimbra, M.A., Silva, T.H., Reis, R.L., Vázquez, J.A., **2017**. *Carbohydr. Polym. 157*,

31–37.

Pudełko, A., Wisowski, G., Olczyk, K., Koźma, E.M., **2019**. *FEBS J. 286*, 1815–1837.

Raman, R., Venkataraman, G., Ernst, S., Sasisekharan, V., Sasisekharan, R., **2003**. *Proc. Natl. Acad. Sci. U.S.A 100*, 2357–2362.

Revuelta, J., Aranaz, I., Acosta, N., Civera, C., Bastida, A., Peña, N., Monterrey, D.T., Doncel-Pérez, E., Garrido, L., Heras, Á., García-Junceda, E., Fernández-Mayoralas, A., **2020**. *ACS Appl. Mater. Interfaces 12*, 25534–25545.

Smock, R.G., Meijers, R., **2018**. *Open Biol. 8*, 180026–180035.

Swann, D.A., Garg, H.G., Silver, F.H., Larsson, A., **1984**. *J. Biol. Chem. 259*, 7693–7700.

Swarup, V.P., Hsiao, T.W., Zhang, J., Prestwich, G.D., Kuberan, B., Hlady, V., **2013**. *J. Am. Chem. Soc. 135*, 13488–13494.

Turnbull, J., Powell, A., Guimond, S., **2001**. *Trends Cell Biol. 11*, 75–82.

Vázquez, J.A., Blanco, M., Fraguas, J., Pastrana, L., Pérez-Martín, R., **2016**. *Food Chem. 198*, 28–35.

Vázquez, J.A., Fraguas, J., Novoa-Carballal, R., Reis, R.L., Pérez-Martín, R.I., Valcarcel, J., **2019**. *Carbohydr. Polym. 210*, 302–313.

Vázquez, J.A., Fraguas, J., Novoa-Carvallal, R., Reis, R., Antelo, L., Pérez-Martín, R., Valcarcel, J., **2018**. *Mar. Drugs 16*, 344–358.

Vessella, G., Traboni, S., Cimini, D., Iadonisi, A., Schiraldi, C., Bedini, E., **2019**. *Biomacromolecules 20*, 3021–3030.

Vessella, G., Vázquez, J.A., Valcárcel, J., Lagartera, L., Monterrey, D.T., Bastida, A., García-Junceda, E., Bedini, E., Fernández-Mayoralas, A., Revuelta, J., **2021**. *Polymers 13*, 313–329.

Volpi, N., **2000**. *Anal. Biochem. 277*, 19–24.

Xu, D., Esko, J.D., **2014**. *Annu. Rev. Biochem. 83*, 129–157.

Zong, C., Venot, A., Li, X., Lu, W., Xiao, W., Wilkes, J.S.L., Salanga, C.L., Handel, T.M., Wang, L., Wolfert, M.A., Boons, G.J., **2017**. *J. Am. Chem. Soc. 139*, 9534–9543.

CHAPTER 4
STUDY FOR REGIOSELECTIVE SULFATION OF POLYSACCHARIDES

4
STUDY FOR REGIOSELECTIVE SULFATION OF POLYSACCHARIDES

4.1 Introduction

Natural sulfated polysaccharides are found in a large variety of living systems and have central functions in biological processes (see also Paragraph 1.2.1). Among them, sulfated GAGs, mainly found in animal species, have attracted much attention thanks to their roles in various physiological and pathological processes such as immunity, angiogenesis, cancer, infectious diseases, etc. (Bedini et al., **2019**). These bioactivities have inspired their use in the development of therapeutics and biomaterials, some of them already available from decades. Heparin, which has been the most extensively used anticoagulant drug in the world since its discovery in the early 1900s (Wardrop and Keeling, **2008**), is the most notorious, but not the only example in this field. For instance, CS-A,C is currently used for the treatment of articular cartilage osteoarthritis (Bishnoi et al., **2016**) and other GAG applications are under development (Kowitsch et al., **2018**; Scott and Panitch, **2013**). However, for most medical uses, native GAGs may exhibit limitations with respect to production cost, batch standardization, immunogenicity, degradability, or other aspects. Engineering of polysaccharides, with the insertion of one or more sulfate groups per repeating unit to obtain GAG analogues and mimics, can overcome some of these challenges and simultaneously unveil novel biomedical applications of sulfated polysaccharides. Indeed, since these artificially sulfated species show unique structural features, they may display altered pharmacokinetic properties with respect to natural sulfated polysaccharides, revealing new possibilities for their use in biomaterials,

drug delivery vehicles, and more (Arlov et al., **2021**). Moreover, in several cases engineered sulfated polysaccharides can be produced in large quantities and at moderately low cost, starting from renewable and/or underutilized raw materials or from microbial production, thus being a more environmentally and economically sustainable alternative to isolation of GAGs from animal tissues (Arlov and Skjåk-Bræk, **2017**; Bedini et al., **2011**; Wang et al., **2015**; Zou and Khor, **2009**).

Over the last decades, several chemical and chemoenzymatic approaches have been developed for the obtainment of a wide variety of engineered sulfated polysaccharides (Caputo et al., **2019**; Wang et al., **2018**; Zeng et al., **2019**). The main efforts have been addressed towards regioselective strategies in order to gain well-defined structures with a precise sulfation pattern, starting from unsulfated polysaccharides with wide availability and ease of purification from non-animal sources. Indeed, the presence of regular repeating units along the polymeric chain can facilitate the elucidation of the structure-activity relationships. Among chemical regioselective sulfation methods, two strategies can be distinguished (Bedini et al., **2017**). On one hand, non-sulfated polysaccharides can be subjected to direct, regioselective sulfation reactions; although this approach has the advantage to afford the target in a single step, it can be employed only to install sulfate groups on the most reactive hydroxyl(s) of the polysaccharides – if any exists – and it is often characterized by low regioselectivity and/or sulfation degree. On the other hand, methods based on multi-step regioselective protection(s)-sulfation-deprotection sequences are centred on the employment of suitable protecting groups to be regioselectively installed on specific hydroxyl position(s) of the polymeric chain, thus enlarging the scope of achievable sulfation patterns.

In this frame, here we investigate the possibility to achieve the regioselective sulfation of naturally occurring polysaccharides, exploiting suitably tailored

multi-step sequences. We also explore the feasibility to employ cyclic protecting groups (*e.g.* acetal/ketal, orthoester, etc.) for the protection of vicinal diols in the repeating units of the polysaccharide chain. This would pave the way to novel, regioselectively modified sulfated polysaccharides, and, from a more general point of view, could enlarge the application of cyclic protecting groups, which are still underexploited in polysaccharide chemistry (Bachelder et al., **2017**; Chien et al., **2019**; Raßloff et al., **2018**). For our study, three polysaccharides (curdlan, M-rich alginic acid, and a marine-sourced bacterial exopolysaccharide) have been selected. Their structural and biological features, together with some reported advances in their chemical modifications, are discussed in more details in the following paragraphs. Notably, their regioselective sulfation — to the best of our knowledge still unexplored in literature apart few, not exhaustive examples on curdlan — could be one of the most cost-effective ways to achieve both an intrinsic improvement of their already existing properties and to introduce completely new activities.

4.1.1. Curdlan

Curdlan is a linear homopolymer, produced by some bacteria as an exopolysaccharide and composed of β-1→3-linked Glc units. It is currently available from mutant *Agrobacterium* strains in high fermentation yield (Kalyanasundaram et al., **2012**) and employed in food industry due to its remarkable rheological and thermal behaviours. Furthermore, its ability to form gel encapsulations with several drugs and above all its roles in both innate and adaptive immunity have fuelled an increasing interest in pharmaceutical applications of curdlan and derivatives thereof (Zhan et al., **2012**). In particular, several curdlan semi-synthetic polysaccharides carrying well-defined structural modifications, especially at the most reactive primary *O*-6 position, have been accessed and demonstrated to have interesting biomedical and pharmaceutical

applications (Zhang and Edgar, **2014**). Among them, curdlan sulfate derivatives recently emerged thanks not only to a highly enhanced water solubility with respect to native curdlan, but also to an efficient adjuvant activity displayed in antitumor and hepatitis B virus immunotherapy both *in vitro* and *in vivo* (Jin et al., **2020**; Li et al., **2014**).

Some regioselectively sulfated curdlan derivatives have been already obtained through a direct sulfation reaction or multi-step protection-sulfation-deprotection sequences. The first approach allowed the insertion of sulfate groups at *O*-6 position with a quantitative DS and at some of the *O*-2 sites of the polysaccharide, the latter being more easily sulfated than *O*-4 ones (Scheme 4.1) (Gao et al., **1997**; Yoshida et al., **1995**). A complementary sulfation pattern with DS = 0.39 and 1.00 for *O*-2 and *O*-4 position, respectively, and no sulfation at *O*-6 site could be accessed by a multi-step strategy relying upon a regioselective protection of the primary hydroxyl at *C*-6 position with a bulky pivaloyl ester, followed by sulfation of the free secondary alcohols and final deacylation (Gao et al., **1997**). A very similar sulfation pattern was postulated for a semi-synthetic polysaccharide obtained by regioselective desulfation with BTSA of a persulfated curdlan derivative (Chaidedgumjorn et al., **2002**; Matsuo et al., **1993**).

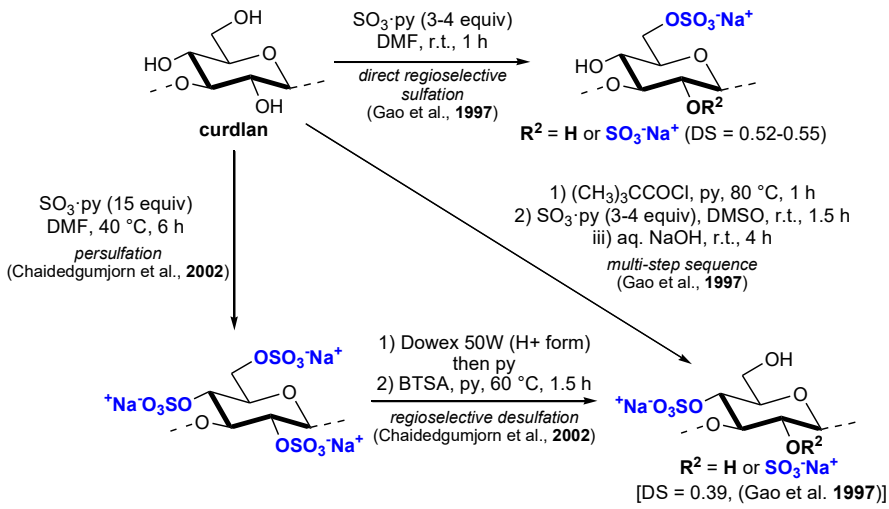

Scheme 4.1. Literature methods to regioselectively sulfated curdlan polysaccharides through direct sulfation, desulfation or multi-step protection-sulfation-deprotection sequence.

4.1.2. Alginates

Alginates are biomacromolecules quite abundant in Nature, present in marine brown algae as structural components and in soil bacteria as capsular polysaccharides. They are widely employed mainly in food, pharmaceutical and textile industry for their properties in viscosity enhancement, gel-forming ability, stabilization of aqueous mixtures, dispersions, emulsions, and encapsulation of drugs and cells (Draget et al., **2006**). Several applications for alginates have been already established or are currently under development (Lee and Mooney, **2012**; Szekalska et al., **2016**).

From a structural point of view, alginates are polysaccharides composed of β-1→4-linked D-ManA and its C-5 epimer L-GulA units. These residues are distributed along the polysaccharide chain in a block-copolymer fashion with homopolymeric regions composed of M-blocks and G-blocks, respectively, and heteropolymeric ones with MG alternating structures (MG-blocks) or more complicate sequences (*e.g.* GGM and MMG) (Aarstad et al., **2012**).

Alginate amount biosynthesized in algae per year is estimated to be more ten times higher than the amount produced and employed by industry in the same period. Such large availability has pushed chemists to investigate the possibility to obtain structurally modified alginate polysaccharides as novel, sustainable materials with enhanced properties with respect to the unmodified polysaccharide or completely new activities otherwise not existing in alginate native form. Several kinds of transformations have been reported (Fernando et al., **2019**; Pawar and Edgar, **2012**; Yang et al., **2011**). Among them, one of the most investigated is the insertion of sulfate groups on alginate backbone (Arlov and Skjåk-Bræk, **2017**). Sulfated alginates, as well as the other semi-synthetic sulfated polysaccharides (Wang et al., **2018**; Zeng et al., **2019**), show interesting anti-coagulant, anti-inflammatory and wound dressing activities. Notably, a low molecular weight alginate sulfated derivative (propylene glycol alginate sodium sulfate, PSS) has been used for more than 30 years as a heparin-like anti-cardiovascular disease drug in China. Nonetheless, a not negligible number of adverse effects has been recorded during the clinical application of PSS (Xue et al., **2016**). The M/G ratio is known to play an important role in both anticoagulant and side effects of PSS (Wu et al., **2014**), but the key factors for SAR studies, not only for PSS but also for alginate sulfate species as well as for sulfated polysaccharides in general, are the degree of sulfation and the distribution of the sulfate groups along the polysaccharide backbone (sulfation pattern) (Freeman et al., **2008**). In semi-synthetic sulfated polysaccharides, the former parameter can be often controlled through stoichiometry, while the latter requires, as discussed above, the development of chemical or enzymatic methods for the regioselective insertion of sulfate groups exclusively on determined positions. Although this goal has been attained for several polysaccharides up to now, to the best of our knowledge such achievement is still missing for any alginate sulfate derivative (Bedini et al., **2017**). Indeed, a quite good control of DS on alginates with homogeneous

monosaccharide sequences (poly-M, poly-G and poly-MG) could be achieved (Arlov et al., **2014**), whereas no control of sulfation pattern — neither between nor within M and G units (*i.e.* M- *vs.* G-, and *O*-2 *vs. O*-3, respectively) — has been reported. Only a slight preference for sulfation of M- over G-units and of *O*-3 over *O*-2 positions has been observed, anyway in the context of an undoubtedly random sulfation pattern (Cong et al., **2014**).

4.1.3. HE800 EPS from *Vibrio diabolicus*

Exopolysaccharides (EPSs) are biomacromolecules that microorganisms secrete in their surrounding environment. They can be capsular polymers, if attached to the cell membrane through the lipopolysaccharides anchored in the membrane or through other specific proteins (Decho, **1990**). Alternatively, they can also be produced as a slime loosely bound around the cell or dispersed in the environment (Sutherland, **1982**). These polysaccharides have mostly a protective role and permit resistance under extreme environmental conditions by participating in the cell membrane integrity, trapping nutrients, allowing adhesion to surfaces, protecting from toxic compounds and adverse conditions, such as freezing (Decho, **1990**; Finore et al., **2014**; Jannasch and Taylor, **1984**).

The growing interest in renewable sources situates EPSs as important products of microbial biotechnologies aimed to convert discarded materials into bioenergy and biomaterials, in order to contribute to a reduction in economic dependence on fossil fuels (Pagliano et al., **2017**). A particular attention has been focused on polysaccharide-producing marine bacteria; indeed, the existence of various extreme habitats in marine ecosystem (*e.g.* deep-sea, hydrothermal vents, volcanic and hydrothermal marine areas, marine salterns, salt lake, and sea ice in polar regions) leads to the presence of unusual microorganisms, secreting very different and peculiar EPS structures with interesting chemical and rheological properties (Casillo et al., **2018**).

Vibrio diabolicus is a facultatively anaerobic, heterotrophic, mesophilic bacterium isolated from the polychaete annelid *Alvinella pompejana* collected from a deep-sea hydrothermal field in the East Pacific Rise (Raguénès et al., **1997**). This strain was described for the first time in 1997 and, on the basis of phenotypic characteristics, phylogenetic analyses, and DNA-DNA relatedness, it was identified as a new species of the genus *Vibrio*, which consists of more than 100 species naturally occurring in marine systems (Reen et al., **2006**), but also associated with a wide variety of molluscs and animals (Romalde et al., **2014**). As many other *Vibrio* bacteria (Bramhachari et al., **2007**; Bramhachari and Dubey, **2006**; Drouillard et al., **2015**; Jiang et al., **2011**; Muralidharan and Jayachandran, **2003**), *V. diabolicus* secretes an EPS (hereinafter referred to as HE800 EPS), whose structure is rich in aminosugars and uronic acids. Its polymer chain consists of a linear tetrasaccharide repeating unit, including two D-GlcA residues, one D-GlcNAc and one D-GalNAc linked together as depicted in Figure 4.1.

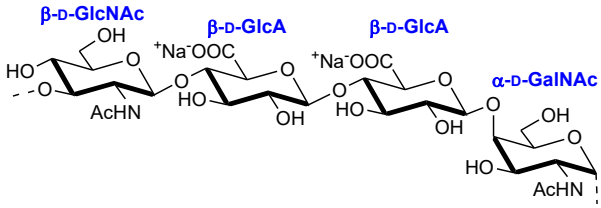

Figure 4.1 HE800 EPS repeating unit.

The resemblance of HE800 EPS chain to GAG structures, due to the presence of both aminosugars and uronic acids, makes it of potential interest in term of biological and biomedical properties and applications. For example, it has been already evaluated its bone regeneration capacity, revealing to act as an efficient filler of bone defects in rat calvaria, without showing any inflammatory activity (Zanchetta et al., **2003**). In addition, the polysaccharide chain may be structurally modified, *e.g.* depolymerized and/or sulfated, opening the way to semi-synthetic macromolecules with new or enhanced bioactivity. To the best of our knowledge,

this approach is still mostly unexplored and only few reports, dealing with chemical modifications of marine EPSs, can be found in literature (Gomez D'Ayala et al., **2008**). In the case of HE800 EPS, low-molecular weight oversulfated derivatives thereof have been obtained through depolymerization of the native polysaccharide, followed by a quantitative, non-regioselective sulfation, and they have shown to exhibit biological activities similar to heparin and other GAGs (Senni et al., **2015**, **2013**).

4.2. Results and Discussion

4.2.1. Regioselective Sulfation of Curdlan

In this section, the semi-synthetic strategies for the access to new curdlan derivatives with unprecedented and well-defined sulfation patterns are discussed. In particular, the possibility to employ a cyclic benzylidene protecting group for *O*-4,6 diols in suitably tailored multi-step sequences is investigated.

Since natural sulfated polysaccharides can cause adverse effects associated with high molecular weight sulfated species (Fonseca et al., **2010**), native curdlan — M_w estimated in the range 50–1000 kDa (Futatsuyama et al., **1999**) — was firstly subjected to a polymer chain shortening by partial acid hydrolysis under described conditions with 1 M $TFA_{(aq)}$ at 60 °C for 3 hours (Grandpierre et al., **2008**; Prieto et al., **2011**). After dialysis of the neutralized reaction mixture with a 3.5 kDa M_w cut-off and freeze-drying, a selective protection of diol at position 4 and 6 of Glc repeating unit was attempted by treating the obtained LMW-curdlan with α,α-dimethoxytoluene in the presence of CSA as acid catalyst (Scheme 4.2), to install a benzylidene cycle, analogously to our previous investigations on chondroitin polysaccharide (see also Chapter 2). Product **50-i** was collected by precipitation and then analysed by ^{1}H-NMR. The presence of aromatic signals at δ 7.60–7.10 ppm together with a broad peak centred at δ 5.49 ppm —the latter accounting for

a benzylidene acetal hydrogen atom— confirmed the presence of the desired protecting group on the polysaccharide (Figure 4.2) (Chien et al., **2019**). Nonetheless, DS could not be easily evaluated because integration of signals at δ 5.0–3.2 ppm relative to Glc repeating unit protons was precluded by a partial overlap with HDO signal at 3.31 ppm. For this reason, the benzylidenation reaction was reiterated under the same reaction conditions described above, to check whether the signals attributable to benzylidene ring and consequently DS could be increased or not. Unfortunately, the obtained product **50-ii** could not be analysed by NMR due to its very low solubility in DMSO-d_6.

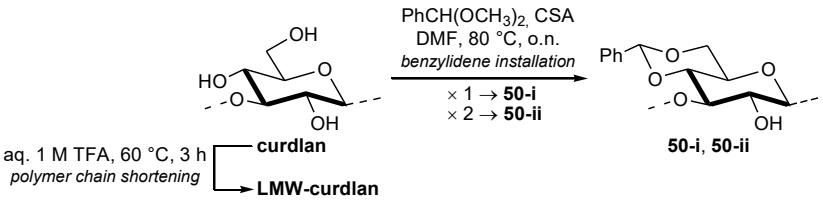

Scheme 4.2. Obtainment of 4,6-diol protected LMW-curdlan.

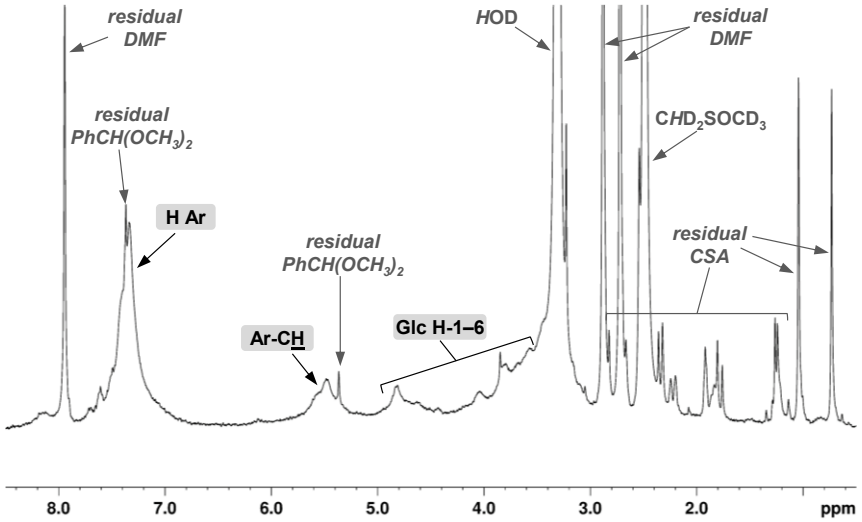

Figure 4.2. ^{1}H-NMR (400 MHz, 298K, DMSO-d_6) of derivative **50-i** (polysaccharide signal assignments are enclosed in rectangles).

Both derivatives **50-i** and **50-ii** were subjected to further reactions, the first one being a protection of the free hydroxyl at position *O*-2 of Glc units with an acetyl group. The reaction was performed with Ac_2O, Et_3N and DMAP to give fully protected derivatives **51-i** and **51-ii** (Scheme 4.3). Noteworthy, even if multi-protection steps are often performed on monosaccharides in a one-pot fashion (Kulkarni et al., **2018**; Traboni et al., **2016**, **2015**), here the benzylidenation and acetylation reactions were conducted independently in order to avoid the stabilization of any intra-glycosidic benzylidene acetal linkage (Laezza et al., **2014**) that could complicate the structure of **51-i,ii** and subsequent derivatives thereof.

The benzylidene ring installed on **51-i,ii** could be removed employing different kinds of reactions (hydrolytic or hydrogenolysis cleavage, reductive opening, and oxidative conditions), as extensively described in the previous chapters (see Paragraph 1.3.1.1). These diversified deprotection conditions can give access to curdlan derivatives with a different pattern of free alcohol moieties on which sulfate groups could be then installed regioselectively.

Firstly, the 4,6-diol reinstatement was attempted. Having discarded hydrogenolytic conditions for the toxicity and the high cost of the palladium catalyst, and for the difficulties related to the purification processes, we focused our attention on the hydrolysis reaction, which could be conducted with a cheaper and greener reagent such as an aqueous solution of acetic acid. Indeed, as described in Chapter 2 (see Paragraph 2.2.1.1), the relative reactivity of benzylidene rings installed on *galacto*-configured units with respect to glycosidic bonds under different hydrolytic conditions was already investigated by us for a chondroitin polysaccharide. By conducting the reaction in 9:1 *v/v* AcOH–H_2O at 50 °C for 48 hours, a high benzylidene cleavage degree could be obtained without a significant polysaccharide chain shortening. Since benzylidene rings on *gluco*-configured 4,6-diols are usually hydrolytically cleaved with a faster kinetics than

on *galacto*- ones (Maki et al., **2020**), **51-i,ii** were subjected to the same hydrolytic conditions indicated above (Scheme 4.3). After purification by a 3.5 kDa M_w cut-off dialysis, derivatives **52-i,ii** with only a negligible amount of residual benzylidene rings, as detected by the very low intensity of the typical benzylidene signals at δ 7.60–7.10 and 5.50 ppm in the ^{1}H-NMR spectrum (Figure 4.3), were obtained.

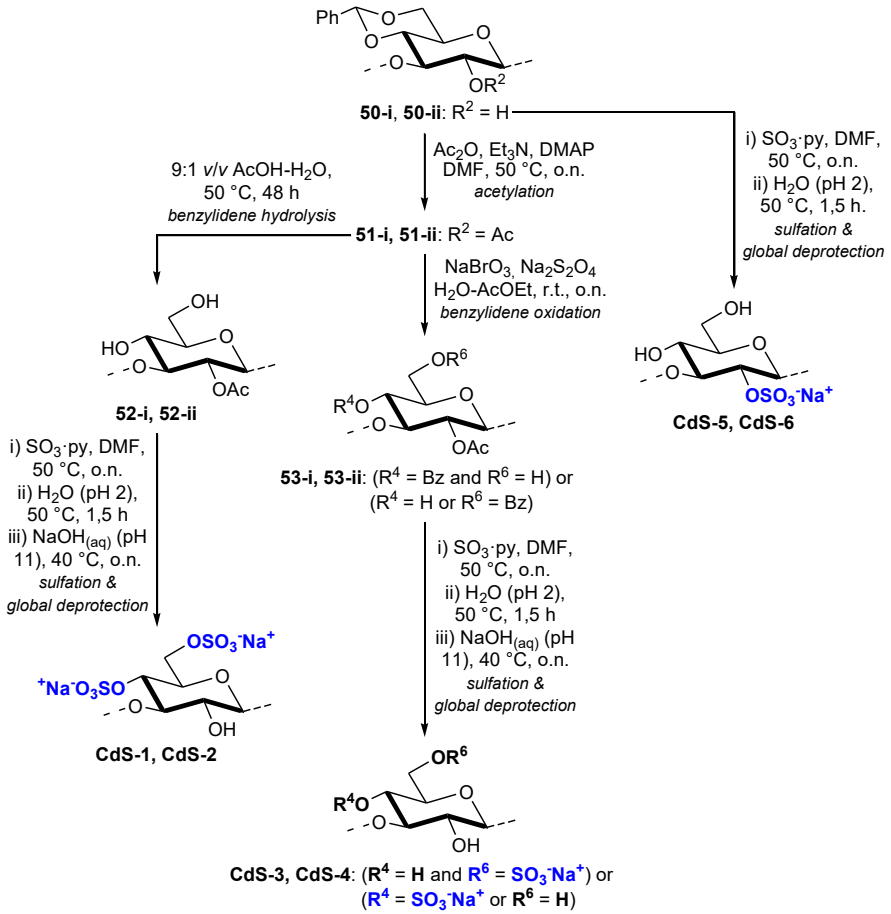

Scheme 4.3. Semi-synthesis of curdlan derivatives with different sulfate group distribution from a common benzylidene-protected derivative.

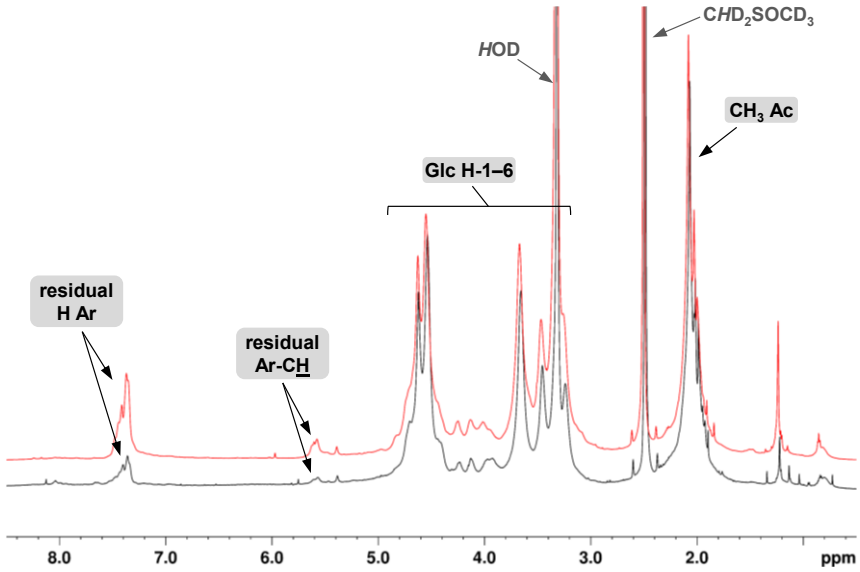

Figure 4.3. ^{1}H-NMR (400 MHz, 298 K, DMSO-d_6) of derivative **52-i** (black) and **52-ii** (red) (polysaccharide signal assignments are enclosed in rectangles).

Benzylidene rings on **51-i,ii** were cleaved also under oxidative conditions (Scheme 4.3), by treatment with sodium bromate and sodium dithionite in a biphasic water–ethyl acetate mixture (Adinolfi et al., **1999**). These reaction conditions should give the protection of one of the two hydroxyls as benzoate ester and the release of the alcohol at the complementary position. ^{1}H-NMR spectrum of products **53-i,ii**, collected as precipitates from the reaction mixtures, showed a negligible amount of residual benzylidene rings, as detected by the very low intensity of the typical PhC*H* acetal signal at 5.50 ppm (Figure 4.4). Moreover, the presence of signals between 8.10 and 7.10 ppm, typical of an aromatic ring with an electron-withdrawing substituent, confirmed the oxidative conversion of the benzylidene into a benzoate ester.

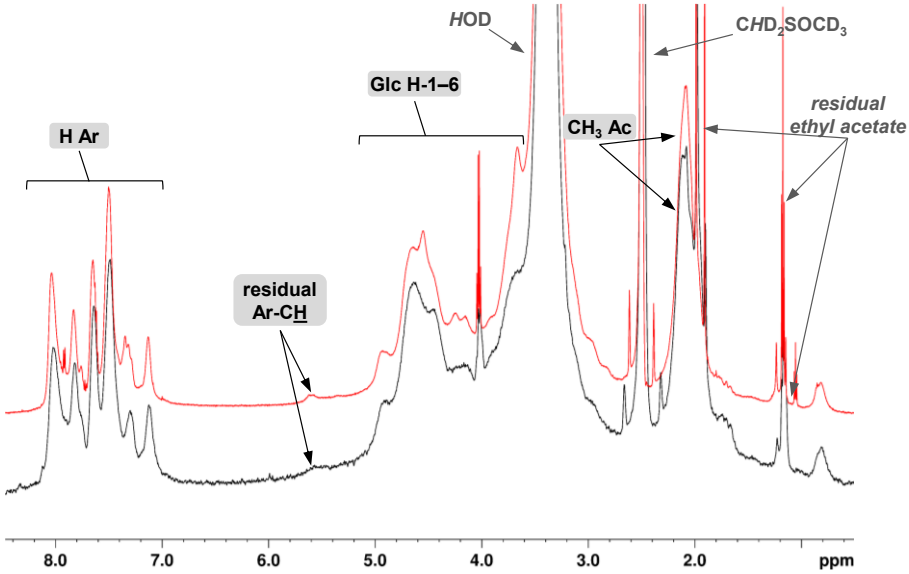

Figure 4.4. ^{1}H-NMR (400 MHz, 298 K, DMSO-d_6) of derivative **53-i** (black) and **53-ii** (red) (polysaccharide signal assignments are enclosed in rectangles).

Concerning benzylidene reductive opening on **51-i,ii**, this was judged less interesting and therefore not attempted. Indeed, the two curdlan sulfate polysaccharides, that could be obtained through semi-synthetic routes relying upon the two different regioselectivities for benzylidene reductive opening, display theoretically a sulfate group at position *O*-4 or *O*-6, respectively. Curdlan polysaccharides with such sulfation pattern have been already obtained, even if a strict sulfate groups regioselectivity was not observed (Scheme 4.1) (Gao et al., **1997**). Furthermore, benzylidene rings conversion into benzyl ethers under reductive conditions requires strictly anhydrous conditions that are not easily achievable for reactions on polysaccharides.

Partially protected derivatives **52-i,ii** and **53-i,ii** were subjected to exhaustive sulfation of the free hydroxyl moieties by treatment with SO_3·pyridine complex in DMF at 50 °C (Scheme 4.3). Then, a global deprotection, firstly under acid aqueous conditions to cleave residual benzylidene rings and then with alkali to

hydrolyse acetate esters, furnished curdlan derivatives **CdS-1,2** and **CdS-3,4** with sulfate groups expected at both or mutually excluded *C*-4 and *C*-6 positions, respectively. The sulfation/deprotection sequence was applied also on benzylidene-protected derivatives **50-i,ii**, skipping the alkaline hydrolysis step, since no acetyl protecting groups were previously installed on the polysaccharide chain. In this case an exclusive sulfation at *C*-2 position of Glc repeating unit was expected for the obtained polysaccharides **CdS-5,6**. Global mass yields, calculated over the whole semi-synthetic sequence from native curdlan to **CS-1,6**, were in the range 37–69% (Table 4.1).

The presence of sulfate groups on the polysaccharide chain of **CdS-1-6** was confirmed by FT-IR measurements: their spectra displayed typical bands at 1204–1219 and 800–808 cm^{-1}, accounting for asymmetric S=O and symmetric C–O–S stretching vibrations, respectively (Jin et al., **2020**), there were not detected in the spectrum of native curdlan (see Figure 4.21–4.23 in Paragraph 4.4.2).

The postulated sulfation patterns for **CdS-1-6** were, then, investigated by ^{1}H- and 2D-NMR analysis. Polysaccharide **CdS-3** was examined first. Its $^{1}H,^{13}C$-DEPT-HSQC spectrum (Figure 4.5B) clearly showed three methylene signals associated to CH_2 atoms at position 6 ($\delta_{H/C}$ 3.94,3.76/62.0, 4.36,4.24/68.4 and 4.57,4.16/68.9 ppm, respectively), thus suggesting the presence of at least three different Glc units within the polysaccharide backbone. Two of them displayed a sulfate group at position 6, as inferred by the downfield shift for both ^{1}H and ^{13}C values. In particular, COSY and TOCSY (Figure 4.25A in Paragraph 4.4.5) cross-peaks analysis revealed that the more intense one ($\delta_{H/C}$ 4.36,4.24/68.4 ppm) is associated to 6-sulfated Glc (Glc6S) units, while the other one ($\delta_{H/C}$ 4.57,4.16/68.9 ppm) is related to 4,6-disulfated Glc (Glc4,6S) residues. Furthermore, non-shifted methylene signals at $\delta_{H/C}$ 3.94,3.76/62.0 ppm could be assigned to 4-sulfated Glc (Glc4S) and unsulfated residues. The former was confirmed by the presence in the $^{1}H,^{13}C$-DEPT-HSQC spectrum of a rather intense signal assigned by COSY and

TOCSY analysis to sulfated *CH*-4 of both Glc4S and minor Glc4,6S. Its remarkable ^{1}H and ^{13}C downfield shift ($\delta_{H/C}$ 4.25/75.9 ppm) with respect to chemical shift values for *CH*-4 Glc units in native curdlan ($\delta_{H/C}$ 3.54/69.3 ppm) (Petersen et al., **2000**) clearly indicated that such signal accounted for 4-*O*-sulfation. Finally, the presence of unsulfated Glc residues was demonstrated by the *CH*-5 signal at $\delta_{H/C}$ 3.52/77.0 ppm in the $^{1}H,^{13}C$-DEPT-HSQC spectrum. Such chemical shift values are in close agreement with literature data for native curdlan (Petersen et al., **2000**). Moreover, they cannot be ascribed to any other *CH*-5 of 4- and/or 6-sulfated Glc residues, for which a ^{1}H-downfield and ^{13}C-upfield shift — typical of a sulfate group placed at an adjacent site (Yates et al., **1996**)— was expected (see Table 4.4 in Paragraph 4.4.2 for full assignment of chemical shifts values for **CdS-3**). The relative integration of the three methylene signal volumes assigned in the $^{1}H,^{13}C$-DEPT-HSQC spectrum to Glc4,6S, Glc6S and Glc4S/Glc units, respectively, was estimated to be 3%, 43% and 54%, assuming that they displayed similar $^{1}J_{C,H}$ coupling constants and that a difference of around 5−8 Hz from the experimental set value did not cause in any case a substantial variation of the integrated peak volumes (Gargiulo et al., **2009**; Guerrini et al., **2005**). Moreover, a 4-sulfated *vs.* 4-unsulfated Glc ratio could be estimated by relative integration of the Glc CH-4 signal at $\delta_{H/C}$ 4.25/75.9 ppm relative to Glc4S and Glc4,6S residues, with respect to *CH*-4 signal of Glc and Glc6S units at $\delta_{H/C}$ 3.54/69.3 ppm (Figure 4.5B). Taking together the integration data, it could be concluded that **CdS-3** displayed, as expected, Glc4S and Glc6S as major monosaccharide units along the polysaccharide chain, even if a not negligible amount of unsulfated Glc residues could also be detected (Table 4.1). Notably, the DS value (0.81) in **CdS-3**, as estimated from the relative amount of sulfated and unsulfated Glc units by NMR integration data, was quite close to the value (0.84) measured by elemental analysis (Table 4.1), thus validating the assignments and the integrations made on the $^{1}H,^{13}C$-DEPT-HSQC spectrum.

Signal assignments, degree of substitution and relative amount estimation of differently sulfated Glc subunits within the polysaccharide backbone could be similarly done for **CdS-4** (Table 4.1, Table 4.4 and Figure 4.24A in Paragraph 4.4.2 for full assignment of chemical shifts values and $^{1}H,^{13}C$-DEPT-HSQC of **CdS-4**, respectively). Noteworthy, a lower amount of unsulfated Glc residues was detected with respect to **CdS-3**. This is in agreement with a more extensive benzylidene protection in **50-ii** with respect to **50-i**, as the former was obtained after two instead of only one benzylidenation cycle on LMW-curdlan. Indeed, a less extensive protection of 4,6-positions with benzylidene rings along the polysaccharide backbone implied a higher amount of acetate esters – installed in the subsequent step – protecting such sites. Since the latter served as permanent protecting groups in the semi-synthetic scheme, they were removed only at the end of the sequence, thus leaving a higher amount of Glc units unsulfated in **CdS-3** with respect to **CdS-4**. Surprisingly, the lower amount of unsulfated Glc residues in **CdS-4** did not cause an increased amount of the expected Glc4S and Glc6S residues, whereas a marked enhancement of Glc4,6S subunits was detected. Our hypothesis is that this unexpected behaviour could be ascribed to a hydrolytic mechanism catalysed by HBrO (generated from $Na_2S_2O_3$ and $NaBrO_3$) (Kikuchi et al., **1998**) that competes with the expected oxidative cleavage of the benzylidene rings (**51-i,ii→53-i,ii**, Scheme 4.3), when the substrate becomes more hydrophilic and therefore can better interact with a polar, hydrosoluble species such as HBrO. Actually, an increased hydrophilicity is expected for the polysaccharide at the late stage of the reaction, when a high number of polar alcohol functionalities has been already restored, and in particular for the reaction starting from **51-ii** rather than **51-i**, as the former should carry more benzylidene rings along the backbone.

Table 4.1. Yields, DS and relative amount of differently sulfated Glc units for **CdS-1–6**.

	Yield[a]	**2-sulfated *vs.* 2-unsulfated Glc**	**4-sulfated *vs.* 4-unsulfated Glc**	**6-sulfated *vs.* 6-unsulfated Glc**	**DS** [b, c]
CdS-1	40%	0:100	78:22 Glc4,6S: 58%; Glc4S: 20%; Glc 14%; Glc6S 8%	66:34	1.20,1.44
CdS-2	69%	0:100	76:24 Glc4,6S: 52%; Glc4S: 24%; Glc: 15%; Glc6S: 9%	61:39	1.14, 1.37
CdS-3	48%	0:100	35:65 Glc6S: 43%; Glc4S: 32%; Glc: 22%; Glc4,6S: 3%	46:54	0.84, 0.81
CdS-4	50%	0:100	53:47 Glc6S: 38%; Glc4,6S: 31%; Glc4S: 22%; Glc: 9%	69:31	1.33, 1.22
CdS-5	46%	46:54	12:88	53:47	1.24, 1.11
CdS-6	37%	49:51	0:100	16:84	0.47, 0.65

[a] Overall mass yield calculated from native curdlan. [b] The first values for each sample are derived by elemental analysis (see Paragraph 4.4.2 for details). [c] The second values for each sample are calculated from the relative amount of differently sulfated Glc units — as estimated by 2D-NMR integration and reported in the third to fifth column – according to equation 4.1:

$$DS = \%2\text{-sulfated} + \%4\text{-sulfated} + \%6\text{-sulfated} \quad \text{(Eq. 4.1)}$$

Structural determination of polysaccharides **CdS-1**,**2** could be made on the basis of the assignments previously done on **CdS-3** (Figure 4.5A). As expected from the semi-synthetic pathway relying upon hydrolytic cleavage of the benzylidene ring to restore the 4,6-diol, the most abundant Glc units within the polysaccharide were characterized by a 4,6-disulfation pattern (Table 4.1). A negligible variation of differently sulfated Glc units were detected between **CdS-1** and **CdS-2**.

Finally, the analysis of a set of 2D-NMR (COSY, TOCSY, ^{1}H,^{13}C-DEPT-HSQC) spectra allowed the structural characterization of **CdS-5** and **CdS-6**. In particular, COSY (Figure 4.25B in Paragraph 4.4.2) cross-peaks analysis revealed that the most ^{1}H-downfield/^{13}C-upfield shifted anomeric signals in the ^{1}H,^{13}C-DEPT-

HSQC spectrum ($\delta_{H/C}$ 5.23–5.04/101.6–98.6 ppm, Figure 4.5C) correlate with strongly $^{1}H,^{13}C$-downfield shifted signals at $\delta_{H/C}$ 4.46/81.7 and 4.27/79.9 ppm, accounting for *O*-sulfated *CH*-2 positions. Instead, the most ^{1}H-upfield/^{13}C-downfield shifted anomeric signals ($\delta_{H/C}$ 4.89–4.67/104.3–102.8 ppm) could be assigned to Glc units not showing sulfation at *O*-2-sites, as their corresponding CH atoms resonate at chemical shift values typical for *CH*-2 Glc units in native curdlan ($\delta_{H/C}$ 3.81–3.57/74.4 ppm) (Petersen et al., **2000**). A relative integration of such anomeric signal groups in the $^{1}H,^{13}C$-DEPT-HSQC estimated 46:54 and 49:51 ratios for 2-sulfated *vs*. 2-unsulfated Glc units in **CdS-5** and **CdS-6**, respectively (Table 4.1). Regarding the eventual presence of sulfate groups at other Glc positions, the assignments previously done on **CdS-3** indicated that **CdS-5** displayed some additional sulfate groups at 4- or 6-position (but not in the same residue as 4,6-disulfated Glc signals were not detected). Their relevance could be evaluated by the relative integration of 4-sulfated *vs.* 4-unsulfated *CH*-4 signals at $\delta_{H/C}$ 4.25/75.9 and 3.76–3.54/69.7–69.0 ppm and of 6-sulfated *vs.* 6-unsulfated CH_2-6 signals at $\delta_{H/C}$ 4.46–4.21/69.3–68.4 ppm and 3.94,3.76/62.0 ppm in the $^{1}H,^{13}C$-DEPT-HSQC spectrum. Ratio estimations for 6-sulfated *vs.* 6-unsulfated Glc residues in **CdS-5** and **CdS-6** were 53:47 and 16:84, respectively, while only in derivative **CdS-5** some 4-sulfated Glc units could be detected, in a 12:88 ratio with respect to 4-unsulfated ones. Taking together the integration data for **CdS-5** and **CdS-6**, it could be concluded that the latter displayed sulfate groups almost exclusively at *O*-2 position, with a similar amount of Glc and Glc2S units distributed along the polysaccharide together with a much lower amount of Glc2,6S and/or Glc6S residues, while a more heterogeneous sulfate distribution was shown by **CdS-5**. The DS decrease in **CdS-6** with respect to **CdS-5** is in agreement with a higher degree of benzylidene protection in **50-ii** rather than in **50-i**, as already described above for **CdS-4** *vs.* **CdS-3** structure comparison.

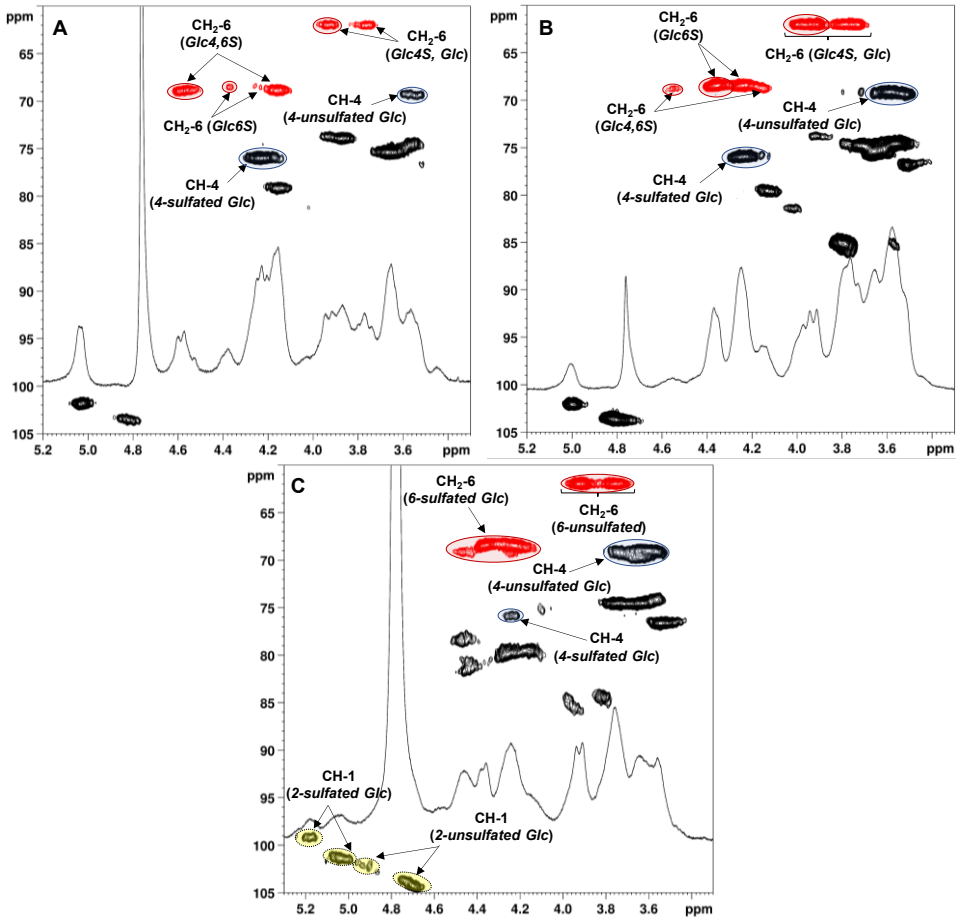

Figure 4.5. $^{1}H,^{13}C$-DEPT-HSQC and ^{1}H-NMR spectra (400 MHz, 298K, D_2O) of (A) **CdS-1**, (B) **CdS-3**, (C) **CdS-5** (densities enclosed in the highlighted areas were integrated for estimation of relative amounts of differently sulfated Glc units).

Finally, an evaluation of the molecular weight distribution of semi-synthetic **CdS-1–5** was also performed by high-performance size-exclusion chromatography combined with a triple detector array (HP-SEC-TDA) (see Table 4.2).

Table 4.2. Hydrodynamic parameters for polysaccharides **CdS-1–5** (very large aggregates accounting for less than 5% on refractive index quantification were not considered reliable on the analysis and thus they were not inserted in the table).

	M_w[a] (kDa)	M_n[b] (kDa)	M_w/M_n	[η] (dL/g)	R_h (nm)	Representativity (%)
CdS-1	393.5	224.6	1.752	0.783	15.64	80.24
	222.2	221.8	1.002	0.298	10.02	14.99
CdS-2	301.9	231.5	1.304	0.903	15.27	100
CdS-3	54.5	38.8	1.406	0.705	8.02	87.73
	31.0	30.2	1.026	0.442	5.99	12.27
CdS-4	73.5	62.9	1.168	0.774	9.44	80.40
	46.1	44.2	1.042	0.177	4.95	13.30
CdS-5	112.0	56.7	1.974	0.184	6.32	92.20
	67.1	57.3	1.172	0.065	4.04	7.80

[a] M_w: weight averaged molecular mass; [b] M_n: number-averaged molecular mass

All the tested samples, except for **CdS-2**, displayed a multimodal distribution (Table 4.2), evidencing a significant polydispersion of the polysaccharides. This could be due to the presence of different molecular weight polysaccharide fractions and/or aggregates. As for intrinsic viscosity ([η]) data, all the samples presented values lower than the ones reported for natural polyanionic biopolymers of similar molecular weight. For example, CS species of 32–52 kDa displayed a [η] of 0.77–1.49 dL/g (Restaino et al., **2017**), whereas HA polysaccharides ranging between 200 and 500 kDa had a [η] of 3.9–6.7 dL/g (La Gatta et al., **2016**). The different correlation between the intrinsic viscosity and the molecular weight values for the semi-synthetic CdS derivatives with respect to these other biopolymers (Table 4.2) was well evidenced by the Mark-Houwink-Sakurada curves (log[η] *vs.* logM_w) for the larger and smaller CdS polysaccharides (**CdS-1** and **CdS-3**, respectively). Both curves were considerably below the correlation curve for a 35-kDa sample of CS (see Figure 4.20 in Paragraph 4.4.2), suggesting

a different and more compact conformation in water for CdS polysaccharides, hypothetically caused by aggregate formation. However, the dimension of the aggregates seems to be dependent on sulfate groups amount and distribution on the polysaccharide chain, as highlighted by the similar M_w data for **CdS-1** and **CdS-2** (both enriched in 4,6-disulfated units, see Table 4.1), that were much higher with respect to **CdS-3–5**, all possessing a single sulfate group in the most abundant residues along the polysaccharide backbone. The same behaviour could be observed for hydrodynamic radius (R_h) data, which depend on dimension and charge. Nevertheless, a more detailed investigation of CdS hydrodynamic properties and their correlation with the proposed structures is mandatory. It is scheduled for the near future and will be reported elsewhere.

4.2.2. Regioselective Sulfation of M-rich Alginic Acid

In this section, multi-step procedures for regioselective sulfation of alginates are discussed and the possibility to install cyclic protecting groups on 2,3-diols of commercially available M-rich alginic acid (M = 85%, G = 15%) is investigated. The semi-synthetic strategy involves also a regioselective opening of the cyclic group leading to polysaccharide derivatives protected exclusively at *O*-2 or *O*-3 and with a free alcohol restored at the complementary position (Scheme 4.4). Then, sulfation and deprotection of such semi-synthetic intermediates will give alginate sulfate polysaccharides theoretically with a high control of their sulfation pattern.

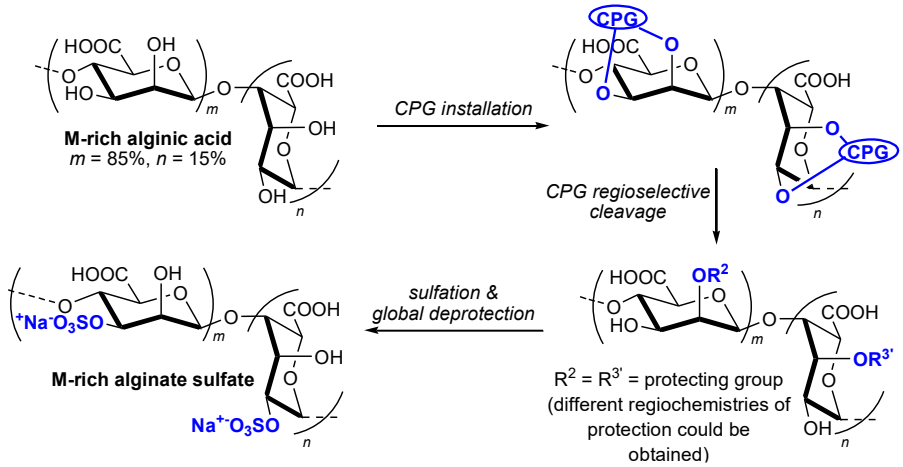

Scheme 4.4. General strategy for regioselective sulfation of alginic acid with regioselective cleavage of a cyclic protecting group (CPG) as key step.

Among the several different cyclic protecting groups, cyclic acetals and orthoesters are often employed for protection of vicinal *cis*-diols, such as *O*-2,3 diol of ManA and GulA units. For our purposes, a benzylidene ring was selected as a representative to be tested for the former category, while orthobenzoate for the latter. The choice was due, in both cases, to the possibility to regioselectively open such cyclic groups under appropriate conditions, as planned in the general strategy. Indeed, the oxidative opening of benzylidene five-membered rings installed on 1,2-*cis*-diol of pyranosides (mono- or oligosaccharides) restores a free alcohol moiety on the equatorial position of the diol, while the axial site results protected with a benzoyl group (Adinolfi et al., **1999**). Analogously, cyclic orthoesters installed on 1,2-*cis*-diol of pyranosides could be subjected to an acid-mediate rearrangement, liberating a free hydroxyl on the equatorial position, while leaving the axial oxygen atom protected with an acyl group (Mukhopadhyay and Field, **2003**).

Hence, the selected cyclic protecting groups were installed on M-rich alginic acid under conditions commonly employed for mono- and oligosaccharides and previously optimized for an unsulfated chondroitin polysaccharide (Bedini et al.,

2012, **2011**). Thus, commercial alginic acid was firstly treated with trimethyl ortobenzoate in DMF with CSA as catalyst. Because of the high lability of cyclic orthoester groups, derivative **54** was not isolated, on the contrary it was reacted one-pot with aqueous acetic acid to open the orthoester ring and furnish derivative **55-i**. This should carry a benzoyl group at axial positions of ManA and GulA units — *i.e. O*-2 position of ManA and *O*-3 site of GulA — and a free hydroxyl at the complementary, equatorial positions (Scheme 4.5).

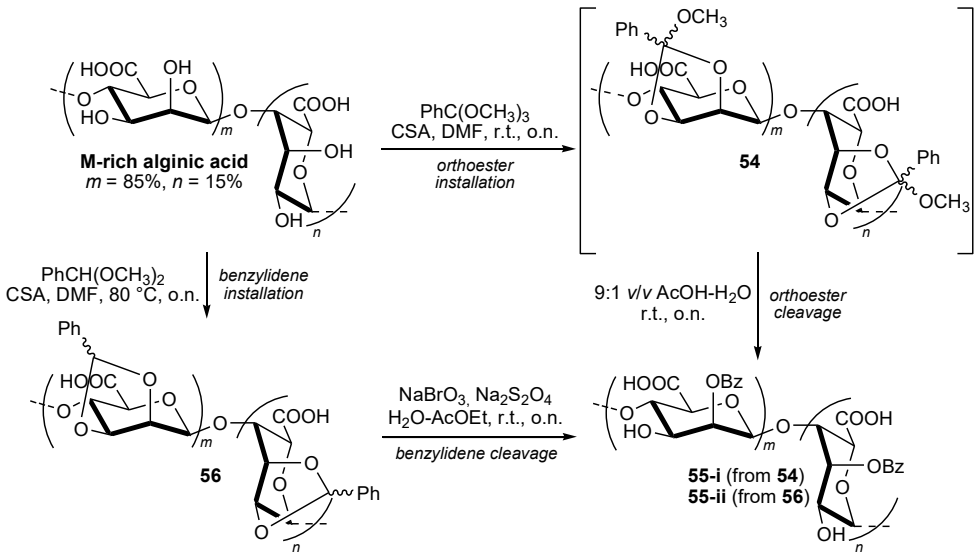

Scheme 4.5. Installation and regioselective cleavage of benzylidene or orthoester CPGs on alginic acid.

By ^{1}H-NMR analysis of derivative **55-i**, the presence of benzoate esters was confirmed; indeed, its spectrum shows typical signals related to aromatic hydrogen atoms (δ 8.20–7.10 ppm) together with signals at δ 5.30–5.75 ppm assignable to ring protons downfield shifted by a with-drawing group such as the benzoyl one (Figure 4.6). However, due to HDO signal overlapping with pyranoside ring atoms, the degree of ester substitution could be not evaluated. Thus, hypothetically assuming a non-quantitative ester substitution, one-pot

orthoester installation and cleavage reactions were repeated on **55-i**, so forcing the insertion of an ester protecting group at the axial position of not reacted *O*-2,3-diols. Nonetheless, no significant differences were detected by comparison between ^{1}H-NMR spectra after one and two orthoester installation/cleavage sequences (Figure 4.6). This could be explained with a very high degree of substitution already achieved after a single one-pot sequence or, alternatively, with the existence along the polysaccharide chain of a certain amount of monosaccharide units recalcitrant to react under the employed reaction conditions.

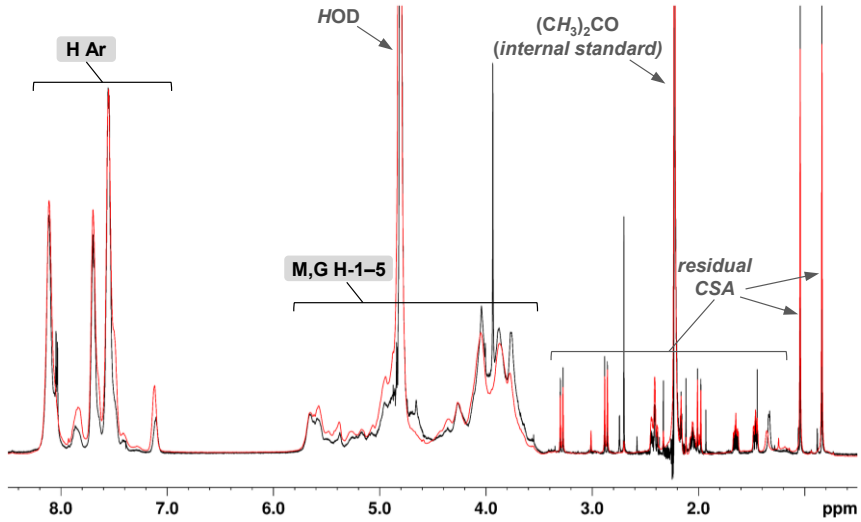

Figure 4.6. ^{1}H-NMR spectrum (600 MHz, D_2O, 298 K) of derivative **55-i** after one (black trace) or two (red trace) orthoester installation/cleavage one-pot sequences (polysaccharide signal assignments are enclosed in rectangles).

A benzylidene ring was also installed on M-rich alginic acid by a reaction conducted twice with α,α-dimethoxytoluene in DMF in the presence of CSA as acid catalyst. Differently from orthoester groups, benzylidene rings are usually stable enough to be isolated and structurally characterized. So, derivative **56**, isolated by precipitation from the reaction mixture, was subjected to 2D-NMR analysis. In its DEPT-HSQC spectrum (Figure 4.7), the presence of four different

acetal signals, at δ_C between 95 and 105 ppm, could be detected. Among them, the most downfield shifted ones at δ_H 5.77 and 6.07 ppm, together with the densities at $\delta_{H/C}$ 7.3–7.6/126–129 ppm attributable to aromatic CH atoms, demonstrated the formation of benzylidene rings on alginic acid. The integral ratio between the two benzylidene acetal CH densities, estimated as 5.1:1, closely resembles the 85:15 M/G ratio of starting alginic acid, thus suggesting that the reaction occurred in a similar way on both M and G units, although the possibility that the two signals were instead related to two different configurations of the five-membered benzylidene ring — with the phenyl group placed in an *endo*- or *exo*-position — cannot be ruled out. In addition to that, the ratio between the sum of integral values for benzylidene acetal densities and for anomeric ones gave a value very close to 1 (1.04), thus suggesting a nearly quantitative degree of benzylidene installation.

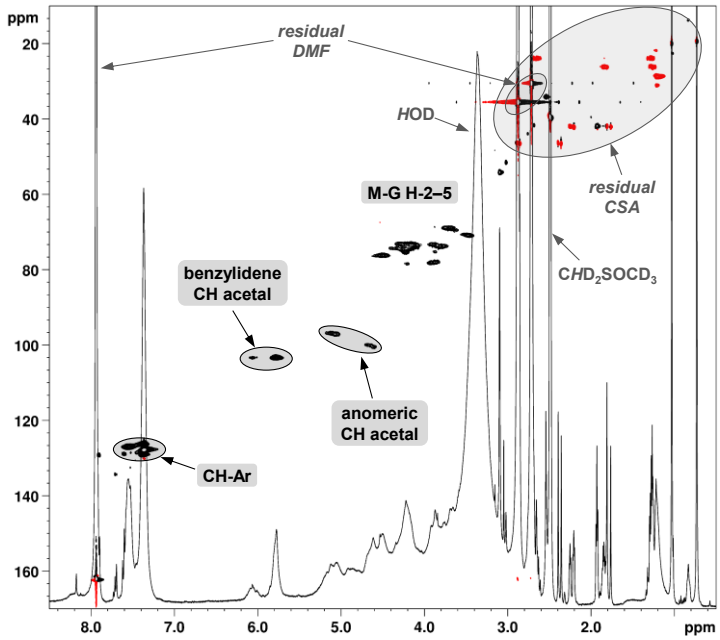

Figure 4.7. $^{1}H,^{13}C$-DEPT-HSQC and ^{1}H NMR spectra (400 MHz, 298 K, DMSO-d_6) of derivative **56** (polysaccharide signals assignments are enclosed in rectangles).

Then, product **56** was submitted to the oxidative opening of benzylidene rings with $NaBrO_3$ and $Na_2S_2O_4$ in water–ethyl acetate biphasic mixture to gain derivative **55-ii**, whose ^{1}H-NMR spectrum was quite comparable to those obtained after the orthoester installation/cleavage sequence (see Figure 4.26 in Paragraph 4.4.3).

Hence, derivatives **55-i** and **55-ii** were both subjected to sulfation with SO_3·py complex in DMF at 50 °C, followed by a global deprotection under aqueous alkaline conditions to remove benzoate esters, affording the semi-synthetic sulfated alginate derivatives, **AS-1,2** (Scheme 4.6). Moreover, with the aim to ease the structural study of these sulfated products, a persulfated derivative was also obtained by subjecting M-rich alginic acid to a direct sulfation under the same conditions employed on **55-i** and **55-ii**.

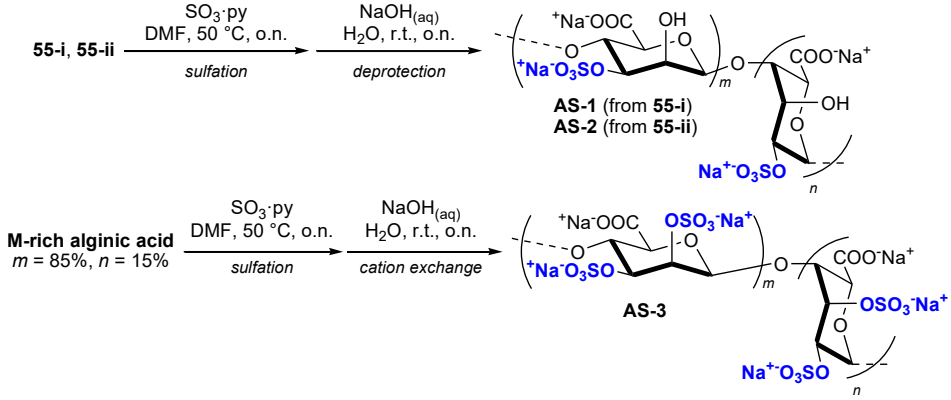

Scheme 4.6. Semi-synthesis of sulfated alginates **AS-1–3**.

Structural characterization of sulfated polysaccharides **AS-1**–**3** was performed with a combination of 1D- and 2D-NMR techniques. First of all, their ^{13}C-NMR spectra were compared with that obtained from starting M-rich alginate, observing a significant difference between the latter and the semi-synthetic sulfated polysaccharides as regards the chemical shifts of ring carbon atoms of ManA and GulA units (Figure 4.8). ^{13}C-NMR signals of both unsulfated and persulfated M-

rich alginate spectra were in full agreement with assignments already reported in literature (Coleman et al., **2011**; Cong et al., **2014**). Remarkably, **AS-1** and **AS-2** showed a slightly different pattern of ^{13}C-NMR signals.

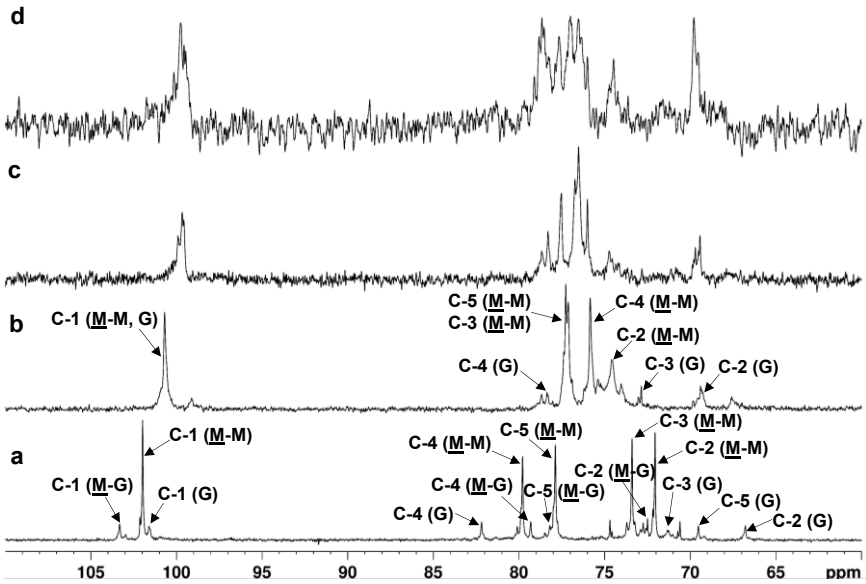

Figure 4.8. Zoom of ^{13}C- NMR spectra (100 MHz, 298 K, D_2O) of: (a) M-rich alginate, (b) **AS-3**, (c) **AS-2**, (d) **AS-1**.

^{1}H,^{13}C-HSQC spectra of **AS-1**–**3** and unsulfated alginate were also measured, focusing their analysis on the most intense densities, related to ManA units, the most abundant on a M-rich alginic acid and its sulfated derivatives. Spectra of both the native polysaccharide and **AS-3** showed five main signals (Figure 4.9), as expected for an unsulfated or persulfated M-rich alginic acid, respectively. Their assignment was performed by comparison with literature data (Coleman et al., **2011**; Cong et al., **2014**) and also with the aid of COSY, NOESY and HMBC 2D-NMR spectra.

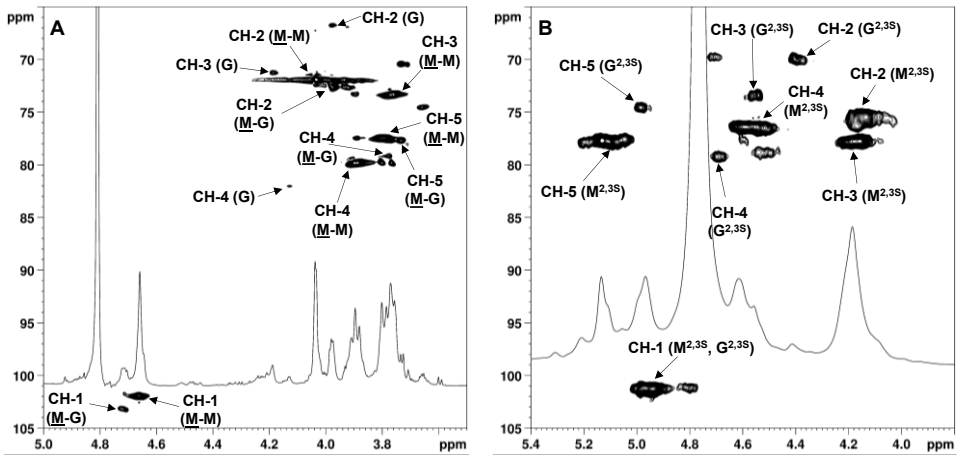

Figure 4.9. $^{1}H,^{13}C$-HSQC and ^{1}H NMR spectra (600 MHz, 298 K, D_2O) of (A) M-rich alginate, (B) **AS-3**.

On the contrary, a much higher number of densities, with a comparable intensity, could be observed in **AS-1** and **AS-2** $^{1}H,^{13}C$-HSQC spectra, thus preventing a precise assignment of all the signals. Despite that, their superimposition with M-rich alginate and **AS-3** $^{1}H,^{13}C$-HSQC spectra (see Figure 4.10 and Figures 4.27, 4.28A in Paragraph 4.4.3) revealed that neither unsulfated nor 2,3-disulfated ManA units could be detected, as clearly evinced, for example, by the absence in the spectrum of **AS-2** of any signal at $\delta_{H/C}$ 4.65–4.70/102.5 and 4.90–5.00/100.8 ppm, previously attributed to anomeric CH atoms of ManA residues in native and persulfated alginic acid, respectively. This demonstrated that the two semi-synthetic sulfated alginate polysaccharides, possessed a non-exhaustive sulfation at *O*-2,3 positions of M units, although the two employed multi-step strategies did not allow a regiocontrol in sulfation pattern.

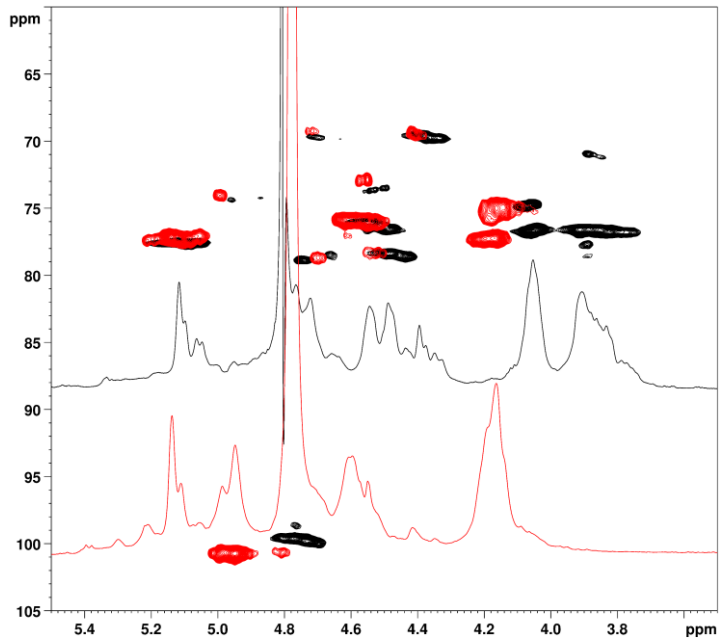

Figure 4.10. $^{1}H,^{13}C$-HSQC and ^{1}H NMR spectra (600 MHz, 298 K, D_2O) of **AS-2** (black) and **AS-3** (red).

To further pursue this aim, a different strategy, based on a three-steps, one-pot sequence for regioselective protection of the polysaccharide, was then tested. This strategy, already developed for chondroitin (see also Chapter 2, Paragraph 2.2.1.2), involves the installation of a cyclic protecting group linking together carboxylic acid and *OH*-3 moieties of ManA units through a 3,6-lactone ring (Elferink et al., **2019**). It is worth noting that the *trans* arrangement of the same groups in GulA residues should prevent the lactone formation, thus ensuring not only an intra-residue (*OH*-3 *vs. OH*-2) but also an inter-residue (M *vs.* G) selectivity. Interestingly, the intra-residue lactonization of alginic acid has been already accomplished through a thermal dehydration under vacuum, though very low substitution degree values (not higher than 0.15) were attained (Anson et al., **2009**). For our purposes, the lactonization reaction was instead performed with Bz_2O in DMF at 85 °C (Kornilov et al., **2001**), then the subsequent one-pot

addition of DMAP and pyridine allowed the protection of the unreacted hydroxyls as benzoate esters and, with the final addition of NaOAc and methanol, the labile lactone was selectively cleaved, thus restoring an alcohol moiety exclusively at position 3 of ManA units (Scheme 4.7). The obtained derivative **58**, recovered by precipitation from the reaction mixture, could not be subjected to NMR analysis since it was insoluble in any deuterated solvent. Therefore, it was directly subjected to sulfation and deprotection under the same reaction conditions already employed for the obtainment of **AS-1-3**.

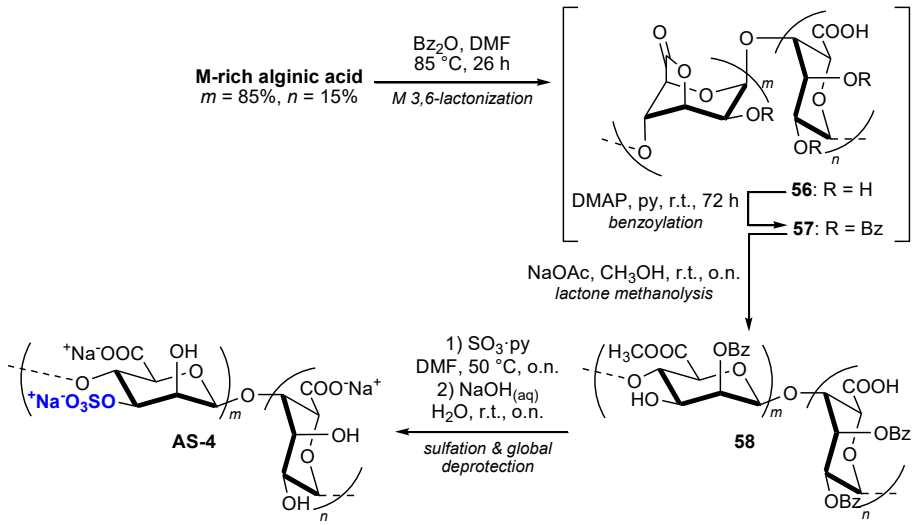

Scheme 4.7. Semi-synthesis of sulfated alginate **AS-4**.

The postulated sulfation pattern for **AS-4** was preliminary studied by ^{13}C-NMR analysis, comparing its ^{13}C-NMR spectrum with those obtained for M-rich alginate and its persulfated derivative (**AS-3**). A different profile in the chemical shift of the ring carbon atoms of M and G units could be easily evidenced between **AS-4** and both M-rich alginate and **AS-3** spectra (Figure 4.11). In particular, in **AS-4** ^{13}C-NMR spectrum the main ring carbon signals are shifted in the region between 76.5–78.2 ppm, with an evident downfield shift of the *C*-3 resonance

with respect to its position in the native polysaccharide, hypothetically due to the expected sulfation, and a concomitant upfield shift of the *C*-4 signal, typical of a sulfate group placed at an adjacent site (Yates et al., **1996**). Moreover, the presence of the signal at 70.1 ppm could be ascribed to non-sulfated *C*-2 positions, adjacent to sulfated *C*-3. This experimental evidence suggested that **AS-4** should possess a non-exhaustive sulfation at *O*-2,3 positions, even though a clear ^{13}C-NMR signal assignment could not be accomplished.

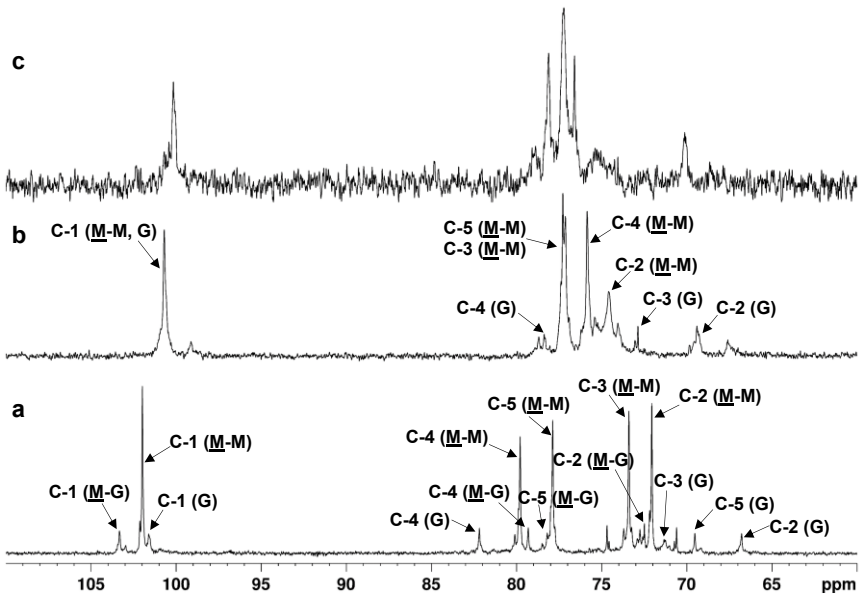

Figure 4.11. Zoom of ^{13}C- NMR spectra (100 MHz, 298 K, D_2O) of: (a) M-rich alginate, (b) **AS-3**, (c) **AS-4**.

To further investigate **AS-4** structure, its ^{1}H,^{13}C-HSQC spectrum was measured (Figure 4.12 and Figure 4.28B in Paragraph 4.4.3); the spectrum showed five main signals, as for native and persulfated alginate, though several satellite peaks for each signal could be noticed. This could be ascribed both to the small percentage of GulA units along the polysaccharide chain and to differently sulfated monosaccharide units, probable due to a non-regioselective protection strategy.

However, a clear assignment of all the densities was not possible, neither by the aid of a set of 2D spectra, including COSY, NOESY and $^{1}H,^{13}C$-HMBC. The implementation of more specific and advanced NMR techniques would be required for a clear assessment of the sulfation regiochemistry in **AS-4**.

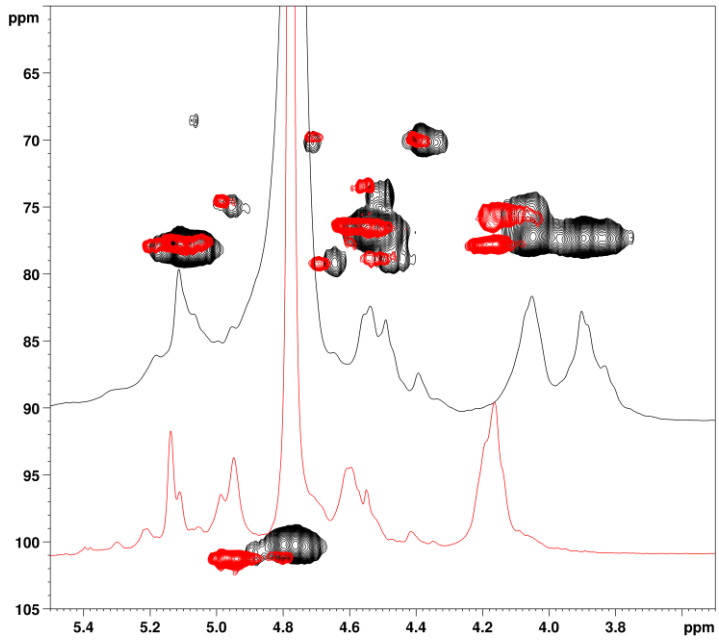

Figure 4.12. $^{1}H,^{13}C$-HSQC and ^{1}H NMR spectra (600 MHz, 298 K, D_2O) of **AS-4** (black) and **AS-3** (red).

Finally, the sulfur content in the semi-synthetic sulfated derivatives, **AS-2**, **AS-3** and **AS-4**, was estimated by elemental analysis, performed in collaboration with Dr. Valentina Gargiulo from *Istituto di Scienze e Tecnologie per l'Energia e la Mobilità Sostenibili* of the Italian National Research Council (CNR-STEMS). The obtained DS values, designed as the average number of sulfate groups per monosaccharide repeating unit, were 1.55, 1.81 and 1.75 for **AS-2**, **AS-3** and **AS-4**, respectively. The data shown by **AS-2** and **AS-4** evidenced a heterogenous sulfation pattern on the polymer chain, even with the presence of disulfated

repeating units counting for a value higher than 1, as instead should be expected for a mono-sulfation. These results suggested, in accordance with the NMR data, that the implemented multi-step strategies did not allow a complete regiocontrol in sulfation pattern. However, both approaches seemed to be promising pathway that have to be optimized once results will be confirmed by further analyses.

4.2.3. Regioselective Sulfation of HE800 EPS from *Vibrio diabolicus*

In this section, the semi-synthetic strategies to obtain regioselectively sulfated GAG-like polysaccharides from a marine-sourced bacterial EPS are examined. The high availability of polysaccharide-producing microorganisms has made bacterial EPSs suitable candidates to produce artificially sulfated polysaccharides, in order to obtain new biomaterials with novel or enhanced biological properties. Furthermore, the regioselective chemical sulfation of such biopolymers could open the way to structure-activity relationship studies aimed to investigate the importance of the sulfate group distribution in determining the diverse biological activities.

We focused our attention on the regioselective sulfation of HE800 EPS, naturally produced under controlled conditions by fermentation of the non-pathogenic marine bacteria, *Vibrio diabolicus* (Raguénès et al., **1997**), and furnished by Dr. Agata Zykwinska group from the Biotechnology and Marine Resources Research Unit of *Institut Français de Recherche pour l'Exploitation de la Mer* (IFREMER). Before any chemical manipulation, the native high-molecular-weight HE800 EPS was subjected by Dr. Zykwinska and co-workers to a free-radical depolymerization step to obtain a low-molecular-weight species (LMW-HE800 EPS) (Senni et al., **2015**).

Our efforts have been focused on the research of appropriate regioselective synthetic procedures to access the sulfation patterns depicted in Figure 4.13, to

obtain differently sulfated HE800 EPS species to be subjected to future physico-chemical and biological assays.

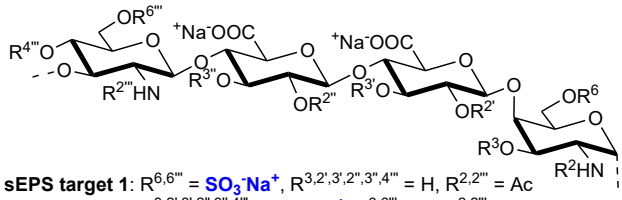

Figure 4.13. Structure of the differently sulfated HE800 EPS (sEPS) targets.

We first focused the attention on the regioselective sulfation of the primary hydroxyl positions of GlcNAc and GalNAc units. As also discussed in Chapter 2 (see Paragraph 2.2.1.1), several procedures for regioselective 6-*O*-sulfation have been reported for different polysaccharide structures, including GAGs (Bedini et al., **2017**). For our purposes, we decided to implement the same strategy already developed by us for mild sulfation of chondroitin derivatives (see Chapter 2, Paragraph 2.2.1.3). This included a cation exchange step to convert the polysaccharide sodium salt in its corresponding tetrabutylammonium salt **59**, then the regioselective 6-*O*-sulfation with SO_3·pyridine complex in DMF at 4 °C, and a final cation re-exchange step to ensure a total conversion of the polysaccharide into its sodium salt form **sEPS-1** (Scheme 4.8).

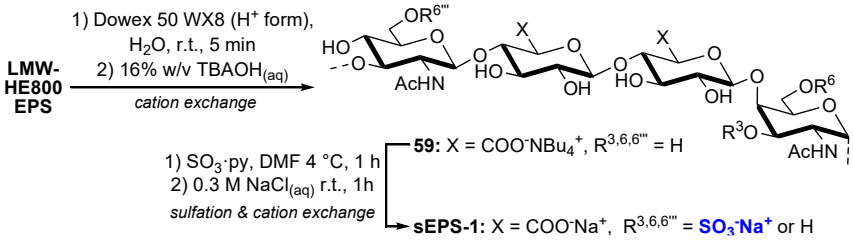

Scheme 4.8. Semi-synthesis of **sEPS-1** through mild sulfation reaction.

Structural characterization of **sEPS-1** was performed through 1D- and 2D-NMR analysis. Its ^{1}H,^{13}C-DEPT-HSQC spectrum (Figure 4.14) displayed two groups of methylene signals ($\delta_{H,C}$ 3.63–3.93/60.6–62.7 and 4.18–4.36/67.3–70.1 ppm) associated to CH_2 atoms at position 6. The non-shifted ones ($\delta_{H,C}$ 3.63–3.93/60.6–62.7 ppm) could be assigned to unsulfated GlcNAc and GalNAc units in accordance with the chemical shift values typical for methylene signals in starting LMW-HE800 EPS (Rougeaux et al., **1999**). On the contrary, the marked downfield shift of the second group of signals ($\delta_{H,C}$ 4.18–4.36/67.3–70.1 ppm) could be ascribed to sulfation at CH_2-6 position of the aminosugar residues. A complete assignment of all the signals was accomplished by comparison with literature data of starting LMW-HE800 EPS (Rougeaux et al., **1999**) and with the aid of COSY, TOCSY, HSQC-TOCSY and HMBC 2D-NMR spectra (see Table 4.7 in Paragraph 4.4.4). Surprisingly, three different signals ($\delta_{H/C}$ 5.42/98.6, 5.55/98.3, 5.62/97.9 ppm, respectively) were associated to anomeric position of GalNAc residues, thus suggesting the presence of at least three different subunits within the polysaccharide backbone. In particular, the most downfield shifted one could be attributed to 3,6-*O*-sulfated GalNAc unit, by means of a HSQC-TOCSY spectrum showing a correlation (also confirmed by COSY spectrum) with the CH signal at $\delta_{H/C}$ 4.50/49.3 ppm, attributable to GalNAc *CH*-2, which in turn was connected to a highly downfield shifted resonance at $\delta_{H/C}$ 4.52/74.7 ppm, that could be attributed to a sulfated *CH*-3 position. The other two anomeric signals at 5.55/98.3 and 5.42/98.6 ppm were instead assigned to *CH*-1 position of 6-*O*-sulfated and unsulfated GalNAc units, respectively. By relative integration of the three anomeric signals in ^{1}H-NMR spectrum of **sEPS-1**, percentage amounts of 6-*O*-sulfation (accounting for both GalNAc3,6S and GalNAc6S units) and 3-*O*-sulfation (representing only GalNAc3,6S units) were estimated as 65% and 16%, respectively. As for the *gluco*-aminosugar, because of the absence of proper signals in the ^{1}H-NMR spectrum, 6-*O*-sulfation percentage amount was estimated

as 67% from the ^{1}H-^{13}C-DEPT-HSQC spectrum by relative integration of the methylene signals assigned to GlcNAc6S and GlcNAc units, at 4.34/68.02 and 3.90/61.7 ppm, respectively.

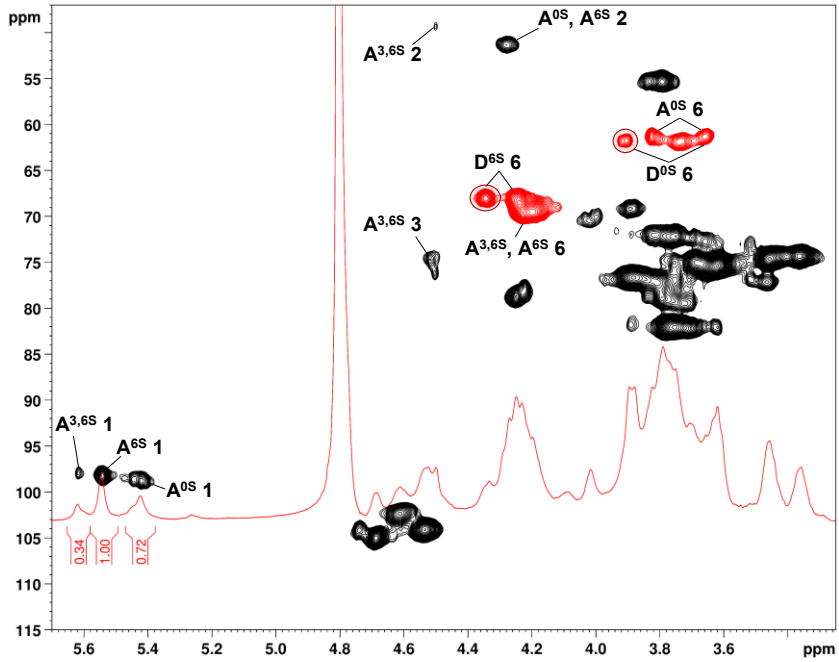

Figure 4.14. Zoom of ^{1}H,^{13}C-DEPT-HSQC and ^{1}H-NMR spectra (600 MHz, 298 K, D_2O) of **sEPS-1**. A: GalNAc, D: GlcNAc. 3,6S, 6S, 0S superscripts represent sulfated positions in GalNAc and GlcNAc units. Densities enclosed in highlighted areas were integrated for estimation of GlcNAc6S/GlcNAc ratio (only some of the assignments are shown).

The second targeted sulfation pattern, displaying sulfate groups at each hydroxyl positions except for the primary ones, could be obtained through a proper 6-de-*O*-sulfation reaction starting from a persulfated HE800 EPS derivative. This oversulfated product was already prepared by Dr. Zykwinska and coworkers under classical sulfation conditions (SO_3·py in DMF) from LMW-HE800 EPS and was employed in studies regarding skin regeneration activity (Senni et al., **2013**). Regioselective 6-de-*O*-sulfation can be conducted employing a silylating agent, such as MSTFA or BTSA. This method can selectively cleave sulfate

groups placed at *O*-6 position of polysaccharides and converts the released primary hydroxyl groups into trimethylsilyl ethers. The alcohol moieties are then restored by silyl ether cleavage on aqueous work-up (Benito-Arenas et al., **2018**; Han et al., **2018**; Kariya et al., **2000**; Toida et al., **2000**). Hence, the per-*O*-sulfated LMW-HE800 EPS was first subjected to a cation exchange step, to convert it into its more soluble pyridinium salt **60** (Scheme 4.9). The subsequent 6-de-*O*-sulfation step was performed using the highly selective silylating agent MSTFA (Benito-Arenas et al., **2018**; Kariya et al., **2000**; Takano et al., **1995**), at 70 °C in pyridine. Then a final cation re-exchange step, to ensure a total conversion of the polysaccharide into its sodium salt form, allowed to gain polysaccharide **sEPS-2**.

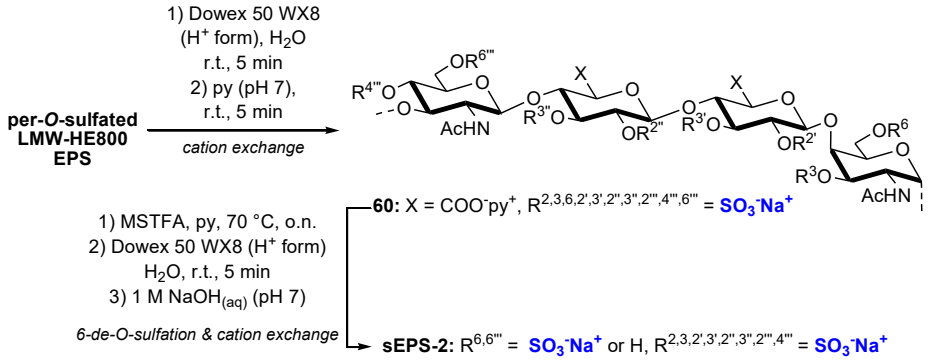

Scheme 4.9. Semi-synthesis of **sEPS-2** through de-*O*-sulfation approach.

Unfortunately, 2D-NMR analysis of **sEPS-2** showed no particular difference with respect to the starting oversulfated product. In particular, no remarkable upfield shift, as expected by the absence of a sulfate group, could be observed for any methylene signals (see Figure 4.29 in Paragraph 4.4.4).

We also explored the possibility to obtain a heparin-like sulfation pattern, with sulfate groups on the amino functions and/or on the primary positions of the two aminosugars in HE800 EPS structure. To this aim, the *N*-acetyl groups of the GlcNAc and GalNAc residues should be first cleaved under appropriate conditions, then the liberated amino functions should be selectively sulfated. This

strategy required the optimization of the *N*-deacetylation reaction conditions. Historically, hydrazinolysis has been the most common method for GAG *N*-deacetylation and several examples have been reported in the past decades on CS, DeS, HS and more complex species such as fCS (Fukuda et al., **1976**; Guo and Conrad, **1989**; Nadkarni et al., **1996**; Shaklee and Conrad, **1984**; Yan et al., **2017**; Zhao et al., **2013**). Reaction parameters, such as temperature, catalyst and reaction time, play a pivotal role in determining the efficiency of this reaction and avoiding, at the same time, the formation of collateral side-products. Indeed, GAG structures are quite labile under the required alkaline condition, that could cause a β-eliminative cleavage at the glycosidic bonds involving *O*-4 linked uronic units, thus resulting in an undesired depolymerization and an increased polydispersity of the product. The choice of the reagent is crucial to reduce this side reaction, with a 70% content of hydrazine in water being the threshold not to be surpassed (Guo and Conrad, **1989**; Zhao et al., **2013**). Reaction temperature can also be a critical parameter affecting the reaction rate and yield; usually, higher temperature values are required and performing the reaction at 90 °C has revealed the best compromise to reach a satisfying deacetylation degree without a significant molecular weight reduction (Yan et al., **2017**; Zhao et al., **2013**). The reaction is often performed in the presence of a catalyst, commonly hydrazine sulfate, which provides protons to accelerate the *N*-deacetylation rate, again avoiding the β-elimination. As for reaction time, there is no standard value since it can be particularly variable depending on the GAG structure to be reacted; so, to vary the reaction time could be an optimal and convenient way to control the degree of deacetylation. Hence, we monitored the *N*-deacetylation, conducted with hydrazine monohydrate (64-65% hydrazine in water) and hydrazine sulfate at 90 °C (Scheme 4.10), on LMW-HE800 EPS derivative, by taking aliquots from the reaction mixture at different times (10, 20, 30, 40 h). After the work-up with ethanol and some drops of saturated aqueous NaCl solution, each aliquot was

dialysed at 4 °C and freeze-dried, then the obtained crude products **61-i-iv** were analysed by ^{1}H-NMR spectroscopy.

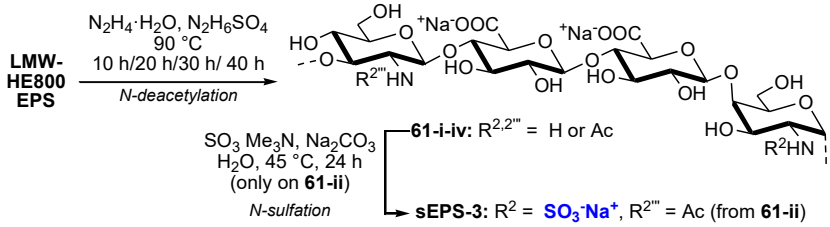

Scheme 4.10. Semi-synthesis of **sEPS-3** through *N*-deacetylation and *N*-sulfation reaction sequence.

The comparison of ^{1}H-NMR spectra of **61-i-iv** with the one displayed by the native polysaccharide (Figure 4.15) evidenced the gradual decrease of the *N*-acetyl signals at 2.04 and 2.06 ppm with the increase of the reaction time. It could be also noticed a lowering of the intensity of the *H*-1 GalNAc signal (δ_H 5.42 ppm) with the concomitant appearance of a resonance at 5.67 ppm, which could be attributed to the anomeric proton of the *N*-deacetylated GalN units. However, at reaction times higher than 20 h (see spectra *d* and *e* in Figure 4.15), overlapped peaks could be observed between 5.62–5.72 ppm, reasonably due to anomeric signals of GalN units in shorter and/or differently degraded polysaccharide chains. For these reasons, a reaction time of 20 h was considered adequate both to have a good deacetylation degree and to avoid polysaccharide depolymerization and/or by-products.

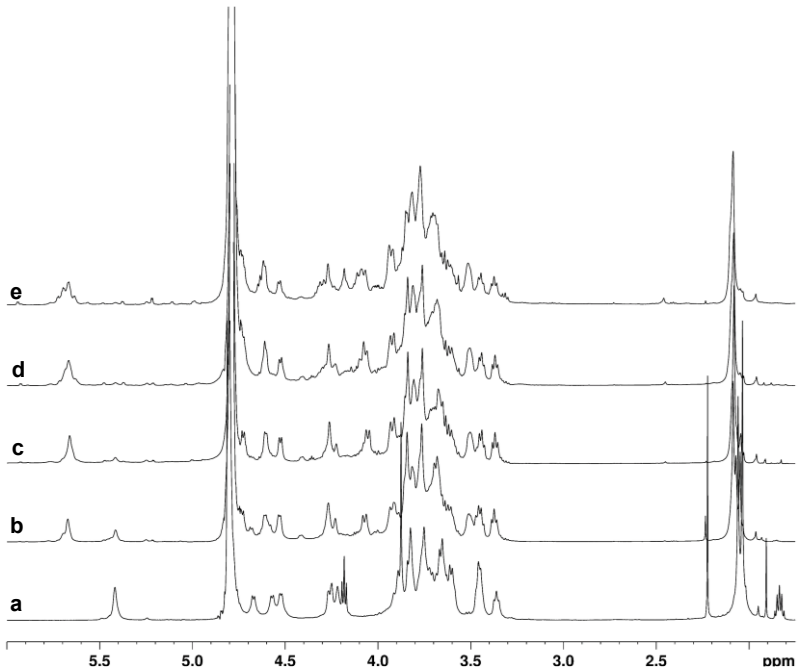

Figure 4.15. ^{1}H NMR spectra (600 MHz, 298 K, D_2O) of (a) LMW-HE800 EPS, (b) **61-i**, (c) **61-ii**, (d) **61-iii**, (e) **61-iv**.

To further investigate this hypothesis, the structural characterization of **61-ii** (obtained with a reaction time of 20 h) was accomplished by 2D-NMR analysis. Its ^{1}H,^{13}C-DEPT-HSQC spectrum (Figure 4.16) displayed four anomeric signals ($\delta_{H,C}$ 5.66/97.2, 4.72/104.2, 4.60/101.5, 4.52/103.9 ppm), that could be assigned also by the aid of COSY and TOCSY 2D-NMR spectra. As also observed by ^{1}H-NMR analysis, the *CH*-1 signal of GalN residue underwent a significant ^{1}H downfield shift with respect to *CH*-1 of GalNAc in starting LMW-HE800 EPS; on the contrary, a comparable shift was not detected in the case of the anomeric resonance relative to the *gluco*-configured aminosugar. A similar situation could be observed for the *CH*-2 signals of the two aminosugars: while the *CH*-2 resonance of the glucosamine units remained unaffected after the *N*-deacetylation reaction, the *CH*-2 signal of the *galacto*-configured aminosugar was largely shielded in the proton dimension and slightly downfield shifted in the ^{13}C

dimension. The observed NMR shifts, in agreement with reported data on *N*-deacetylation of CS samples (Mans et al., **2015**), suggested that the *N*-deacetylation reaction involved exclusively the amide group on the GalNAc units, leaving unaltered the GlcNAc residues. These could not be deacetylated even under prolonged reaction times, which caused, instead, extensive degradation of the polysaccharide structure, as noticed in ^{1}H-NMR spectra of **61-iii** and **61-iv** (see Figure 4.15).

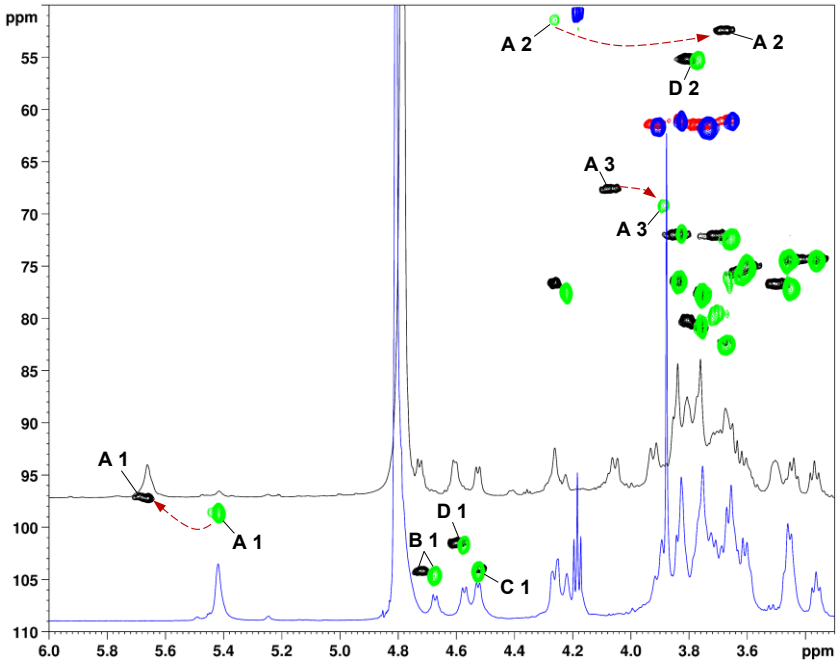

Figure 4.16. Zoom of ^{1}H,^{13}C-DEPT-HSQC and ^{1}H-NMR spectra (600 MHz, 298 K, D_2O) of LMW-HE800 EPS (green/blue: ^{1}H,^{13}C-DEPT-HSQC NMR spectrum; blue: ^{1}H-NMR spectrum) and **61-ii** (black/red: ^{1}H,^{13}C-DEPT-HSQC NMR spectrum; black: ^{1}H NMR spectrum). A: **GalNAc** or **GalN**, B: →4)-**GlcA**-(1→4)-GalNAc, C: →4)-**GlcA**-(1→4)-GlcA, D: **GlcNAc**. Red arrows show shifts of GalN(Ac) signals from LMW-HE800 EPS to **61-ii**. (Only some of the assignments are shown)

Polysaccharide **61-ii**, displaying only one free amino group per repeating unit, was subjected to a chemoselective sulfation reaction, with $SO_3 \cdot Me_3N$ complex and sodium carbonate in water at 45 °C, in order to install a sulfate group only on the

amino function, leaving unaffected all the free hydroxyl positions (Scheme 4.10). Product **sEPS-3**, obtained after dialysis and freeze-drying, was then analysed by 2D-NMR spectroscopy to validate the expected structure. Significant shifts of the newly sulfated GalN *CH*-1, *CH*-2 and *CH*-3 signals could be observed by comparison of its $^{1}H,^{13}C$-DEPT-HSQC spectrum with the one displayed by **61-ii** (Figure 4.17). In particular, the addition of a sulfate group at the GalN nitrogen atom of **61-ii** to gives **sEPS-3** deshielded the *CH*-2 resonance in the ^{13}C dimension, in accordance with literature NMR data of *N*-sulfated CS polysaccharides (Mans et al., **2015**).

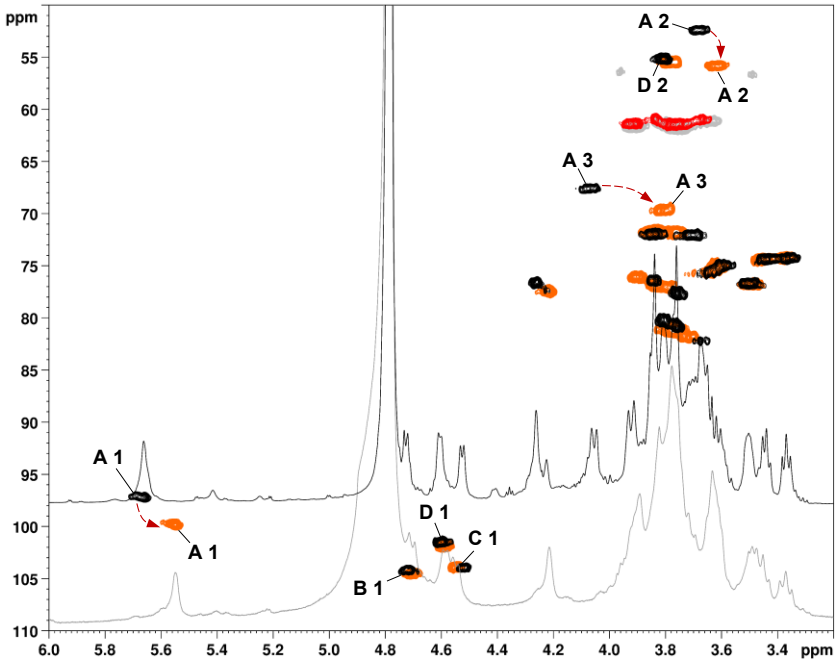

Figure 4.17. Zoom of $^{1}H,^{13}C$-DEPT-HSQC and ^{1}H-NMR spectra (600 MHz, 298 K, D_2O) of **sEPS-3** (orange/grey: $^{1}H,^{13}C$-DEPT-HSQC spectrum; grey: ^{1}H-NMR spectrum), **61-ii** (black/red: $^{1}H,^{13}C$-DEPT-HSQC spectrum; black: ^{1}H-NMR spectrum). A: **GalNAc** or **GalN**, B: →4)-**GlcA**-(1→4)-GalNAc, C: →4)-**GlcA**-(1→4)-GlcA, D: **GlcNAc**. Red arrows indicate the shift of GalN signals from **61-ii** to **sEPS-3**. (Only some of the assignments are shown)

In order to obtain a heparin-like sulfation pattern, also the two primary positions of the aminosugars residue should be sulfated. To this aim, we performed on **sEPS-3** the 6-*O*-sulfation procedure, already employed for **sEPS-1**. Unfortunately, in this case no reaction occurred, and the starting product was recovered completely unreacted as evidenced by a preliminary ^{1}H-NMR analysis (data not shown). Future work will be necessary in order to seek a new approach for the obtainment of the heparin-like derivative.

Finally, we also decided to investigate whether a cyclic protecting group could be regioselectively installed on the LMW-HE800 EPS structure, to open the way to a new sulfation pattern. Interestingly, the HE800 EPS repeating unit shows only one diol, comprising position 4 and 6 on the GlcNAc residue, that could be protected with a cyclic protecting group. Among the several different cyclic protecting groups, cyclic acetals are often employed for protection of 1,3-diols, such as *O*-4,6 one of GlcNAc unit. For our purposes, a benzylidene ring was selected thanks to its relative stability and ease of insertion. Thus, the selective protection of GlcNAc *O*-4,6 diol was attempted by treating the unsulfated LMW-HE800 EPS with α,α-dimethoxytoluene in the presence of CSA as acid catalyst (Scheme 4.11), to install a benzylidene cycle, analogously to our previous investigations (see Paragraphs 4.2.1 and 4.2.2). The obtained product **62**, recovered by precipitation from the reaction mixture, was then subjected to exhaustive sulfation of the free hydroxyl moieties by treatment with SO_3·pyridine complex in DMF at 50 °C (Scheme 4.11). Then, a global deprotection, under acid aqueous conditions to cleave benzylidene rings, furnished derivative **sEPS-4** with sulfate groups expected at all the positions expect for the GlcNAc ones.

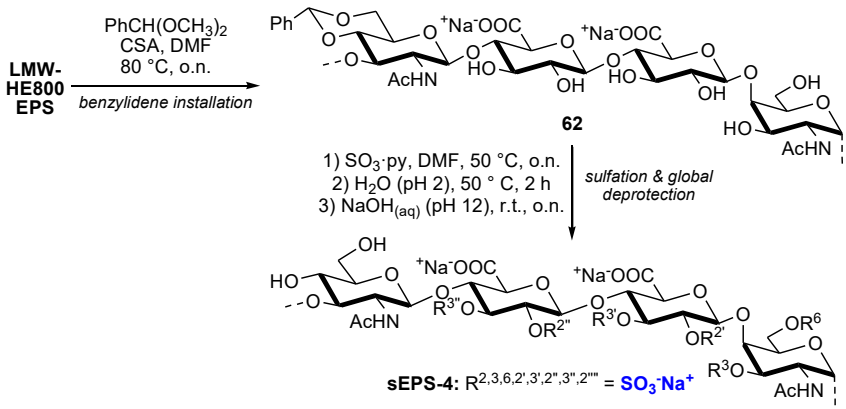

Scheme 4.11. Semi-synthesis of **sEPS-4** through cyclic group installation.

The postulated structure for derivative **sEPS-4** could be not confirmed by 2D-NMR spectra analysis. Indeed, the only *CH*$_2$ multiplicity-edited signals in the ^{1}H,^{13}C-DEPT-HSQC spectra were found at ^{1}H and ^{13}C downfield chemical shifted values ($\delta_{H/C}$ 4.24–4.29/70.0 and 4.20–4.67/68.9 ppm, respectively; see Figure 4.18), strongly suggesting that GalNAc and GlcNAc *O*-6 positions were both sulfated. Actually, a comparison of the ^{1}H,^{13}C-DEPT-HSQC spectra between **sEPS-4** and per-*O*-sulfated LMW-HE800 EPS (see Figure 4.30 in Paragraph 4.4.4) revealed a close resemblance, thus suggesting that this multi-step strategy, relying upon the benzylidene protection of LMW-HE800 EPS before treatment with SO_3·py in order to avoid per-*O*-sulfation, was not successful. A detailed analysis of a full set (COSY, TOCSY, DEPT-HSQC, HMBC and HSQC-TOCSY) of 2D-NMR spectra of **sEPS-4** suggested that the acid catalyst employed in the benzylidenation reaction was responsible instead for a significant shortening of the polysaccharide chain. Indeed, a highly ^{1}H-downfield and ^{13}C-upfield shifted anomeric signal at $\delta_{H/C}$ 6.24/93.7 ppm could be detected in the ^{1}H,^{13}C-DEPT-HSQC spectrum, and assigned by COSY, HMBC and HSQC-TOCSY correlations to an α-configured 1,4,6-trisulfated GlcNAc pseudo-reducing unit.

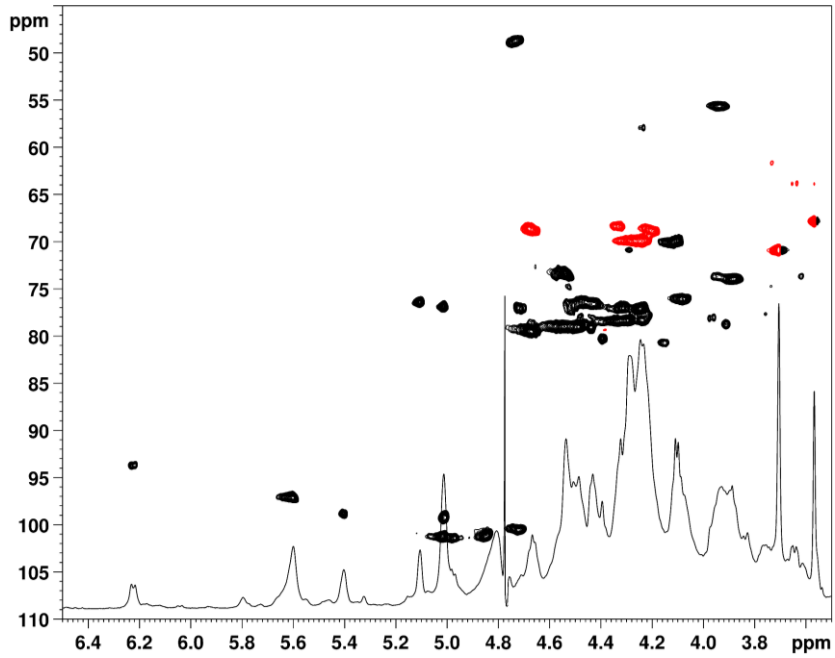

Figure 4.18. ^{1}H and ^{1}H,^{13}C-DEPT-HSQC NMR spectra (600 MHz, 298K, D_2O) of **sEPS-4**.

As confirmation of the polysaccharide chain shortening, the densities at $\delta_{H/C}$ 5.02/76.7 and 5.12/76.1 ppm, detected exclusively in the ^{1}H,^{13}C-DEPT-HSQC spectrum of **sEPS-4**, could be assigned to *CH*-3 and *CH*-4 atoms, respectively, of a 2,3,4-trisulfated GlcA residue at the non-reducing end of the polysaccharide chain. Notably, signals of different terminal residues at both reducing and non-reducing ends could not be found, thus suggesting that the β-1→4 glycosidic linkage between GlcNAc and GlcA units is much more labile with respect to the other ones constituting the LMW-HE800 EPS. Indeed, it is known that the carboxylic acid moiety can accelerate the hydrolysis of the glycosidic bond involving a 4-linked hexuronic acid by its destabilization through a hydrogen-bond forming a pseudo-pyranosidic ring. By also considering other (stereo)-electronic effects —*e.g.* a hexuronic acid stabilizes its own glycosidic bonds while the acetamido moiety of *N*-acetylated aminosugars can ease the cleavage of the

vicinal 1,2-*trans*-configured glycosidic bond by an anchimeric assistance effect—the observed selectivity in the acid-catalyzed shortening of LMW-HE800 EPS was not surprising at all (Knirel et al., **2019**).

As further confirmation of the polysaccharide chain shortening in **sEPS-4** and, more generally, to have a complete structural characterization of the semi-synthesized LMW-HE800 EPS derivatives **sEPS-1,3,4**, their weight- and number-averaged molecular weights (M_W and M_n, respectively) as well as their polydispersity (as M_w/M_n ratio) were measured by HPSEC-MALS analysis. A significant chain shortening with respect to starting LMW-HE800 EPS was detected for both **sEPS-3** and **sEPS-4**, even if no dramatic increase of polydispersity index was noted (Table 4.3). On the contrary, **sEPS-1** showed a moderately higher M_w value (27 kDa) with respect to the starting polysaccharide, probably due to the high number of sulfate groups on the polymeric chain together with a lower depolymerization compared to the other two derivatives. In all cases, the observed chain shortening was expected due to the acid conditions of the sulfation reaction; besides, the remarkable decrease in M_w value of **sEPS-3** could be also attributed to the *N*-deacetylation alkaline step.

Table 4.3. Molecular mass data of semi-synthetic **sEPS-1,3,4**.

	DS	M_w[a] **(kDa)**	M_n[b] **(kDa)**	M_w/M_n
LMW-HE800 EPS	0	24.0 ± 0.1	17.6 ± 0.2	1.36 ± 0.02
per-*O*-sulfated LMW-HE800 EPS	fully *O*-sulfated	16.4 ± 0.2	12.6 ± 0.3	1.30 ± 0.04
sEPS-1	GlcNAc 6-sulfation: 0.64 GalNAc 6-sulfation: 0.65 GalNAc 3-sulfation: 0.16	27.2 ± 0.1	18.8 ± 0.2	1.45 ± 0.02
sEPS-3	GalNS *N*sulfation : 1.00	5.4 ± 0.1	4.2 ± 0.1	1.29 ± 0.04
sEPS-4	fully *O*-sulfated	12.3 ± 0.4	7.5 ± 0.6	1.6 ± 0.1

[a] weight-averaged molecular mass; [b] number-averaged molecular mass.

4.3. Conclusions

In this chapter, the research for new semi-synthetic strategies for the regioselective sulfation of different naturally occurring polysaccharides (curdlan, M-rich alginic acid, the marine-sourced bacterial HE800 EPS) was attempted. These polysaccharides, already in their native unsulfated form, exhibit interesting biological activities and their regioselective sulfation could be one of the most cost-effective ways both to achieve an intrinsic improvement of their already existing properties and to introduce completely new ones (*e.g.* anticoagulant activity).

Regioselective sulfation of polysaccharides can be obtained through direct, regioselective sulfation/desulfation reactions, or multi-step procedures. In this work, these strategies were applied depending on the different targeted sulfation pattern: direct methods were used for sulfation or desulfation of primary (more reactive) sites, whereas multi-step procedures were employed for the less reactive positions. In the latter case, the use of cyclic protecting groups for regioselective protection of vicinal diols was also explored. In all cases, the semi-synthetic procedures were applied on laboratory-scale quantities (from tens to hundreds of milligrams), making still far a set-up for a preparative industrial synthesis. However, the low price of the used reagents, together with the abundance of the starting materials, especially in the case of curdlan and M-rich alginate, could be useful advantaged to be considered for a future up-scaling of such approaches.

In the case of curdlan, the use of a cyclic benzylidene protecting group for Glc *O*-4,6-diols on its LMW-derivative opened an access to new polysaccharide species with unprecedented sulfation patterns. Three different semi-synthetic pathways were investigated, one relying upon the sulfation of a benzylidene-protected intermediate and the others based on the sulfation of two polysaccharide derivatives obtained after hydrolytic or oxidative cleavage, respectively, of benzylidene protecting groups. The obtained curdlan sulfate polysaccharides were

structurally characterized by a detailed 2D-NMR analysis, associated with FT-IR spectroscopy and elemental analysis. For some of the semi-synthetic derivatives, NMR characterization revealed the presence of unprecedented Glc sulfation patterns as main motifs along the polysaccharide chain, *i.e.* 4,6-disulfated for **CdS-1,2**, 4- and 6-sulfated for **CdS-3**, and 2-sulfated for **CdS-6**. This achievement enlarges the number of curdlan sulfate polysaccharides on which structure-activity relationship studies could be done. In this context, the immunological properties of **CdS-1–6** are currently under investigation and results will be reported at due time.

The study of regioselective sulfation of a commercially available M-rich alginic acid was based on the installation of different cyclic protecting groups on ManA and GulA 2,3-diols. A more classical approach for protection of vicinal diols was first attempted by employing an orthoester and a benzylidene group, respectively, that were then cleaved under proper, regioselective opening conditions. A different approach, based on a three-step, one-pot sequence, with a 3,6-lactonization as key step, was also tested. The three strategies gave derivatives with free alcohol moieties at selected positions, which were then sulfated and deprotected to give three alginate sulfate polysaccharides (**AS-1**, **AS-2**, **AS-4**). NMR characterization, also by comparison with data of M-rich alginic acid and its per-*O*-sulfated derivative, together with DS evaluation by elemental analysis showed a heterogenous sulfation pattern for the three semi-synthetic derivatives. Future works will be necessary to implement multi-step strategies able to allow a complete regiocontrol of the sulfation pattern in order to obtain M-rich alginate sulfate derivatives for structure-activity relationship investigations.

Regioselective sulfation of the LMW-HE800 EPS polysaccharide gained three sulfated derivatives with a different substitution pattern, which was scrutinized by NMR analysis. A mild sulfation procedure allowed to obtain derivative **sEPS-1** with sulfate groups placed at the primary positions of GalNAc and GlcNAc

subunits and at some *O*-3 positions of GalNAc. A *N*-deacetylation, followed by a regioselective *N*-sulfation gave the monosulfated derivative **sEPS-3** with sulfate groups exclusively attached at nitrogen atom of GalN units. This approach could also pave the way to a heparin-like EPS polysaccharide by optimizing reaction conditions for sulfation at primary alcohol positions of the *N*-sulfated derivative. Finally, the use of a benzylidene protecting group in a multi-step sequence was also investigated to access another sulfation pattern on LMW-HE800 EPS. A preliminary ^{1}H-NMR analysis of the obtained sulfated derivative **sEPS-4** suggested a partial sulfation, in accordance with the implemented semi-synthetic strategy; however, a complete 2D-NMR analysis is mandatory for a clear assessment of the sulfation pattern of such compound. The three semi-synthetic sulfated HE800 EPS derivatives will be included in a preliminary study aimed to decipher the effect of different sulfation patterns on their bioactivities. In particular, with the final aim to find new GAG-like molecules, analyses to assess the affinity to growth factors and to evaluate the anti-coagulant and anti-thrombotic activities could be performed on the EPS derivatives. Work is in progress to this aim and will be published as soon as possible elsewhere.

4.4. Experimental Section

4.4.1. General Methods

Curdlan (hydrated form, max 10% loss on drying, CAS n° 54724-00-4) and M-rich alginic acid (average M_W > 5000 Da, CAS n° 29894-36-8) were purchased from Carbosynth Ltd. LMW-HE800 EPS and per-*O*-sulfated LMW-HE800 EPS were obtained at the laboratories of Dr. Agata Zykwinska group (*Laboratoire Ecosystèmes Microbiens et Molécules Marines pour les Biotechnologies*, Biotechnology and Marine Resources Research Unit, *Institut Français de Recherche pour l'Exploitation de la Mer*, IFREMER) according to reported

procedures (Senni et al., **2015**), starting from microbial-sourced HE800 EPS (Rougeaux et al., **1999**).

Commercially grade reagents and solvents were used without further purification, except where differently indicated. The term "deionized water" refers to water purified by a Millipore Milli-Q Gradient system. Centrifugations were performed with an Eppendorf Centrifuge 5804 R instrument at 4 °C (3500 rpm, 5 min). Dialyses were conducted on Spectra/Por 3.5 kDa cut-off membranes at 4 °C. Freeze-dryings were performed with a 5Pascal Lio 5P 4K freeze dryer.

NMR spectra were recorded on a Bruker DRX-400 (^{1}H: 400 MHz, ^{13}C: 100 MHz), or on a Bruker Avance-III HD (^{1}H: 600 MHz, ^{13}C: 150 MHz) instrument equipped with a cryo probe, in D_2O (acetone as internal standard, ^{1}H: $(CH_3)_2CO$ at δ 2.22 ppm; ^{13}C: $(CH_3)_2CO$ at δ 31.5 ppm), or DMSO-*d*$_6$ (^{1}H: CHD_2SOCD_3 at δ 2.49 ppm; ^{13}C: CD_3SOCD_3 at δ 39.5 ppm). Data were processed using the data analysis packages integrated with Bruker TopSpin® 4.0.5 software. Gradient-selected COSY, NOESY and TOCSY experiments were performed using spectral widths of 6000 Hz in both dimensions, using data sets of 2048 × 256 points. TOCSY and NOESY mixing times were set to 120 ms and 200 ms, respectively. DEPT-HSQC and HMBC experiments were measured in the ^{1}H-detected mode via single quantum coherence with proton decoupling in the ^{13}C domain, using data sets of 2048 × 512 points and typically 60 increments (120 for HMBC).

FT-IR spectra of CdS samples were recorded on a Nicolet 6700 spectrometer (Thermo Scientific) in the ATR mode, using Omnic software. Elemental analysis of CdS samples was performed on a FlashSmart Elemental Analyzer (ThermoFisher Scientific). A Viscotek™ instrument (Malvern) was used to determine molecular mass data for CdS samples. Elemental analysis of alginate sulfate samples was performed with a LECO CHN 628 instrument for the determination of C, N, H and with a LECO SC 144 DR instrument for C, S. A HPSEC instrument coupled with a MALS (Dawn Heleos-II, Wyatt Technology)

and a differential RI (Optilab Wyatt technology) detector was employed for determination of molecular mass data of sulfated HE800 EPS derivatives.

4.4.2. Semi-Synthetic Procedures and Characterization of Curdlan Sulfate Polysaccharides

Conversion of curdlan into LMW-curdlan. A fine suspension of curdlan (271 mg, 1.67 mmol RU) in deionized water (27 mL) was treated with 1 M $TFA_{(aq)}$ (2.2 mL) and then stirred at 60 °C for 3 hours. Thereafter, the reaction mixture was neutralized by addition of 4 M $NaOH_{(aq)}$. The mixture was dialyzed and then freeze-dried to afford LMW-curdlan as a white powder (258 mg, 95% weight yield).

Example of benzylidenation. LMW-curdlan (230 mg, 1.42 mmol RU) was suspended in dry DMF (10.7 mL) and then heated to 80 °C. After 2 h stirring, a very fine suspension was obtained. It was cooled to r.t. and then treated with α,α-dimethoxytoluene (2.13 mL, 14.2 mmol) and then CSA (82.3 mg, 0.354 mmol). The mixture was stirred for 20 h at 80 °C. Thereafter, it was cooled to r.t. and treated with diisopropyl ether (45 mL). The obtained white precipitate was collected by centrifugation and then dried under vacuum to afford **50-i** (326 mg, 142% weight yield) as a yellowish powder.

Example of acetylation. A fine suspension of **50-i** (220 mg, 0.879 mmol RU) in dry 2:1 *v*/*v* CH_3CN–DMF (8.1 mL) was treated with Ac_2O (3.32 mL, 35.2 mmol), Et_3N (2.45 mL, 17.6 mmol) and finally with DMAP (39.4 mg, 0.352 mmol). The suspension was stirred at 50 °C for 20 h, then cooled to r.t. and treated with diisopropyl ether (60 mL) to give a brownish precipitate. This was collected by centrifugation and dried under vacuum to give **51-i** (302 mg, 137% weight yield) as a brownish powder.

Example of benzylidene hydrolysis. A suspension of **51-i** (108 mg, 0.368 mmol RU) in 9:1 *v*/*v* AcOH–deionized water (3.4 mL) was stirred at 50 °C for 48 h. The

resulting clear solution was diluted with deionized water (15 mL), dialyzed and freeze-dried. Derivative **52-i** (74.3 mg, 69% weight yield) was obtained as a yellowish powder.

Example of benzylidene oxidative cleavage. A suspension of **51-i** (89.9 mg, 0.308 mmol RU) in ethyl acetate (2.1 mL) was treated with a 0.47 M solution of $NaBrO_3$ in deionized water (1.95 mL). A 0.51 M solution of $Na_2S_2O_4$ in deionized water (1.52 mL) was then added portionwise over a period of 10 min. The triphasic mixture was vigorously stirred at r.t. for 20 h under visible light irradiation. The yellowish solid was then collected by centrifugation and dried under vacuum to afford derivative **53-i** (70.6 mg, 78% weight yield).

Example of sulfation and global deprotection. Polysaccharide **53-i** (65.2 mg, 0.212 mmol RU) was suspended in dry DMF (1.8 mL) and then treated with a 1.05 M solution of SO_3·py complex in dry DMF (4.0 mL, 4.2 mmol). After 20 h stirring at 50 °C, the obtained clear solution was cooled to r.t. and then a saturated NaCl solution in acetone (15 mL) was added. The obtained yellowish precipitate was collected by centrifugation and then dissolved in deionized water (10 mL). The resulting acid solution (pH ~ 2) was heated to 50 °C and stirred for 1.5 hours. Thereafter, it was treated at r.t. with 4 M $NaOH_{(aq)}$ to adjust pH to 12. The solution was stirred at r.t. for 20 h and then neutralized with 1 M $HCl_{(aq)}$. Dialysis, freeze-drying and further purification of the obtained material by filtration on a Sep-Pak C18 cartridge followed again by freeze-drying, yielded polysaccharide **CdS-3** (32.5 mg, 50% weight yield) as a white amorphous solid.

Degree of sulfation. For the evaluation of the degree of sulfation by CHNS elemental analysis, the samples (~3–5 mg) were weighted and mixed in a tin capsule with V_2O_5 as oxidizer. They were then combusted in a furnace with the following set of parameters: temperature furnace = 950°C, temperature oven = 65 °C, He carrier flow = 140 mL/min, O_2 flow = 250 mL/min flow, oxygen injection end = 3 sec, sampling delay time = 12 sec, run time = 720 sec. Experiments were

performed for each sample in triplicate. Degree of sulfation values were calculated according to Equation 4.2 (M_C = atomic mass carbon, M_S = atomic mass sulphur, n_C = number of carbon atoms per repeating unit):

$$DS = (S\ wt.\% \cdot M_C \cdot n_C)/(C\ wt.\% \cdot M_S) \qquad \text{(Eq. 4.2)}$$

Hydrodynamic analyses. A detailed hydrodynamic analysis was carried out using SEC equipped with a triple detector array (SEC-TDA) by Viscotek (TDA305, Malvern). The system consisted of two gel-permeation columns set in series (TSK-GEL GMPWXL, 7.8x30.0 cm, Tosoh Bioscience), a RI detector, a laser detector made of a RALS detector and a LALS one, and a four-bridge viscosimeter. The RI increment of solution (dn/dc) of a β-glucan in water (0.151 mL/g) was used for calculations. An appropriate amount of each CdS sample was dissolved in pure water and stirred overnight at r.t. The suspension was then centrifuged, and the supernatant was recovered, filtered on 0.22 µm filters (Millipore) and analyzed for hydrodynamic characterization in duplicate. Sample molecular weight (weight average molar mass, M_w; number-averaged molar mass, M_n; polydispersity index, M_w/M_n), molecular size (hydrodynamic radius, R_h), and intrinsic viscosity ([η]) distributions were derived.

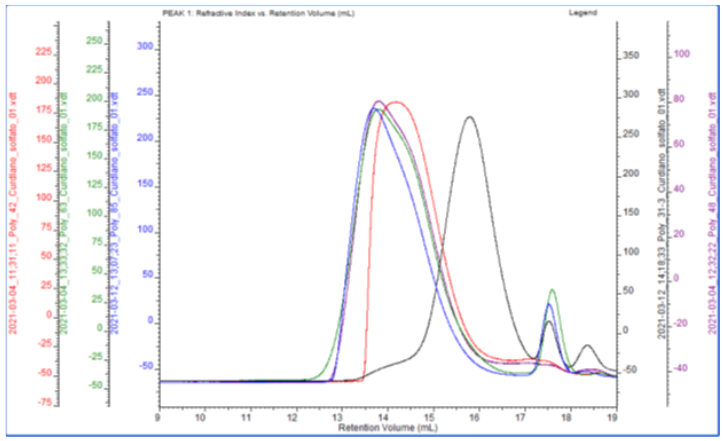

Figure 4.19. RI chromatograms overlay: **CdS-1** (red), **CdS-2** (blue), **CdS-3** (purple), **CdS-4** (green) and **CdS-5** (black).

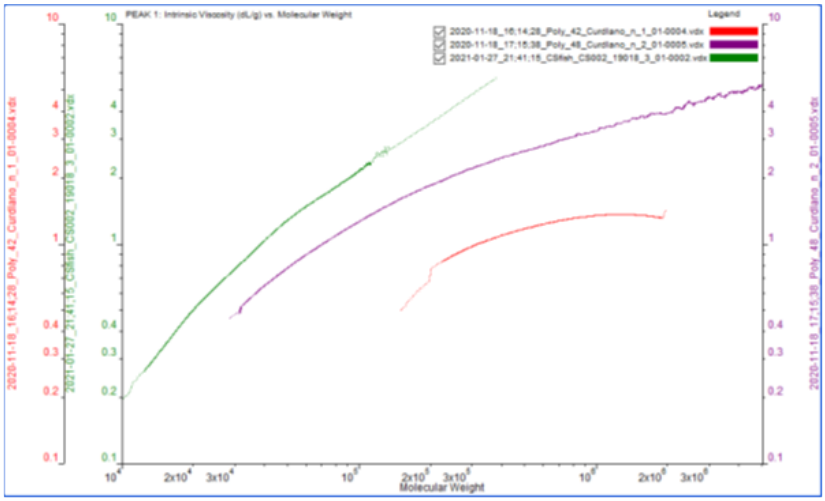

Figure 4.20. Mark-Houwink-Sukurada curves overlap for **CdS-1** (red), **CdS-3** (purple) and a 35-kDa chondroitin sulfate sample (green).

FT-IR spectra

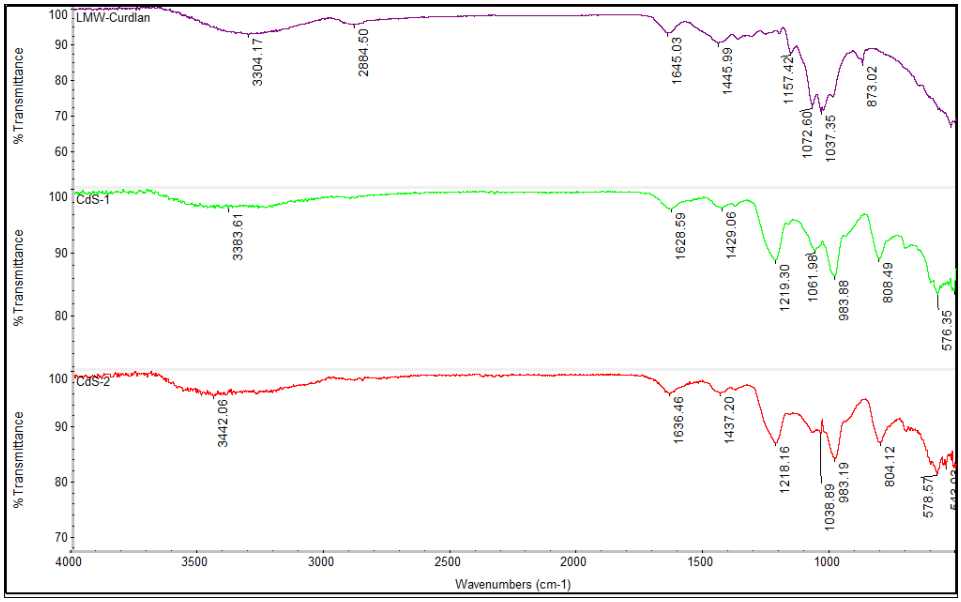

Figure 4.21. FT-IR spectra of LMW-curdlan (purple), **CdS-1** (green), **CdS-2** (red).

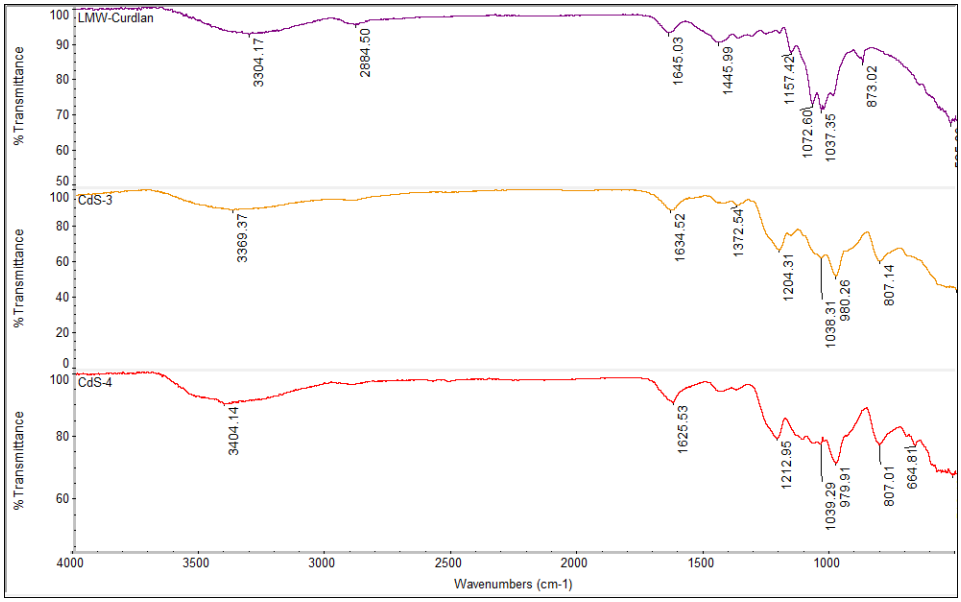

Figure 4.22. FT-IR spectra of LMW-curdlan (purple), **CdS-3** (orange), **CdS-4** (red).

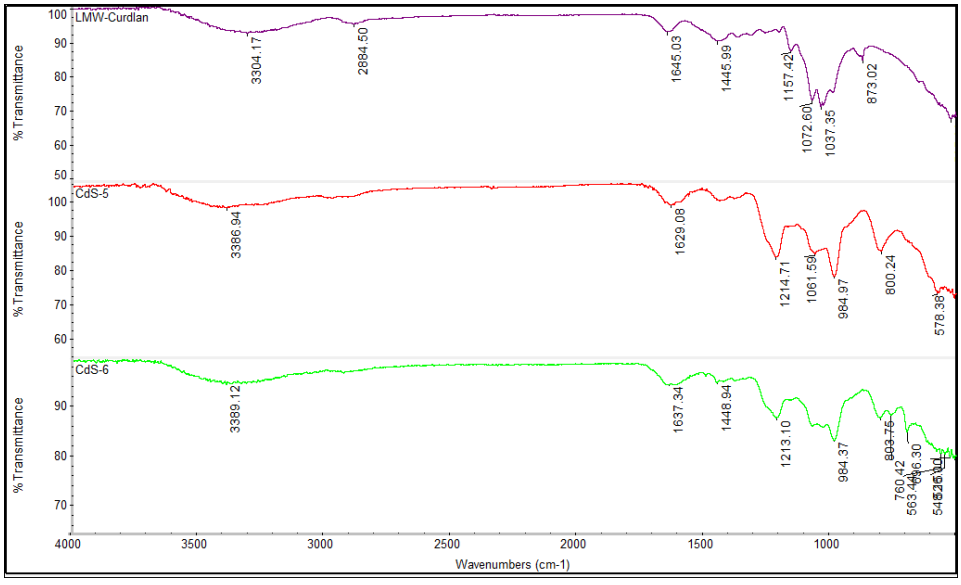

Figure 4.23. FT-IR spectra of LMW-curdlan (purple), **CdS-5** (red), **CdS-6** (green).

^{1}H and ^{13}C NMR Chemical Shifts Attributions

Table 4.4. ^{1}H (plain) and ^{13}C NMR (italic) chemical shift attribution of differently sulfated Glc units in **CdS-1-6**. [a,b]

Subunit	*Product*	1	2	3	4	5	6
Glc4S	**CdS-1–4**	4.81 *103.6*	3.71 *74.6*	4.13 *79.5*	4.25 *75.9*	3.65 *75.5*	3.94, 3.76 *62.0*
Glc6S	**CdS-1–4**	4.99 *102.0*	3.56 *74.5*	3.79 *85.1*	3.59 *69.0*	3.65 *75.5*	4.36, 4.24 *68.4*
Glc4,6S	**CdS-1–4**	5.03 *101.8*	3.65 *75.4*	*4.15* *79.2*	4.25 *75.9*	3.87 *74.1*	4.57, 4.16 *68.9*
Glc2S	**CdS-5,6**	5.24, *98.8* 5.19, *99.1* 5.06, *101.3* 5.04, *101.1*	4.46, *81.7* 4.27, *79.9*	4.16, *79.5* 3.98, *84.6*	3.77–3.56 *69.3*	n.d.[c]	4.36, 4.24, *68.4* (Glc2,6S) 3.94, 3.76, *62.0* (Glc2S)
Glc	**CdS-1–6**	4.78 *103.9*	3.56 *74.5*	3.79 *85.1*	3.54 *69.3*	3.52 *77.0*	3.94, 3.76 *62.0*

[a] NMR experiments conducted in D_2O at 298 K. [b] Chemical shifts expressed in δ relative to internal acetone (^{1}H: $(CH_3)_2CO$ at δ = 2.22 ppm; ^{13}C: $(CH_3)_2CO$ at δ= 31.5 ppm. [c] Not determined.

1D- and 2D-NMR Spectra

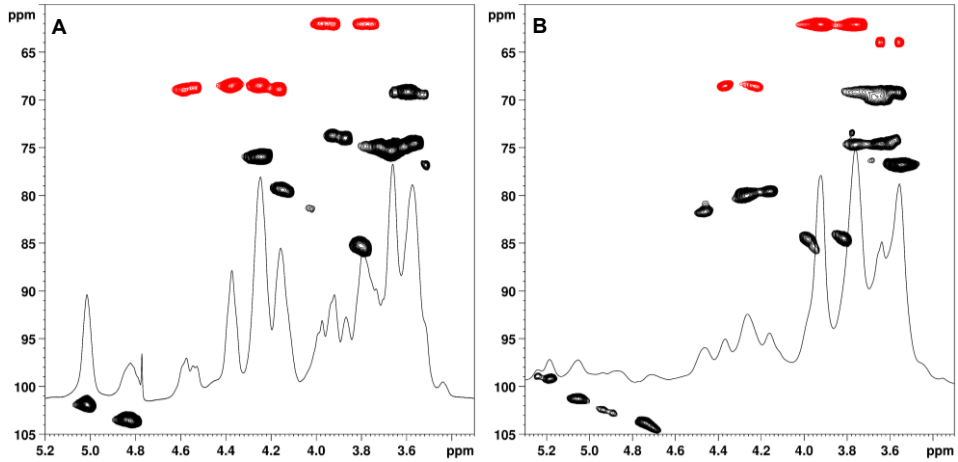

Figure 4.24. ^{1}H,^{13}C-DEPT-HSQC and ^{1}H-NMR spectra (400 MHz, 298K, D_2O) of (A) **CdS-4**, (B) **CdS-6**.

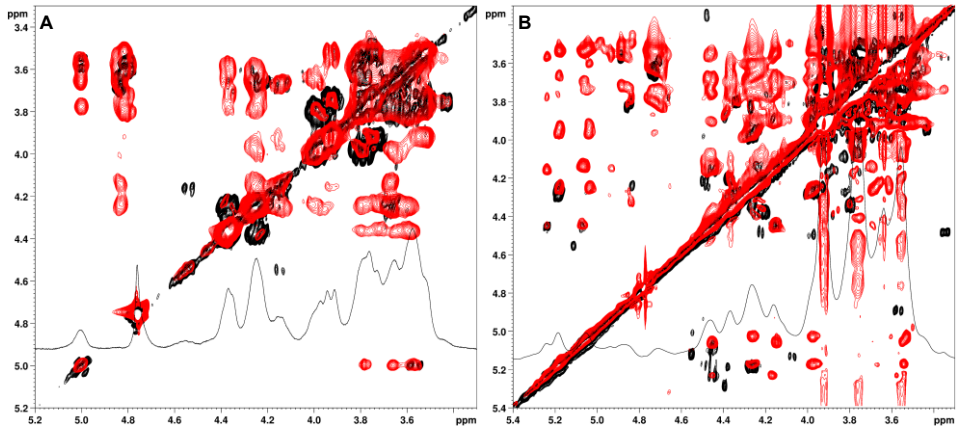

Figure 4.25. ^{1}H, COSY (black) and TOCSY (red) NMR spectra of (A) **CdS-3** (400 MHz, 298K, D_2O), (B) **CdS-6** (600 MHz, 298K, D_2O).

4.4.3. Semi-Synthetic Procedures and Characterization of Alginate Sulfate Polysaccharides

Derivative 55-i. M-rich alginic acid (85.0 mg, 0.481 mmol RU) was suspended in dry DMF (3.8 mL). After 90 min stirring at r.t., trimethyl orthobenzoate (752 μL, 4.38 mmol) and then CSA (140 mg, 603 μmol) were added. The suspension was stirred at r.t. for 20 h, then deionized water (15 mL) was added. The resulting milky suspension was stirred for 2 h, then subjected to dialysis and freeze-drying. The whole procedure was performed twice. Polysaccharide **55-i** (94.4 mg, 111% weight yield) was obtained as a yellowish powder.

Derivative 56. A suspension of M-rich alginic acid (196 mg, 1.11 mmol RU) in dry DMF (15 mL) was briefly stirred at 80 °C and then treated at r.t. with α,α-dimethoxytoluene (816 μL, 5.44 mmol) that was freshly dried over 4Å MS, and then with a 0.21 M solution of CSA in dry DMF (0.77 μL). The mixture was vigorously stirred at 80 °C for 20 h, then cooled to r.t. and treated with diisopropyl ether (40 mL) to give a white precipitate. The mixture was stored at −28 °C for some hours, then the solid was collected by centrifugation. After overnight drying

under vacuum, derivative **56** (175 mg, 89% weight yield) was obtained as a white powder.

Derivative 55-ii. Polysaccharide **56** (473 mg, 1.78 mmol RU) was suspended in ethyl acetate (20 mL) and treated with a 0.27 M solution of $NaBrO_3$ in deionized water (20 mL). Then a 0.24 M solution of $Na_2S_2O_4$ in deionized water (18 mL) was added portionwise. The yellowish triphasic reaction mixture was vigorously stirred at r.t. for 20 h. Thereafter, the solid was collected by centrifugation and dried under vacuum overnight. The biphasic liquid mixture was partitioned in a separation funnel, the water phase collected and then subjected to dialysis and freeze-drying. The obtained yellowish residue was combined with the previously collected solid to afford derivative **55-ii** (190 mg, 40% weight yield).

Derivative 58. M-rich alginic acid (196 mg, 1.11 mmol RU) was suspended in dry DMF (8.8 mL) and briefly stirred at 85 °C. The resulting, fine, yellowish suspension was treated with Bz_2O (7.57 g, 33.5 mmol) at r.t. under Ar atmosphere. The mixture was vigorously stirred at 85 °C for 26 h, then cooled to r.t. and treated with pyridine (4.9 mL) and DMAP (182 mg, 1.49 mmol). After 72 h stirring at r.t., dry methanol (7.5 mL) and NaOAc (137 mg, 1.67 mmol) were added and stirring was continued overnight. Thereafter, a further amount of methanol (16 mL) was added, and the reaction mixture was concentrated to approximately 20 mL volume by rotoevaporation. The residue was treated at 0 °C with diisopropyl ether (9 mL) to give a white precipitate. The mixture was stored at −28 °C overnight, then the solid was collected by centrifugation and further purified by dissolving it in DMSO (9 mL) and then precipitating with 2:1 *v*/*v* acetone–diisopropyl ether (45 mL). After overnight drying under vacuum, derivative **58** (190 mg, 97% weight yield) was obtained as a white powder.

General procedure for sulfation and global deprotection. Polysaccharide **58** (or M-rich alginic acid or **55-i,ii**) (180 mg) was suspended in dry DMF (5.2 mL) and then treated with a 1.45 M solution of SO_3·py complex in dry DMF (7.5 mL).

After 20 h stirring at 50 °C, a saturated NaCl solution in acetone (11 mL) was added at r.t. and the mixture was then stored at −28 °C for 2 h. The obtained white precipitate was collected by centrifugation and then dissolved in deionized water (5.0 mL). The mixture was then treated with 4 M $NaOH_{(aq)}$ to adjust pH to 12, stirred at r.t. overnight, and then 1 M $HCl_{(aq)}$ was added until neutralization. Dialysis and subsequent freeze-drying yielded polysaccharide **AS-4** (or **AS-1,3**) (248 mg, 138% weight yield; 109% for **AS-1**, 181% for **AS-3**) as a white amorphous solid. To obtain polysaccharide **AS-2**, after the sulfation step, the obtained precipitate, collected by centrifugation, was dissolved in deionized water and the resulting acid mixture (pH ~ 12) was heated to 50 °C. After 2 h stirring at 50 °C, the mixture was cooled and then treated with 4 M $NaOH_{(aq)}$ to adjust pH to 12. The solution was stirred at r.t. for 20 h and then neutralized with 1 M $HCl_{(aq)}$. Dialysis and subsequent freeze-drying gave polysaccharide **AS-2** (148% weight yield).

Elemental analysis data

Table 4.5. Elemental analysis data (C, H, N).

Sample	Weight (g)	C wt.%	H wt.%	N wt.%	Others wt.%
M-rich alginic acid	0.0155	28.679	4.0336	0	67.2874
	0.0161	27.716	3.9595	0	68.3245
Average		*28.1975*	*3.99655*	*0*	*67.80595*
AS-2	0.0112	16.914	2.9335	1.133	79.0195
	0.012	16.662	2.9346	1.0861	79.3173
Average		*16.788*	*2.93405*	*1.10955*	*79.1684*
AS-3	0.0083	16.112	2.5844	0.0552	81.2484
	0.0062	16.066	2.2682	0.8675	80.7983
		16.089	*2.4263*	*0.8675*	*80.6172*
AS-4	0.0156	17.951	2.4887	0.8927	78.6676
	0.0154	17.991	2.14	0.8632	79.0058
Average		*17.971*	*2.31435*	*0.87795*	*78.8367*

Table 4.6. Elemental analysis data (C, S).

Sample	Weight (g)	S wt.%	C wt.%	Others wt.%
M-rich alginic acid	0.0817	0.35158	28.345	71.30342
	0.076	0.3277	28.182	71.4903
Average		*0.33964*	*28.2635*	*71.39686*
AS-2	0.0806	11.863	17.2	70.937
	0.0804	11.743	17.048	71.209
Average		*11.803*	*17.124*	*71.073*
AS-3	0.0628	12.667	15.638	71.695
	0.0573	12.311	15.364	72.325
Average		*12.489*	*15.501*	*72.01*
AS-4	0.084	13.543	17.13	69.327
		13.109	17.075	69.816
Average		*13.326*	*17.1025*	*69.5715*

Average values of S wt.% and C wt.% were used for DS calculation according to the following Equation 4.2.

1D- and 2D-NMR Spectra

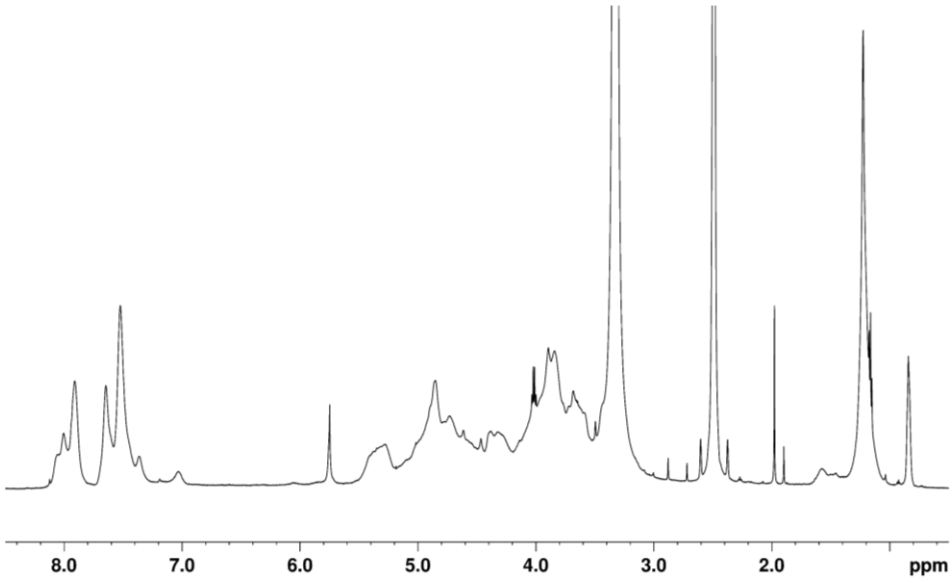

Figure 4.26. ^{1}H NMR (600 MHz, 298K, DMSO-d_6) of M-rich alginic acid derivative **55-ii.**

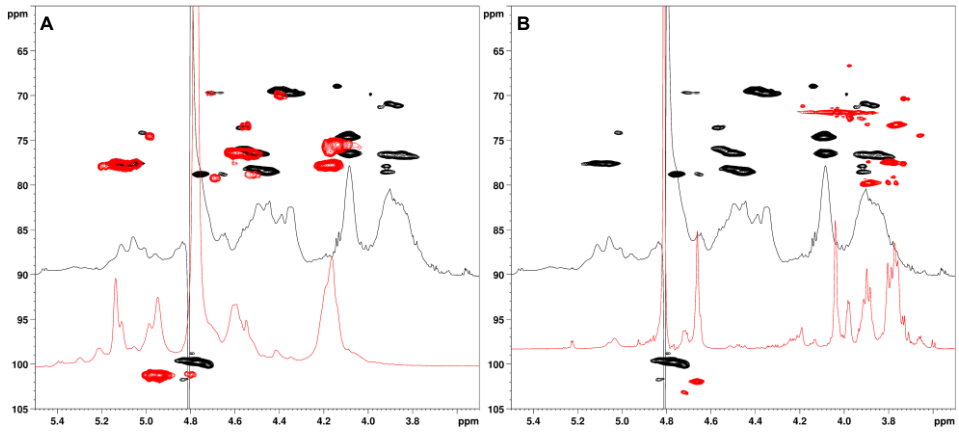

Figure 4.27. $^{1}H,^{13}C$-HSQC and ^{1}H-NMR spectra (600 MHz, 298 K, D_2O) of (A) **AS-1** (black) and **AS-3** (red), (B) **AS-1** (black) and M-rich alginic acid (red).

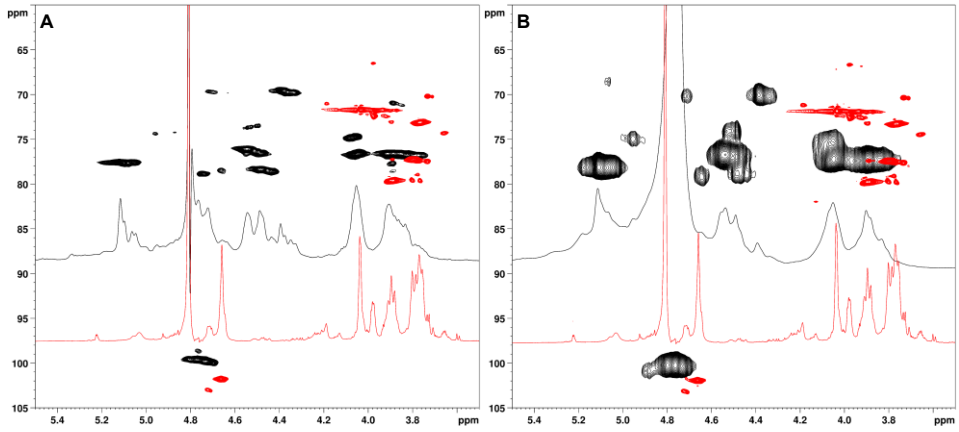

Figure 4.28. $^{1}H,^{13}C$-HSQC and ^{1}H NMR spectra (600 MHz, 298 K, D_2O) of (A) **AS-2** (black) and M-rich alginic acid (red). (B) **AS-4** (black) and M-rich alginic acid (red).

4.4.4. Semi-Synthetic Procedures and Characterization of Sulfated HE800 EPS Polysaccharides

Derivative 59. LMW-HE800 EPS (33.9 mg, 34.4 μmol RU) was dissolved in deionized water (750 μL) and passed through a short Dowex 50 WX8 column (H^+ form, 20-50 mesh, approx. 4 cm^3). Elution with deionized water was continued until a neutral pH of the eluate was detected. The eluted fraction was then

neutralized with some drops of an aqueous solution of TBAOH (16% *w*/*v* TBAOH in H_2O). After freeze-drying, product **59** (43.8 mg, 129% weight yield) was obtained as a white waxy solid.

Derivative sEPS-1. A suspension of **59** (41.2 mg, 33.2 μmol RU) in dry DMF (2.5 mL) was treated with a 0.40 M solution of SO_3·py complex in dry DMF (550 μL, 199 μmol). After 1 h stirring at 4 °C, some drops of 1 M $NaHCO_{3(aq)}$ were added to adjust pH to 7 at r.t. and then 0.3 M $NaCl_{(aq)}$ (5 mL) was added. The mixture was stirred for 1 h at r.t., then dialyzed and freeze-dried. The obtained product was dissolved in deionized water and passed through a short Dowex 50 WX8 column (H^+ form, 20-50 mesh, approx. 4 cm^3), continuing the elution with deionized water until a neutral pH of the eluate was detected. The eluted solution was adjusted to pH 10 with 1 M $NaOH_{(aq)}$, then dialyzed and freeze-dried to afford product **sEPS-1** (15.9 mg, 39% weight yield) as a white waxy solid.

Derivative 60. Per-*O*-sulfated LMW-HE800 EPS (18.8 mg, 9.13 μmol RU) was dissolved in deionized water (1.0 mL) and passed through a short Dowex-50 WX8 column (H^+ form, 20–50 mesh, approx. 4 cm^3). Elution with deionized water was continued until pH of the eluate was neutral. The obtained eluate was treated with some drops of pyridine to neutralize the solution. Freeze-drying of the collected eluate gave pyridinium salt **60** (17.1 mg, 91% weight yield).

Derivative sEPS-2. A suspension of **60** (17.1 mg, 8.30 μmol RU) in pyridine (1.7 mL) was treated with MSTFA (31 μL, 0.16 mmol) and heated at 70 °C. After 20 h stirring, the mixture was cooled to r.t., then deionized water (3 mL) was added giving a turbid mixture that was dialyzed for one day. Thereafter, the mixture was passed through a short Dowex-50 WX8 column (H^+ form, 20–50 mesh, approx. 4 cm^3), continuing the elution with deionized water until a neutral pH of the eluate was reached. Then some drops of 1 M $NaOH_{(aq)}$ were added to neutralize the solution. Dialysis and subsequent freeze-drying gave polysaccharide **sEPS-2** (12.2 mg, 65% weight yield).

Study of *N*-deacetylation on LMW-HE800 EPS. LMW-HE800 EPS (40.5 mg, 50.5 μmol RU) was dissolved in $N_2H_4 \cdot H_2O$ (1.0 mL), then $N_2H_4 \cdot H_2SO_4$ (10.0 mg, 76.8 μmol) was added. The suspension was flushed under Ar atmosphere and heated at 90 °C. At different times, 250 μL aliquots were collected, cooled to r.t. and treated with ethanol (1.0 mL) and a few drops of brine. The mixtures were dialyzed and, after freeze-drying, the obtained solid residues (**61-i–iv**) were weighted and subjected to ^{1}H NMR analysis in D_2O.

Derivative sEPS-3. Polysaccharide **61-ii** (15.6 mg, 19.3 μmol RU) was dissolved in deionized water (3.9 mL) and treated with Na_2CO_3 (25.0 mg, 23.6 μmol) and $SO_3 \cdot Me_3N$ complex (25.0 mg, 18.0 μmol) and heated at 45°C. After 4 h stirring, additional $SO_3 \cdot Me_3N$ (25.0 mg, 18.0 μmol) was added to the solution. After 20 h stirring at 45°C, the obtained solution was cooled to r.t., dialyzed and freeze-dried to yield derivative **sEPS-3** (12.4 mg, 79% weight yield).

Derivative 62. LMW-HE800 EPS (20.8 mg, 25.9 μmol RU) was suspended in DMF (1.0 mL) and then heated to 80 °C. After 1 h stirring, a very fine suspension was obtained. It was cooled to r.t. and treated with α,α-dimethoxytoluene (39 μL, 259 μmol) and then with CSA (1.5 mg, 6.5 μmol). The mixture was stirred for 20 h at 80 °C. Thereafter, it was cooled to r.t. and treated with diisopropyl ether (5 mL). The obtained white precipitate was collected by centrifugation and then dried under vacuum to afford derivative **62** (24.8 mg, 119% weight yield).

Derivative sEPS-4. A suspension of **62** (17.8 mg, 20.0 μmol RU) in dry DMF (500 μL) was treated with a 0.4 M solution of $SO_3 \cdot$py complex in dry DMF (2.7 mL, 1.1 mmol). After overnight stirring at 50°C, the obtained clear solution was cooled to r.t. and then a saturated NaCl solution in acetone (5 mL) was added. The obtained white precipitate was collected by centrifugation and then dissolved in deionized water (minimal amount). The acid solution (pH ~ 2) was heated to 50 °C and stirred for 2.5 hours. Thereafter, it was treated at r.t. with 4 M $NaOH_{(aq)}$ solution to adjust pH to 12. The solution was stirred at r.t. for 20 h and then

neutralized with 1 M $HCl_{(aq)}$. Dialysis and freeze-drying yielded polysaccharide **sEPS-4** (31.5 mg, 177% weight yield).

Determination of molecular mass. The molecular weight analyses of the sulfated HE800 EPS samples were performed by a HPSEC system composed of an HPLC system Prominence (Shimadzu Co), a PL aquagel-OH MIXED, 8 μm guard column (7.5 × 50 mm, Agilent Technologies), and a PL aquagel-OH MIXED separation column (7.5 × 300 mm, Agilent Technologies). The eluent was 0.1 M NH_4OAc. The molecular weight was calculated using a RI increment characteristic of polysaccharides, dn/dc = 0.145 mL/g.

^{1}H and ^{13}C NMR Chemical Shifts Attributions

Table 4.7. ^{1}H (plain) and ^{13}C NMR (italic) chemical shift attribution of LMW-HE800 EPS and per-*O*-sulfated LMW-HE800 EPS. [a]

Product	***Subunit***	**1**	**2**	**3**	**4**	**5**	**6**	***Other signals***
LMW-HE800 EPS[b]	*GalNAc*	5.42 *99.0*	4.27 *51.3*	3.89 *69.2*	4.22 *77.6*	3.83 *71.9*	3.66/3.83 *61.3*	NAc 2.00–2.06/*23.4*
	*→4)-**GlcA**- (1→4)-GalNAc*	4.68 *104.7*	3.46 *74.6*	3.60 *78.3*	3.67 *79.4*	3.84 *76.6*	---	
	*→4)-**GlcA**- (1→4)-GlcA*	4.53 *104.2*	3.36 *74.5*	3.60 *78.3*	3.75 *80.7*	3.75 *77.9*	---	
	GlcNAc	4.58 *101.8*	3.77 *55.4*	3.67 *79.4*	3.65 *72.5*	3.45 *77.5*	3.73/3.92 *61.8*	
per-*O*-sulfated LMW-HE800 EPS[c]	*GalNAc*	5.60 *97.5*	4.68 *48.5*	4.44 n.d.[d]	4.57 *73.7*	4.16 *70.1*	4.22/4.29 *69.5*	NAc 2.02/*23.6* 2.10/*23.7*
	*→4)-**GlcA**- (1→4)-GalNAc*	5.15 *92.3*	4.42 n.d.[d]	4.81 *78.6*	4.34 *78.5*	n.d.[d]	---	
	*→4)-**GlcA**- (1→4)-GlcA*	5.00 *102.3*	4.46 n.d.[d]	4.72 *78.1*	n.d.[d]	n.d.[d]	---	
	GlcNAc	4.80 *100.9*	4.01 *55.2*	4.11 *76.0*	4.49 n.d.[d]	3.92 *73.9*	4.21/4.63 *68.5*	

[a] Chemical shifts are expressed in δ relative to internal acetone (^{1}H: $(CH_3)_2CO$ at δ = 2.22 ppm; ^{13}C: $(CH_3)_2CO$ at δ = 31.5 ppm). [b] NMR experiments conducted in D_2O (600 MHz, 298 K). [c] NMR experiments conducted in D_2O (400 MHz, 298 K). [d] not detected.

Table 4.8. ^{1}H (plain) and ^{13}C NMR (italic) chemical shift attribution of **sEPS-1**, **61-ii**. [a]

Product	*Subunit*	**1**	**2**	**3**	**4**	**5**	**6**	*Other signals*
sEPS-1[b]	*GalNAc*	5.61 *98.0* 3,6S	4.50 *49.3* 3,6S	4.51 *74.5* 3,6S	4.50 *76.3* 3,6S	4.01 *70.4* 3,6S/6S	4.17/4.25 *69.6* 3,6S/6S	NAc: 2.00–2.12 22.7–24.5
		5.54 *98.3* 6S	4.28 *51.1* 6S	3.88 *69.2* 6S/0S	4.25 *78.8* 6S			
		5.42 *98.8* 0S	4.26 *51.3* 0S		4.22 *78.0* 0S	3.83 *71.9* 0S	3.65/3.82 *61.3* 0S	
	*{→4)-**GlcA**-(1→4)-GalNAc}^{i}*	4.68 *105.1*	3.45 *74.5*	3.63 *75.3*	3.74 *82.0*	3.89 *76.6*	---	
	*{→4)-**GlcA**-(1→4)-GalNAc}^{ii}*	4.74 *104.1*	3.40 *74.3*					
	*→4)-**GlcA**-(1→4)-GlcA*	4.53 *104.1*	3.36 *74.2*	3.61 *74.9*	3.77 *82.0*	3.81 *79.0*	---	
	GlcNAc	4.61 *102.7*	3.79 *55.3*	3.71 *79.2*	3.68 *75.1* 6S	3.69 *72.2* 6S	4.25/4.34 *67.8* 6S	
					3.65 *72.7* 0S	3.46 *77.0* 0S	3.73/3.90 *61.8* 0S	
61-ii[c]	*GalN*	5.66 *97.2*	3.68 *52.4*	4.07 *67.6*	4.25 *76.6*	3.83 *72.0*	3.67/3.83 *60.9*	NAc 2.07/*23.8*
	*→4)-**GlcA**-(1→4)-GalNAc*	4.71 *104.2*	3.43 *74.4*	3.63 *75.5*	3.67 *82.2*	3.84 *76.4*	---	
	*→4)-**GlcA**-(1→4)-GlcA*	4.52 *103.9*	3.36 74.3	3.59 *79.4*	3.80 *80.2*	3.75 *77.6*	---	
	GlcNAc	4.56 *101.5*	3.80 *55.1*	3.75 *80.8*	3.70 *72.0*	3.50 *76.7*	3.77/3.92 *61.4*	

The superscripts *i* and *ii* represent the same residue type with different neighbouring residues. [a] Chemical shifts are expressed in δ relative to internal acetone (^{1}H: $(CH_3)_2CO$ at δ = 2.22 ppm; ^{13}C: $(CH_3)_2CO$ at δ = 31.5 ppm). [b] NMR experiments conducted in D_2O (600 MHz, 298 K). [c] NMR experiments conducted in D_2O (400 MHz, 298 K).

Table 4.9. ^{1}H (plain) and ^{13}C NMR (italic) chemical shift attribution of **sEPS-3**. [a,b]

Product	*Subunit*	1	2	3	4	5	6	*Other signals*
sEPS-3	*GalNS*	5.54 *99.9*	3.61 *55.8*	3.81 *69.7*	4.21 *77.4*	3.82 *71.6*	3.63/3.82 *61.2*	NAc 2.04/*23.9*
	→4)-***GlcA***- *(1→4)-GalNAc*	4.70 *104.5*	3.45 *74.3*	3.62 *75.5*	3.71 *81.4*	3.89 *76.1*	---	
	→4)-***GlcA***- *(1→4)-GlcA*	4.54 *103.9*	3.37 *74.2*	3.61 *75.2*	3.79 *81.2*	3.82 *76.9*	---	
	GlcNAc	4.59 *101.9*	3.77 *55.5*	3.76 *80.9*	3.76 *71.8*	3.49 *76.7*	3.76/3.90 *61.7*	

[a] NMR experiments conducted in D_2O (400 MHz, 298 K). [b] Chemical shift expressed in δ relative to internal acetone (^{1}H: $(CH_3)_2CO$ at δ = 2.22 ppm; ^{13}C: $(CH_3)_2CO$ at δ = 31.5 ppm).

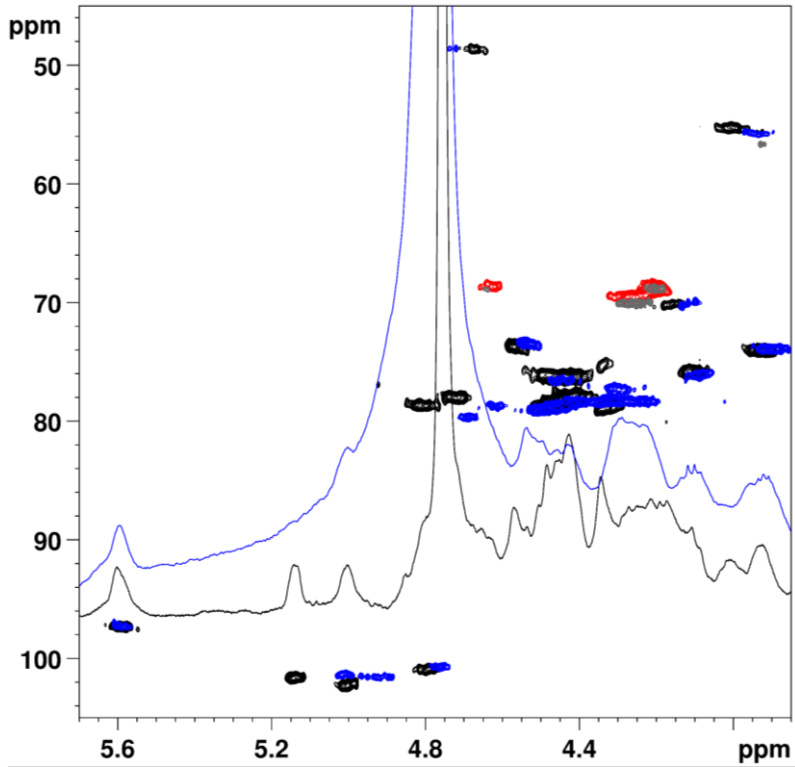

Figure 4.29. Zoom of ^{1}H,^{13}C-DEPT-HSQC ^{1}H-NMR spectra (400 MHz, 298 K, D_2O) of per-*O*-sulfate LMW-HE800 EPS (black/red: ^{1}H,^{13}C-DEPT-HSQC NMR spectrum, black: ^{1}H-NMR spectrum) and **sEPS-2** (blue/grey: ^{1}H,^{13}C-DEPT-HSQC NMR spectrum; blue: ^{1}H-NMR spectrum).

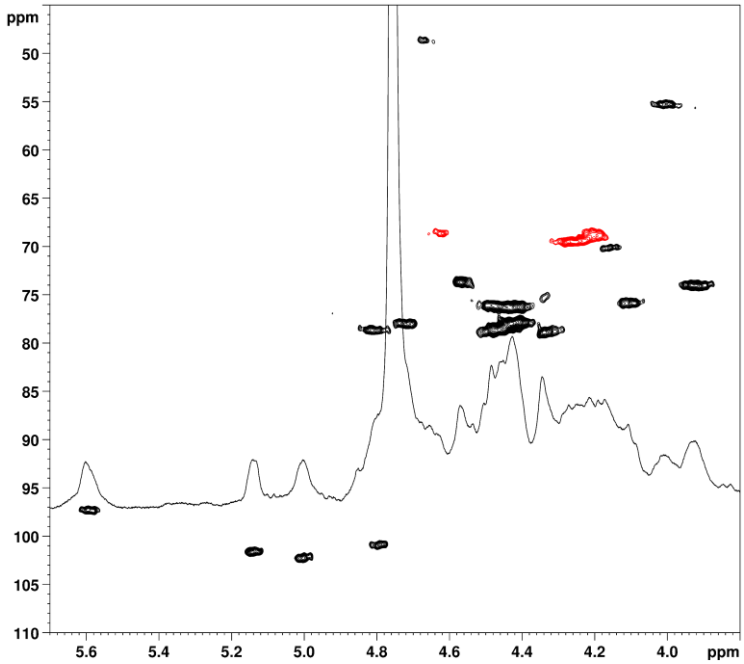

Figure 4.30. Zoom of ^{1}H and $^{1}H,^{13}C$-DEPT-HSQC NMR spectra (400 MHz, 298K, D_2O) of per-*O*-sulfated LMW-HE800 EPS.

References

Aarstad, O.A., Tøndervik, A., Sletta, H., Skjåk-Bræk, G., **2012**. *Biomacromolecules 13*, 106–116.

Adinolfi, M., Barone, G., Guariniello, L., Iadonisi, A., **1999**. *Tetrahedron Lett. 40*, 8439–8441.

Anson, S.I., Novikova, E. V., Iozep, A.A., **2009**. *Russ. J. Appl. Chem. 82*, 1095–1097.

Arlov, Ø., Aachmann, F.L., Sundan, A., Espevik, T., Skjåk-Bræk, G., **2014**. *Biomacromolecules 15*, 2744–2750.

Arlov, Ø., Rütsche, D., Korayem, M.A., Öztürk, E., Zenobi-wong, M., **2021**. *Adv. Funct. Mater. 31*, 2010732–2010784.

Arlov, Ø., Skjåk-Bræk, G., **2017**. *Molecules 22*, 793.

Bachelder, E.M., Pino, E.N., Ainslie, K.M., **2017**. *Chem. Rev. 117*, 1915–1926.

Bedini, E., De Castro, C., De Rosa, M., Di Nola, A., Iadonisi, A., Restaino, O.F., Schiraldi, C., Parrilli, M., **2011**. *Angew. Chem., Int. Ed. 50*, 6160–6163.

Bedini, E., De Castro, C., De Rosa, M., Di Nola, A., Restaino, O.F., Schiraldi, C., Parrilli, M., **2012**. *Chem. - Eur. J. 18*, 2123–2130.

Bedini, E., Corsaro, M.M., Fernández-Mayoralas, A., Iadonisi, A., **2019**. Chondroitin, Dermatan, Heparan, and Keratan Sulfate: Structure and Functions, in: Cohen, E., Merzendorfer, H. (Eds.), *Extracellular Sugar-Based Biopolymers Matrices*. Springer Nature Switzerland, Cham, Switzerland, pp. 187–233.

Bedini, E., Laezza, A., Parrilli, M., Iadonisi, A., **2017**. *Carbohydr. Polym. 174*, 1224–1239.

Benito-Arenas, R., Doncel-Pérez, E., Fernández-Gutiérrez, M., Garrido, L., García-Junceda, E., Revuelta, J., Bastida, A., Fernández-Mayoralas, A., **2018**. *Carbohydr. Polym. 202*, 211–218.

Bishnoi, M., Jain, A., Hurkat, P., Jain, S.K., **2016**. *Glycoconjugate J. 33*, 693–705.

Bramhachari, P. V., Kavi Kishor, P.B., Ramadevi, R., Kumar, R., Rama Rao, B., Dubey, S.K., **2007**. *J. Microbiol. Biotechnol. 17*, 44–51.

Bramhachari, P.V., Dubey, S.K., **2006**. *Lett. Appl. Microbiol. 43*, 571–577.

Caputo, H.E., Straub, J.E., Grinstaff, M.W., **2019**. *Chem. Soc. Rev. 48*, 2338–2365.

Casillo, A., Lanzetta, R., Parrilli, M., Corsaro, M.M., **2018**. *Mar. Drugs 16*, 69–103.

Chaidedgumjorn, A., Toyoda, H., Woo, E.R., Lee, K.B., Kim, Y.S., Toida, T., Imanari, T., **2002**. *Carbohydr. Res. 337*, 925–933.

Chien, C.-Y., Enomoto, Y., Iwata, T., **2019**. *ACS Sustainable Chem. Eng. 7*, 9857–9864.

Coleman, R.J., Lawrie, G., Lambert, L.K., Whittaker, M., Jack, K.S., Grondahl, L., **2011**. *Biomacromolecules 12*, 889–897.

Cong, Q., Xiao, F., Liao, W., Dong, Q., Ding, K., **2014**. *Int. J. Biol. Macromol. 69*, 252–259.

Decho, A.W., **1990**. *Oceanogr. Mar. Biol. 28*, 73–153.

Draget, K.I., Moe, S.T., Skjåk-Bræk, G., Smidsrød, O., **2006**. Alginates, in: Stephen, A.M., Phillips, G.O., Williams, P.A. (Eds.), *Food Polysaccharides and Their Applications*. CRC Press, Boca Raton (FL), pp. 289–334.

Drouillard, S., Jeacomine, I., Buon, L., Boisset, C., Courtois, A., Thollas, B., Morvan, P.Y., Vallée, R., Helbert, W., **2015**. *Mar. Drugs 13*, 6723–6739.

Elferink, H., Mensink, R.A., Castelijns, W.W.A., Jansen, O., Bruekers, J.P.J., Martens, J., Oomens, J., Rijs, A.M., Boltje, T.J., **2019**. *Angew. Chem., Int. Ed. 131*, 8838–8843.

Fernando, I.P.S., Kim, D., Nah, J.W., Jeon, Y.J., **2019**. *Chem. Eng. J. 355*, 33–48.

Finore, I., Di Donato, P., Mastascusa, V., Nicolaus, B., Poli, A., **2014**. *Mar. Drugs 12*, 3005–3024.

Fonseca, R.J.C., Oliveira, S.N.M.C.G., Pomin, V.H., Mecawi, A.S., Araujo, I.G., Mourão, P.A.S., **2010**. *Thromb. Haemostasis 103*, 994–1004.

Freeman, I., Kedem, A., Cohen, S., **2008**. *Biomaterials 29*, 3260–3268.

Fukuda, M., Kondo, T., Osawa, T., **1976**. *J. Biochem. 80*, 1223–1232.

Futatsuyama, H., Yui, T., Ogawa, K., **1999**. *Biosci., Biotechnol., Biochem. 63*, 1481–1483.

Gao, Y., Fukuda, A., Katsuraya, K., Kaneko, Y., Mimura, T., Nakashima, H., Uryu, T., **1997**. *Macromolecules 30*, 3224–3228.

Gargiulo, V., Lanzetta, R., Parrilli, M., De Castro, C., **2009**. *Glycobiology 19*, 1485–1491.

La Gatta, A., De Rosa, M., Frezza, M.A., Catalano, C., Meloni, M., Schiraldi, C., **2016**. *Mater. Sci. Eng., C 68*, 565–572.

Gomez D'Ayala, G., Malinconico, M., Laurienzo, P., **2008**. *Molecules 13*, 2069–2106.

Grandpierre, C., Janssen, H.G., Laroche, C., Michaud, P., Warrand, J., **2008**. *Carbohydr. Polym. 71*, 277–286.

Guerrini, M., Naggi, A., Guglieri, S., Santarsiero, R., Torri, G., **2005**. *Anal. Biochem. 337*, 35–47.

Guo, Y., Conrad, H.E., **1989**. *Anal. Biochem. 176*, 96–104.

Han, W., Li, Q., Lv, Y., Wang, Q.C., Zhao, X., **2018**. *Carbohydr. Res. 460*, 8–13.

Jannasch, H.W., Taylor, C.D., **1984**. *Annu. Rev. Microbiol. 38*, 487–487.

Jiang, P., Li, J., Han, F., Duan, G., Lu, X., Gu, Y., Yu, W., **2011**. *PLoS One 6*, e18514.

Jin, Y., Mu, Y., Zhang, S., Li, P., Wang, F., **2020**. *Int. J. Biol. Macromol. 146*, 273–284.

Kalyanasundaram, G.T., Doble, M., Gummadi, S.N., **2012**. *AMB Express 2*, 40.

Kariya, Y., Kyogashima, M., Suzuki, K., Isomura, T., Sakamoto, T., Horie, K., Ishihara, M., Takano, R., Kamei, K., Hara, S., **2000**. *J. Biol. Chem. 275*, 25949–25958.

Kikuchi, D., Sakaguchi, S., Ishii, Y., **1998**. *J. Org. Chem. 63*, 6023–6026.

Knirel, Y.A., Naumenko, O.I., Senchenkova, S.N., Perepelov, A. V., **2019**. *Russ. Chem. Rev. 88*, 406–424.

Kornilov, A. V., Sukhova, E. V., Nifantiev, N.E., **2001**. *Carbohydr. Res. 336*, 309–313.

Kowitsch, A., Zhou, G., Groth, T., **2018**. *J. Tissue Eng. Regen. Med. 12*, e23–e41.

Kulkarni, S.S., Wang, C.-C., Sabbavarapu, N.M., Podilapu, A.R., Liao, P.-H., Hung, S.-C., **2018**. *Chem. Rev. 118*, 8025–8104.

Laezza, A., De Castro, C., Parrilli, M., Bedini, E., **2014**. *Carbohydr. Polym. 112*, 546–555.

Lee, K.Y., Mooney, D.J., **2012**. *Prog. Polym. Sci. 37*, 106–126.

Li, P., Tan, H., Xu, D., Yin, F., Cheng, Y., Zhang, X., Liu, Y., Wang, F., **2014**. *Carbohydr. Polym. 110*, 446–455.

Maki, Y., Nomura, K., Okamoto, R., Izumi, M., Mizutani, Y., Kajihara, Y., **2020**. *J. Org. Chem. 85*, 15849–15856.

Mans, D.J., Ye, H., Dunn, J.D., Kolinski, R.E., Long, D.S., Phatak, N.L., Ghasriani, H., Buhse, L.F., Kauffman, J.F., Keire, D.A., **2015**. *Anal. Biochem. 490*, 52–54.

Matsuo, M., Takano, R., Kamei-Hayashi, K., Hara, S., **1993**. *Carbohydr. Res. 241*, 209–215.

Mukhopadhyay, B., Field, R.A., **2003**. *Carbohydr. Res. 338*, 2149–2152.

Muralidharan, J., Jayachandran, S., **2003**. *Process Biochem. 38*, 841–847.

Nadkarni, V.D., Toida, T., Van Gorp, C.L., Schubert, R.L., Weiler, J.M., Hansen, K.P., Caldwell, E.E.O., Linhardt, R.J., **1996**. *Carbohydr. Res. 290*, 87–96.

Pagliano, G., Ventorino, V., Panico, A., Pepe, O., **2017**. *Biotechnol. Biofuels 10*, 113–136.

Pawar, S.N., Edgar, K.J., **2012**. *Biomaterials 33*, 3279–3305.

Petersen, B.O., Krah, M., Duus, J.Ø., Thomsen, K.K., **2000**. *Eur. J. Biochem. 267*, 361–369.

Prieto, M.A., Vázquez, J.A., Murado, M.A., **2011**. *Process Biochem. 46*, 1579–1588.

Raguénès, G., Christen, R., Guezennec, J., Pignet, P., Barbier, G., **1997**. *Int. J. Syst. Bacteriol. 47*, 989–995.

Raßloff, J., Zhang, Q., Mischnick, P., **2018**. *Cellulose 25*, 4929–4940.

Reen, F.J., Almagro-Moreno, S., Ussery, D., Boyd, E.F., **2006**. *Nat. Rev. Microbiol. 4*, 697–704.

Restaino, O.F., Finamore, R., Diana, P., Marseglia, M., Vitiello, M., Casillo, A., Bedini, E., Parrilli, M., Corsaro, M.M., Trifuoggi, M., De Rosa, M., Schiraldi, C., **2017**. *Anal. Chim. Acta 958*, 59–70.

Romalde, J.L., Diéguez, A.L., Lasa, A., Balboa, S., **2014**. *Front. Microbiol. 4*, 413.

Rougeaux, H., Kervarec, N., Pichon, R., Guezennec, J., **1999**. *Carbohydr. Res. 322*, 40–45.

Scott, R.A., Panitch, A., **2013**. *Wiley Interdiscip. Rev.: Nanomed. Nanobiotechnol. 5*, 388–398.

Senni, K., Gueniche, F., Changotade, S., Septier, D., Sinquin, C., Ratiskol, J., Lutomski, D., Godeau, G., Guezennec, J., Colliec-Jouault, S., **2013**. *Mar. Drugs 11*, 1351–

1369.

Senni, K., Gueniche, F., Fioretti, F., Godeau, G.J., Colliec-Jouault, S., Ratiskol, J., Sinquin, C., Raguénès, G., Courtois, J., Guézennec, J., **2015**. Sulfated depolymerized derivatives of exopolysaccharides from mesophilic marine bacteria, method for preparing same, and uses thereof in tissue regeneration. US 9,125,883.

Shaklee, P.N., Conrad, H.E., **1984**. *Biochem. J. 217*, 187–197.

Sutherland, I.W., **1982**. *Adv. Microb. Physiol. 23*, 79–150.

Szekalska, M., Pucibowska, A., Szymanska, E., Ciosek, P., Winnicka, K., **2016**. *Int. J. Polym. Sci. 2016*, 1–17.

Takano, R., Kanda, T., Hayashi, K., Yoshida, K., Hara, S., **1995**. *J. Carbohydr. Chem. 14*, 885–888.

Toida, T., Suzuki, A., Nakajima, K., Chaidedgumjorn, A., Imanari, T., **2000**. *Glycoconjugate J. 17*, 393–399.

Traboni, S., Bedini, E., Giordano, M., Iadonisi, A., **2015**. *Adv. Synth. Catal. 357*, 3562–3572.

Traboni, S., Bedini, E., Iadonisi, A., **2016**. *Beilstein J. Org. Chem. 12*, 2748–2756.

Wang, Junlong, Yang, W., Wang, Jiancheng, Wang, X., Wu, F., Yao, J., Zhang, J., Lei, Z., **2015**. *Carbohydr. Polym. 133*, 320–327.

Wang, Z., Xie, J., Shen, M., Nie, S., Xie, M., **2018**. *Trends Food Sci. Technol. 74*, 147–157.

Wardrop, D., Keeling, D., **2008**. *Br. J. Haematol. 141*, 757–763.

Wu, J., Zhao, X., Ren, L., Xue, Y., Li, C., Yu, G., Guan, H., **2014**. *Carbohydr. Polym. 104*, 23–28.

Xue, Y.-T., Ren, L., Li, S., Wang, L.-L., He, X.-X., Zhao, X., Yu, G.-L., Guan, H., Li, C., **2016**. *Carbohydr. Polym. 144*, 330–337.

Yan, L., Li, J., Wang, D., Ding, T., Hu, Y., Ye, X., Linhardt, R.J., Chen, S., **2017**. *Carbohydr. Polym. 178*, 180–189.

Yang, J.-S., Xie, Y.-J., He, W., **2011**. *Carbohydr. Polym. 84*, 33–39.

Yates, E.A., Santini, F., Guerrini, M., Naggi, A., Torri, G., Casu, B., **1996**. *Carbohydr. Res. 294*, 15–27.

Yoshida, T., Yasuda, Y., Mimura, T., Kaneko, Y., Nakashima, H., Yamamoto, N., Uryu, T., **1995**. *Carbohydr. Res. 276*, 425–436.

Zanchetta, P., Lagarde, N., Guezennec, J., **2003**. *Calcif. Tissue Int. 72*, 74–79.

Zeng, K., Groth, T., Zhang, K., **2019**. *ChemBioChem 20*, 737–746.

Zhan, X.B., Lin, C.C., Zhang, H.T., **2012**. *Appl. Microbiol. Biotechnol. 93*, 525–531.

Zhang, R., Edgar, K.J., **2014**. *Biomacromolecules 15*, 1079–1096.

Zhao, L., Lai, S., Huang, R., Wu, M., Gao, N., Xu, L., Qin, H., Peng, W., Zhao, J., **2013**. *Carbohydr. Polym. 98*, 1514–1523.

Zou, Y., Khor, E., **2009**. *Carbohydr. Polym. 77*, 516–525.